The measurement and modelling of vapour-liquid equilibria in ternary systems containing polar, cross-associating, and associating compounds

by

Andrew Cameron Thompson

Thesis presentation in partial fulfilment

of the requirements for the Degree

of

MASTERS in ENGINEERING

CHEMICAL ENGINEERING

in the Faculty of Engineering

at Stellenbosch University

Supervisor

Prof. A.J. Burger

Co-supervisor

Dr. J.T. Cripwell

December 2020

Plagiarism Declaration

By submitting this thesis electronically, I declare that the entirety of the work contained therein is my own, original work, that I am the sole author thereof (save to the extent explicitly otherwise stated), that reproduction and publication thereof by Stellenbosch University will not infringe any third party rights and that I have not previously in its entirety or in part submitted it for obtaining any qualification.

Date: December 2020

Abstract

The accurate production of simple binary vapour liquid equilibria (VLE) data sets is time consuming and expensive, and the measurement of similar data sets for multicomponent systems is even more laborious and tricky. Therefore, generic thermodynamic models that can predict VLE behaviour accurately are required for the optimisation and design of many processes within industry. This is especially true for complex systems such as polar, associating, and cross-associating mixtures.

For the majority of complex VLE mixtures, thermodynamic models incorporating binary interaction parameters (BIPs) are required for an accurate representation.

Models in the perturbation theory equations of state (EoS) use pure component data to predict phase equilibria. In doing so, these models predict rather than correlate VLE and phase equilibria. Perturbation theory models such as CPA-GV, SAFT-VR-Mie-GV, and sPC-SAFT-GV have been proved accurate for the prediction of binary systems and assumed to be accurate for multicomponent systems. However, **there is a need to systematically test the assumption that these models can accurately predict complex multicomponent mixtures with a similar accuracy that they do for binary systems**. This study therefore produced carefully measured new equilibrium data on the ternary VLE of four systems, as well as the nine binary systems within the ternary systems. Each system contained 1-propanol and 2-butanone, with the third component being either one of three different C_4 esters, or 2-propanol. These data sets were then used to test and evaluate the applicability and accuracy of the aforementioned EoS.

The data of the nine binary and the four-ternary isobaric VLE systems were produced at 101.3 kPa with the use of a Gillespie type still. This still had experimental uncertainties in temperature of ± 0.62 K and pressure of ± 0.046 bar. The liquid and vapour samples were analysed using a GC and had experimental uncertainties of ± 0.016 mole fraction. The experimental procedure with the Gillespie still and the GC analysis was verified using vapour pressure of the binary systems that occur in all four ternary systems, 1-propanol/2-butanone, and existing literature data. All VLE data were thermodynamically consistent, passing both the McDermott-Ellis and the L/W consistency tests.

The deviations from the ideal state in the ternary systems were found to correspond to similar deviations in the binary mixtures. This was further evidenced with distillation boundaries when two azeotropes existed (methyl propionate and propyl formate systems) with the 2-propanol system displaying the largest deviations from the ideal state, and the ethyl acetate system behaving the most ideal.

Accurate results were found for the binary modelling, with both the SAFT-VR-Mie-GV and sPC-SAFT-GV models being able to cope with the cross-association and the non-ideal nature of the systems, having AAD values for the nine binary systems of 0.614 K and 0.011 mole fraction and 0.589 K and 0.011 mole fraction, respectively.

In the ternary systems, the two models that accurately predicted the binary systems also predicted the ternary systems accurately, with comparable results with NRTL and each other. The AAD values of the four ternary systems were 0.820 K and 0.015 mole fraction, and 0.720 K and 0.017 mole fraction, respectively. **This work therefore shows that the SAFT type models display strong potential to predict the vapour-liquid equilibria in ternary systems containing polar, non-associating and associating compounds.**

Opsomming

Die akkurate produksie van eenvoudige binêre damp ekwilibria (VLE) datastelle is tydrowend en duur, en die meting van soortgelyke datastelle vir multkomponentstelsels is selfs meer moeisaam en bedrieglik. Daarom word generiese termodinamiese modelle wat VLE-gedrag akkuraat kan voorspel benodig vir die optimering en ontwerp van baie prosesse in die industrie. Dit is veral waar vir komplekse stelsels soos polêre, assosiërende, en kruisassosiërende mengsels.

Vir die meeste van komplekse VLE-mengsels, word termodinamiese modelle wat binêre interaksie parameters (BIPs) inkorporeer, benodig vir akkurate voorstelling.

Modelle in die steuringteorie toestandsvergelykings (EoS) gebruik suiwer komponent data om fase-ekwilibria te voorspel. Deur dit so te doen voorspel hierdie modelle VLE en fase-ekwilibria eerder as om dit te korreleer. Steuringteorie modelle soos CPA-GV, SAFT-VR-Mie-GV, en sPC-SAFT-GV is reeds akkuraat bewys vir die voorspelling van binêre stelsels en word aangeneem om akkuraat te wees vir multikomponentstelsels. Daar is egter ’n behoefte om die aanname sistematies te toets dat hierdie modelle komplekse multikomponentmengsels akkuraat kan voorspel met ’n eenderse akkuraatheid as vir binêre stelsels. Hierdie studie het daarom versigtig gemete, nuwe ekwilibriumdata op die ternêre VLE van vier stelsels geproduseer, sowel as die nege binêre stelsels binne die ternêre stelsels. Elke stelsel het 1-propanol en 2-butanon bevat, met die derde komponent wat of een van drie C_4-esters was, of 2-propanol. Hierdie datastelle is toe gebruik om die toepaslikheid en akkuraatheid van die voorafgenoemde EoS te toets en evalueer.

Die data van die nege binêre en die vier- ternêre isobariese VLE-stelsels is geproduseer by 101.3 kPa met die gebruik van ’n Gillespie-tipe distilleerder. Hierdie distilleerder het eksperimentele onsekerhede in temperatuur van ± 0.62 K en druk van ± 0.046 bar. Die vloeistof- en dampsteekproewe is geanaliseer deur ’n GC te gebruik en het eksperimentele onsekerhede van ± 0.016 molfraksie. Die eksperimentele prosedure met die Gillespie-distilleerder en die GC-analise is geverifieer deur dampdruk van die binêre stelsels te verifieer wat in al vier ternêre stelsels voorgekom het, 1-propanol/2-butanon, en bestaande literatuur data. Alle VLE-data is termodinamies konsekwent, en slaag so beide die McDermott-Ellis en die L/W-konsekwentheidstoetse.

Die afwykings van die ideale toestand in die ternêre stelsels is gevind om met eenderse afwykings in die binêre mengsels ooreen te stem. Hierdie is verder bewys met distillasiegrense wanneer twee aseotrope bestaan het (metielpropionaat- en propielformaatstelsels) met die

2-propanolstelsels wat die grootste afwykings van die ideale toestand vertoon het, en die etielasetaatstelsels wat hom die mees ideaal gedra het.

Akkurate resultate is gevind vir die binêre modellering, met beide die SAFT-VR-Mie-GV en sPC-SAFT-GV-modelle wat die kruisassosiërende en die nie-ideale natuur van die stelsels kon hanteer, wat gemiddelde AAD-waardes vir die nege binêre stelsels van 0.614 K en 0.011 molfraksie en 0.589 K en 0.011 molfraksie, onderskeidelik, gehad het.

In die ternêre stelsels het die twee modelle wat die binêre stelsels akkuraat kon voorspel, ook die ternêre stelsels akkuraat voorspel, met vergelykbare resultate met NRTL en mekaar. Die gemiddelde AAD-waardes vir die vier ternêre stelsels was 0.820 K en 0.015 molfraksie en 0.720 K en 0.017 molfraksie, onderskeidelik. Hierdie werk het daarom gewys dat die SAFT-tipe modelle sterk potensiaal wys om die damp-vloeistofekwilibria in ternêre stelsels wat polêre, nie-assosiërende en assosiërende samestellings bevat, te voorspel.

Acknowledgements.

This project was made possible by the support of the following people. I would like to thank:

- Prof A. J. Burger, for your unwavering calmness, and valuable guidance, always ensuring that I had the correct focus.
- Dr J. T. Cripwell, for the fantastic insight you had into the work, which helped me look at the project from many different angles that never occurred to me. Your patience and the amount of time you spent helping me, was really appreciated.
- Dr. F. Shaahmadi, your support and expert knowledge, as well as your eagle eyes for mistakes was extremely appreciated.
- Mrs H. Botha, Mrs L. Simmers, and Mr J. van Rooyen, for the help with understanding the analytical side of the work.
- Mr J. Waardenburg, Mr A, Cordier, and Mr B. Koopman, for helping rebuild the still.
- Ms D. de Klerk, without you in the labs, working your ridiculous hours, the experimental procedure would have been far less eventful.
- Mr J. Lamprecht, thank you for being the ‘resident electrician’, helping me understand the basics and resurrecting the still.
- My colleagues in office C416 both past and present, thank you for immediately welcoming me in. It is a shame that this year has taken the turn it has.
- My family, Kim, Bruce, Amy. Thank you for all the support, encouragement, and advice you have given to me throughout my study, as well as housing me during the pandemic. It is deeply appreciated.
- My Wife, thank you for allowing me to further my education at a later age. We made a good choice.

Abbreviations

AAD	Absolute average deviation
ADC	Analogue to digital converter
CPA	Cubic-plus association
EoS	Equation of state
FID	Flame ionisation detector
GC-MS	Gas chromatography mass spectrometry
GV	Gross and Vrabec
JC	Jog and Chapman
LLE	Liquid-liquid equilibrium
NRHB	Non-random hydrogen bonding model
NRTL	Non-random two-liquid model
PC-SAFT	Perturbed chain statistical associating fluid theory
PHCT	Perturbed hard chain model
PR	Peng Robinson model
RK	Redlich-Kwong model
SAFT	Statistical associating fluid theory model
SAFT-VR Mie	Statistical associating fluid theory variable range Mie potential
SRK	Soave-Redlich-Kwong model
UNIQUAC	Universal quasichemical model
VLE	Vapour-liquid equilibrium
VLLE	Vapour-liquid-liquid equilibrium

Roman Symbols

A	Helmholtz energy
Ar	Area
a	Dispersion energy perturbation
C	Number of components
D	Dipole moment
d	Temperature dependant segment diameter
F	Degrees of freedom
f	fugacity
G	Gibbs free energy
H	enthalpy
K	Response factor
k_{ij}	Binary interaction parameter
M	Number of reactions
M_i	Number of association sites
$\bar{m}$	Mean segment number
n	Moles
N_{av}	Avogadro's number
P	Pressure
Ph	Number of phases
R	Universal gas constant
S	Entropy
T	Temperature
V	Volume

Roman Symbols

x	Liquid mole fraction
y	Vapour mole fraction
Z	Compressibility factor

Greek Symbols

β	Isothermal compressibility
γ	Activity coefficient
Δ^{AB}	Association strength
ε	Segment potential energy
ρ	Reduced density
Θ	Partial molar property
κ	Association volume
μ	Chemical potential
π	Pi
ρ	Molar density
σ	Temperature independent segment diameter
Φ	Fugacity coefficient
ω	Acentric factor

Subscripts/Superscripts

AB	Sites A and B
Assoc	Association
B	Boil
Chain	Chain formation
Disp	Dispersion
E	Excess property
Hs	Hard sphere
i,j	Component i and j
L	Liquid
max	maximum
Res	Residual
Sat	Saturated
Seg	Segment
V	Vapour
Vap	Vaporisation
0	Standard state

Contents

1. Introduction

From raw materials to intermediate chemicals in a reaction stream, there is a need for separation, in order to ensure a purified product. The most common industrial processes used to achieve this result is distillation. The overall design of the distillation process is entrenched, and mostly optimised, and therefore any further improvements to the physical process are difficult [1].

Distillation is still very energy intensive [1]. In order to optimise the systems, a knowledge of the vapour-liquid equilibrium (VLE) of specific mixtures and specific thermodynamic models is required. The best way to achieved this knowledge is through the generation of experimental data [2].

In complex systems containing non-ideal mixtures, binary interaction parameters (BIPs) are used in majority of thermodynamic models to form an accurate representation of phase behaviour. These BIPs are derived from experimental VLE data. The accuracy of the data has a direct impact on the accuracy of the model [3]. These binary BIPs and models can then be used to predict multi-component systems. These models that require the production of experimental data are expensive and time consuming, there is therefore a need for accurate models that can predict systems, without the use of BIPs.

1.1. Phase Equilibrium

In order to produce experimental VLE data, it is necessary to know when phase equilibrium occurs. Phase equilibrium occurs when Gibbs energy is at a minimum, and consequently, the chemical potential of each component (i), as well as the temperature and the pressure of each phase, is equal amongst all the possible phases [4].

$$\begin{aligned} \mu_i^a &= \mu_i^b = \cdots = \mu_i^c \\ T^a &= T^b = \cdots = T^c \\ P^a &= P^b = \cdots = P^c \end{aligned} \qquad 1.1$$

Chemical potential is a theoretical definition of equilibrium, whereas temperature and pressure are physical properties. With all three equations of Equation 1.1[5] being required to have phase equilibrium, it is necessary to use the theoretical term and to find a solution to an abstract mathematical problem. This transforms the mathematical solution into a meaningful physical term [6].

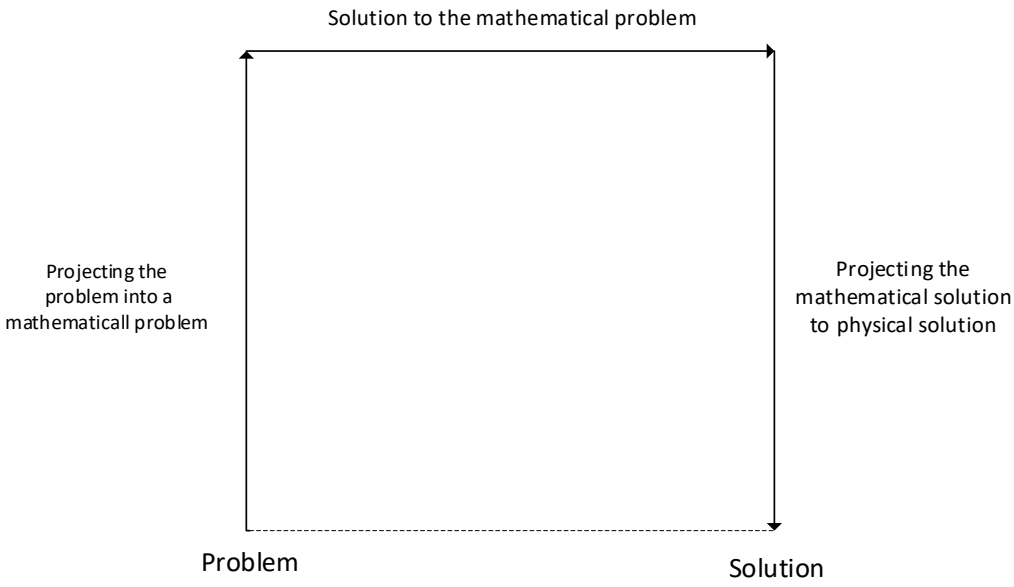

Figure 1.1: The solving of thermodynamic problems using the abstract mathematical term (taken and re-drawn from Prausnitz, et al. 1986 [6])

Using the theoretical definition and creating a mathematical solution (Figure 1.1) can be accomplished by equating chemical potential to fugacity (Equation 1.2).

$$\mu_i - \mu_i^0 = RTln(\frac{f_i}{f_i^0}) \qquad 1.2$$

In which fugacity can be thought of as the tendency of a molecular species to escape from a specific phase [7]. A chemical equilibrium is achieved when the fugacity of each component is equal in each phase (Equation 1.3) [5].

$$f_i^L(T,P,x) = f_i^V(T,P,y) \qquad 1.3$$

In order to use the mathematical solution and find a physical solution (Figure 1.1), the fugacity coefficient (Φ_i) is defined by using the phi-phi method (Equation 1.4) [5].

$$f_i^L(T,P,x) = x_i\Phi_i^L(T,P,x)P = f_i^V(T,P,y) = y_i\Phi_i^V(T,P,y)P \qquad 1.4$$

In which the fugacity coefficient can further be described as (Equation 1.5) [8], [9].

$$RTln(\Phi_i) = \int_\infty^V \left[\left(\frac{\partial P}{\partial N_i}\right)_{T,V,N_j} - \frac{RT}{V}\right] dV - RTln(Z) \qquad 1.5$$

The deviations from an ideal gas state (Equation 1.5 integral term) can be found using an equation of state (EoS). This EoS allows physical properties, such as temperature, pressure, and composition, to be used to describe the phase equilibrium of a system [9]. These physical properties can be found in vapour-liquid equilibrium experiments.

1.1.1. Vapour-liquid equilibrium

When looking at experimental phase equilibrium data collection in the industry, there are three differing views [10], namely:

a) There are enough data sets;
b) There are not enough data sets; and
c) There are too many differing data sets.

With many simulators being available to chemical engineers, the mind-set of “there are enough data sets” relies on satisfactory answers being received, without having to consider further thermodynamic data. However, this mind-set has been shown by Dorn and Pfohl (2002) to be risky, as experiments have shown different solutions to the same problem by using different simulators. The mindsets of “there are not enough data sets” and “there are too many differing data sets” result in the need for further accurate data production [10].

The majority of experimental VLE data are produced for binary systems, even though most industrial situations contain multiple components. Accurate multicomponent data is rare even for common well-defined mixtures [9]. This is because of the high cost of equipment and labour, as well as being time-consuming. All these factors increase in significance for multicomponent mixtures [11].

Correlative models can be used to accurately model multicomponent systems for both close-to-ideal [9], [12], [13] and complex non-ideal mixtures [9], [11], [14]. However, because these models depend on the generation of VLE data, correlative modelling remains expensive and time-consuming. Predictive models are useful as they can be used without data. Phase equilibria can be predicted by using pure component data, and without the need for BIPs.

1.1.2. Association theory equations of state

It is desirable to have a model that can predict highly-complex mixtures, such as cross-associating mixtures, and a unified model that can accurately predict different types of phase equilibria and mixtures without the need for BIPs [15].

Association type EoSs are models that can be used for this purpose. The different theories include the chemical theory (PHCT [16]), the quasi-chemical theory (NHRB [17]), and the perturbation theory (SAFT [18], [19], CPA [20]), with the perturbation theory EoS being the most successful [9].

1.1.3. Perturbation theory equations of state.

The original perturbation theory model, Statistical associating fluid theory (SAFT), and the family of models that built on it are based on the perturbation theory derived by Wertheim [21]–

[24]. The original SAFT EoS is therefore described using residual Helmholtz energy (Equation 1.6). This is equated to the Helmholtz energy of the hard sphere, dispersive forces, the chain formation, and the association between segments [9].

$$a^{res} = \left(a^{hs} + a^{disp}\right)^{seg} + a^{chain} + a^{assoc} \qquad 1.6$$

Variations to the SAFT model differ in the attractive contribution to the residual Helmholtz energy, such as in SAFT-VR-Mie [25]. Further differences in the simplification of the chain and dispersion terms by substituting these terms for a Cubic EoS (SRK), lead to the cubic-plus association model (CPA). An additional Helmholtz energy polar term such as the Gross and Vrabec polar term (GV) [26] can also be added to all perturbation type models[9].

Work has been done on increasing the accuracy of these models for binary systems. There is still a need to assess if these perturbation theory models can accurately predict highly non-ideal multicomponent systems. A common hypothesis is held with the SAFT family of models, that the scaling up of binary model predictions to multicomponent predictions is accurate [27]–[30]. However, without the explicit systematic evaluation of the models' for multicomponent systems, this hypothesis cannot be verified. There is a possibility that the predictions may not be reliable, without certain adjustments being made to the model's parameters [31].

1.2. Problems Faced

Perturbation theory thermodynamic models, such as the CPA + GV, SAFT-VR Mie-GV and sPC-SAFT-GV, consider the self-association and in some cases the cross-association between compounds. These models have been used successfully in binary systems containing these types of components [32], [33], and there is an assumption that this can be scaled up to ternary and higher order mixtures without the need for correlative BIPs. However, there is a lack of experimental work to prove this assumption.

Some work has been done on both binary and ternary systems for polar associating compounds such as ketone-alcohol-water [34] and short chained ketone-ester-alcohol [35]. However, there is a lack of ternary equilibrium data for similar polar, associating, and cross-associating mixtures using mid-length ketones, mid-length esters, and mid length alcohols, that will allow for the systematic testing of the predictive nature of a thermodynamic model.

The chemicals used in this study were chosen for their polar, self-associating, and cross-associating nature (ketone-alcohol-alcohol and ketone-alcohol-ester). This is because such systems show a strong deviation from the ideal state, with the cross-association difficult for predictive thermodynamic models to accurately predict. The four systems tested in this work all contain 2-butanone and 1-propanol to isolate the effects of the third component in

each system. The third component was either one of three mid-length C4 esters (ethyl acetate, methyl propionate, propyl formate) or an alcohol (2-propanol).

Deviation in ideal behaviour is assured in each system with polar associating components 1-propanol, and polar cross-association component 2-butanone, the third component in each system is either polar cross-associating (C_4 esters) or polar associating (2-propanol) this will result in a non-ideal system. With the movement of the functional group (Figure 1.2 a, b, c) and a change in functional group (Figure 1.2 d) allows for a systematic test of the effect of the third component, as well as a systematic test of the possible flaws in a model.

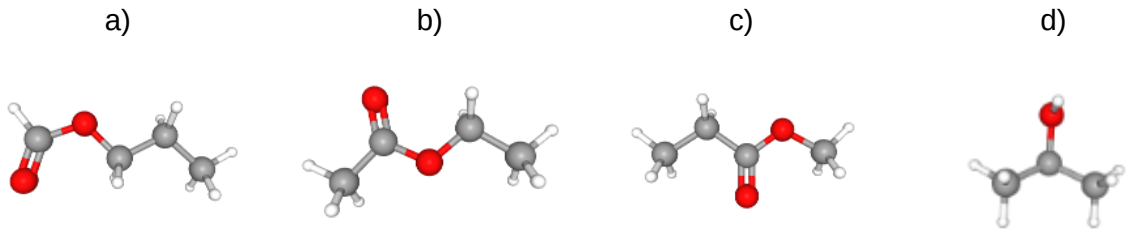

Figure 1.2: 3D formulae of the three C4 esters and 2-propanol, to show the moving of the functional group and the changing of the functional group. a) propyl formate, b) ethyl acetate, c) methyl propionate, d) 2-propanol

1.3. Aims and Objectives

The key aim of the study is to generate ternary isobaric vapour liquid equilibria for associating ketone-alcohol-alcohol and ketone-alcohol-ester mixtures. And then to evaluate whether sPC-SAFT-GV, SAFT-VR-Mie-GV and CPA-GV models can be used to accurately predict the phase behaviour of the polar associating and non-associating compounds for both binary and ternary data.

The objectives of the study are outlined below.

1.3.1. Objective 1: Generate binary VLE data

The initial experimental phase involves the collection of nine binary vapour-liquid equilibrium data sets for the components in the ternary systems. These consist of systems where the data are readily available, namely:

a) 1-propanol + 2-butanone;
b) 1-propanol + 2-propanol;
c) 1-propanol + ethyl acetate;
d) 1-propanol + methyl propionate;
e) 2-butanone + 2-propanol;
f) 2-butanone + ethyl acetate;

and those where no binary data exists, namely:

a) 1-propanol + propyl formate;
b) 2-butanone + methyl propionate;
c) 2-butanone + propyl formate.

And to assess the possible outcome of the ternary data.

1.3.2. Objective 2: Generate Ternary VLE

Due to the lack of ternary data with polar associating and non-associating compounds, four systems with no existing data were measured. Attention is paid to the effect of the placement of the functional group and the type of functional group in these systems and the subsequent effect it has on the resulting equilibria. These consist of systems containing C_4 esters, namely:

a) 1-propanol + 2-butanone + ethyl acetate;
b) 1-propanol + 2-butanone + methyl propionate;
c) 1-propanol + 2-butanone + propyl formate;

and systems containing an alcohol, namely,

a) 1-propanol + 2-butanone + 2-propanol.

1.3.3. Objective 3a: Model experimental binary data using sPC-SAFT-GV SAFT-VR-Mie-GV and CPA-GV

The three models, sPC-SAFT, SAFT-VR-Mie + GV, and CPA + GV are used to predict the VLE data of the nine binary systems. To test the effectiveness of the predictive nature of each model. Attention is paid as to which model predicts the binary systems in the most accurate way, and to assess which model should predict the ternary systems the most accurately.

1.3.4. Objective 3b: Model experimental ternary data using sPC-SAFT-GV SAFT-VR-Mie-GV and CPA-GV

The same three models that were used to predict the binary models are used to predict the ternary models. Attention is to be paid to how accurate the models predict the ternary data, in comparison to how accurately the binary data was modelled.

2. Literature Review

2.1. Low-pressure Vapour-liquid Equilibrium

The phase behaviour of mixtures is fundamental to in the manufacturing process [6], therefore, it is important to know when phase equilibrium occurs. Phase equilibrium occurs when the Gibbs energy of a compound within a system is at a minimum.

$$0 = (dG_i)_{T;P} \tag{2.1}$$

This, in turn leads, to the chemical equilibrium occurring when the chemical potential of each component (i) is equal through all possible phases (a, b, c) [4].

$$\mu_i^a = \mu_i^b = \cdots = \mu_i^c \tag{2.2}$$

However, this is a theoretical definition of chemical equilibrium, and there is a need to take these abstract terms and transform it into a more physically meaningful term. The terms that are more easily found during experiments are temperature, pressure and composition [6].

Temperature and pressure are basic intensive variables when working with phase behaviour. It is easy to determine what effect these variables are having on pure components; however, most studies are conducted on the phase behaviour of mixtures for two main reasons.

1. It provides a way of studying the forces involved between molecules without relying on pure component data. Using pure component data to study the forces relies on calculating the average of the forces between the same molecules (α-α), (β-β) and between the different molecules (α-β), (β-π). Other than for very simple substances, such as an ethanol/propanol mixture [36], these interactions are more complicated, and the degree to which the forces occur between molecules in mixtures is observed mainly in experimental work [37].
2. The addition of extra degrees of freedom derived from the Gibbs phase rule (Equation 2.3) leads to possible outcomes not found in pure components, such as the effect on equilibrium of varying composition [37].

The Gibbs phase rule can be described by the equation in 2.3 where F is the degrees of freedom, C is the number of components in the mixture, M is the number of reactions taking place, and Ph is the number of phases present [5].

$$F = C - M - Ph + 2 \tag{2.3}$$

Therefore, in a system with two phases, such as the binary and ternary systems being tested in this work, the number of degrees of freedom (intensive variables) needed (temperature,

pressure, liquid mole fraction, or vapour mole fraction) is governed by the number of components in the system.

2.2. Binary Vapour-liquid Equilibrium

Three ways are used to describe various states of matter, namely, solid, liquid and vapour. For most pure components, it is possible to find the melting, boiling and freezing points that correspond to the changing of the various states. These changes can be shown in a phase diagram. However, phase diagrams are not limited to only showing single component systems and in the case of binary VLE the equilibrium between the phases can be shown [38].

The equilibrium involving the solid state is outside the scope of this project and therefore only the equilibrium conditions between vapour and liquid are evaluated. There are three possible outcomes with the mixture of two liquids [38]:

a) There will be complete solubility and the liquids will mix;
b) There will be partial solubility and the liquids will partially mix; and
c) The liquids will be completely immiscible and there will be no mixing.

Because of these outcomes, there is the potential for a vapour-liquid, vapour-liquid-liquid, and, at elevated pressures, a liquid-liquid equilibrium. All the compounds within the scope of this project are completely soluble with each other and therefore only vapour-liquid equilibrium is evaluated.

Plotting the experimental data on phase diagrams can give a clear indication of the relationship between the two compounds. This can be shown in three different ways, namely a P-x-y, a T-xy, or simply an x-y and, as stated in Section 2.1, there are two degrees of freedom in a binary system. If one intensive variable is fixed, for example pressure in an isobaric case, any change in temperature will result in a change in composition [38].

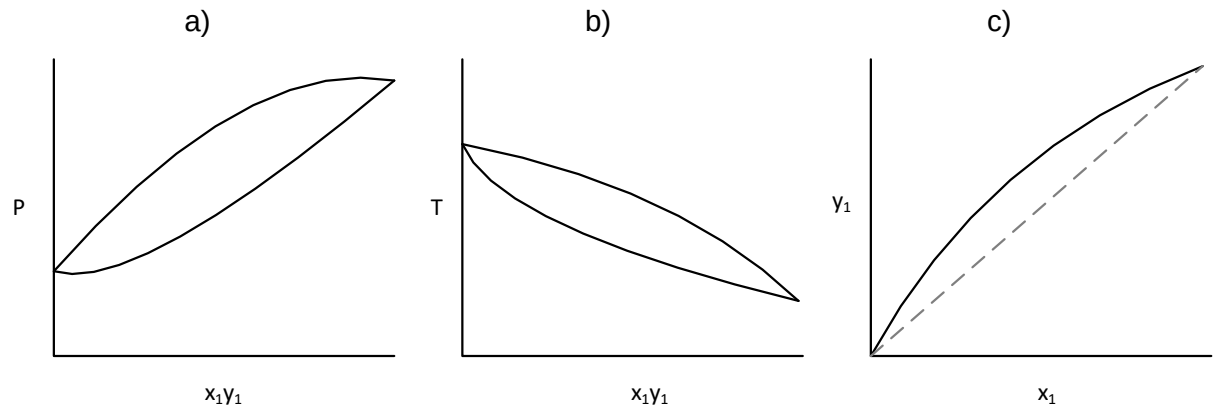

Figure 2.1: An example of a) a P-x-y diagram, b) a T-xy diagram, and c) a x-y diagrams for binary VLE

2.2.1. Binary azeotropes

An ideal mixture is bound by Raoult's law in which the vapour pressure of a component in a mixture is equal to the mole fraction pure vapour pressure of the same component (Equation 2.4) [39].

$$P_A = x_A P_A^0$$

$$P_B = x_B P_B^0 \qquad 2.4$$

$$P_{Tot} = P_A + P_B$$

Raoult's law leads to the composition diagram in Figure 2.2 a) and is consistent for ideal mixtures. Few real mixtures act in an ideal way and deviations from Raoult's law occur for the majority of mixtures. This deviation is either a positive deviation (Figure 2.2 b) or a negative deviation (Figure 2.2 b).

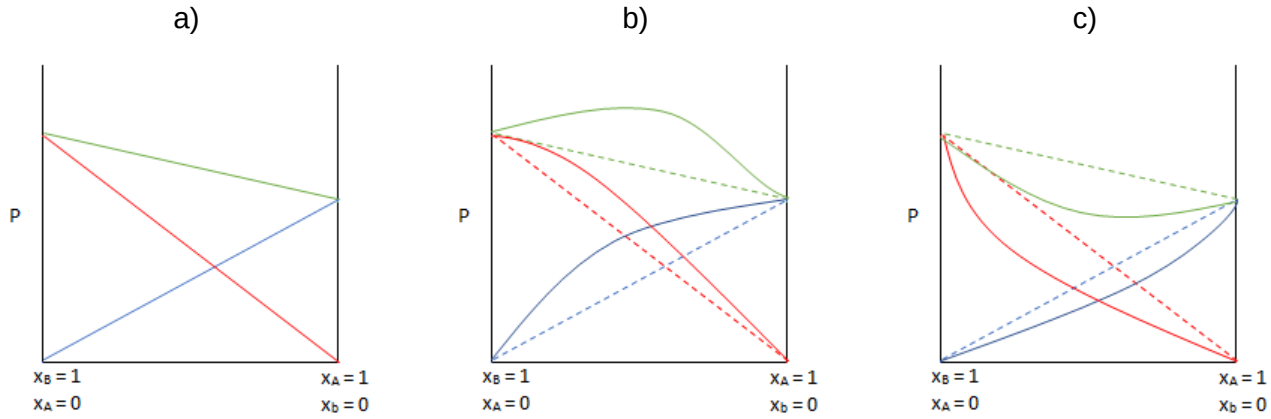

Figure 2.2: Binary mixture and Raoult's law. The blue line is the partial pressure of A, the red line is the partial pressure of B, and the green line is the total pressure of the mixture. a) An ideal mixture, b) a positive deviation from Raoult's law, c) a negative deviation from Raoult's law.

In some cases, the deviation from Raoult's law can be large enough to cause maxima or minima points on the phase diagram [4]. These points are described as azeotropes and occur when the composition of the liquid phase and of the vapour phase are equal. Boiling of the mixture results in no change. The presence of an azeotrope is of interest to chemical engineers as it complicates distillation, requiring the need for changes in condition or the addition of an extractant [40].

The forces between the molecules can either favour mixing (like molecules) or oppose it (unlike molecules). These types of forces are what give us the different types of azeotropes, as can be seen in Figure 2.3 [40]. If the unlike interactions between the molecules are stronger than the like interactions, a maximum in the T-xy curve is formed, and when the like interactions are stronger than the unlike interactions, a minimum occurs in the T-xy curve [4].

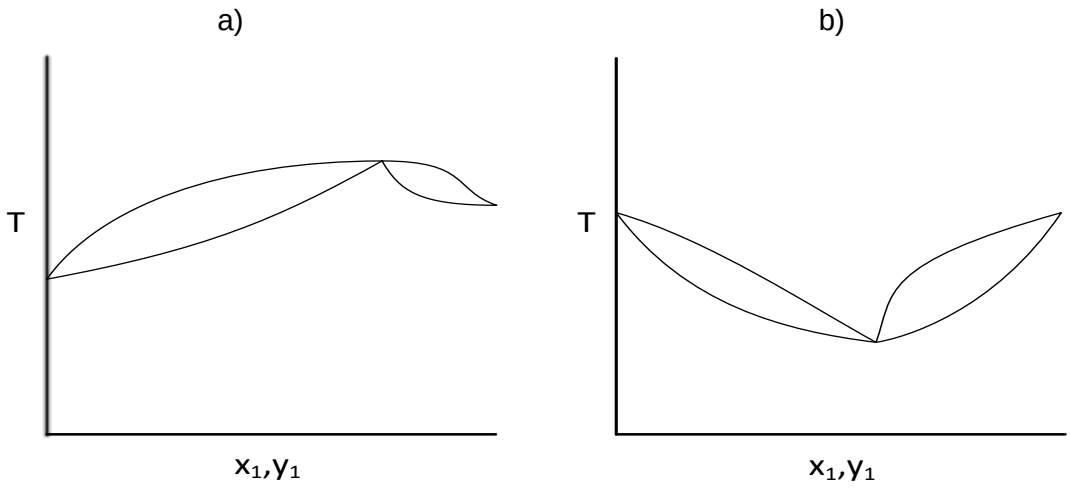

Figure 2.3: Examples of azeotropic systems. a) a maximum boiling T-xy diagram. b) a minimum boiling T-xy diagram

2.3. Ternary Vapour-liquid Equilibrium

As with the binary systems (Section 2.2), ternary systems that do not have completely soluble components are beyond the scope of this project. Therefore, only ternary VLE data are evaluated.

As stated in Section 2.2 a ternary system has three components in a mixture and will have three degrees of freedom. Therefore, if three intensive variables are set, any other intensive variables are defined [38].

To graphically represent ternary mixtures, a 3D plot is required. This is to show all three compositional variables as well as temperature. However, in an isobaric case, where the pressure is constant and the composition of the three components is known, the temperature will be defined. It is therefore possible to show ternary VLE data on a 2D triangular diagram.

Although a right-hand triangle representation is possible, these diagrams are usually used for high concentration of one of the components. This leaves the more convenient equilateral Gibbs triangle (Figure 2.4), in which X,Y, and Z represent the three components [41].

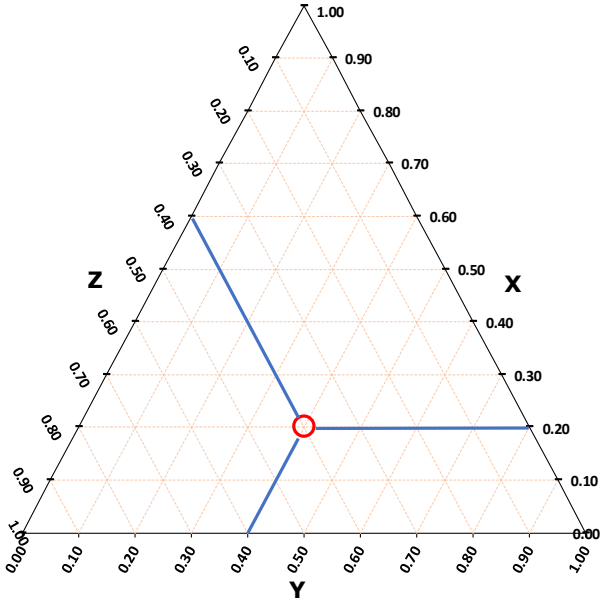

Figure 2.4: Example of a Gibbs triangle with an (X,Y,Z) composition of (0.20; 0,40; 0.40)

2.3.1. Tie lines

When two phases form in ternary VLE, the composition of each phase will lie on either side of a straight isothermal tie-line, with the original mixture lying on the line between the two points [42]. An example of the tie-line can be seen in Figure 2.5.

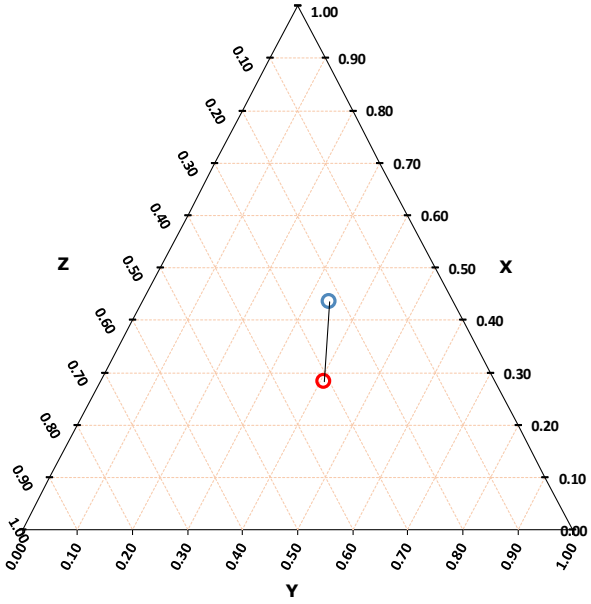

Figure 2.5: Example of isothermal tie-line (black line) with the equilibrium compositions of liquid (red circle) and vapour (blue circle) on either side of the tie line

These ternary tie-lines can be shown for all experimental compositions, with each tie-line representing a temperature. Alternatively, if one takes an isomorphous diagram, in which each binary VLE system lies on each axis and the temperature is increasing in the Z plane, this allows a surface to form, where the vapour surface is on top and the liquid below (Figure

2.6 a). If the isomorphous diagram is cut at a certain temperature, it gives a surface in which liquid-vapour exists (Figure 2.6 b). Tie-lines can be created at this specific temperature on the liquid-vapour surface. These diagrams are an effective means of displaying the experimental equilibrium measurements of ternary systems.

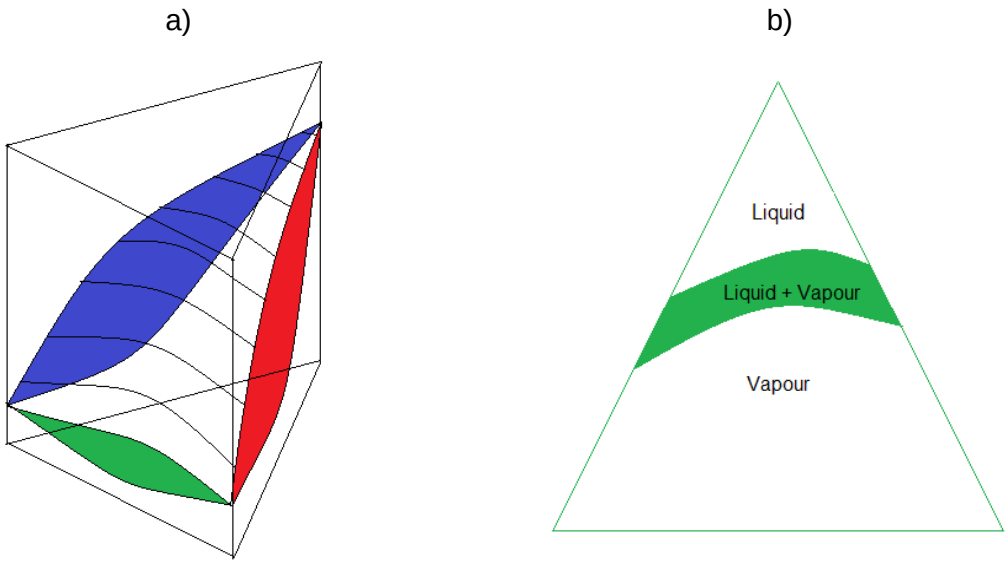

Figure 2.6: a) Example of an isomorphous diagram in which Temperature is in the Z plane and the equilateral triangle lies in the x-y plane. The three binary systems in (blue, red, and green), surface shown by black lines, b) Example of a liquid-vapour surface at a certain temperature

2.4. Experimental Equilibrium Measurements

There are five broad categories of VLE data gathering techniques. All these techniques have engrained errors in them and do not yet give completely thermodynamically consistent data. However, with constant improvements in technology, there are varying measures of accuracy for each method [39]. The five categories are:

a) Distillation method
b) Dew and bubble point method
c) High dilution method
d) Static method
e) Circulation method

The distillation method, although very simple, accounts for large errors because of the need to distil small volumes in order to not change the composition of the original mixture and to prevent condensation forming on cold walls. This leads to inaccurate measurements and is therefore seldom used [39]. The dew and bubble point method is more accurate, but it can only be used in binary VLE measurements [43] , and is therefore not suitable for this work. The high dilution method is also more accurate but it does not allow measurements to be taken

along the whole range of compositional values [44], this in turn does not allow for a systematic testing of multicomponent systems. This leaves the static and circulation stills.

2.4.1. Static still

The two most commonly used equilibrium stills are the static still and the circulation still. The static method is initially simple, in which a solution is placed within an evacuated cylinder. This cylinder in turn is placed within a thermostat. The cylinder is then rotated, and the liquid and vapour form an equilibrium. Although the initial process is simple the removal of the gas sample becomes complicated. At low pressures in order to get an accurate reading of equilibrium, there is a need to evacuate almost all the vapour from the still. This leads to large disturbances to the equilibrium and inaccurate results [45].

Methods have been improved open to get more accurate results at low pressures, such as method used by Scatchard et al. 1964 [46], in which extremely accurate results were found. This shows that Static still can be accurately used for low pressure systems, however static still run isothermal equilibrium [45]. With the majority of distillation being run at isobaric conditions, it is important to use a method that can be run at isobaric conditions such as a circulation still.

2.4.2. Circulation stills

When using a circulation still, the mixture is placed in a boiling chamber (A) and boiled. The mixture's boiled vapours go to receiver (B) where condensation occurs and the condensed liquid returns to A (Figure 2.7). This sequence continues until a steady state is reached, which occurs when the concentration of each component does not change over time. With the pressure constant, the equilibrium temperature and composition can be tested (Figure 2.7) [45].

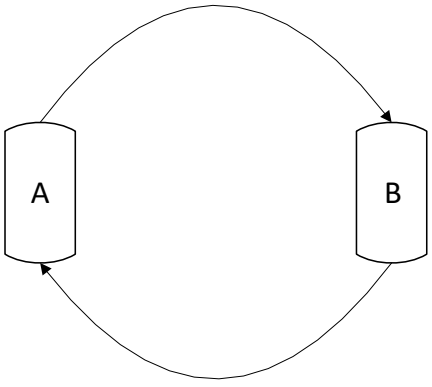

Figure 2.7: Schematic of circulating phase equilibrium stills (taken and re-drawn from Hala et al. 1967)

2.4.3. Othmer still

The first circulation still to successfully circulate vapour and create a phase equilibrium was the Othmer still (Figure 2.8) [47]. In this still, the vapour is recycled, and the liquid remains in the boiling chamber.

Heat is added to the boiling chamber (C) until boiling occurs and, consequently, the vapours fill the entire chamber, with the initial air within the flask being dispelled. The vapours flow through an enveloped vapour tube where it comes into contact with a thermometer (E) and then through a condenser (G), where the initial condensate fills a receiver, with the excess condensate returning to the distillation flask [45].

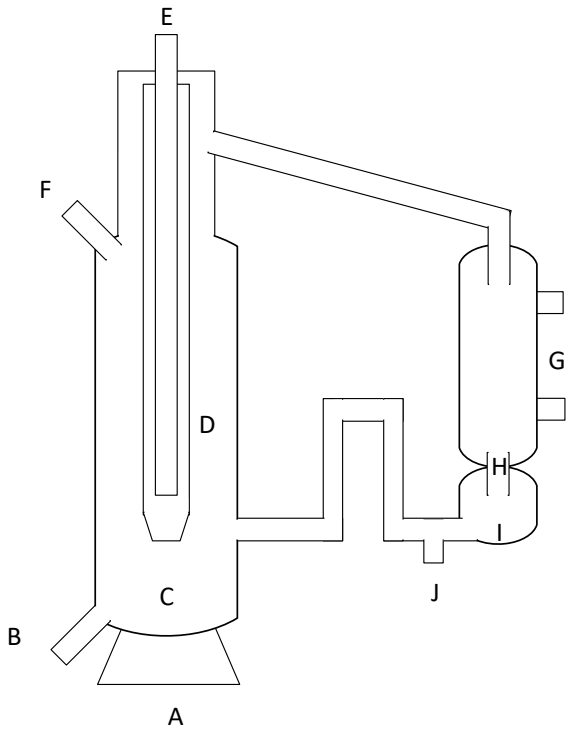

Figure 2.8: Othmer still (taken and re-drawn from Othmer and Coats, 1928) A) heater; B) liquid sample point; C) boiling chamber; D) vapour tube; E) thermometer; F) air venting valve; G) condenser; H) drop counter; I) condensate receiver; J) vapour sample point

Although the system is simple, the results contain some flaws.

a) Although the vapours around the vapour tube will help prevent condensation the cooling of the chamber will cause some condensation to form. This is especially problematic in high boiling systems.
b) The boiling and recirculation of the colder condensate does not ensure a well-mixed liquid and leads to concentration gradients.
c) When withdrawing the condensed vapour sample, contamination occurs with mixing from the returning condensate.

d) Only measuring the vapour temperature does not lead to an accurate reading of the equilibrium temperature.

Although improvements have been made to the Othmer-type still, the measurement of the boiling point remains imprecise. This can be rectified by circulating both the liquid and vapour phases, which allows for a more accurate measurement of the temperature [45].

2.4.4. Gillespie still

The Gillespie still, which uses a Cottrell tube, allows both the liquid and the vapour to circulate through the system [45]. The Cottrell tube allows for the thermometer to be placed above the boiling mixture (in the vapour phase), while the action of boiling the liquid, pumps the liquid containing vapour slugs through the tube and into contact with the thermometer. The Gillespie still allows for a more accurate temperature measurements [48].

A small volume approximately 100 ml of the mixture is placed in the boiling chamber (A). An internal heater (B) creates bubbles that ensure the mixing and carrying of liquid and vapour through a Cottrell tube (D). The equilibrium mixture encounters the thermometer (E) in the equilibrium chamber. The Gillespie still is designed to separate the liquid and the vapour phases further, before they return to the boiling chamber Figure 2.9 [49].

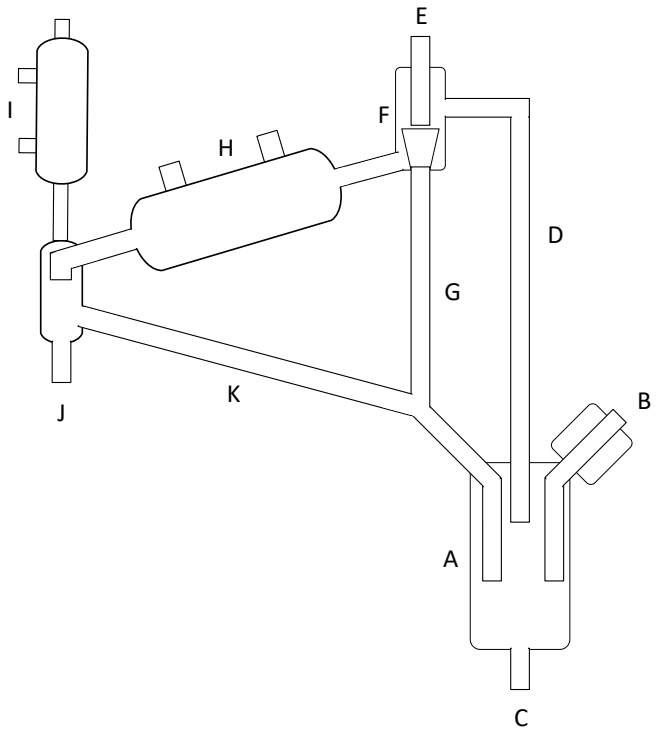

Figure 2.9: Gillespie still (taken and re-drawn from Gillespie, 1946 [49]) A) boiling chamber; B) internal heater; C) liquid sample point; D) Cottrell tube; E) thermometer; F) phase separation chamber; G) liquid return; H) primary condenser; I) secondary condenser; J) vapour sample point; K) vapour return

Although the Gillespie still has come up with a solution to make temperature measurement more accurate, it has a few flaws of its own [45], for example:

a) The intensity of the boiling has an impact on the phase equilibrium. If the boiling rate is too high, then imperfect separation will occur, and if it is too low then it will cause the vapour to rise without carrying the liquid;
b) There is still a possibility of partial condensation within the still;
c) The still requires approximately three hours to reach equilibrium [50][51]; and
d) The liquid samples are not an accurate representation of the equilibrium concentration as the sample is taken from the boiling flask.

The improvements made by various authors to the Gillespie still have addressed the majority of the flaws. In this work a Gillespie-type still designed in-house by Gowda, 2018 [52] is used to collect the VLE experimental data of complex associating, cross-associating and polar mixtures. It is important to understand the effect these complex compounds have on VLE data.

2.5. Associating Compounds and Mixtures

Association is the ability of like molecules (self-association) and unlike molecules (cross-association) to form chemical clusters, through strong intermolecular forces such as hydrogen bonds[4]. Association effects phase equilibrium and phase behaviour, due to the formation of these clusters [19].

According to Vinogradov and Linnell, 1971[53], compounds can be divided up into the following four types of substances [54]:

a) molecules that have an electron donor group (e.g. chloroform);
b) molecules that have an electron acceptor group (e.g. ketones and esters);
c) molecules that have both electron donor and acceptor groups (e.g. alcohols); and
d) molecules that have neither group (e.g. hydrocarbons)

However, in order to arrive at the definition of association, it is less important to look at the “type” of compound, but rather at the variability of a specific compounds ability to associate. This is because some compounds that do not show self-association will cross-associate with compounds that self-associate themselves. It is, therefore, better to define a compound by its “degree” of association [54].

Table 2.1: Properties important to association of ethers, esters, ketones, and alcohols [55], [56]

	T_B (K)	M (g/mol)	ΔH_{vap} (kJ/mol)	ΔS_{vap} (J/molK)	dipole moment (D)
diethyl ether	307.6	74.1	26.5	86.2	1.3
ethyl methanoate	327.5	74.1	29.9	91.5	1.8
ethyl acetate	352.6	88.1	32.2	91.3	1.7
methyl propionate	350.2	88.1	31.9	91.1	1.9
propyl formate	354.7	88.1	33.6	94.7	1.9
acetone	329.2	58.1	29.1	88.4	2.9
2-butanone	352.7	72.1	31.3	88.7	3.3
1-propanol	370.9	60.1	41.4	111.6	1.7
2-propanol	355.4	60.1	39.9	112.3	1.7
1-butanol	390.9	74.1	43.3	110.8	1.8

Table 2.1 is used to reinforce what was said above, namely, that associations are not definite, but rather, they occur on a varying spectrum, from weak to strong associations [54]. The indicators in Table 2.1 can be used to assume the strength of association within the molecule.

The first indicator used for association of a compound is the boiling point (T_B). This can be attributed to the association forces within the molecule that attract other molecules and cause stronger intermolecular forces and higher boiling points. This needs to be looked at with reference to the molecular weight. Therefore, by looking at components of similar molecular weight, it can be seen that the boiling point increases from ethers, to esters, to ketones, to alcohols [54].

Another indicator is the enthalpy of vaporisation (ΔH_{vap}) in which the degree of association increases with the increasing of ΔH_{vap}. This trend can be seen in Table 2.1 where an increase can be seen from diethyl ether to butanol [54].

Another strong indicator of association is “Troutons constant” or the entropy of vaporisation (ΔS_{vap}). In Table 2.1 the alcohols have the highest value and therefore have strongest association attributes. It is interesting to note that the rest of the compounds have comparable entropies of vaporisation. It is also important to note that the ketones are more polar than the

other components, with a dipole moment of around 3D, compared to between 1-2D for the other components [54].

From this, it can be determined that ketones, esters, ethers, and alcohols all have varying degrees of association [54]. Alcohols that have the highest degree of association will self-associate, while ketones and esters, which have slightly lower degrees of association, will not self-associate but will cross-associate with the alcohols[57].

Systems containing these sorts of compounds (alcohols, esters, ketones) will show a deviation from the ideal state, due to this varying degree of association.

2.5.1. Choice of experimental data

As stated, above, systems with alcohols, esters and ketones will show a deviation from the ideal state. Gathering data for systems containing these compounds will be advantageous when testing the validity of certain thermodynamic models, due to the non-ideal behaviour, especially when considering multicomponent systems [9].

Medium length esters (C_4; propyl formate; ethyl acetate; methyl propionate), medium length alcohols (C_3; 1-propanol; 2-propanol), and a medium length ketone (C_4; 2-butanone) are the compounds tested in this work.

In order to systematically isolate the effect that different compounds have on a mixture, 1-propanol and 2-butanone will be consistent in all ternary systems. This allows for the effect of the moving of the functional group between the three C_4 esters and the changing of the functional group to an alcohol to be tested.

The ternary systems, in which no literature data exist, are as follows:

a) 1-propanol/2-butanone/propyl formate;
b) 1-propanol/2-butanone/ethyl acetate;
c) 1-propanol/2-butanone/methyl propionate; and
d) 1-propanol/2-butanone/2-propanol.

As four ternary systems will be tested, there will be nine different binary systems each, either with 1-propanol or 2-butanone. The binary systems tested in this project with available data can be seen in Table 2.2:

Table 2.2: Literature vapour-liquid equilibrium data for 1-propanol + X and 2-butanone + X systems. a) Azeotropic data

1-Propanol + X	**T(K) range**	**P(bar) range**	**Reference**
2-butanone	278.15-323.15		Garriga et al. (1996) [58]
		1.013	Martinez et al. (2008) [59]
2-propanol	298.15		Yamamoto and Shibata (1999) [60]
		1.013	Gultekin (1989) [61]
		1.013	Ballard and winkle (1952) [62]
		1	Gabaldon et al. (1996) [63]
Ethyl acetate		1.013	Murtie and Winkle (1958) [64]
Methyl propionate	303.15		Fernandez et al. (1985) [65]
		1.013	Susial and Ortega (1989) [66]
2-Butanone + X			
2-propanol	278.15-323.15		Garriga et al. (1996) [58]
		1.013	Martinez et al. (2008) [59]
		0.013	Olaya et al. (2002) [67]
Ethyl acetate		1.013	Nagata (1963) [68]
		1.013[a]	Yan et al. (2001) [69]
Propyl formate		1.6	Falcon et al. (1996) [70]

Although data is available for some of the binary systems, majority of the systems have one or fewer data sets at the pressure range tested. It is therefore important to find the binary VLE for all nine systems, as well as for the four ternary systems, through experimental testing. Once these data sets are collected, it is important to test if they are thermodynamically accurate, using a thermodynamic consistency test.

2.6. Consistency Testing of VLE Data

Consistency testing is an important step in the validation of measured data. With consistency testing helping to prove that the data is in fact at equilibrium and therefore, with further

validation, accurate. The consistency of the VLE data is conducted using experimental uncertainty, experimental data, and the Gibbs-Duhem equation.

2.6.1. Gibbs-Duhem equation

The Gibbs-Duhem equation which is represented in terms of entropy (S), temperature (T), volume (V), pressure (P), mole fraction (x_i) and chemical potential (μ), can be seen in the equation below.

$$0 = S\mathrm{d}T - V\mathrm{d}P + \sum x_i \mathrm{d}\mu_i \qquad 2.5$$

In the case that both temperature and pressure are constant, it can be seen that the equation will simplify down to just the chemical potential term (Equation 2.6).

$$0 = \sum x_i \mathrm{d}\mu_i \qquad 2.6$$

This simplification allows for the knowledge that at constant temperature and pressure the chemical potential of the system will not change on its own. This is also true for other partial molar properties [71]. In the special case of a binary system in which X_i (a thermodynamic partial molar property) is expressed by Equation 2.7 [71].

$$x_1 dX_{1,m} + x_2 dX_{2,m} = 0 \qquad 2.7$$

This in turn can lead to the use of activity coefficients. If the activity coefficient of one of the substances in the mixture is known γ_1, then the activity coefficient of second substance can also be found γ_2. This can be seen in Equation 2.8. [71].

$$ln\left(\frac{\gamma_1}{\gamma_1^*}\right) = -\int_{\gamma_1^*}^{\gamma_1} \left(\frac{x_2}{x_1}\right) d\ln(\gamma_2) \qquad 2.8$$

If there are two different procedures to calculate the two different activity coefficients, then the data set that is derived from these experiments can be tested to see if it is, in fact, consistent. It is also important to note that the deviation from Raoult's Law of both components should result in both having either a higher or lower vapour pressure compared to that of an ideal mixture [72].

2.6.2. Point-to-point method

Using the Gibbs-Duhem equation, the point-to-point method can be used to ensure that a data set will be consistent. Equation 2.9 is a simplification of Equation 2.7 [72].

$$x_1\left(\frac{d\ln(\gamma_1)}{dx_1}\right) + x_2\left(\frac{d\ln(\gamma_2)}{dx_1}\right) = 0 \qquad 2.9$$

Using equation 2.9 and plotting it compared to varying compositions, the corresponding activity coefficients can be found. The slope of the corresponding curve generates the

left-hand side of the equation. If the slope is equal to zero, then the data can be considered consistent. This is done for each point. Although this method is mathematically correct, it is not used often, due to the complexity of getting the correct tangent between the points. It is not useful as a mathematical check but it is useful as a visual check and therefore it can be useful as a quick guide [72].

2.6.3. Area test

An area test using the Gibbs-Duhem equation can be used to test the consistency of the experimental VLE data. Integrating the Gibbs-Duhem equation from a value of $x_1 = 0$ to $x_1 = 1$ gives areas for the two curves. This can be seen in Equation 2.10. where $Ar_1 and\ Ar_2$ are the areas of the curves one and two [72].

$$\int_0^1 ln(\gamma_1)\,\mathrm{dx}_1 + \int_1^0 ln(\gamma_2)\,\mathrm{dx}_2 = \mathrm{Ar}_1 + \mathrm{Ar}_2 = 0 \qquad 2.10$$

The areas of the two curves need to be equal to satisfy the equation (Equation 2.10). However, because of introduced error (experimental, human, equipment, or error occurring through extrapolating or fitting curves of best fit), it can be assumed that the criteria for consistency of data is met if Equation 2.11 is met [72].

$$\frac{\big||\mathrm{Ar}_1| - |\mathrm{Ar}_2|\big|}{|\mathrm{Ar}_1| + |\mathrm{Ar}_2|} \leq 0.02 \qquad 2.11$$

Both the point-to-point and the area methods are limited because the Gibbs-Duhem approach is only affective when the temperature and the pressure in the system have been kept constant. Keeping both temperature and pressure constant is impossible when doing VLE experiments. Thus these exact methods cannot be used to check for consistency; however, they are very important with the understanding tests for consistency [72].

2.6.3.1. The McDermott-Ellis test

Tests, such as the Li and Lu consistency test [73], propose a test where the only constraint is that the points are not widely separated and therefore the integration of these points is small, while integrating the entire data set. However, these types of tests do not detect systematic errors. This leaves the potential that the data tested may deviate from consistency [74]. Tests developed by McDermott and Ellis 1965 overcame this discrepancy.

The McDermott-Ellis test can be seen as a ‘local’ test that uses the area integral and the trapezoidal rule (Equation 2.12), over a small range of values, instead of the entire data set; for example between adjacent points [75].

$$\int_{x_{1,a}}^{x_{1,b}} \ln\left(\frac{\gamma_1}{\gamma_2}\right) dx_1 = \int_{T_a}^{T_b} \frac{\Delta H}{RT^2} dT - \int_{P_a}^{P_b} \frac{\Delta V}{RT} dP + \frac{G^E}{RT} \quad 2.12$$

Which in turn simplifies to equation 2.13 [74].

$$\sum_{i=1}^{N} (x_{i,a} + x_{i,b})(ln\gamma_{i,b} - ln\gamma_{i,c}) = 0 \quad 2.13$$

For a perfectly thermodynamic consistent system equation 2.13 would be equal to zero. However, this does not occur due to the experimental error and uncertainty. There needs to be a maximum allowable deviation from this case. This maximum deviation derived by Wisniak and Tamir 1977 [76] can be seen in Equation 2.14.

$$D_{\max} = \sum_{i=1}^{N} (x_{i,a} + x_{i,b}) \left(\frac{1}{x_{i,a}} + \frac{1}{x_{i,b}} + \frac{1}{y_{i,a}} + \frac{1}{y_{i,b}}\right) \Delta x + 2 \sum_{i=1}^{N} \left(\left|ln\gamma_{i,b} - ln\gamma_{i,c}\right|\right) \Delta x + \sum_{i=1}^{N} (x_{i,a} + x_{i,b}) \frac{\Delta P}{P} + (x_{i,a} + x_{i,b}) B_i \left(\frac{1}{|T_a + C_i|^2} + \frac{1}{|T_b + C_i|^2}\right) \Delta T \quad 2.14$$

Where Δx, ΔP, and ΔT are the experimental uncertainties, B_i and C_i are Antoine's constants, and temperature is measured in degrees Celsius. Each data point is considered consistent if the D_{max} value is greater than the left-hand side of Equation 2.14.

2.6.3.2. The Wisniak L-W test

The L-W test was derived by Wisniak 1993 [77] and can use both the point-to-point method and the area test. It is a method that describes the bubble point of a mixture and can be used to test both binary and multicomponent systems.

$$G^E = RT \sum_{i=1}^{n} x_i \ln\gamma_i \quad 2.15$$

Equation 2.15, where G^E is the excess Gibbs free energy, that can be used together with the boiling point (Equation 2.16) [72] and the assumption that the vapour phase of the mixture acts like an ideal gas. This assumption can be made due to the low pressure at which these tests take place. As a result, the non-ideal state, can be assumed to only appear in the liquid phase [76]. Equation 2.17 shows that the activity coefficient can be described by the liquid and vapour partial pressures. Therefore, the L-W test will only work at low pressures.

$$\left(\frac{d\ln\left(P_i^0\right)}{dT}\right) = \left(\frac{\Delta h^{vap}}{RT^2}\right) \quad 2.16$$

$$\gamma_i = \left(\frac{y_i P}{x_i P_i^0}\right) \quad 2.17$$

With the assumption of low pressure and the boiling point of a component, the equation can be simplified to Equation 2.18 [72]. A further rearrangement expresses the equation by two terms L_i and W_i. This can be seen in Equation 2.19.

$$G^E = RT\omega + \sum x_i \Delta S_i^0 \left(T_i^0\right) - T\Delta S^0 \quad 2.18$$

$$L_i = \left(\sum x_i \left(\frac{\Delta S_i^0}{\Delta S^0}\right)\left(T_i^0\right) - T\right) = \left(\left(\frac{G^E}{\Delta S^0}\right) - \left(\frac{RT}{\Delta S^0}\right)\omega\right) = W_i \quad 2.19$$

Equation 2.20 can be used as a form of point-to-point method for multicomponent systems, to test if each separate point is consistent.

$$0.92 < \frac{L_i}{W_i} < 1.08 \quad 2.20$$

However, when looking at the consistency of binary and multicomponent systems, it is important to use the area test to ensure that the system is consistent, as a whole. Therefore, the area of L_i and the area of W_i needs to be found. Consistency can be evaluated using Equation 2.21 and Equation 2.22 with maximum D values of below 5 [72].

$$L = \int_0^1 L_i dx_1 = \int_0^1 W_i dx_1 = W \quad 2.21$$

$$D = 100\frac{|L - W|}{L + W} \quad 2.22$$

Since the L-W test can be used for both binary and multicomponent components while considering the area and point-to-point test, it can be considered a useful and accurate measure of thermodynamic consistency. The only downfall is that there is a need to find data that is not generated in the testing of the system. One is required to source this data from previously conducted studies in the literature. There are errors associated with this data and these errors are more serious for multicomponent systems [72].

With thermodynamically consistent experimental data of polar, self-associating, and cross-associating binary and ternary VLE, there is a need to predict these models using a thermodynamic model. The two main types of thermodynamic models are the equations of state, and the activity coefficient models.

2.7. Equations of state and activity coefficient models

Equation 2.23 is derived using the phi-phi method in so doing ensuring an EoS model will be used to describe both liquid and vapour phases [9]. Where the basis of EoS models are derived using the Van der Waal cubic EoS [78].

$$f_i^L(T,P,x) = x_i\Phi_i^L(T,P,x)P = f_i^V(T,P,y) = y_i\Phi_i^V(T,P,y)P \qquad 2.23$$

Many modifications have been successfully made to the Van der Waal EoS while still using the one fluid mixing rule, with notable examples such as Redlich-Kwong (RK) [79], Soave-Redlich-Kwong (SRK) [80], and Peng-Robinson (PR) [81] models. However, these EoS's are only used to model simple systems with small deviations from the ideal state, such as hydrocarbon and inorganic mixtures [9].

The use of the gamma-phi method (Equation 2.24) [5] allows for the use of an activity coefficient model which is used only for mixtures containing either liquids or solids.

$$f_i^L(T,P,x) = x_i\Phi_i^{L,sat}(T,P)\gamma_i(T,P,x)P_i^{sat}(T) = f_i^V(T,P,y) = y_i\Phi_i^V(T,P,y)P \qquad 2.24$$

Activity coefficient models allow for the modelling of more complex VLE systems by quantifying the deviation of the activity coefficients from Raoult's law [9]. Many iterations of these activity models exist such as Wilson [82] , NRTL [83], and UNIQUAC [84] models.

There are some limitations to these activity coefficient models such the confusion surrounding the selection of the correct model for the correct system type [15]. Another limitation is the correlative nature of the activity coefficient models.

These models have a proven ability to model highly complex systems. They require the use of existing data, in the form of BIPs, to model a system. If there is no data available, experimental work is needed. This experimental work is time-consuming and expensive. The need for predictive models that are accurate is becoming ever more important, as many companies in the chemical industry are reducing the time and resources that are spent on applied thermodynamics [10].

There are models, such as UNIFAC, a predictive model that was developed by improving the Wilson and UNIQUAQ model. These models use pure component data to form a predictive type model [85]. The UNIFAC model has been extensively used and modelling is reasonably accurate for complex mixtures. However, the model struggles with highly complex multicomponent mixtures with associating compounds [9].

2.8. Prediction of Phase Equilibrium of Associating Interactions

The prediction of phase equilibrium for substances and mixtures that associate is important to industry but is still problematic. These associating interactions are significant in the overall intermolecular interactions and need to be implicitly considered when looking at predictive phase equilibrium models [86].

Associating mixtures form long-lived dimers, or even higher multimers. This leads to very strong intermolecular interactions. Although these forces are not as strong as true chemical bonds, they do fall in between the chemical bonds and Van der Waal forces and need to be treated differently when modelled. One way of accurately predicting these associating mixtures is the use of association theory models [87].

2.9. Perturbation Theory Equations of State

Although other association type models exist, the most common type is the perturbation theory EoS, such as SAFT and CPA. These models are thermodynamic EoS that help to describe systems containing molecules and mixtures of associating spheres. These types of molecules and mixtures do not behave in an ideal fashion because they contain molecules that have either hydrogen bonds or donor/acceptor pairs, such as an alcohol, a ketone, or an ester [18].

The SAFT and CPA models have a basis in the perturbation theory. The perturbation theory can be used to describe the bulk fluid behaviour as well as the site-to-site interaction and was largely developed in work done by Wertheim, 1984a, 1984b, 1986a, 1986b [21]–[24]. Wertheim used perturbation theory to expand Helmholtz energy into a sum of integrals, in which many of these integrals must be equal to zero. This resulted in a simplified expression of Helmholtz energy which allowed the SAFT and CPA model to be developed [19].

2.9.1. The SAFT model

The first SAFT model was developed in a series of papers by Chapman, 1989,1990 [18], [19]. A reference fluid is required to model an equation of state. This fluid exhibits real behaviours that the model will try to represent. SAFT uses a reference fluid that has both chain length (or molecular shape), and molecular association. This is used instead of the hard sphere reference fluid that is used in many other equations of state [19]. This allows for a more predictive EoS for systems involving associating molecules.

Figure 2.10 shows the formation of a molecule in the SAFT reference fluid. The reference fluid is formed (a) and is first assumed to be full of hard spheres. The dispersive forces are added to the spheres, indicated by the dotted circle surrounding the spheres (b). The spheres form a chain (c) and interaction sites, which are represented by the grey circles (d), are added to the chains which allow the chains to be able to associate.

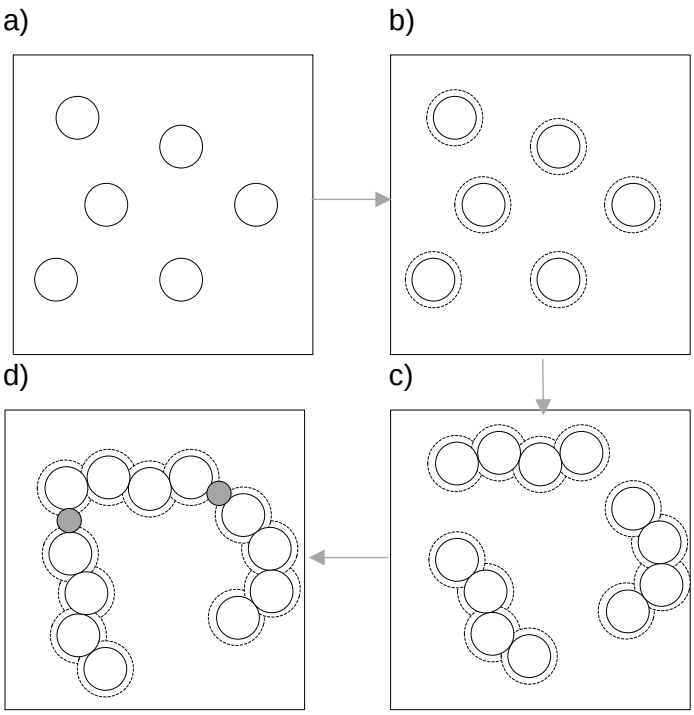

Figure 2.10: Formation of a molecule in the SAFT reference fluid: a) the initial hard chain fluid; b) dispersive forces added; c) chains form; d) association sites are added (taken and re-drawn from Kontogeorgis and Folas, 2010 [9])

Each of the steps in Figure 2.10 contribute to the Helmholtz energy of the system as seen in Equation 2.25.

$$\frac{\mathrm{A}}{\mathrm{NRT}}^{\mathrm{res}} = \mathrm{a}^{\mathrm{res}} = \mathrm{a}^{\mathrm{seg}} + \mathrm{a}^{\mathrm{chain}} + \mathrm{a}^{\mathrm{assoc}} \qquad 2.25$$

Equation 2.25 considers the residual Helmholtz energy (a^{res}) as a sum of three Helmholtz energy terms, as well as being the deviation from an ideal gas $a^{res} = a - a^{ideal}$. The first term (a^{seg}) considers the segment-segment interactions. The second term (a^{chain}) considers the covalent bonds that form in a chain-like fashion amongst the segments. The third term (a^{assoc}) considers the associating interactions between the molecules [18].

The segment and association term remain fairly constant, however, differences in the reference fluid and the dispersion term have led to many different iterations of the SAFT model. The first major modification to the dispersion term was by Huang and Radosz, 1990 [88] with SAFT-HR, where a square-well potential function was used, instead of an LJ potential function (Figure 2.11) [19], [88]. Further developments to the dispersion term resulted in further iterations to the SAFT models such as PC-SAFT[89] which was simplified to sPC-SAFT [90] (Section 2.9.3.) and, SAFT-VR [91], [92] in which further improvements lead to SAFT-VR-Mie [25],[91] (Section 2.9.4.),

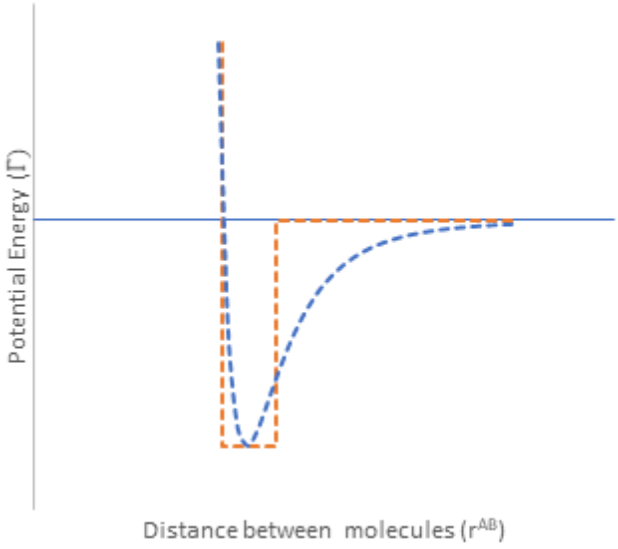

Figure 2.11: Strength of association model using square-well method (orange dashed line) and Lennard-Jones method (blue dashed line) for a random mixture. Taken and re-drawn from [19]

Other extensions and modifications have been made to the SAFT models in which changes were not made to the dispersion term. Examples of this is the CPA EoS (Section 2.9.2) or the addition of polar terms to the Helmholtz energy (Section 2.9.5).

2.9.2. CPA EoS

The CPA EoS is a simplification of the SAFT model which is a combination of the cubic equation SRK [80] and the association term, similar to that in the SAFT model [94]. This model was developed for the oil and gas industry to model polar and hydrogen bonding component interactions when there is no need for the use of the full SAFT model [94].

When the CPA models a component that does not associate or hydrogen bond, the CPA is reduced to the SRK model. However, the parameters used are regressed from the pure components vapour pressure and density [35]. This strikes a balance between the accuracy of the model and its simplicity [9].

As the CPA uses a cubic equation of state, the reference fluid is represented by hard spheres, and uses the defined intermolecular potential function [35]. The association term adds association sites to the hard sphere (Figure 2.12). Since the molecule is represented by a hard sphere, there is no chain term and the chain length has no influence on the model [35].

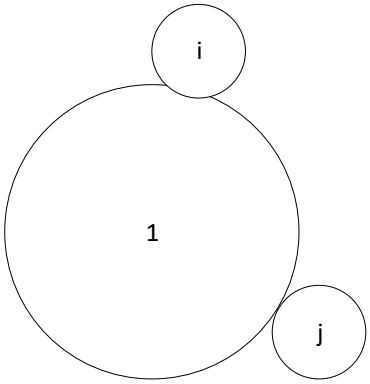

Figure 2.12: Example of the CPA reference fluid, a hard sphere (1) with two association sites, i and j. (taken and re-drawn from de Villiers, (2011))

The CPA and other SAFT variants association term uses two different mixing rules, namely the CR1 [94] and the ECR [28] mixing rules. The CR1 rule is able to model non-self-associating and cross-associating compounds and is therefore used in this project [9].

The CPA model is a very commonly-used model in the oil and gas industry, where the majority of mixtures are alcohol-hydrocarbon or water-hydrocarbons mixtures [95]–[97]. Work has also been done on systems involving cross-associating systems such as ketones and esters [98].

Although good results have been seen, there are still limitations to the model [35]:

a) The CPA model cannot account for the cross-association of compounds that do not self-associate;
b) It does not account for polar interactions such as those evident in ketones and esters; and
c) Multicomponent mixtures often require large BIPs for an accurate representation of the mixture.

2.9.3. sPC-SAFT EoS

A more complicated model compared to CPA, the PC-SAFT model shares the same terms as the original SAFT model, except for the dispersion term. This dispersion term accounts for the dispersion between the chains, rather than the dispersion between the hard spheres [9].

This results in the reference fluid and the formation of the molecules following a different path (Figure 2.13) compared to the path previously described in Figure 2.10. In the PC SAFT, the reference fluid: a) the fluid is assumed to full of hard spheres; b) chains form; c) dispersive forces are added to the chains, shown by the dotted circles; d) the association sites are added to the chain (Figure 2.13).

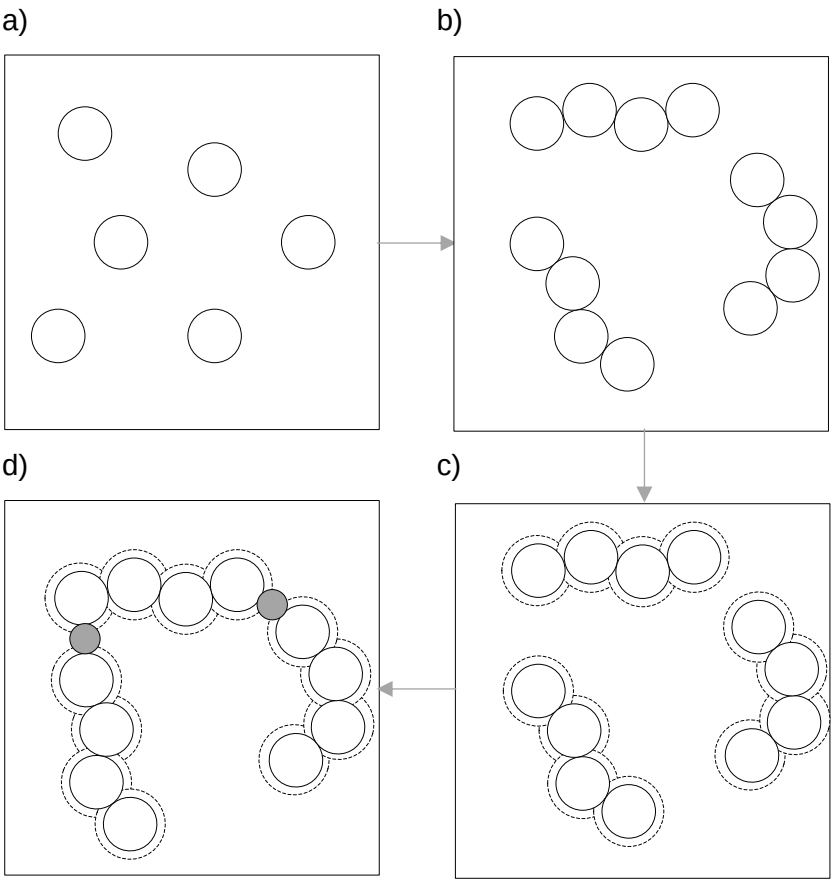

Figure 2.13: Formation of a molecule in the PC SAFT reference fluid: a) the initial hard chain fluid; b) chains form; c) dispersive forces added; d) association sites are added (taken and re-drawn from Kontogeorgis and Folas, 2010[1])

A modified square-well potential is used, as proposed by Chen and Kreglewski 1977 [99], to explain the soft repulsion experienced by real fluids [100] (Figure 2.14).

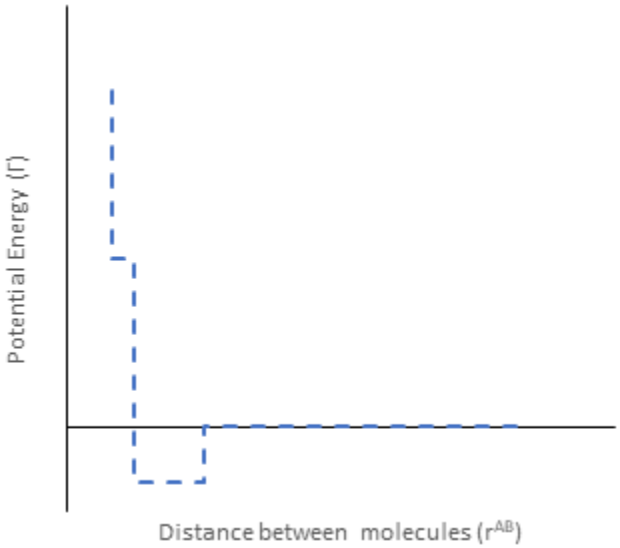

Figure 2.14: Modified square-well potential used in PC-SAFT (Re-drawn and adapted from Cripwell, 2017 [100])

A simplification of the PC SAFT model leads to simplified PC SAFT (sPC-SAFT), this simplification of the model cuts down the simulation time by 30% [90] without showing less accurate results, leading to a model that is more likely to be used.

The first simplification to the sPC-SAFT equation assumes that the mixture has segments with similar-sized segment diameters. The second simplification is a simplification to the radial distribution function [90].

The sPC-SAFT model requires five pure component parameters for associating components: segment diameter (σ); segment energy (ε); the number of hard spheres (m); the association energy (ε^{AB}); association volume (K^{AB}) and three pure component parameters for non-associating components: σ; ε; m [9].

The sPC-SAFT model showed greater accuracy than the original SAFT model. This proves that valid improvements were made [101] and has been applied to a wide range of phase equilibria. This is especially true in systems involving a polar hydrogen-bonding component and a non-polar non-hydrogen-bonding component [102]–[104], while some work is being done on polar associating components [35], [105].

Although promising results have been seen with the use of the sPC-SAFT model, there are still limitations [35]:

a) Polar compounds, such as ketones and esters, have poor descriptions when using the sPC-SAFT model;
b) When looking at compounds that cross-associate but do not associate themselves difficulties in the accuracy of the model is noticed; and
c) Mixtures containing strong polar compounds, such as alcohols, require large BIPs to accurately represent the data.

There is a need for improvements to the model, such as giving it an extra polar term, to ensure more accurate predictions.

2.9.4. SAFT-VR-Mie EoS

The SAFT-VR EoS equation is identical to the original SAFT equation, however, a different dispersion term is used. The original SAFT dispersion term had a potential function (LJ potential function) that is expressed in terms of segment diameter (σ) and segment energy (ε) [9].

The SAFT-VR model is based on the square-well potential function, an extra parameter, the square-well width (λ), is needed to describe the reference fluid. Hence, there is a need for an extra-pure component parameter. The square-well width varies the attraction forces of the

segment, hence SAFT- 'Variable Range'. It is standard to want to describe a pure component with as few pure component parameters as possible. However, the addition of the square-well width helps to predict many of the more complex systems deviations from the ideal state [9].

Improvements to the SAFT-VR model by Lafitte et al. 2006 ,2007 [25], [93], move away from using the square-well potential function and uses the soft-core Mie potential function. This improves the repulsive interactions described by the reference fluid (SAFT-VR-Mie) [25], [93].

In the SAFT-VR-Mie equation, up to six pure component parameters are required to describe the component. The following six associating components are required: segment diameter (σ), segment energy (ε), the number of hard spheres (m), the association volume (ε^{AB}), and the range of association (r_{AB}^{c}). Only four non-association components are required, namely σ, m, ε and λ.

The SAFT-VR-Mie model is more accurate in modelling than the original SAFT. However as with the two previous models, the model has some limitations.

a) As with the previous two models SAFT-VR-Mie has poor predictions for polar models
b) Cross-association of molecules that do not self-associate but do cross-associate, is hard to accurately model

2.9.5. Addition of a polar term

VLE is affected by the interactions of polar systems. The previously described models do not take the effect of polarity explicitly into account, and therefore, a term can be added to Helmholtz energy to describe the polar interactions (Equation 2.26).

$$\frac{\mathrm{A}^{\mathrm{res}}}{\mathrm{NRT}} = \mathrm{a}^{\mathrm{res}} = \mathrm{a}^{\mathrm{seg}} + \mathrm{a}^{\mathrm{chain}} + \mathrm{a}^{\mathrm{assoc}} + \mathrm{a}^{polar} \qquad 2.26$$

Two of these polar interactions are described in work conducted by Jog and Chapman, (1999) [106] and Jog et al. (2001) [107], (JC polar) and work done by Gross and Vrabec, (2006) [26], (GV).

2.9.5.1. GV term

The GV term is a third-order perturbation theory polar term, written in terms of Pade approximations. The testing of simulated data, using the GV term, resulted in a good description of polar mixtures [26]. This term explicitly accounts for the polar interactions of compounds used in this work.

The GV term introduces the number of polar segments term (n_p), this pure component parameter can be added to each model used in this study. Although other polar terms exist

such as the JC polar term. The testing of the polar term with polar/polar mixtures shows that the GV term has more accurate predictions than the JC polar term [108]. Therefore, the GV term is used in this study.

3. Methodology

With the focus of the work shifting from the premise to the means by which the work was done, this chapter lays out the materials, apparatus, methods, and uncertainty of measurement.

3.1. Materials

All chemicals for this project were purchased from Sigma Aldrich. The chemicals used in the phase equilibrium experiments are shown in Table 3.1, together with the mass percentage purity.

Table 3.1: List of chemicals used in ternary and binary experiments with purities

Component	Assay (mass%)	CAS Number
Methyl ethyl ketone	99.7%	79-93-3
1-propanol	99.8%	71-23-8
2-propanol	99.8%	67-63-0
Ethyl acetate	99.7%	141-78-6
Methyl Propionate	99.7%	554-12-11
Propyl formate	97.0%	110-74-7

All the chemicals were analysed using gas chromatography-mass spectrometry (GC-MS) to ensure that no significant impurity peaks were present. The outcome of this analysis showed that all the component purities were equal to, or greater than, the manufactures stated purity, with all the chemicals being at least 99.7% pure. This included five propyl formate tests on 100 ml bottles, which were all greater than 99.7% pure (99.71%, 99.79%, 99.81%, 99.81%, and 99.83% respectively). This is significantly greater than the manufacturer's stated 97%. Therefore, the components were considered suitable for use in phase equilibrium testing. Technical grade argon (Afrox) was used to control overpressure within the still.

3.2. Apparatus

A glass Gillespie VLE still, built in-house by Gowda, 2018 [52], was used to measure phase equilibrium data (Figure 3.1)..

3.2.1. Unit description

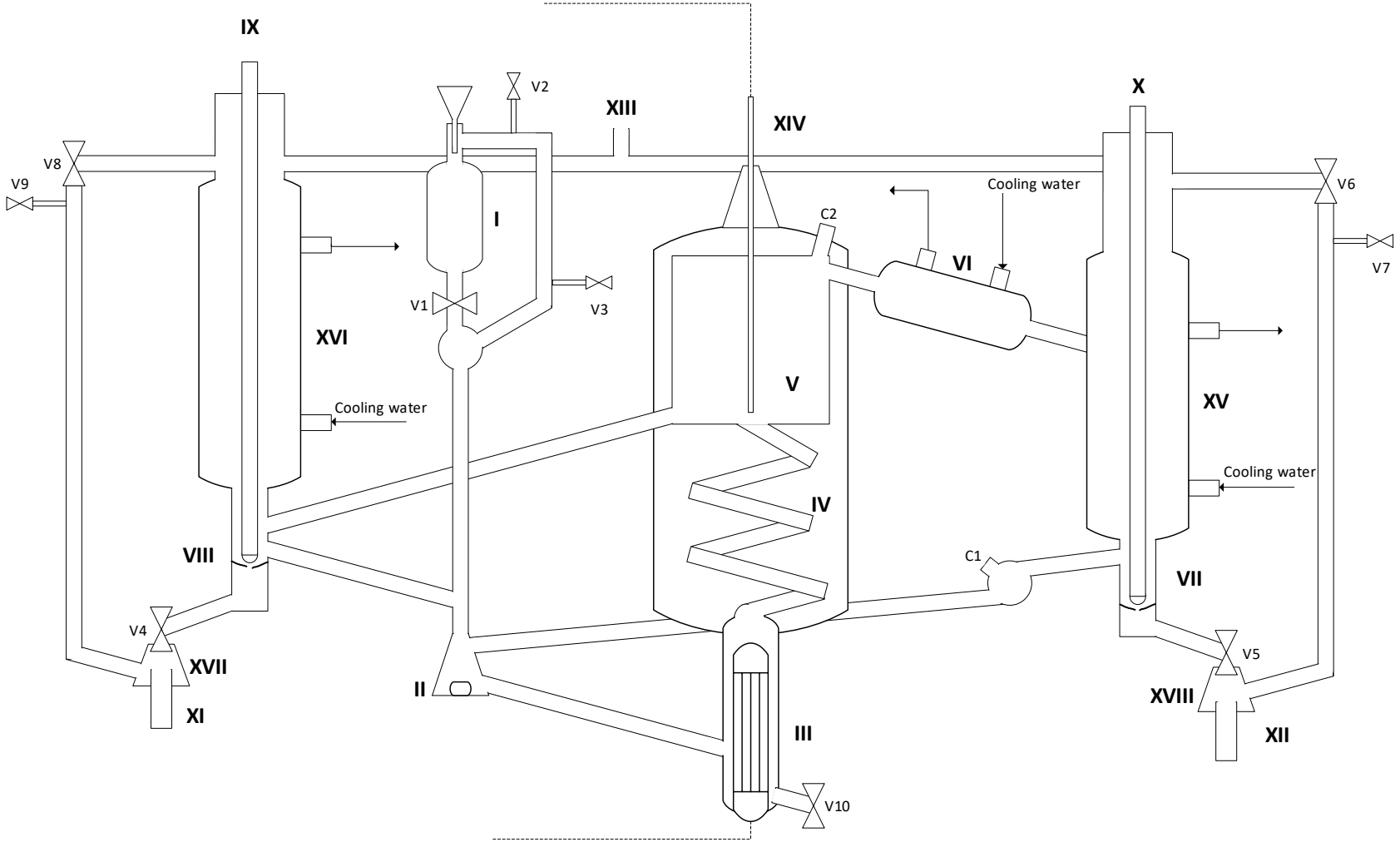

Figure 3.1: Set-up of the glass Gillespie still used for phase equilibrium experimentation (re-drawn and adapted with permission from Gowda (2018))

Table 3.2: Annotations of the Gillespie type still

Notation	Description
I	Feed chamber
II	Mixing chamber and magnetic stirrer
III	Heating chamber and cartridge heater
IV	Cottrell tube
V	Gillespie chamber
VI	1st Vapour condenser (Liebig style)
VII	Vapour sample well
VIII	Liquid sample well
IX	Liquid glass rod with magnetic ends
X	Vapour glass rod with magnetic ends
XI	Liquid sample tube
XII	Vapour sample tube
XIII	Over- and under-pressure control entry point
XIV	PT100 temperature probe
XV	2nd Vapour condenser (Dimroth style)
XVI	Liquid condenser (Allihn style)
XVII	Liquid collection point
XVIII	Vapour collection point

Continuous circulation is achieved by supplying heat, via the Cartridge heater (Figure 3.1 (III)), to the system. This Results in an evaporated vapour with entrained liquid, this evaporated mixture enters the Cottrell tube (IV), which in turn comes into contact with the equilibrium thermometer (XIV). The resulting mixture separates into the liquid and vapour fractions within the Gillespie chamber (V) and passes through condensers (VI and XV) before returning to the mixing chamber (II). Within the mixing chamber a magnetic stirrer ensures that the initial concentration is well-mixed. Continuous circulation is then reached, due to this continuous circulation, equilibrium is achieved at a fast rate. It takes approximately 60 - 90 minutes to reach this point. A more detailed step by step procedure can be seen in Appendix C, with reasoning behind the method seen in Section 3.3

3.3. Experimental Procedure

3.3.1. Still preparation

One needs to ensure that there are no residual liquids before using the still. Therefore, it is important to wash the still, using a solvent (methanol) that is completely soluble with the compounds used in this study, and then to dry the still thoroughly, using compressed air (described in further detail in Section 3.3.6).

The Gillespie still can be used at either over or under pressure, using a vacuum pump for under pressure and argon gas for over pressure. The three-way valve needs to be opened towards the desired run type and all valves (V1-V9) need to be closed including the caps (C1 and C2). Depending on which way the three-way valve is opened, either the vacuum pump is turned on or the argon canister is opened. However, the pressure control valve must be left closed. A submersible pump can now be turned on to ensure cooling water is running through the condensers (VI, XVI, XV). Approximately 110 ml of feed mixture, enough to completely submerge the cartridge heater, can be added to feed chamber (I). Opening valve V1 allows the mixture into the mixing chamber (II) and the boiling chamber (III). Cap C1 and valve V1 can be closed.

The magnetic stirrer can be switched on and power can be switched on for the cartridge heater. The heating power is controlled through the use of a potentiometer and an adjustable dial. This dial must be left closed with no voltage passing through to the cartridge heater.

3.3.2. Experimental run

Once the still is prepared an experimental run can proceed. Because the ambient pressure in Stellenbosch is below standard atmospheric pressure, all experimental runs are to be run at 1.013 bar and the three-way valve is to be opened to over pressure. In the very uncommon event of the ambient pressure being above atmospheric pressure, the three-way valve is to be opened to under pressure. With the argon canister already opened, the control valve can be opened until the pressure reading on the Yokogawa EJX510A pressure transmitter reads 1,013 bar with fluctuations of less than 0.001 bar.

The dial-controlled heater can now be adjusted to ensure the setting for the system is correct. The heater’s power setting is important because if the power is too high it will cause large pressure fluctuations. Although the pressure fluctuations are over-exaggerated (Figure 3.2), the pressure fluctuations will result in a change in composition. The sampled composition will lie on a different phase envelope. This results in a composition that is not in equilibrium with the temperature and constant pressure recorded.

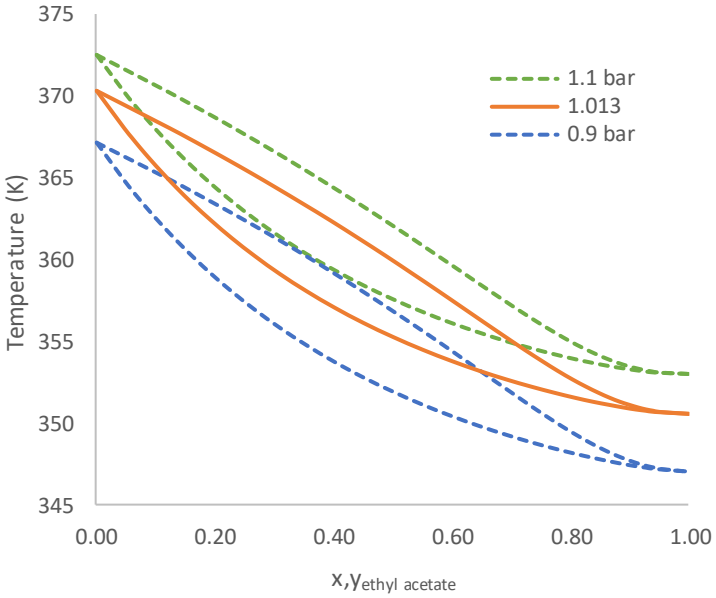

Figure 3.2: Example of pressure fluctuations caused by too high heater power settings, for the 1-propanol/ethyl acetate system

With the initial concentration of the feed mixture in the still remaining constant, the heater's power affects the mass balance ratio of liquid to vapour. Figure 3.3 illustrates that if the heater's power is insufficient the mixture will lie at A and no vapour will be formed. Increasing the heater's power will result in boiling when bubble point (B) is reached. However very little vapour return will be noticed. Using the correct heater power will result in a central concentration with equal liquid and vapour flow rate (C), with equilibrium vapour and liquid compositions of F. A further increase in the heater's power will result in dew point (D), and any further increase will result in no-liquid return (E).

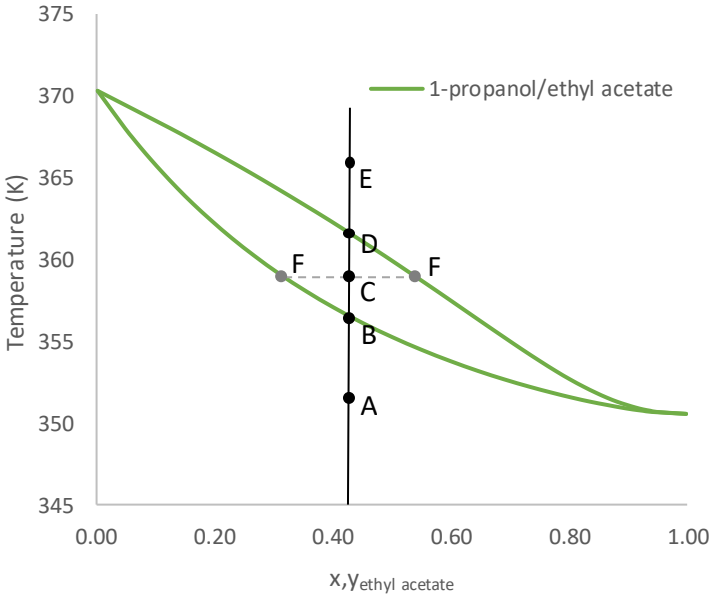

Figure 3.3: Example of the effects of increasing heater power on vapour liquid composition from completely under-heating the mixture(A) to over-heating the mixture (E)

Boiling will occur after approximately 10 minutes of operating at an appropriate heat setting. As stated above, an equal return from both liquid and vapour is required, with liquid and vapour drops one second apart, for accurate sampling, unequal return may result in imperfect separation with more of the volatile components favouring the vapour phase. The potentiometer can be further adjusted to meet these criteria.

The concave shape of the two sample wells (VII, VIII) collects the initial return of liquid and vapour, with later returns flowing over the top of the collected liquid. With equilibrium not yet reached constant flushing is required. As the still gradually heats up (Figure 3.4 G to H) slight changes occur in the equilibrium concentration (K to L). If flushing does not occur, then the concentration within the two sample wells will not change (K). However, this flushing, causes slight changes to the mass balance of the system and there is a shift in concentration (H to I). A further increase in heat results in a move from I to J and an equilibrium concentration of M. Flushing is done every 20 minutes and just before taking a sample.

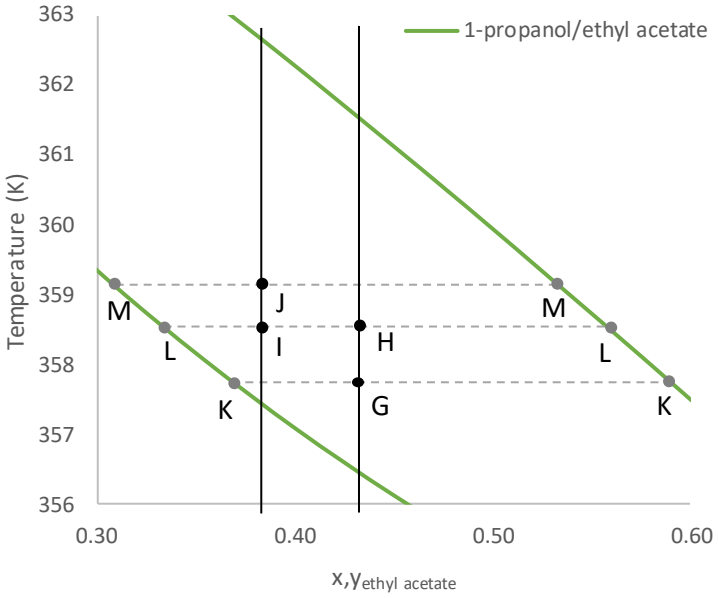

Figure 3.4: Example of the changing concentration with flushing and time: of the 1-propanol/ethyl acetate system. Where: G) the original mixtures concentration and temperature, H) temperature of initial concentration after heating, I) change in concentration after flushing, J) Increase in temperature over time, K) initial concentrations of liquid and vapour, L) concentrations of liquid and vapour after sampling and increase in temperature, M) final concentration of the liquid and vapour after heating

Flushing the still entails the placement of a magnet above the magnetic end of the two glass rods (IX, X) allowing all the liquid in the concave area to flow into the liquid and vapour sample area. Valves V4 and V5 are opened and the liquid flows to the sample tubes (XI, XII) and is discarded.

3.3.3. Sampling

After the last flush when the temperature is constant (fluctuations of less than ±0.03K) samples can be taken and the temperature recorded. The samples are taken in separate sample tubes to those used during flushing. These tubes are washed with wash methanol and dried with compressed air before use. The sampling process follows a similar procedure to that of flushing (3.3.2).

When the system is at equilibrium, the magnet is placed on the end of the two glass rods for a shorter period than previously. This allows for approximately 0.1 ml to flow into the sample area and into the sample tubes. This sample is deposited into 2 ml sample vials (Borosilicate glass vials with PTFE lined caps). The equilibrium temperature was monitored during this sampling procedure to ensure no changes in temperature occurred.

3.3.4. Design of binary experiments

When testing the binary systems (Figure 3.5), the starting point is the pure component with the higher boiling point (‘component 1’). Once the start point is determined, 110 ml of this

component is added to the still. Approximately 10 ml of pure ‘component 2’ is added. This moves the concentrations of both liquid and vapour towards the concentration of pure ‘component 2’. 10 ml of pure ‘component 2’ is continuously added until the mixture in the still is at approximately 50% concentration (grey points of Figure 3.5). Then the still is drained and washed, a detailed explanation of draining and washing procedure is given in Section 3.3.6. The process is then repeated in reverse, by adding 110 ml of pure ‘component 2’ to the still, and adding 10 ml of pure ‘component 1’, until the concentration of the mixture is approximately 50% (blue points of Figure 3.5).

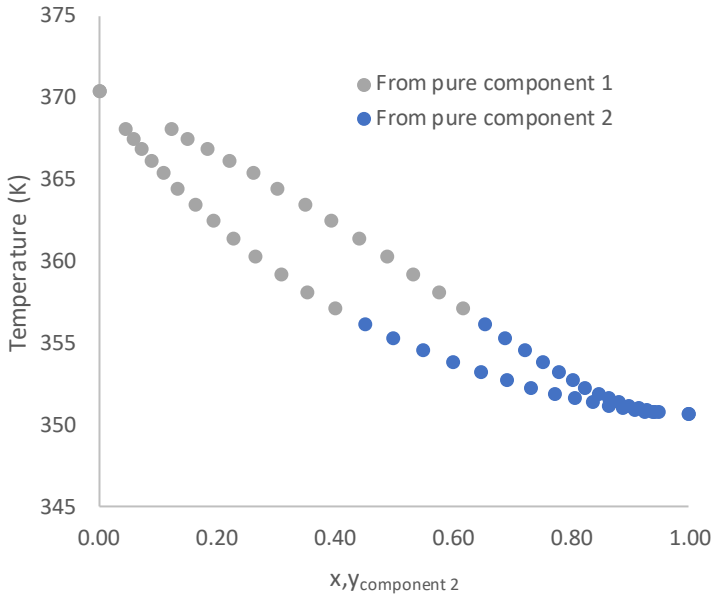

Figure 3.5: Design of binary experiments, starting from pure component 1 and moving down the phase envelope. Then starting at pure component 2 and moving up the phase envelope

3.3.5. Design of ternary experiments

In a similar way to binary systems, a ternary plot starts with a pure component (comp2) with trace amounts of the other two components (comp1 and comp3). This starting point is indicated by the red circle in Figure 3.6. The addition of component 1 to the mixture causes a shift in the mixture’s feed concentration to the point shown by the blue circle. The addition of component 3 causes a further shift in the mixture to the point represented by the orange dot in Figure 3.6. The sequential adding of components 1 and 3 is continued until the mixture’s feed concentration reaches the central point (green dot).

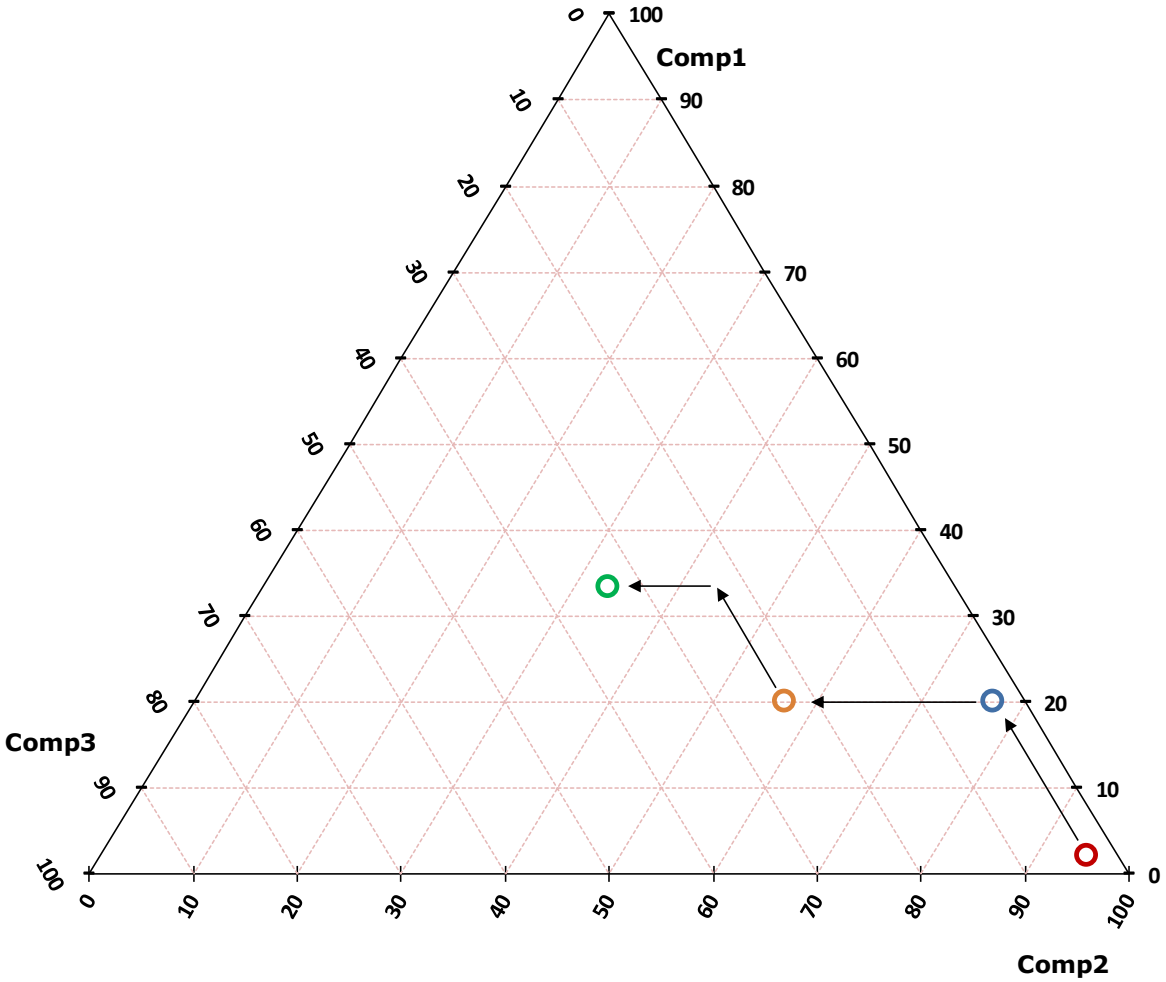

Figure 3.6: Sequential adding of components to ternary plot, each dot representing the concentration of the feed mixture

Once this centre point is reached (close to a mixture of 33,3% of each component), the contents of the still is drained (procedure shown in Section 3.3.6) but not washed. The still has residual liquid from all three components. In order to populate a different region with a high concentration of the other components, the process needs to be repeated with different components as the starting point. Thus, adding a new pure component is the next starting point with the same process being followed. Once all the pure components have been used, the spaces where no data is shown can be populated by using various starting points (Figure 3.7), for example, starting near pure component 2 and adding only pure component 1, thereby moving upwards on the component 1 axis and not towards the centre of the Gibbs triangle.

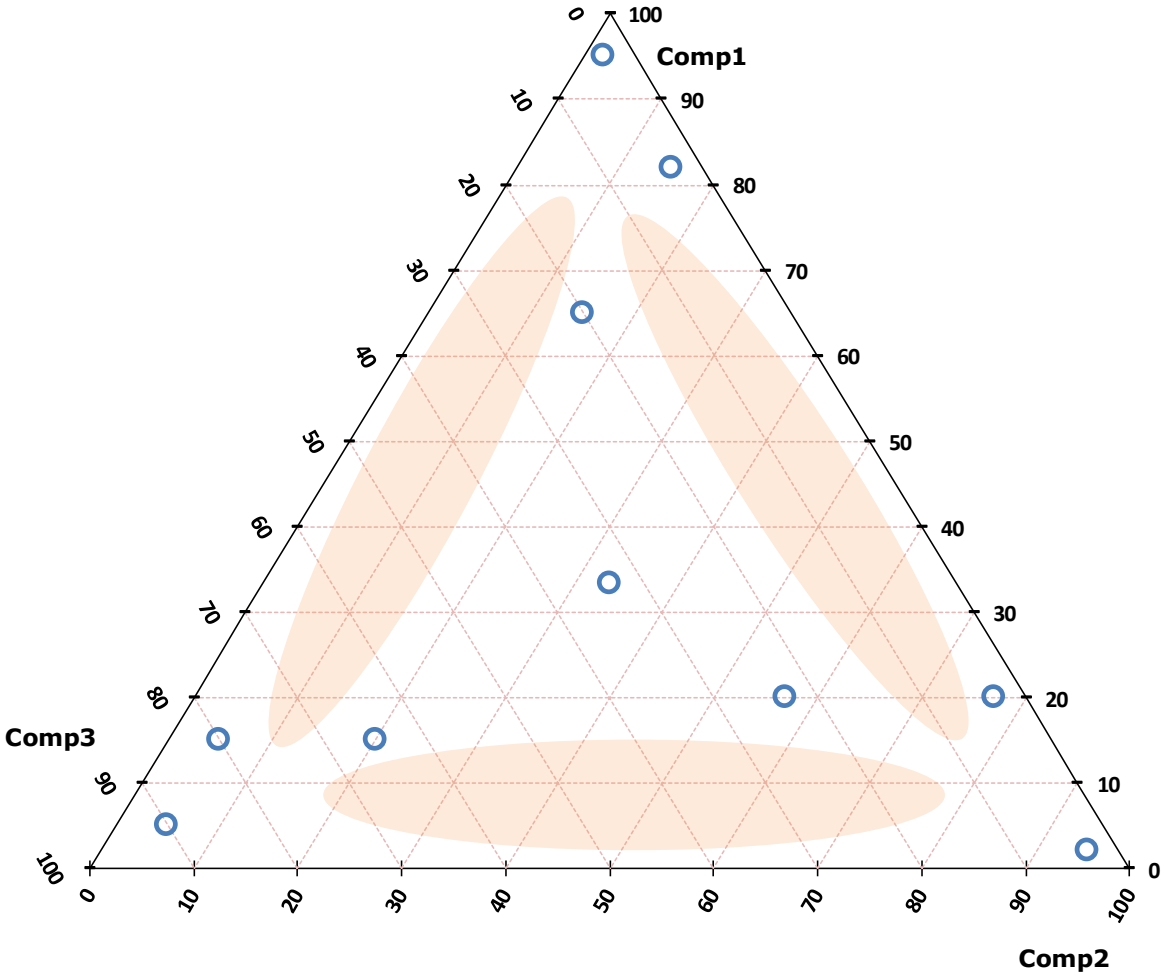

Figure 3.7: Spaces in which data needs to be filled

3.3.6. Draining and washing

Once the binary or the ternary plot is populated, the still needs to be drained and washed to prepare for the testing of a new system. This is to ensure that no residual liquids can contaminate the next system.

Before draining and washing the still, the immersion heater needs to be turned off and the mixture inside the still allowed to cool down. After about 45 minutes, the mixture should be at ambient temperature and safe to remove from the system. Opening valve V10 allows the mixture that was in both the heating and mixing chamber to flow into a beaker. Once all the mixture has been removed (except for small volumes within the heating chamber below the outlet to valve V10) wash acetone can be added.

Approximately 110 ml is added to the feed chamber and, subsequently, to the mixing and heating chamber. This wash acetone acts as a solvent removing any of the non-volatile components that are still present within the still. At ambient pressure the immersion heater is turned on with the potentiometer turned to an appropriate power. The wash acetone will be

allowed to circulate within system for approximately 45 minutes (while still lifting the glass rods at 15-minute intervals to ensure the vapour and liquid collection points are also washed), before being allowed to cool and drain through valve V10.

The still is left to dry overnight with all the values (V1-V10) and caps (C1 and C2) opened, and with the immersion heater unscrewed and removed.

3.3.7. Analysis of samples

Once an experimental sample has been taken for either a binary or ternary system, there is a need to analyse the sample. This is done by diluting the sample with a solvent (methanol), and testing the outcome compared to the outcome from a known mass of an internal standard (2-pentanol).

1. A Capped sample vial and a GC-sample vial are loaded with ≈ 1.5 ml of solvent.
2. 30 µL of the internal standard is added to the capped sample vial and weighed.
3. 80 µL of the liquid or vapour sample is added to the capped sample vial and weighed.
4. 80 µL of the mixture in the capped sample vial is added to the GC-sample vial (Figure 3.8).

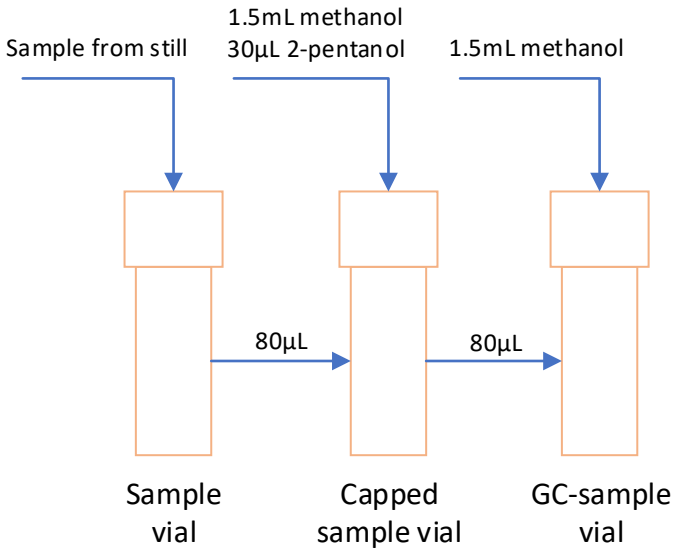

Figure 3.8: Dilution and preparation of GC vial for analysis

The diluted samples are run through an Agilent 7820A GC with an auto sampler and a flame ionisation detector (FID). A run-time of 10 minutes in a non-polar column with dimensions 60m x 0.18mm x 0.1µm, operating at 280°C, is sufficient to get separate area peaks for all components involved.

The mass of each component in the sample mixture can be determined using the weighed mass of the internal standard and the area of the peaks. This is because the ratio of the area

of the internal standard and the components peak are proportional to the internal standard and components mass.

$$\frac{Area_{IS}}{Area_{component}} = K\frac{Mass_{IS}}{Mass_{component}} \quad 3.1$$

In Equation 3.1, the response factor (K) is determined for each component prior to an experimental run. In order to generate a straight-line fit representing the response factor for each component, five known masses of both the internal standard and the component are run through the GC three separate times (Appendix D).

3.3.8. Equipment uncertainty

The uncertainties of the experimental data are obtained using the expanded uncertainty method, in accordance with the standards set by the guide to uncertainty in measurement, "*Evaluation of measurement data-Guide to the expression of uncertainty in measurement (GUM).57"* [109]. In this study an uncertainty coverage factor of 2 is used which gives a 95% confidence level.

$$u_c(y) = \sqrt{\sum_{i=1}^{N}\left(\frac{\delta f}{\delta x_i}\right)^2 u^2(x_i) + 2\sum_{i=1}^{N-1}\sum_{J=i+1}^{N}\left(\frac{\delta f}{\delta x_i}\right)\left(\frac{\delta f}{\delta x_j}\right)u(x_i x_j)} \quad 3.2$$

Using Equation 3.2 the uncertainties of the input variables can be expressed in terms of the output variables. In which y denotes the output variable, x_{ii} the input variable, f is the relationship between both the input and the output variable, u is the standard uncertainty of the input or output and $u(x_i x_j)$ is the covariance between input variables.

3.3.9. Uncertainty in temperature

The following factors are considered when testing for the uncertainty in temperature:

a) A temperature indication uncertainty of 0.08 K which is a combination of precision resolution and hysteresis;
b) Uncertainty due to calibration of 0.31 K; and
c) Fluctuations in temperature prior to reading of a maximum of 0.03 K.

In the factors stated above there is a covariance between the uncertainty of temperature indication and the uncertainty due to calibration as both these factors depend of the indicated temperature. The standard uncertainty of experimental uncertainty is therefore $u_c(T)$=0.31 K and with a coverage factor of two $u_c(T)$=±0.62 K.

3.3.10. Uncertainty in pressure

As with the uncertainty in temperature the following factors are considered when testing the uncertainty in pressure:

a) A pressure indicator uncertainty of 0.0108 bar which includes repeatability, stability, and the thermal effect;
b) Uncertainty of calibration of 0.0103 bar; and
c) Pressure fluctuations of 0.01 bar noticed prior to sampling.

Due to the use of the pressure indicator there is covariance between the calibration uncertainty and the indicator uncertainty. Therefore, the standard uncertainty in pressure is $u_c(P)=0.023$ bar. With a coverage factor of two the uncertainty in pressure is $u_c(P)=0.046$ bar.

3.3.11. Uncertainty in composition

Additional sources of uncertainty are inherent in the analysis of the samples, from the weighing of the samples (±0.01 mg) to the reproducibility of the GC. Although calibration curves allow the GC to reproduce accurate results, wear-and-tear on the GC can cause slight shifts in the calibration curves leading to errors in the compositional data.

The exacted masses, which are made up of each component in a completed ternary system, were tested to determine the inherent error in the GC. Three samples containing five different variants of masses were prepared. With the exact masses of each component known, the mole fraction could be compared to the mole fraction determined by the GC. From this analysis the maximum error in composition was found to be ±0.013 mole fraction and the average error was 0.008 mole fraction.

This manual repeatability tests lead to an uncertainty in composition of $u_c(\text{composition})=0.016$ mole fraction with a coverage factor of two.

4. Experimental Results

4.1. Experimental Verification

Confidence in experimentally measured data is created by verifying the equilibrium still and the experimental procedure. The pure components and their subsequent vapour pressures can be used to verify the measurements of the equilibrium still (pressure and temperature). A binary system with existing literature VLE data can be compared with the experimentally produced data for the same system and used to verify the experimental and analytical procedures (composition).

4.1.1. Vapour pressure verification

Using the Gibbs phase rule, the pure components at saturation contain only one degree of freedom and therefore, for every pressure there can only be one temperature [37]. Based on this principle, the vapour pressure found from the experimental work is compared to vapour pressure correlations from the DIPPR database [110].

Figure 4.1 a) illustrates this comparison, with a maximum deviation from the DIPPR correlations of less than 1% and 95% of the deviations less than 0.7%. This comparison of the maximum deviations of each system to the DIPPR correlation (Table 4.1) shows a high degree of accuracy of the vapour pressures. This is well within the uncertainty of pressure of ±0.046 bar, used in these results. This degree of accuracy indicates that there are reliable and repeatable pressure and temperature measurements (Figure 4.1 a).

Because of the small deviations from the DIPPR correlations can't be seen in Figure 4.1 a. Figure 4.1 b) is used to show the percentage difference of each component. With the deviations being within the uncertainty of pressure in these experiments, the experimental pressure and temperature in further experiments, using the Gillespie still, can be validated.

Table 4.1: DIPPR correlation uncertainties and ranges for the six pure components

Compound	Uncertainty	Temperature range (K)	Pressure range (bar)
1-propanol	<3%	146.95 – 536.80	4.274×10^{-12} – 51.69
2-butanone	<1%	186.46 – 536.70	9.175×10^{-6} – 42.07
Propyl formate	<1%	180.25 – 538.00	2.110×10^{-6} – 40.28
Ethyl acetate	<1%	189.60 – 523.30	1.431×10^{-5} – 38.50
Methyl propionate	<1%	185.65 – 530.60	6.341×10^{-6} – 40.28
2-propanol	<1%	185.26 – 508.30	6.102×10^{-8} – 47.71

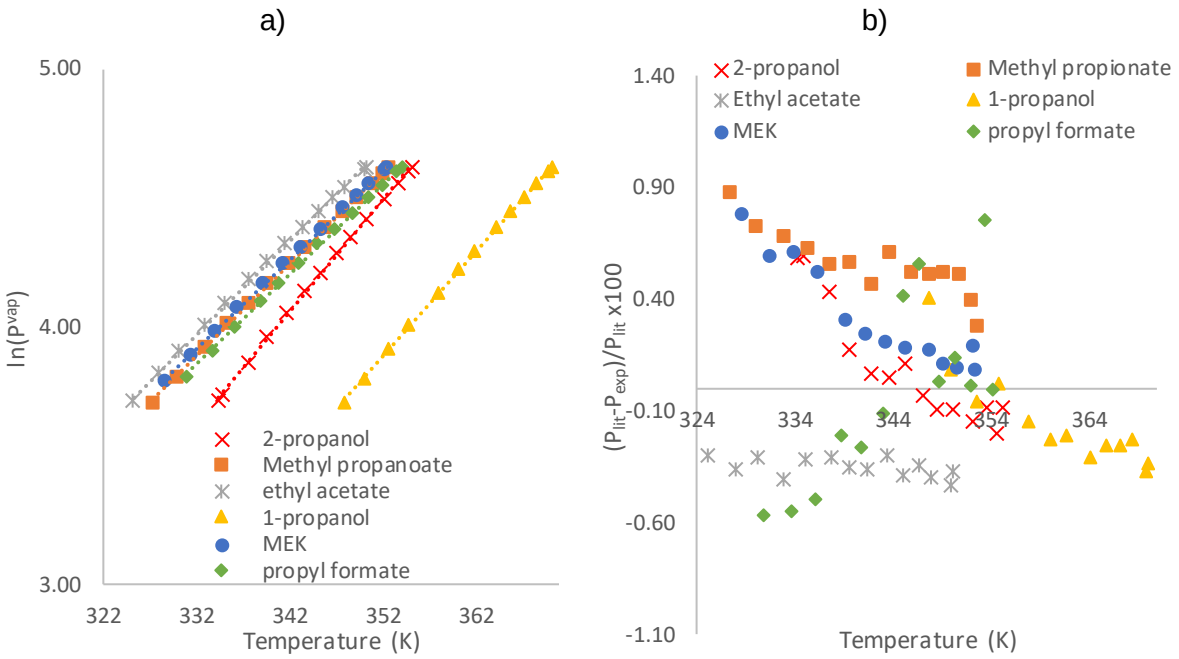

Figure 4.1: a) Deviation of experimental vapour pressure from DIPPR correlations. b) vapour pressure of the pure components used in experiments, DIPPR correlations indicated by the dashed line, and the experimental data by the coloured markers b) Deviation of experimental vapour pressure from DIPPR correlations.

4.1.2. Behaviour of pure component vapour pressures

A comparison of vapour pressures of the six pure components (Figure 4.1 a) show a decrease in P^{sat} for the two propanol components (1-propanol to 2-propanol). This is a result of the structural isomer changing the position of the hydroxyl group to the centre of the carbon chain and dampening the polar and associating behaviour of the compound. This same effect is seen with the lowering of P^{sat} of propyl formate to ethyl acetate. The initial shortening of the carbonyl group (R-O-C) and lengthening of the acyl group (R-C=O) leads to this decrease in P^{sat} for propyl formate to ethyl acetate which is expected. Further shortening of this group to the smallest carbonyl group of the C_4 esters (from ethyl acetate to methyl propionate) results in an increase in P^{sat}. This is evident due to the further increase in the dipole-dipole forces and lessening of steric hindrance on the carbonyl group. The shielding and subsequent opening of the carbonyl can be seen in Figure 4.2.

a) b) c)

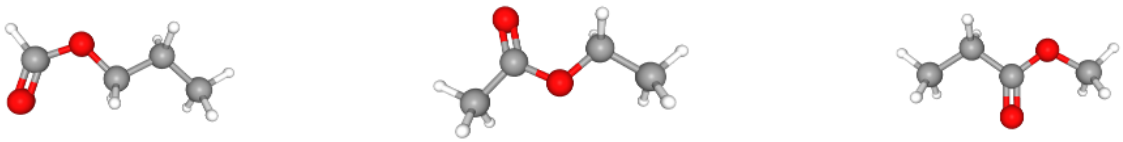

353.6 K 350.2 K 352.4 K

Figure 4.2: 3D formulae of the three C_4 esters with the normal boiling points presented, to show the dampening and effect of moving the hydroxyl group towards the centre and then away from the centre of the carbon chain. a) propyl formate with a boiling point of 353.6 K, b) ethyl acetate with a boiling point of 350.2 K, c) methyl propionate with a boiling point of 352.6 K

The vapour pressures of the three C_4 esters and 2-butanone are extremely similar, with 1-propanol being an outlier (Figure 4.1 a) It can therefore be assumed that the cross-association effects of these components are similar, and that the effect of steric hindrance and the addition of a carboxyl group is negligible.

4.1.3. Binary data verification

The temperature and pressure measurements are validated using the pure component vapour pressures. Validation of the still and sampling techniques have on the composition is still required. This can be done by comparing literature VLE data to VLE data generated using the Gillespie style equilibrium still.

The binary system of 1-propanol/2-butanone is common for all the ternary systems being tested and therefore is the binary system chosen to validate the experimental procedure in measuring composition. The literature system of 1-propanol/2-butanone experimentally produced by Martinez et al. 2008 [59] passes both the L/W and the McDermott-Ellis consistency test with an L/W D value of 1.840. A comparison of the literature data and the experimental data is shown in Figure 4.3. The experimental data in Figure 4.3 (a) lies on the same phase envelope as the literature data, which indicates that experimental data is reliable.

The experimental data was found in two separate runs, with each run starting at 1-propanol and moving towards a higher concentration of 2-butanone . Then starting at 2-butanone and moving towards a higher concentration of 1-propanol . There is a clear overlap in the data between the two runs, indicating confidence in the repeatability of the experimental data.

In Figure 4.3 (b) slight differences in composition are noticed between the experimental and literature data. However, when considering the uncertainty in concentration (0.016 mole fraction), the difference is within the uncertainty of composition. Further repeatability is noticed between the two separate experimental runs (Figure 4.3 b). The excess Gibbs free energy of the experimental data also agrees well with literature (Figure 4.3 c). Due

to the use of activity coefficients in calculating excess Gibbs free energy, it is a useful tool in assessing the consistency of the experimental data collected.

The experimental data of 1-propanol/2-butanone also passes both the L/W and the McDermott-Ellis consistency tests. There is an L/W D value of 1.613.

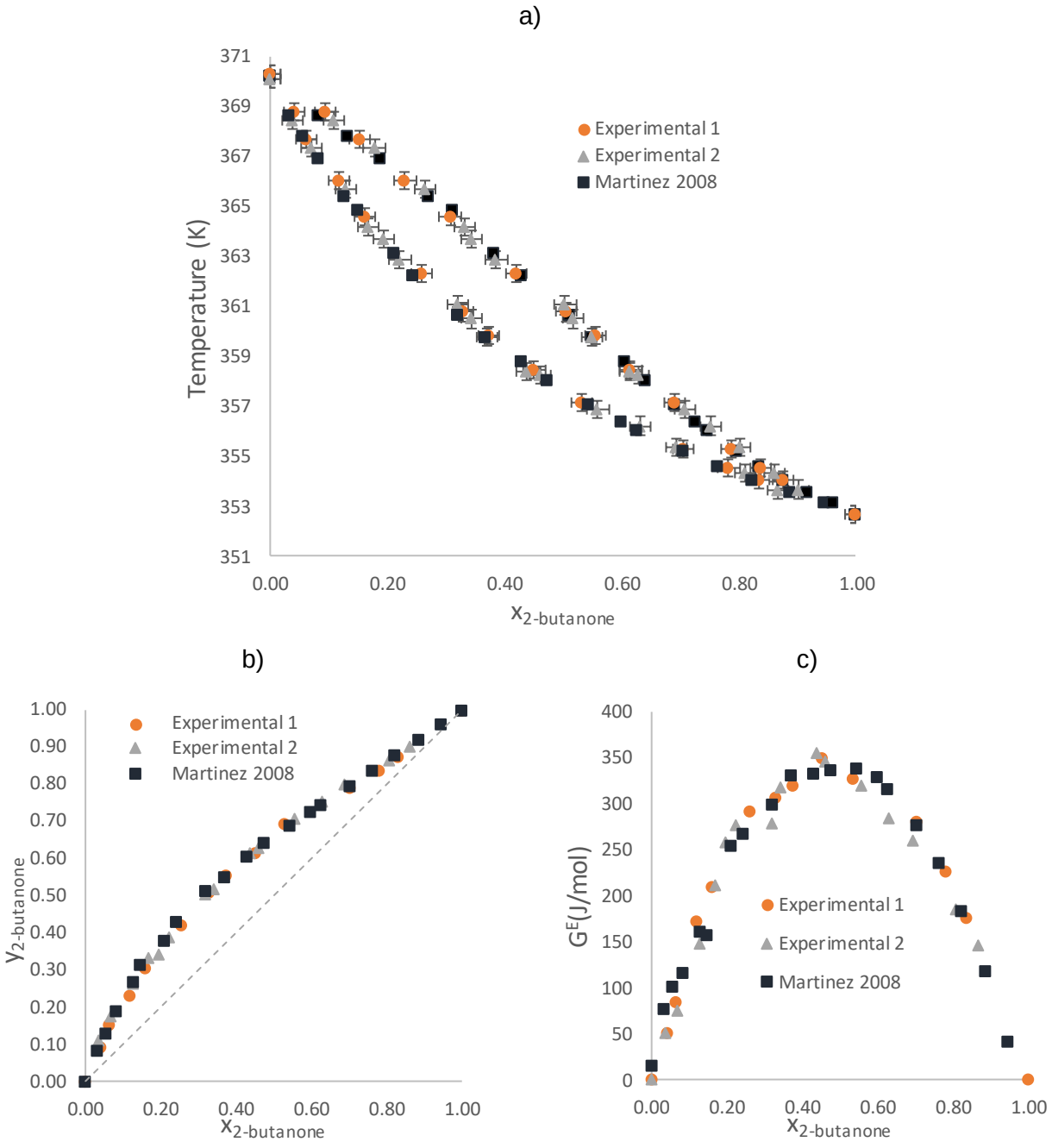

Figure 4.3: a) T-xy diagram of 1-propanol/2-butanone compared to literature data, b) x-y diagram of 1-propanol/2-butanone compared to literature data, c) excess Gibbs free energy comparing experimental and literature values

4.1.4. Still verification

Confidence was found in the temperature and pressure measurements, when using the vapour pressures and DIPPR correlations of the pure components. The 1-propanol/2-butanone system, with a good compositional agreement to the literature data, gives confidence in the repeatability of the data, and the accuracy of the sampling and analytical procedure gives confidence in the composition. This allows for confidence in the results of further binary and ternary data experimentally found.

4.2. Binary systems in the 1-propanol/2-butanone/propyl formate system

In the ternary 1-propanol/2-butanone/propyl formate system there are three corresponding binary systems. The three binary systems being 1-propanol/2-butanone (Figure 4.3), 1-propanol/propyl formate (Figure 4.4 a), and 2-butanone/propyl formate (Figure 4.4 b).

In the 1-propanol/propyl formate system an azeotrope exists at high concentrations of propyl formate (352.60 K and 0.076 mole fraction of 1-propanol). The 1-propanol/propyl formate system passes both the McDermott-Ellis point-to-point test, with all D values lower than the D_{max}, and the L/W area test with a L/W D value of 1.130.

At high concentrations of 2-butanone in the 2-butanone/propyl formate system, slight deviations can be seen in the Gibbs excess energy function (Figure 4.4 f). The low amount of separation, as shown with low partition coefficients (K_i) and relative volatilities (Section 4.7, Figure 4.15), exaggerates this deviation, with the uncertainty of composition being greater than the (y-x) values. Both systems pass both the McDermott-Ellis point-to-point test and the L/W area test with a L/W D value of 0.665.

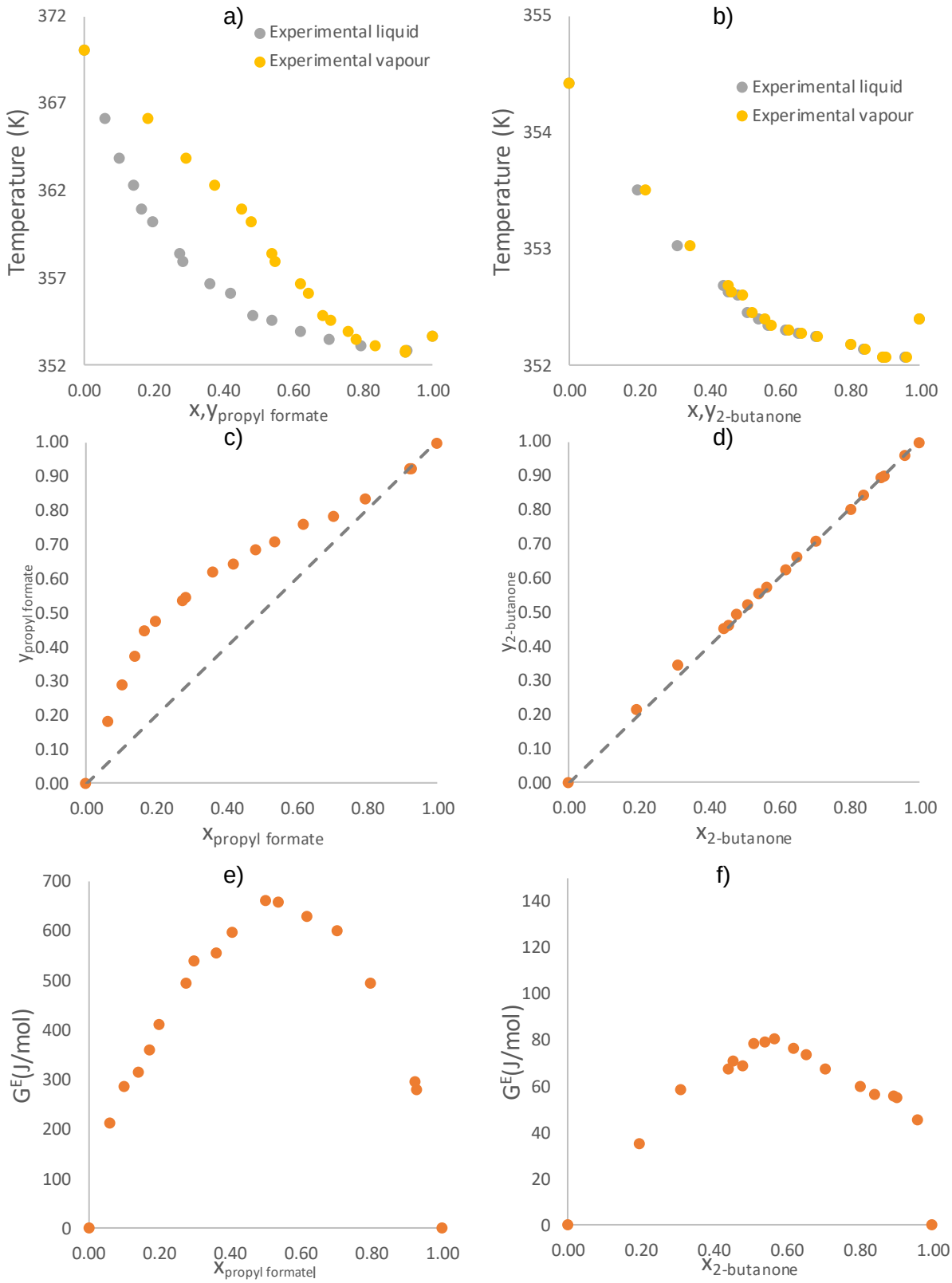

Figure 4.4: a) Experimental T-xy data for 1-propanol/propyl formate system, b) experimental T-xy data for 2-butanone/propyl formate system, c) experimental xy data for 1-propanol/propyl formate system, d) experimental xy data for 2-butanone/propyl formate system, e) excess Gibbs energy function for the 1-propanol/propyl formate system, f) excess Gibbs energy function for the 2-butanone/propyl formate system

Using the three binary systems plotted on the same axis it can be used to see what trend the liquid and vapour surface will take in the ternary system (Figure 4.5). A shortening of the tie lines can be expected as the concentration of 1-propanol decreases, which is shown by little to no separation in the middle section (propyl formate) of Figure 4.5.

Due to the three binary systems showing two azeotropes. There is a distillation boundary between the two azeotropes expected at low concentrations of 1-propanol, with no tie lines crossing this boundary.

Larger separation is expected at lower concentrations of 2-butanone due to the larger amount of separation seen in the 1-propanol/propyl formate system compared to that of the 1-propanol/2-butanone system (Figure 4.5). Deviations from an ideal state are expected at low concentrations of 1-propanol. Due to the two binary azeotropes at both high and low concentrations of propyl formate, by keeping the concentration of 1-propanol low, there is expected to be deviations for all concentrations of propyl formate.

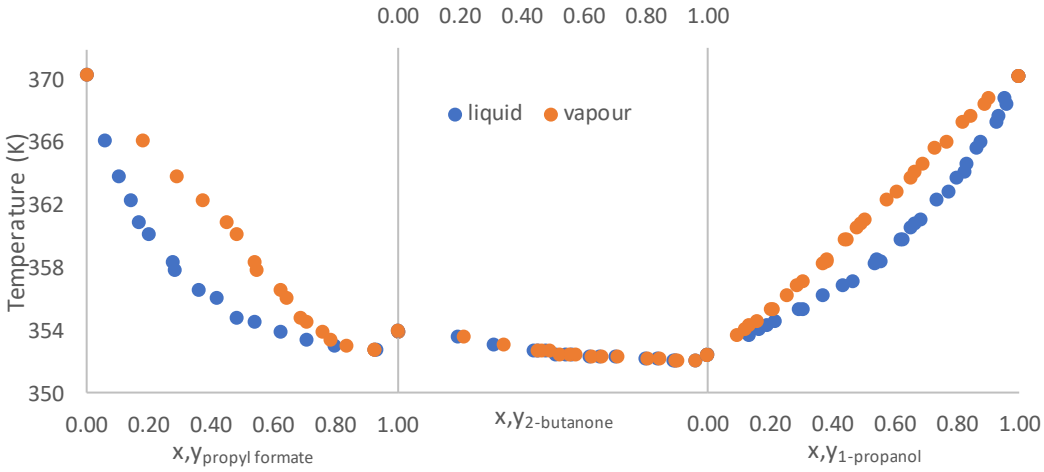

Figure 4.5: Binary systems 1-propanol/2-butanone, 2-butanone/propyl formate, and 1-propanol/propyl formate used to create a ternary diagram of 1-propanol/2-butanone/propyl formate

4.3. Binary systems in the 1-propanol/2-butanone/ethyl acetate system

The ternary system containing the ethyl acetate system contains two additional binary systems, namely, 1-propanol/ethyl acetate and 2-butanone/ethyl acetate (Figure 4.6).

Slight differences are seen in the 2-butanone/ethyl acetate system at low concentrations of ethyl acetate (Figure 4.6 c). In the 2-butanone/ethyl acetate system differences in the azeotropic position are evident, 349.95 K and 0.756 mole fraction of 2-butanone in literature compared to 349.94 K and 0.83 mole fraction of 2-butanone experimentally found. However, the experimentally found azeotropic is similar to the azeotropic data found by Gmelhling et al. 1996 [111], with an azeotropic position of 349.95K and 0.8343 mole fraction

of 2-butanone. As there little to no separation it is difficult to find the correct azeotropic composition.

Both systems pass the McDermott-Ellis point-to-point consistency test and the L/W area test, with a D value in the L/W area test of 2.230 and 1.388, respectively.

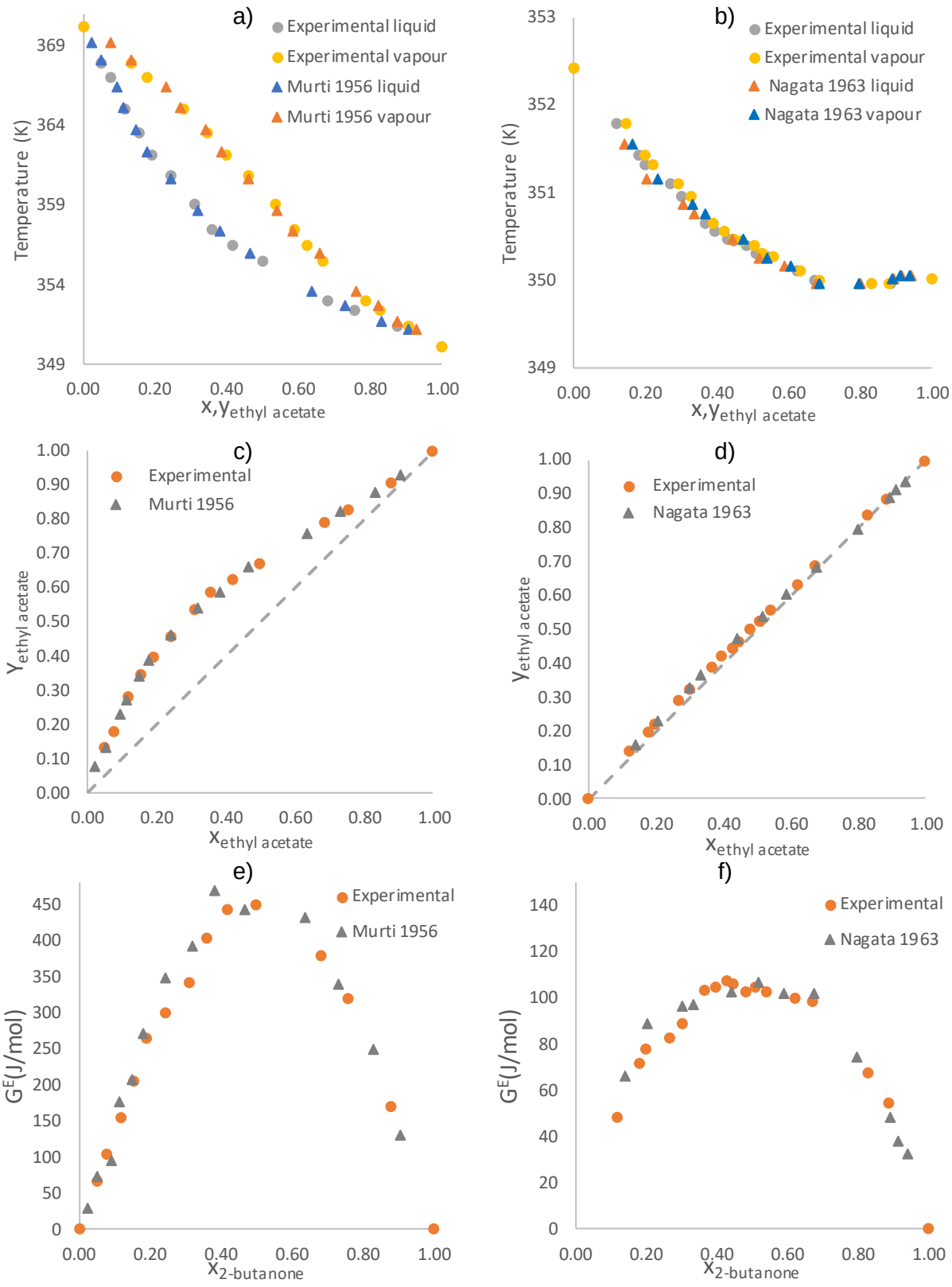

Figure 4.6: a) Experimental T-xy data for 1-propanol/ethyl acetate system, b) experimental T-xy data for 2-butanone/propyl formate system, c) experimental xy data for 1-propanol/ethyl acetate system, d) experimental xy data for 2-butanone/propyl formate system, e) excess Gibbs energy function for the 1-propanol/propyl formate system, f) excess Gibbs energy function for the 2-butanone/propyl formate system

The three binary systems plotted on the same axis (Figure 4.7) shows that a shortening of tie lines can be expected as the concentration of 1-propanol decreases. The tie lines will also increase when going from a low to a high concentration of ethyl acetate, while keeping the 2-butanone constant. This is evident by the greater separation of the 1-propanol/ethyl acetate system compared to the 1-propanol/2-butanone system. This will also result in higher temperatures for increasing concentration of 2-butanone while keeping 1-propanol constant.

The one azeotrope present in the 2-butanone/ethyl acetate system shows that there will be deviations from the ideal state at high concentrations of ethyl acetate. No other azeotrope exists, and it is therefore assumed that the ternary system containing ethyl acetate will show the least deviations from the ideal state.

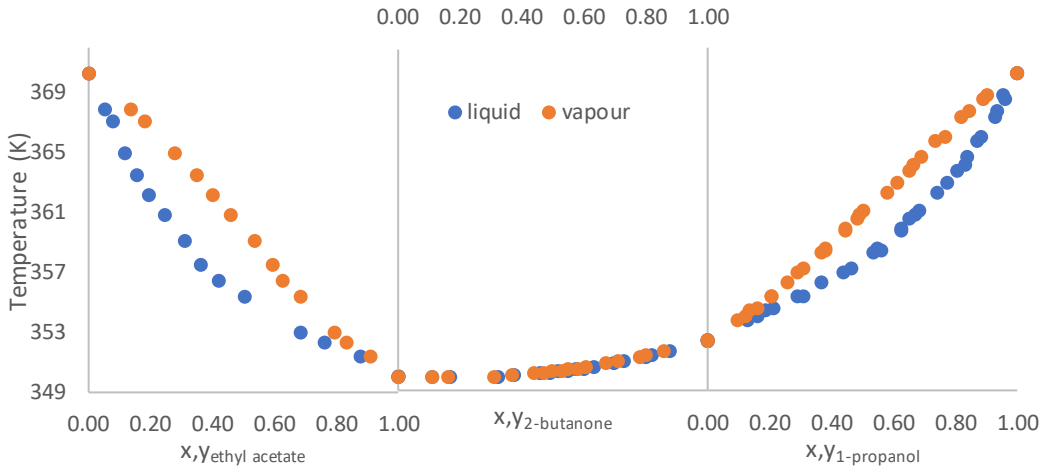

Figure 4.7: Binary systems 1-propanol/2-butanone, 2-butanone/ethyl acetate, and 1-propanol/ethyl acetate used to create a ternary diagram of 1-propanol/2-butanone/ethyl acetate

4.4. Binary systems in the 1-propanol/2-butanone/methyl propionate system

1-propanol/methyl propionate, and 2-butanone/methyl propionate are the two additional systems within the methyl propionate ternary system (Figure 4.9).

The differences between the literature and experimental data are seen at high concentrations of methyl propionate in the 1-propnaol/methyl propionate system (Figure 4.9 a). There is a minimum temperature in the literature data of 351.85 K while in the experimental data there is a minimum temperature 352.16 K. This is a difference of 0.31 K. Although this difference is large, it is still within the temperature uncertainty of ±0.62 K within the system.

In the literature data a minimum azeotrope is not present, however, the minimum temperature in the data drops below the normal boiling point of methyl propionate (351.85 K compared to 352.61 K). This indicates that a minimum azeotrope should be present. It can therefore be

assumed that the azeotropic point of 351.86 K and 0.937 mole fraction of methyl propionate, is correct (Figure 4.8).

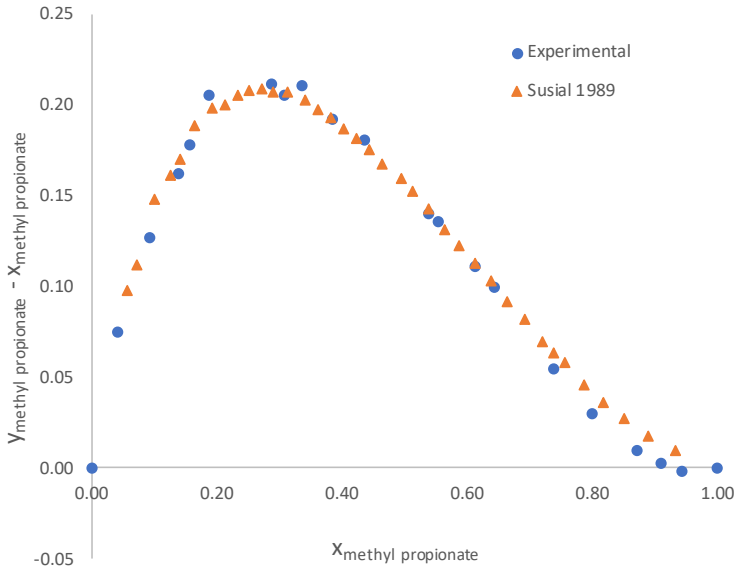

Figure 4.8: (y-x) vs x plot, showing the existence of an azeotropic point in the 1-propanol/methyl propionate system

Due to the extremely similar boiling points of 2-butanone and methyl propionate, little to no separation is expected. This small separation can be seen by the x vs y plot following the 45^{o} line (Figure 4.9 d). Small partition coefficients and small relative volatilities reiterate this point (Section 4.7, Figure 4.15). As a result of the similar boiling points, there are similar dipole-dipole moments creating a larger deviation from the ideal state.

The 1-propanol/methyl propionate and the 2-butanone/methyl propionate systems both pass the McDermott-Ellis point-to-point consistency test and the L/W area consistency test, with a D value for the L/W test of 2.017 and 2.590, respectively.

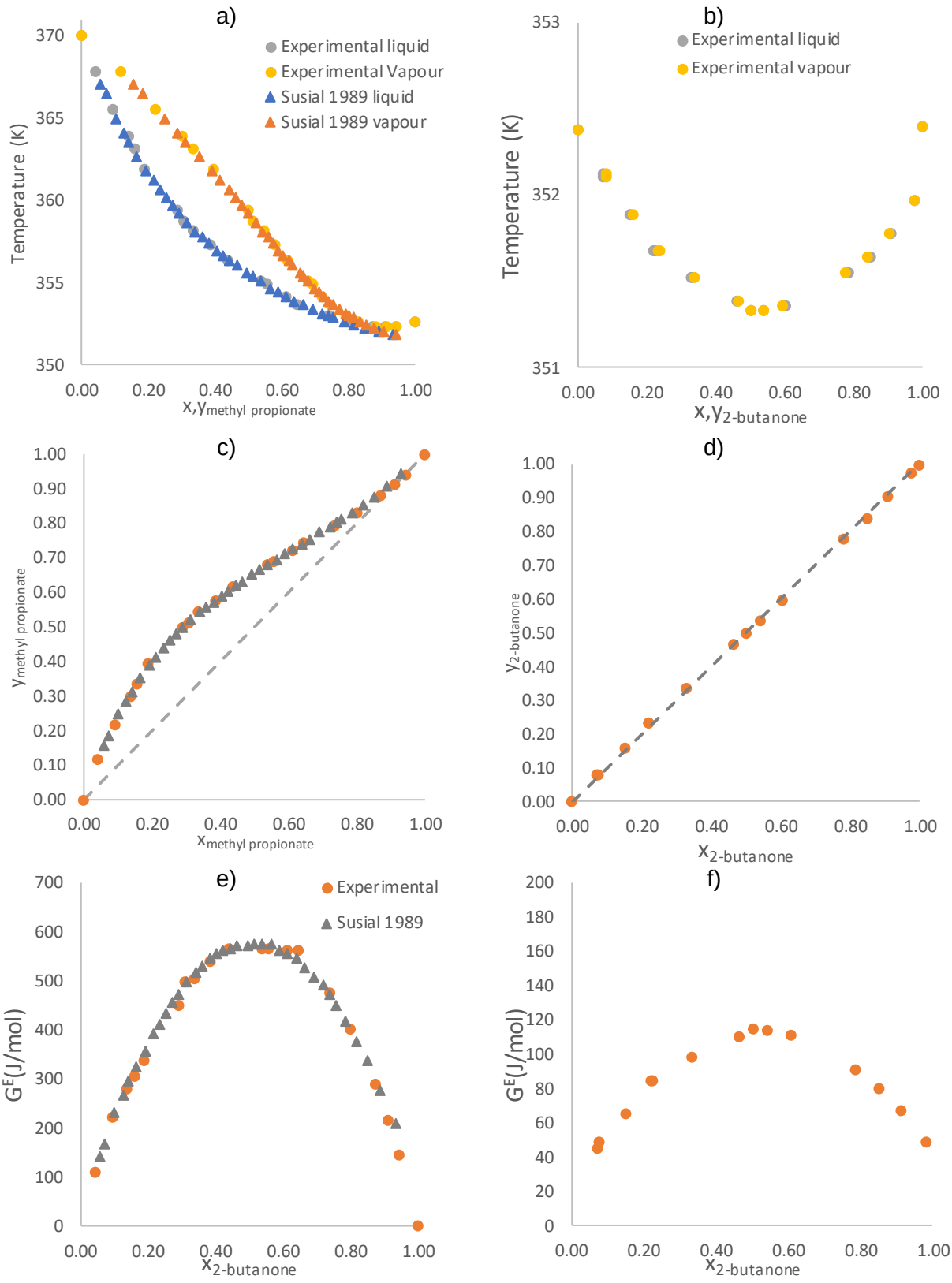

Figure 4.9: a) Experimental T-xy data for 1-propanol/methyl propionate, b) experimental T-xy data for 2-butanone/methyl propionate system, c) experimental xy data for 1-propanol/methyl propionate system, d) experimental xy data for 2-butanone/methyl propionate system, e) excess Gibbs energy function for the 1-propanol/methyl propionate system, f) excess Gibbs energy function for the 2-butanone/methyl propionate system

The three binary systems plotted on the same axis (Figure 4.10) indicated a shortening of tie lines can be expected as the concentration of 1-propanol decreases. This is due to the very similar boiling points of 2-butanone and methyl propionate.

A liquid-vapour surface at a constant temperature is expected to slope towards lower concentrations of 1-propanol when increasing the concentration of 2-butanone. This is due to the larger separation which is apparent in the 1-propanol/methyl propionate system compared to the 1-propanol/2-butanone system.

With two azeotropes in the 1-propanol/methyl propionate system and in the 2-butanone/methyl propionate system, deviations at low concentrations of 1-propanol are predicted. These deviations occur at both medium concentrations of methyl propionate and high concentrations of methyl propionate.

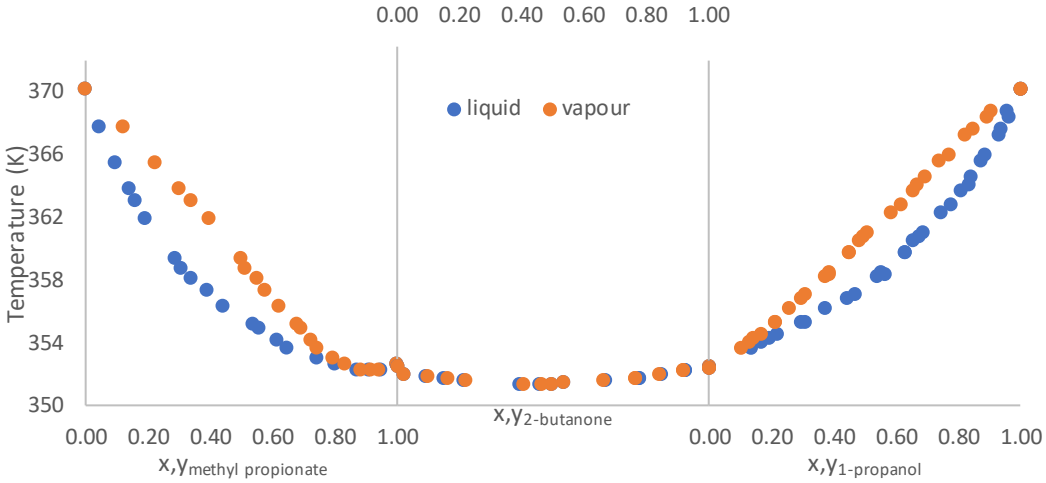

Figure 4.10: Binary systems 1-propanol/2-butanone, 2-butanone/methyl propionate, and 1-propanol/methyl propionate used to create a ternary diagram of 1-propanol/2-butanone/methyl propionate

4.5. Binary systems in the 1-propanol/2-butanone/2-propanol system

To test the effect of the changing of the functional group, two additional binary VLE systems are required in the 2-propanol ternary system, namely, 1-propanol/2-propanol and 2-butanone/2-propanol respectively (Figure 4.11).

The experimental data is in good agreement with the literature data of the 2-butanone/2-propanol system (Figure 4.11 c), with the systems having very similar azeotropic points (350.50 K and 0.62 mole fraction of 2-butanone).

In the 1-propanol/2-propanol system (Figure 4.11 a) the experimental data can be seen to only agree with Ballard et al. 1952 [62]. All three systems do however agree in the xy diagram (Figure 4.11 c) and therefore the differences occur between the two literature sources can be

seen to be in temperature. Seeing the scatter in the excess Gibbs free energy for the Ballard et al. 1952 [62] systems leads to the expectation that the data is thermodynamically inconsistent. Although this may be the case it can also show that there is a small deviation from the ideal state. This is expected having two components that a chemically very similar, that will both hydrogen bond with themselves and with each other at similar strengths.

Both systems pass both the McDermott-Ellis point-to-point test and the L/W area test with D values of 1.248 and 2.26, respectively.

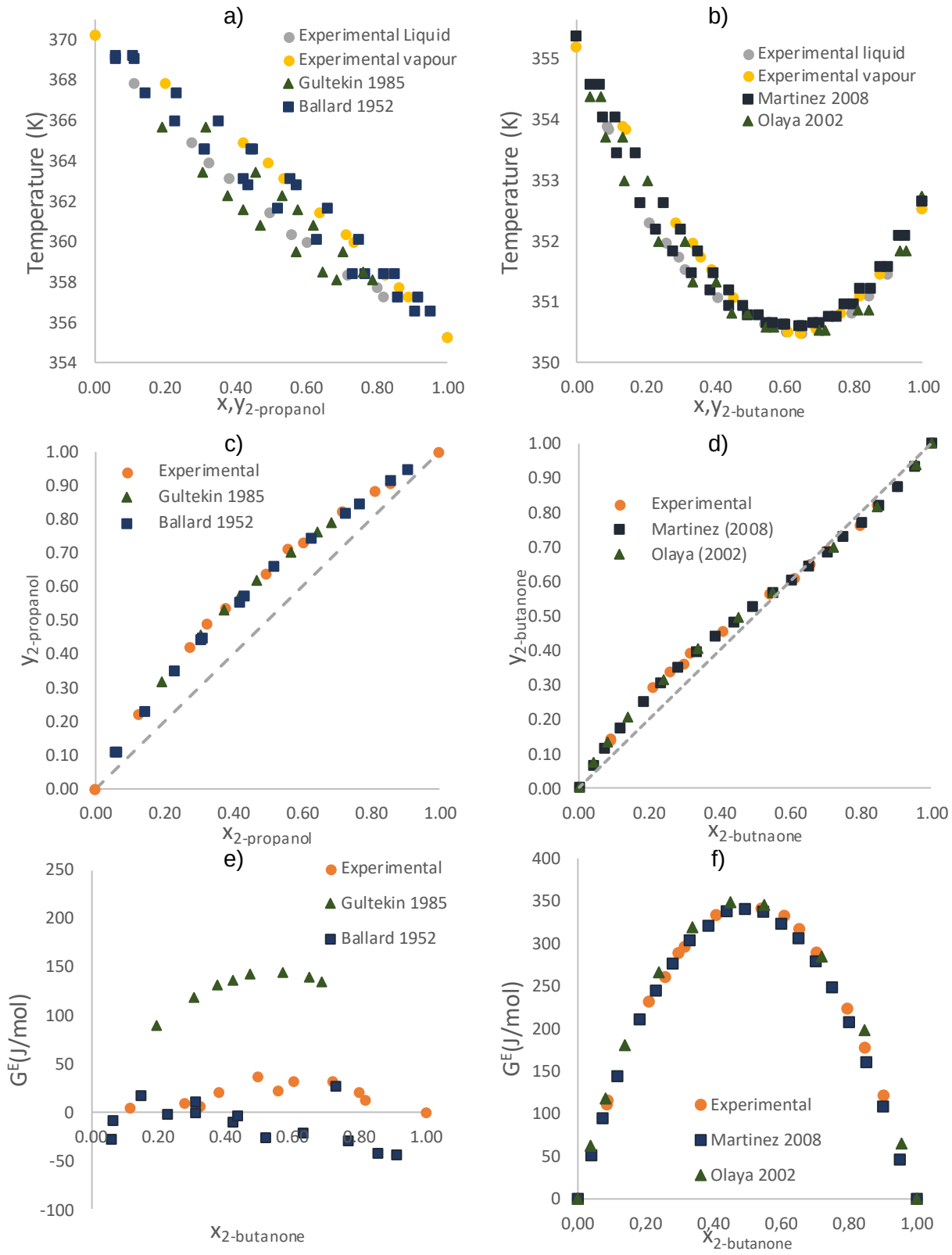

Figure 4.11: a) Experimental T-xy data for 1-propanol/2-propanol system, b) experimental T-xy data for 2-butanone/2-propanol system, c) experimental xy data for 1-propanol/2-propanol system, d) experimental xy data for 2-butanone/2-propanol system, e) excess Gibbs energy function for the 1-propanol/2-propanol system, f) excess Gibbs energy function for the 2-butanone/2-propanol system

The three binary systems plotted on the same axis (Figure 4.12) indicates there will be a shortening of tie lines with decreasing concentration of 1-propanol. However, these tie lines will not be as short as in the ternary systems containing the C_4 esters as a greater separation is evident in the 1-propanol/2-propanol system. Higher temperatures are expected when moving to higher concentrations of 2-propanol while keeping the concentration of 1-propanol constant.

A greater deviation from the ideal state is expected compared to that of the three C_4 ester ternary systems. This is noticed with a larger deviation in temperature in the 2-butanone/2-propanol system, due to the stronger hydrogen bonding between the two components.

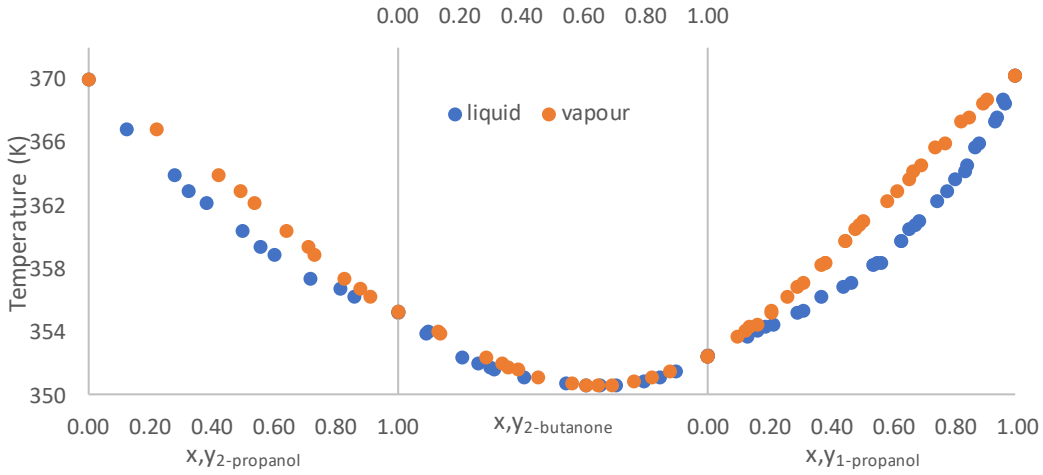

Figure 4.12: Binary systems 1-propanol/2-butanone, 2-butanone/2-propanol, and 1-propanol/2-propanol used to create a ternary diagram of 1-propanol/2-butanone/2-propanol

4.6. 1-propanol systems

Each system contains 1-propanol. The effect that 1-propanol has on each binary system is important to understand as it will impact how they interact within the ternary systems.

The binary systems with 1-propanol (Figure 4.13 a) show a small deviation from an ideal state due to the larger differences in the boiling points. All systems show a similar behaviour at high 1-propanol concentrations. This is especially true for the three C_4 systems as they have almost identical phase envelopes. This is expected as the cross-association between the C_4 components and 1-propanol is dilute. It is therefore hard to distinguish between the cross-association effects of each C_4 isomer, while the self-association of 1-propanol dominates. It is therefore expected that at high temperatures within the ternary systems, interactions close-to-ideal will be expected, with little deviations between the systems.

The binary system of 1-propanol/methyl propionate and 1-propanol/propyl formate both showcase a minimum azeotrope at 0.068 and 0.076 mole fraction of 1-propanol (Figure

4.13 b), whereas the binary system of 1-propanol/ethyl acetate does not have an azeotrope. The azeotrope is formed as a result of being in high concentrations methyl propionate with stronger hydrogen bonding occurring between the 1-propanol/methyl propionate and 1-propanol/propyl formate molecules, than the diluted 1-propanol/1-propanol hydrogen bonds. It can be assumed that an azeotrope does not form in the ethyl acetate system due to the shielding of the carbonyl group and the decrease in hydrogen bond strength. It is therefore expected that the system of ethyl acetate will interact in a more ideal way at low concentrations of 1-propanol compared to the systems containing methyl propionate and propyl formate.

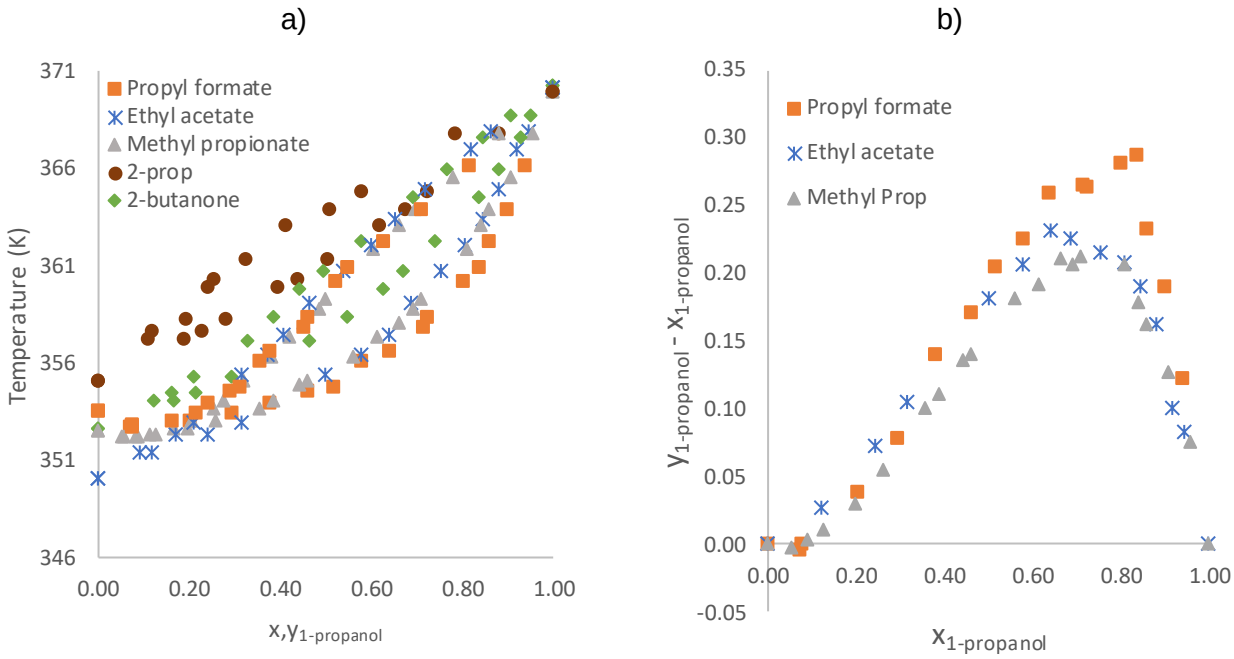

Figure 4.13: a) combined T-xy data of the 1-propanol/(2-propanol 2-butanone C4 esters) systems at 1,013 bar, b) (y-x) vs x plot, showing the azeotropic points of C_4 esters

4.7. 2-butanone systems

Due to the large difference in boiling point, the system of 1-propanol/2-butanone shows a very small deviation from an ideal state (Figure 4.14 a). However, the close boiling points of the 2-butanone/ (C_4 esters/2-propanol) systems all result in minimum boiling azeotropes.

These minimum azeotropes, especially in the 2-butanone/C_4 ester systems, occur at a high concentration of the lower boiling point component, 0.04 mole fraction of 2-butanone for the 2-butanone/propyl formate system and 0.96 mole fraction of 2-butanone for the 2 butanone/ethyl acetate system (Figure 4.14 b). This is due to the close boiling points exhibited by the two components in which the more polar molecules have a greater dipole-dipole interactions at high concentrations. Due to the incredibly close boiling points (352.38 K and 352.40 K respectively) and the similar forces between the models in the 2-butanone/methyl propionate system, the azeotrope occurs at 0.515 mole fraction of

2-butanone. The minimum azeotropic point of the 2-butanone/2-propanol system also occurs a at higher concentration of the lower boiling point component, 0.38 mole fraction 2-butanone, in which hydrogen bonding occurs between the 2-butanone and 2-propanol.

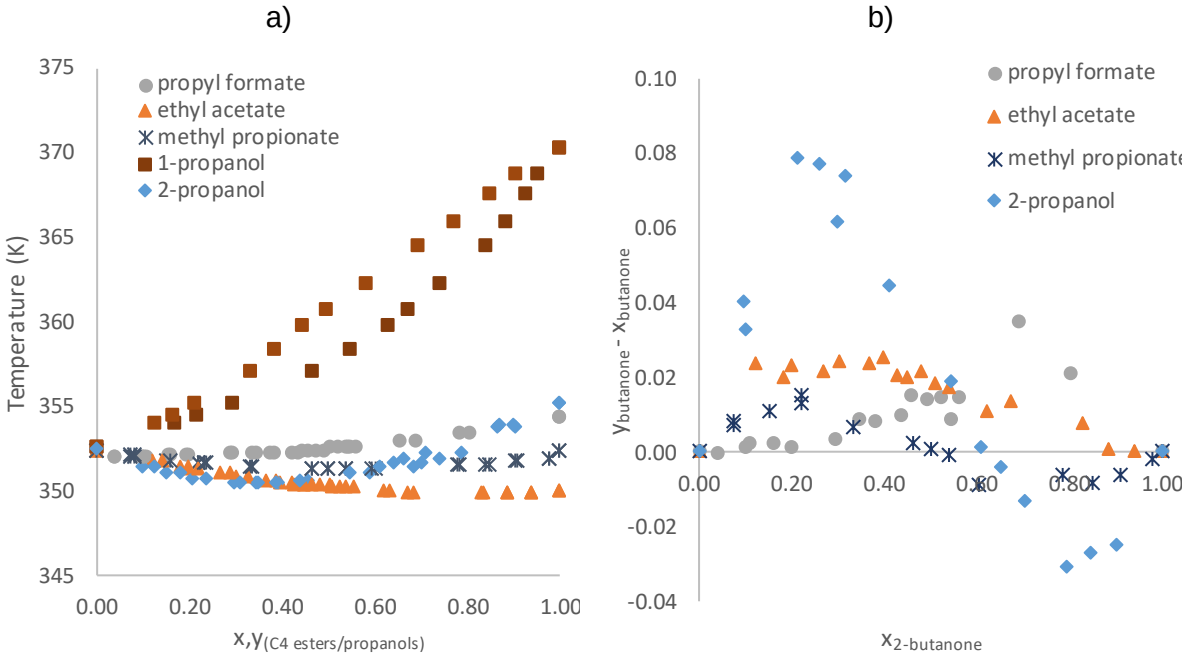

Figure 4.14: a) Combined T-xy data for 2-butanone/(C_4 ester propanol) systems at 1.013 bar, b) (y-x) vs x plot, showing the azeotropic points of C_4 esters and 2-propanol

Due to the close boiling points exhibited in the 2-butanone/C_4 ester systems deviations from the ideal state are noticed. This also leads to a small separation in these systems (Figure 4.15). The 2-butanone/2-propanol system shows larger deviations from an ideal state due to the stronger hydrogen bonding between the components. However, the slightly larger differences in boiling points lead to the slightly larger separation between the components (Figure 4.14). This in turn will lead to larger tie lines compared to those in the three C_4 ester systems.

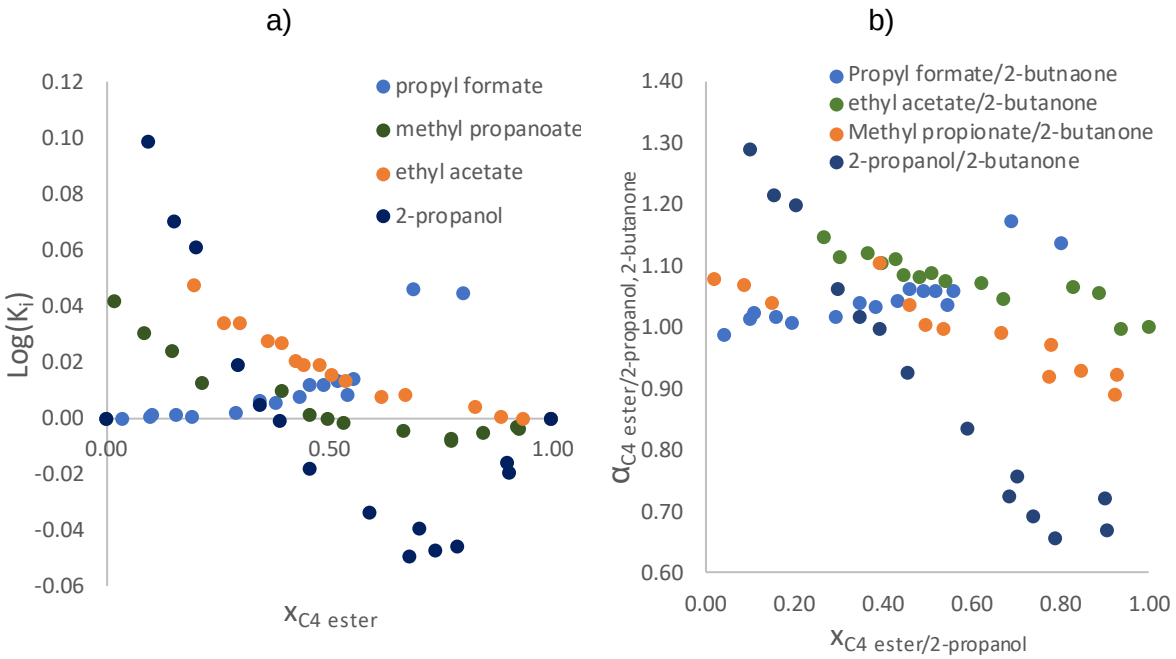

Figure 4.15: The small amount of separation in the 2-butanone/C_4 ester systems, shown by a) partition coefficients, b) relative volatilities

From the outcomes of the binary systems, predictions can be made as to how the ternary systems containing these components will interact. At high concentrations of 1-propanol it can be assumed that all four ternary systems will interact similarly, acting in a near ideal way. As the concentration of 1-propanol decreases, the interactions will be more non-ideal, with the shortening of the tie lines. It is also expected for the ternary system containing 2-propanol to interact in the most no-ideal way due to its self-associating characteristics.

It is expected that at low concentrations of 1-propanol the ternary system containing propyl formate will interact in the most non-ideal way compared to the other C_4 systems. Whereas, the ternary system containing ethyl acetate will interact in the most ideal way.

Due to the azeotropes evident in the 1-propanol/propyl formate and the 1-propanol/methyl propionate systems, a greater deviation from the ideal state is expected in these two ternary systems at low concentrations of 2-butanone compared to the ternary ethyl acetate system. The azeotrope at medium concentrations of 2-butanone in the 2-butanone/methyl propionate system will also cause deviation at medium concentration of 2-butanone in the ternary methyl propionate system.

5. Ternary Vapour-liquid equilibrium Results

With the temperature, pressure, and composition verified as previously described (Section 4.1), the new ternary systems can be populated with a high degree of confidence. The effect of the changing functional group can be tested by looking at four ternary systems each containing 1-propanol, 2-butanone and either C_4 ester or 2-propanol.

Ternary VLE data is usually represented using a Gibbs triangle in which the experimental composition is placed on an equilateral triangle, with the three pure components represented by the corners of the triangles (x, y, z).

The composition in Figure 5.1a can be read by taking the axis shown by x and moving 180^o, the axis shown by y and moving 60^o, and the z axis and moving 300^o, to meet at the point corresponding to the composition (0.50, 0.30, 0.20). The shifting of the point corresponds to a new composition of (0.30, 0.30, 0.40) (Figure 5.1 b).

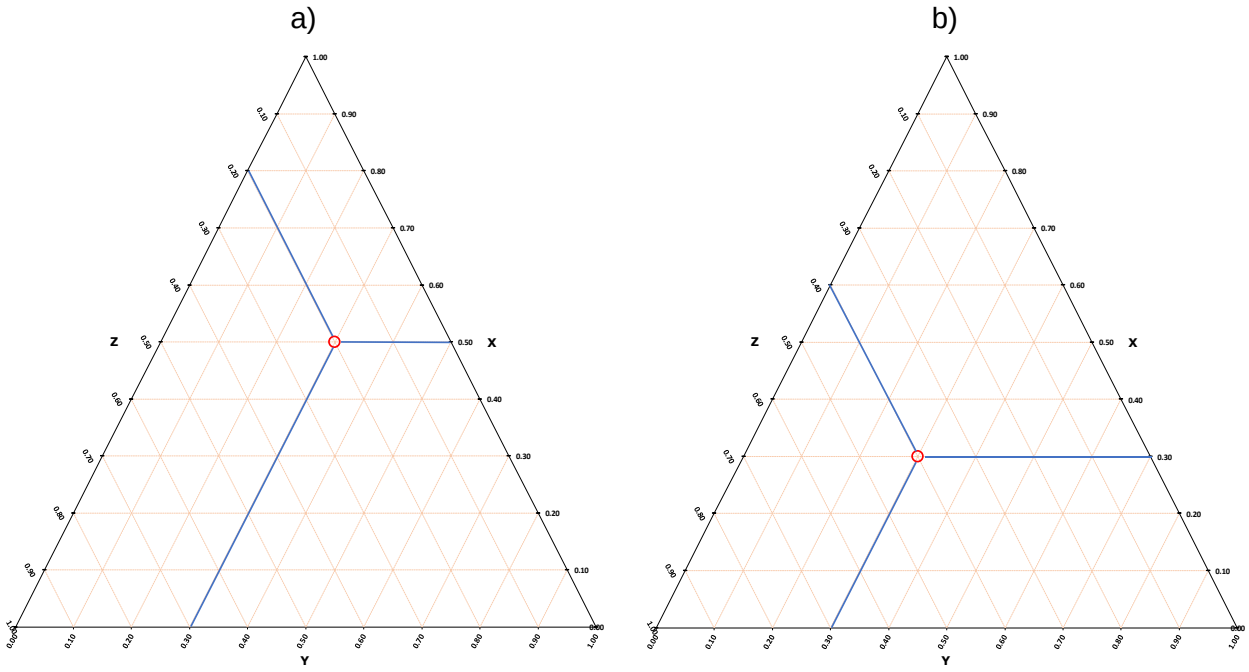

Figure 5.1: Example of four different compositions, and how to read the Gibbs triangle. a) (x, y, z) composition of (0.50, 0.30, 0.20), b) (x, y, z) composition of (0.30, 0.30, 0.40)

5.1. 1-propanol/2-butanone/propyl formate

Figure 5.2 shows the experimental results of the ternary system containing 1-propanol/2-butanone/propyl formate. Good repeatability is found near the centre point of the Gibbs triangle where there is overlap of run one and run three, as well as an overlap of run three and run five (Figure 5.2).

There is evidence of a distillation boundary, as indicated by the liquid having a lower concentration of propyl formate and 1-propanol, x = (0.05; 0.03; 0.92) y = (0.05; 0.03; 0.91), resulting in an inverted liquid-vapour surface (Figure 5.2). As tie lines approach the approximate distillation boundary shown in Figure 5.2 (dashed grey line), it is expected to see a shortening of tie lines. This is due to the strong dipole-dipole forces between the propyl formate/propyl formate becoming more prevalent then the hydrogen bonding between 1-propanol/1-propanol, 1-propanol/propyl formate, 1-propanol/2-butanone and the dipole-dipole forces between 2-butanone/2-butanone.

The 1-propanol/2-butanone/propyl formate system passes both the McDermott-Ellis point-to-point test, with all D values below D_{max} and the L/W area test with a D value of 2.200.

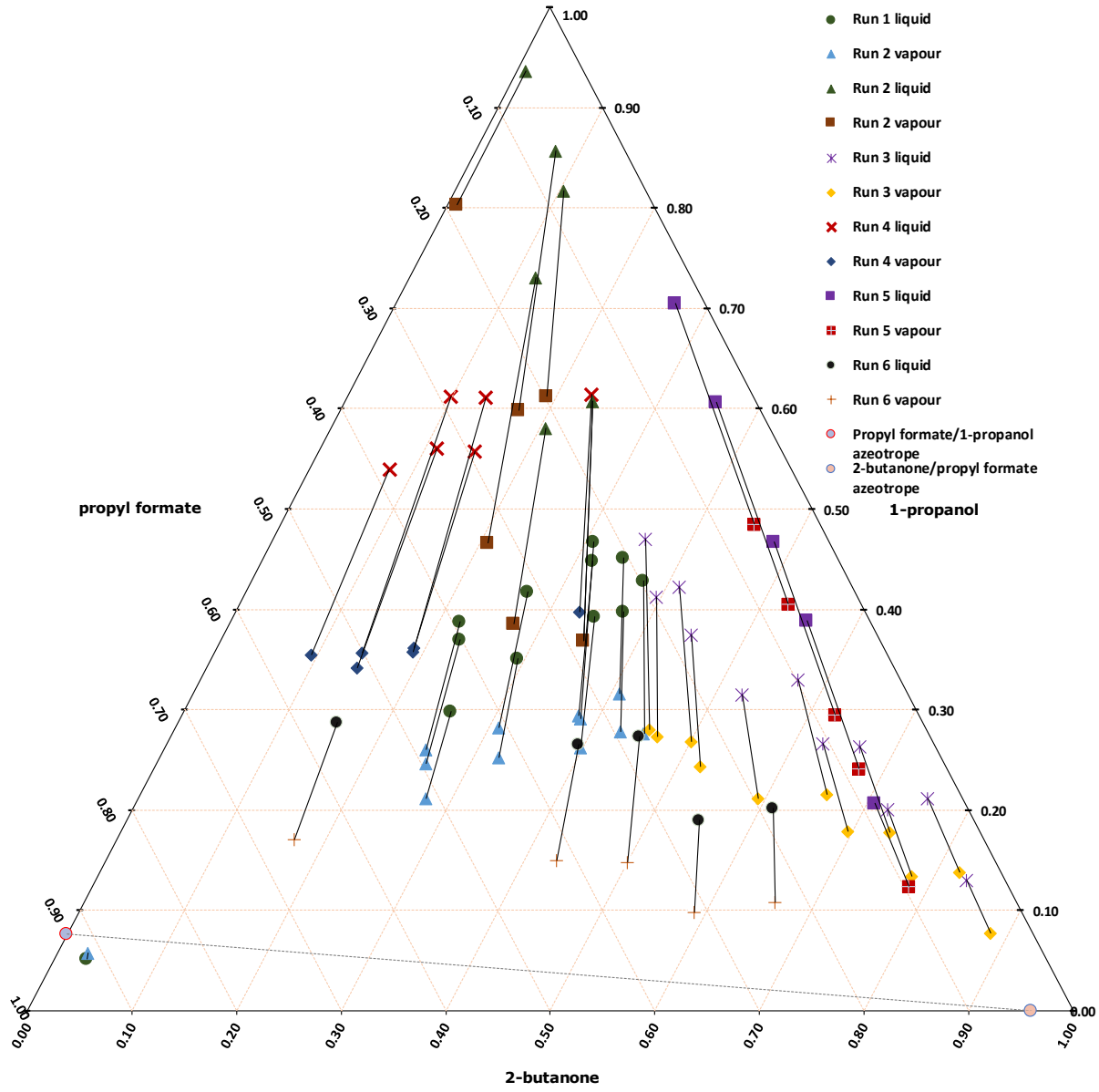

Figure 5.2: x-y-z diagram of the ternary system containing 1-propanol/2-butanone/propyl formate. Dashed grey line indicating an approximation of the distillation boundary

5.2. 1-propanol/2-butanone/ethyl acetate

Figure 5.3 shows the experimental results of the ternary system containing 1-propanol/2-butanone/ethyl acetate. There is clear overlap in the results as shown near the centre point of the Gibbs triangle and this indicates good repeatability of the data. The tie lines increase in size, and separation becomes easier when moving from low concentrations of 1-propanol to high concentrations of 1-propanol. In this region, there is easier separation due to the stronger hydrogen bonds between 1-propanol/1-propanol than other combinations resulting in a more ideal system.

Low concentrations of 1-propanol show a decreasing of tie line sizes. An increase of 2-butanone at high concentration ethyl acetate, approximately (0.20; 0.40; 0.40) to (0.02; 0.86; 0.12), shows a change in slope. This is due to the small amount of separation apparent in the 2-butanone-ethyl acetate system and the increase in dipole-dipole bonding between 2-butanone/2-butanone molecules. This change in slope is also noticeable as the data points move towards the binary azeotropic point of 2-butanone/ethyl acetate (0.00; 0.83; 0.17).

The 1-propanol/2-butanone/ethyl acetate system passes both the McDermott-Ellis point-to-point test with all D values below D_{max} and the L/W area test with a D value of 2.186.

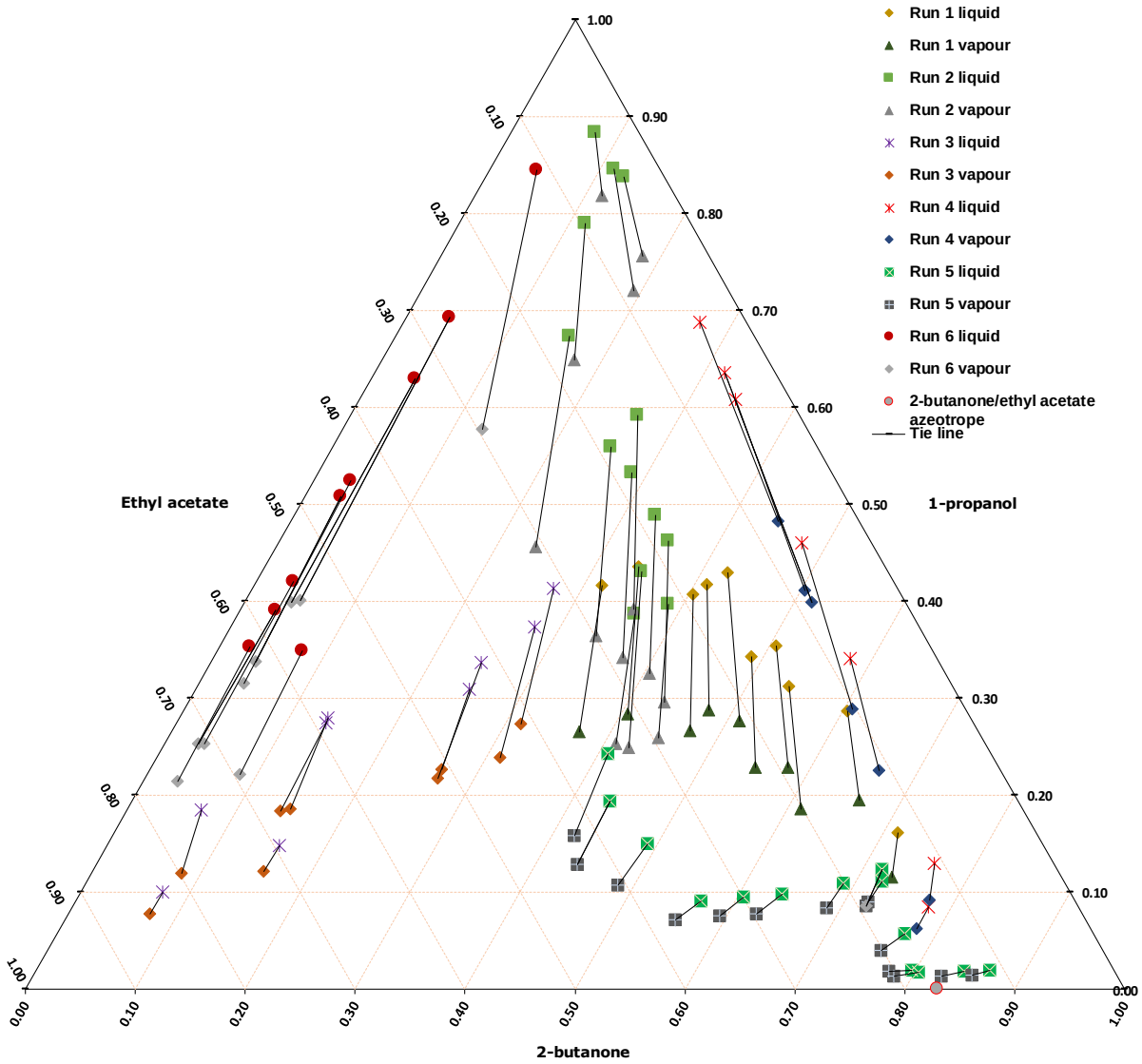

Figure 5.3: x-y-z diagram of the ternary system containing 1-propanol/2-butanone/ethyl acetate

5.3. 1-propanol/2-butanone/methyl propionate

Figure 5.4 shows the experimental results of the ternary system containing 1-propanol/2-butanone/methyl propionate. The shortening of tie lines can be seen at low

concentrations of 1-propanol. This is expected because of the extremely close boiling points of 2-butanone and methyl propionate. The two binary azeotropes, 1-propanol/methyl propionate (0.06; 0.00; 0.94) and 2-butanone/propyl formate (0.00; 0.48; 0.52) create a distillation boundary that does not pass through any experimental ternary data. An approximation of the distillation boundary is shown by the dashed grey line linking the two binary azeotropes. Evidence of the distillation boundary is shown with the inverting of the liquid-vapour surface with the liquid having a lower concentration of 1-propanol, x = (0.04; 0.04; 0.92) and y = (0.05; 0.04; 0.91).

The 1-propanol/2-butanone/methyl propionate system passes both the McDermott-Ellis point-to-point test, with all D values below D_{max} and the L/W area test with a D value of 2.202.

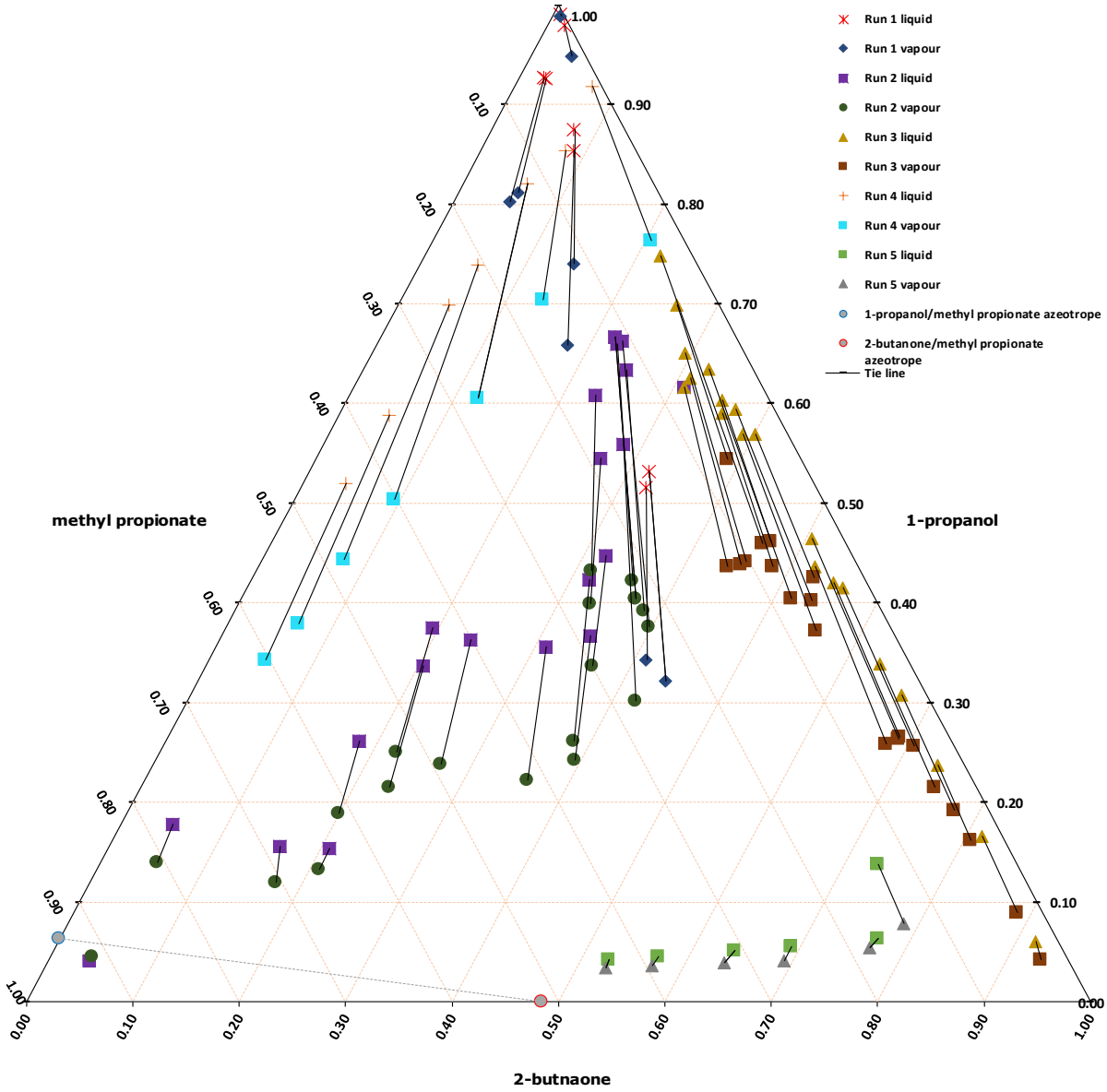

Figure 5.4: x-y-z diagram of the ternary system containing 1-propanol/2-butanone/methyl propionate. Dashed grey line indicating an approximation of the distillation boundary

5.4. 1-propanol/2-butanone/2-Propanol

Figure 5.5 shows the experimental results of the ternary system containing 1-propanol/2-butanone/2-propanol. Because only the 2-butanone/2-propanol system contains an azeotrope, a distillation boundary is expected at low concentrations of 1-propanol. When compared to the ternary data involving the C_4 esters, the ternary system of 1-propanol/2-butanone/2-propanol shows a more stable separation of the phases with similar-sized tie-lines, at different concentrations.

There is a deviation from the ideal state at higher concentrations of 1-propanol compared to the C_4 systems, with the changing of the tie line slope (0.35; 0.38; 0.27) to (0.05; 0.18; 0.77).

The 1-propanol/2-butanone/2-propanol system passes both the McDermott-Ellis point-to-point test, with all D values below D_{max} and the L/W area test with a D value of 1.580.

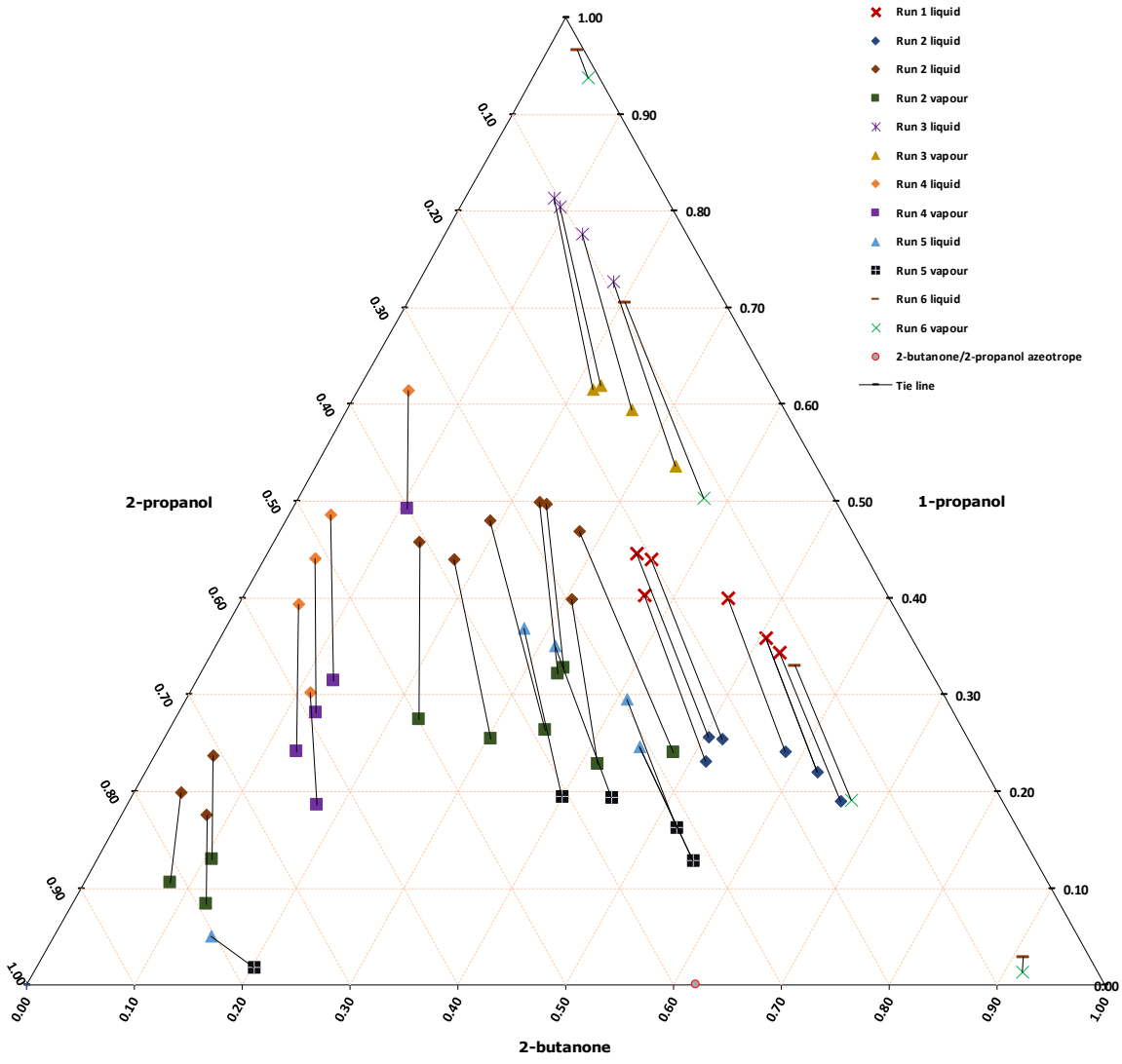

Figure 5.5: x-y-z diagram of the ternary system containing 1-propanol/2-butanone/2-propanol

5.4.1. Effect of placement of functional group and type of functional group

The Gibbs Triangle is useful diagram for representing ternary systems but does not consider the temperature that is measured during experiments. In order to plot temperature, a graph is needed in which a 3D surface is created. Taking Gibbs triangles at specific temperatures (Figure 5.6 a) allows for each temperature to be plotted on a 2D graph. The graph shows the concentrations that are only vapour, and only liquid, and both liquid and vapour at that specific temperature (Figure 5.6 b).

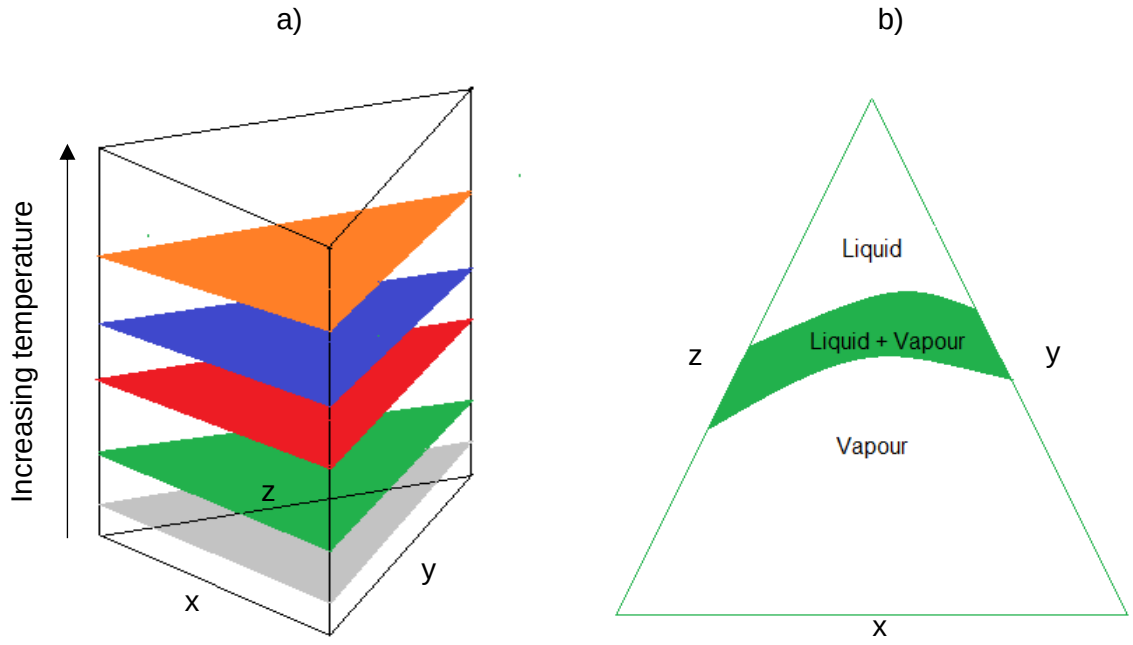

Figure 5.6: Surface temperature Gibbs triangles a) taking Gibbs triangles from a surface graph, with increasing temperature b) vapour liquid surface of a Gibbs triangle at a specific temperature

Using the concentrations that are experimentally found at a certain temperature, as well as the experimentally found points of the binary systems, a good approximation of the liquid-vapour surface can be found.

In order to build the approximations of the vapour-liquid curve, experimentally found data for both the binary systems and the ternary system is needed, this gives at least three different liquid and three different vapour concentrations, allowing an approximation of the smooth vapour-liquid curve to be plotted at the specific temperature (Figure 5.7).

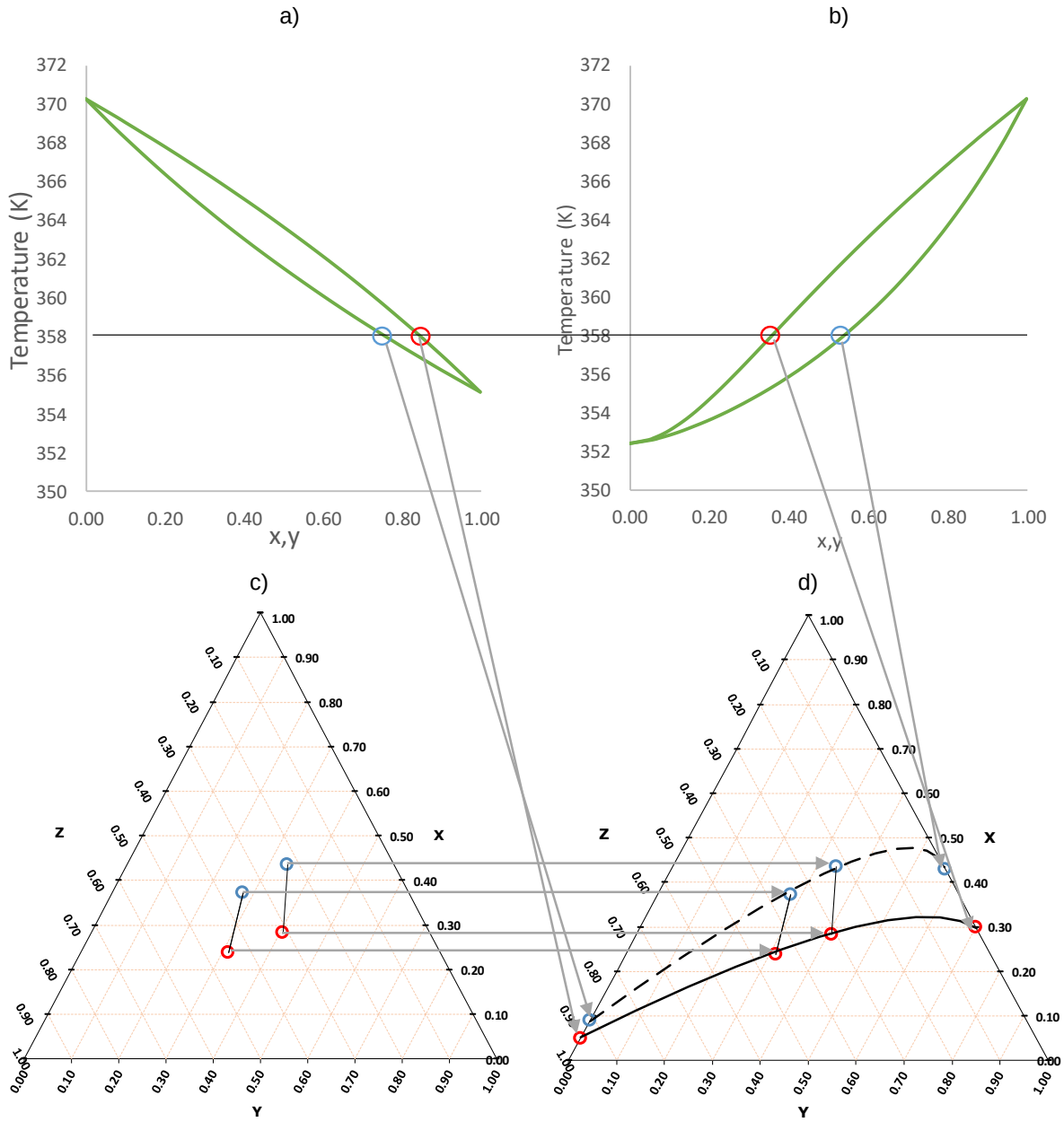

Figure 5.7: constructing a vapour liquid curve at a certain temperature, using ternary and binary data. a) binary points at temperature A. b) binary points in second system at temperature A. c) Ternary points at temperature A. d) Vapour-liquid curve approximated using binary and ternary points at temperature A

The liquid-vapour surfaces at different temperatures can be examined using the concept demonstrated in Figure 5.6 and Figure 5.7. With two components remaining constant throughout the four ternary systems, it can be assumed that the differences between the experimental data occur due to the third component. When analysing the three ternary systems containing the C_4 esters, any differences in concentration and temperature can be attributed to the shifting of the carboxyl group. While differences in concentration and temperature in the ternary system which contain 2-propanol can be attributed to the hydroxyl group.

Figure 5.8 shows the cross section of the surface plot for five increasing temperatures in the four different ternary systems. Each temperature's surface boundary is shown by a specific colour. The vapour boundary is indicated by the solid line and the liquid boundary by the dotted line. The experimental composition is shown by the colour that represents the temperature at which it was found.

In the ternary system containing 2-propanol, higher temperatures are seen at lower concentrations of 1-propanol (towards the base of the triangle) when compared to temperatures in the C_4 ester systems (Figure 5.8 d). This is due to the greater deviation from the ideal state in this system, with the stronger self/cross-associations in the two alcohols, compared to only the cross-associations of the ester/ketone/alcohol in the C_4 ester systems. The liquid-vapour surface can be seen to move towards higher concentrations of 1-propanol when going from low to high concentrations of 2-butanone (Figure 5.8 a). This shows that higher temperatures are observed at higher concentrations of 2-butanone.

The three C_4 systems show different outcomes of the vapour-liquid surface when compared to the 2-propanol system (Figure 5.8 a, b, c), with more ideal liquid-vapour surfaces. The liquid-vapour surface of all three C_4 ester systems trend towards lower concentrations of 1-propanol when it moves from low to high concentrations of 2-butanone, for example, the liquid boundary in Figure 5.8. This indicates that lower temperatures are observed at higher concentrations of 2-butanone. This shape of the liquid-vapour surface is due to the slightly more polar nature of the ketone compared to the C_4 esters.

There is increasing dipole-dipole forces from ethyl acetate – methyl propionate – propyl formate, amongst the three C_4 systems (Figure 5.8 a, b, c). This is important when looking at the differences between the three systems. At lower temperatures, the liquid-vapour surfaces of the propyl formate and methyl propionate systems are at lower concentrations of 1-propanol compared to the ethyl acetate system. Looking at the vapour boundary surface, at 353.6 K and medium concentrations of the C_4 esters, Figure 5.8 a (0.15; 0.52; 0.33), Figure 5.8 b (0.24; 0.45; 0.33), Figure 5.8 c (0.20; 0.47; 0.33). This is in line with the increasing dipole-dipole forces, with stronger hydrogen bonds forming between 1-propanol/propyl formate compared to the other two systems, as well as the ethyl acetate system showing the smallest deviation from an ideal state.

At high temperatures these effects are less pronounced, and all four systems show similar liquid-vapour surfaces. This is due to the stronger hydrogen bonding between 1-propanol/1-propanol components, resulting in near ideal interactions in all four systems.

It should be noted that the saddle point shown in (Figure 5.8 a) is an approximation, without more experimental data in this region, the exact curve is not known. The existence of the

'inversion' is known with the two binary azeotropes, binary data at 353.6 K for all three systems, and two binary points in the 1-propanol/propyl formate system, this region is highlighted by the blue circle. More data generation in this region at that temperature (which in this work is a dependant variable and not fixed) is needed.

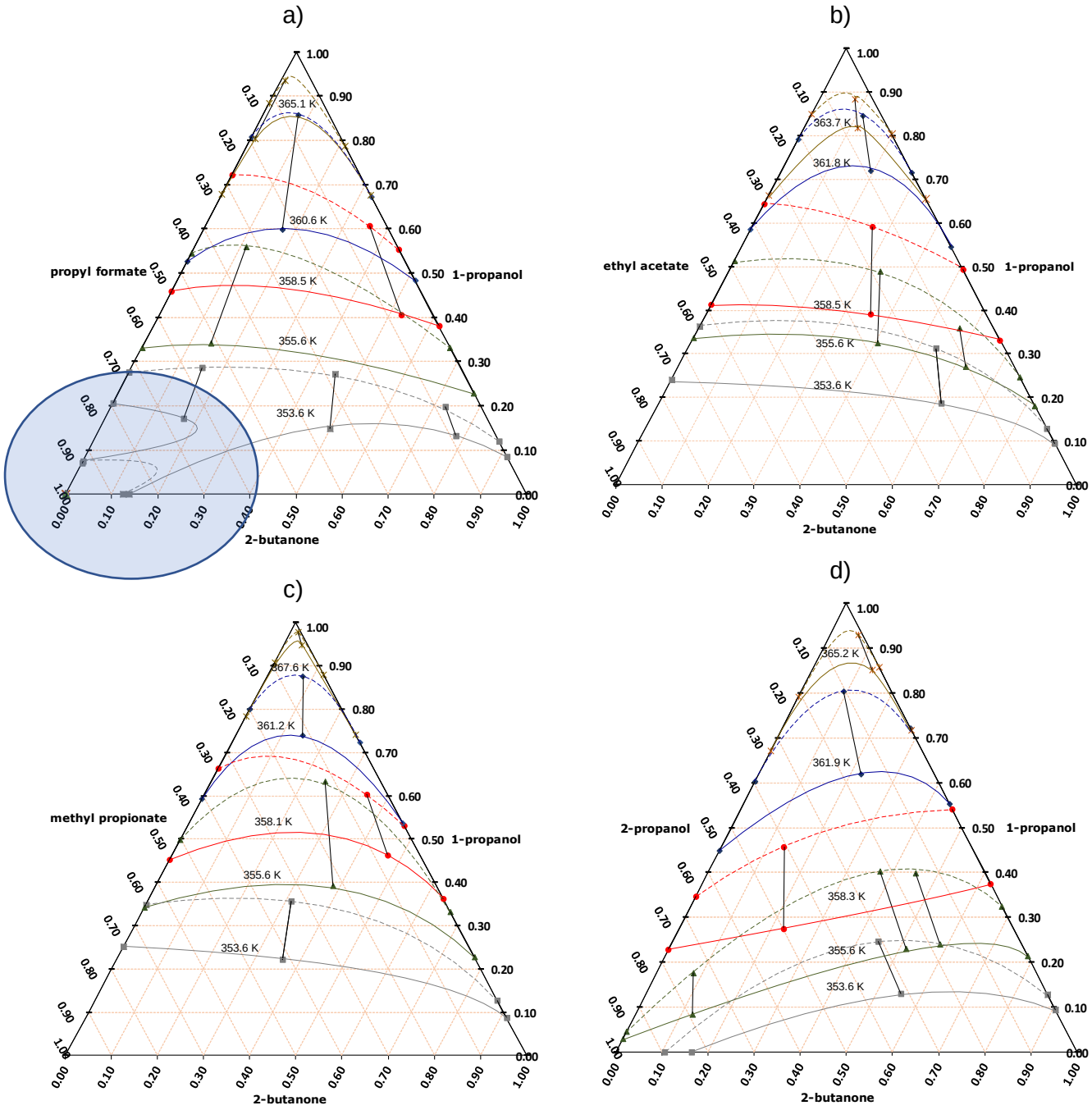

Figure 5.8: Temperature profiles of the four ternary systems a) propyl formate, b) ethyl acetate, c) methyl propionate, d) 2-propanol. The dotted line is the liquid boundary, while the solid line is the vapour boundary. In which the blue circle highlights the 'inversion' in the vapour-liquid surface in which more data is needed for a more accurate estimation.

In order to gain a better understanding of the effect of the changing functional groups and the movement of the functional group, the liquid-vapour surface at a specific temperature in which

each system had experimental data was compared between the four ternary systems (Figure 5.9).

These four temperatures in which experimental data was measured for all four systems were 353.63 K, 354.87 K, 355.60 K, and 356.65 K. The liquid-vapour surface that occurs at these temperatures is plotted on four separate Gibbs triangles, with the 2-propanol/C_4 esters lying on the left-hand side axis (Figure 5.9 a, b, c, d). Each temperature will have the same composition of binary 1-propanol/2-butanone. This is represented by the grey square markers on the 1-propanol axis.

In all four cases, the 2-propanol ternary system shows the greatest deviation from the ideal state, with lower concentrations of 1-propanol for all temperatures. This deviation is more evident as the concentration of 2-propanol increases, and the hydrogen bonding between the two alcohols increases.

When looking at the three C_4 ester systems, the deviations are less exaggerated. At the lowest temperature where all 4 systems had experimental data was 353.63 K, the propyl formate system shows the largest deviation from the ideal state compared to the other two ester systems. This manifests with an inversion of the liquid-vapour surface at high concentrations of propyl formate, as would be expected with the two azeotropes that are in the binary systems containing propyl formate.

In the propyl formate system, for all temperatures, the deviation from the ideal state is noticed at higher concentrations of propyl formate, looking at the liquid boundary at 354.87 K at approximately (0.53; 0.03; 0.44) (Figure 5.9 b)There is a deviation from the ideal state, with a large curve of the liquid boundary. With the binary azeotrope in the 2-butanone/propyl formate being at high concentrations of propyl formate, this is expected. As the temperatures increase, the concentration of propyl formate decreases and the deviation from the ideal state is less pronounced. Compared to the other two C_4 ester systems, the differences are noticed at high concentrations of propyl formate. As the temperature increases and the concentration of propyl formate is low, the system interacts more ideal way and shows little deviation from the ethyl acetate system.

In the methyl propionate system, the deviation from ideal state and the differences from the other two C_4 ester systems is noticed, mostly at medium concentrations of both 2-butanone and methyl propionate, as seen at the vapour boundary at 355.60 K at approximately (0.41; 0.25; 0.34) (Figure 5.9 c), deviations from the ideal state are noticed. Although the deviation is expected at medium concentrations of 2-butanone and methyl propionate, due to the binary azeotrope occurring at these concentrations, the deviation is greater than expected. Especially at concentrations of 1-propanol in which the hydrogen bonds should dampen the dipole

moment experienced between the 2-butanone and methyl propionate components. With methyl propionate and 2-butanone having very similar boiling points, the hydrogen bonding between 1-propanol/2-butanone and 1-propanol/methyl propionate will be very similar and therefore greater separation will occur.

In the ethyl acetate system there are only small deviations from the ideal state. The dampening of the polar and associating behaviour of the compound with the shifting of the hydroxyl group results in the most ideal system.

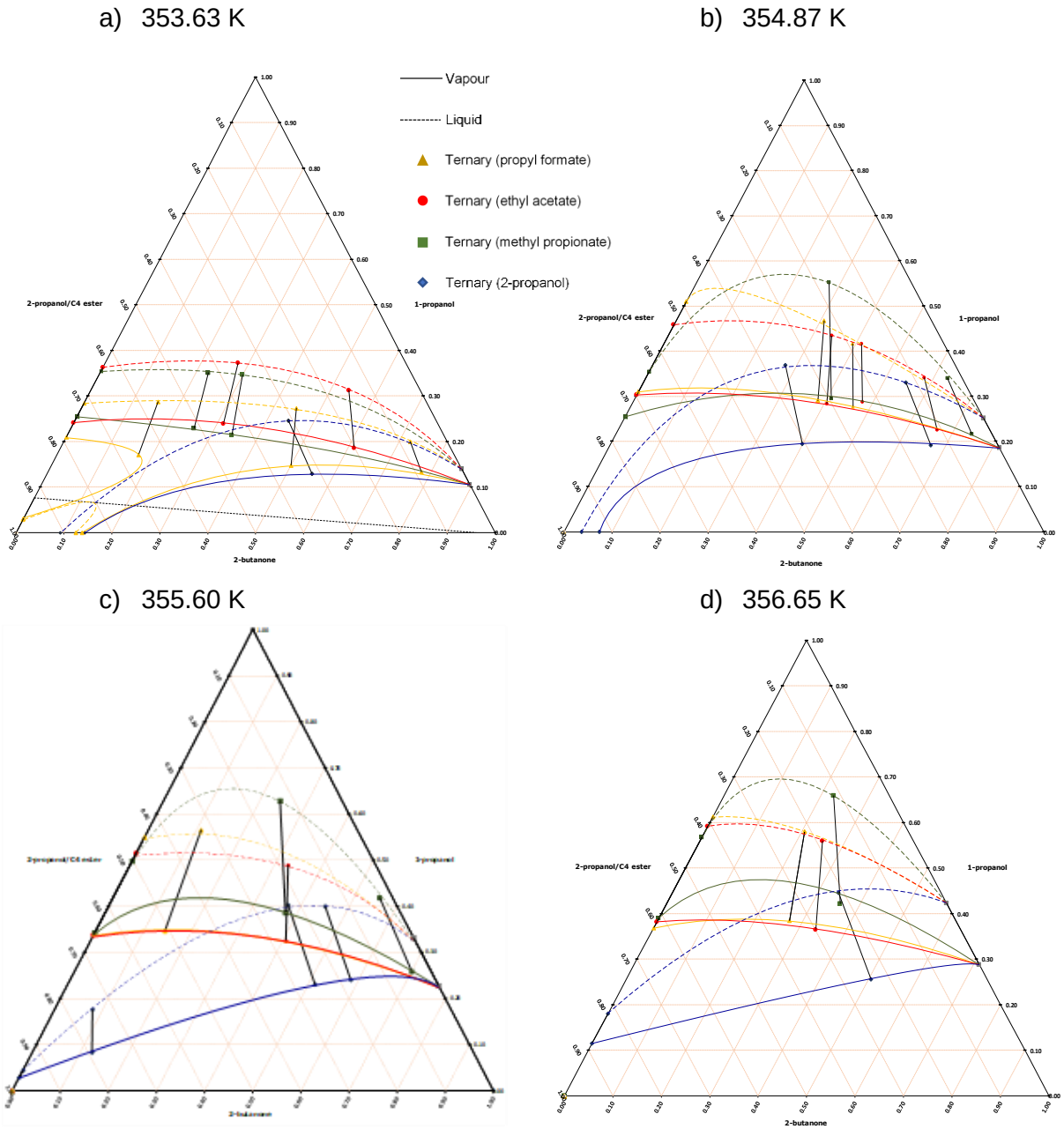

Figure 5.9: Isothermal section of experimental data at a) 353.63 K, b)354.87 K, c) 355.60 K, d) 356.65 K. The grey square markers in each graph corresponding to the 1-propanol/2-butanone binary composition for each temperature

6. Modelling

Work has been done on proving the predictive nature of SAFT-VR-Mie + GV and sPC-SAFT + GV for binary polar systems [32], [33], [112]. However, little work has been done on predicting multicomponent systems. It is therefore of interest as to how accurately these perturbation type models predicts binary systems and whether they predict ternary systems with a similar accuracy.

6.1. Activity coefficient model NRTL

The activity coefficient model NRTL[83] is applied to correlate the experimental VLE data. It requires BIPs in order to accurately model a system, and therefore will not be able to predict the outcome of a binary or ternary system without the use of VLE data. Using NRTL, together with the binary systems measured in this work, however, can be useful in showing the accuracy of a correlative model, and therefore, used as a benchmark for how well the perturbation theory models predicts the systems.

According to the NRTL model, the activity coefficients at specified temperature and liquid compositions are calculated as follows:

$$\ln \gamma_i = \left(\frac{\sum_{j=1}^{n} \tau_{ji} x_j G_{ji}}{\sum_{k=1}^{n} x_k G_{ki}}\right) + \sum_{j=1}^{n} \left(\frac{x_j G_{ij}}{\sum_{k=1}^{n} x_k G_{kj}}\right) \times \left(\tau_{ij} - \frac{\sum_{m=1}^{n} \tau_{mj} x_m G_{mj}}{\sum_{k=1}^{n} x_k G_{kj}}\right) \quad 6.1$$

where

$$G_{ij} = \exp\left(\alpha_{ij} \tau_{ij}\right) \quad 6.2$$

And

$$\tau_{ij} = \frac{A_{ij}}{RT} \quad 6.3$$

where τ_{ij} is the BIP, α_{ij} is the non-randomness parameter, R is the gas constant, and T is the absolute temperature. An extensive number of NRTL BIPs are available in literature. However due to binary systems in this work having no existing binary data, and therefore no BIPs, the regression was used for all the systems. NRTL BIPs are also considered a linear function of temperature because of the strong dependence of the excess Gibbs energy on temperature as follows:

$$A_{ij} = A_{ij}^0 + A_{ij}^1 T \quad 6.4$$

The regression of the two parameters (A_{ij}^0 and A_{ij}^1) was done by minimizing the objective function (OF). through the regression of a MATLAB optimisation function.

$$OF = \sum_{i=1}^{N} \left| \frac{T_i^{exp} - T_i^{calc}}{T_i^{exp}} \right| + \sum_{i=1}^{N} \left| y_i^{exp} - y_i^{calc} \right| \qquad 6.5$$

By setting the non-randomness parameter (α_{ij}) for each system to 0.3, as this results in an accurate output for the model [113], the accuracy of the NRTL model to correlate phase equilibrium can be assessed. Firstly visually, by plotting the model's outcome and the experimental data on the same graph, and secondly statistically using the average absolute deviation (AAD) (equation 6.6).

$$AAD(F) = \frac{1}{Z_T} \sum |F_i^{exp} - F_i^{calc}| \qquad 6.6$$

Where Z_T is the total number of data points in the system, F^{exp} is the experimentally measured variable and F^{calc} is the calculated variable such as temperature or vapour mole fraction.

Using the binary systems within the ternary system of 1-propanol/2-butanone/propyl formate (Figure 6.1) it can be seen that the correlation of the NRTL model is accurate, showing a decent fit for all three binary systems. A slight deviation in the dew point of the 2-butanone/propyl formate system is noticed in which a smaller amount of separation is seen. this can be expected however, due to the experimentally found separation being bellow the uncertainty of composition. This shows a good chance of an accurate correlations of the ternary system containing propyl formate. Similar outcomes for the binary systems in the other three ternary systems can be seen in Appendix G.

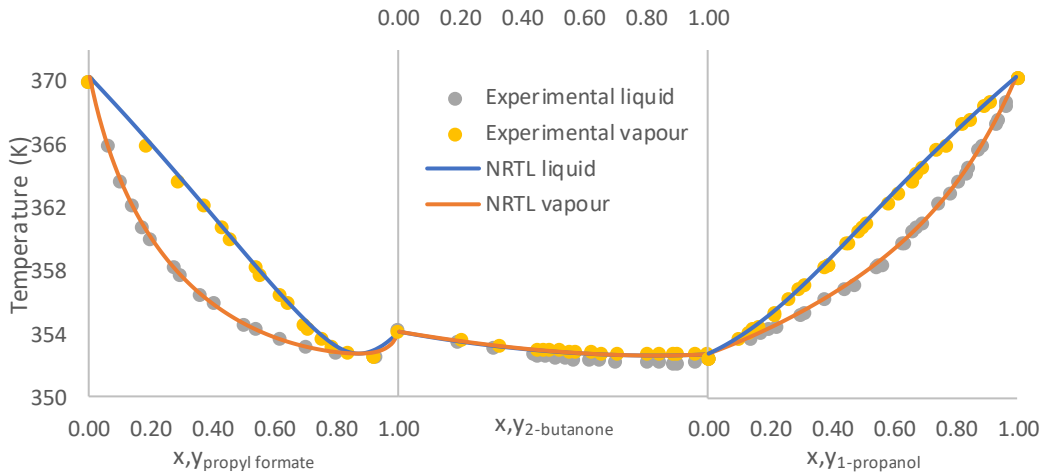

Figure 6.1:NRTL correlative outcomes of the binary systems 1-propanol/2-butanone, 2-butanone/propyl formate, and 1-propanol/propyl formate used to create a ternary diagram of 1-propanol/2-butanone/propyl formate.

Table 6.1: NRTL binary parameter correlation for the nine binary systems, as well as the absolute average deviation of the model from temperature and vapour composition

1-propanol/2-butanone/propyl formate						
Mixture	Aij0	Aij1	Aji0	Aji1	AAD(T)	AAD(y1)
1-propanol/2-butanone (1)	9934.9	-29.242	13477	-31.340	0.331	0.009
1-propanol (1)/propyl formate	1180.4	-7.5790	3043.6	6.4440	0.425	0.009
2-butanone (1)/propyl formate	249820	-706.00	-316620	896.00	0.215	0.003
Average					0.324	0.007

1-propanol/2-butanone/ethyl acetate						
Mixture	Aij0	Aij1	Aji0	Aji1	AAD(T)	AAD(y1)
1-propanol/2-butanone (1)	9934.9	-29.242	13477	-31.340	0.331	0.009
1-propanol (1)/ethyl acetate	7315.5	-16.972	7153.5	-18.244	0.213	0.005
2-butanone (1)/ethyl acetate	-16792	46.302	7999.1	-20.171	0.206	0.002
Average					0.250	0.005

1-propanol/2-butanone/methyl propionate						
Mixture	Aij0	Aij1	Aji0	Aji1	AAD(T)	AAD(y1)
1-propanol/2-butanone (1)	9934.9	-29.242	13477	-31.340	0.331	0.009
1-propanol (1)/methyl propionate	-2352.2	12.196	30197	-83.494	0.288	0.003
2-butanone (1)/methyl propionate	2322.2	-8.2240	2317.7	-3.7600	0.273	0.002
Average					0.297	0.005

1-propanol/2-butanone/2-propanol						
Mixture	Aij0	Aij1	Aji0	Aji1	AAD(T)	AAD(y1)
1-propanol/2-butanone (1)	9934.9	-29.242	13477	-31.340	0.331	0.009
1-propanol (1)/2-propanol	1576.6	-10.349	-35471	106.59	0.161	0.005
2-butanone (1)/2-propanol	2123.8	-5.1040	2997.5	-5.2780	0.051	0.004
Average					0.181	0.006

Using the AAD values for the temperature and the vapour mole fraction (Table 6.1), the maximum absolute average deviation in temperature for the NRTL correlation is 0.425 K, with a maximum deviation in mole fraction of 0.009. This reiterates what an accurate prediction would be for the perturbation type models.

Further evidence of a good correlation of the binary data is seen looking at the Gibbs free energy of the system, in which the experimental data in all four ternary systems agrees with the NRTL correlation (Figure 6.2.).

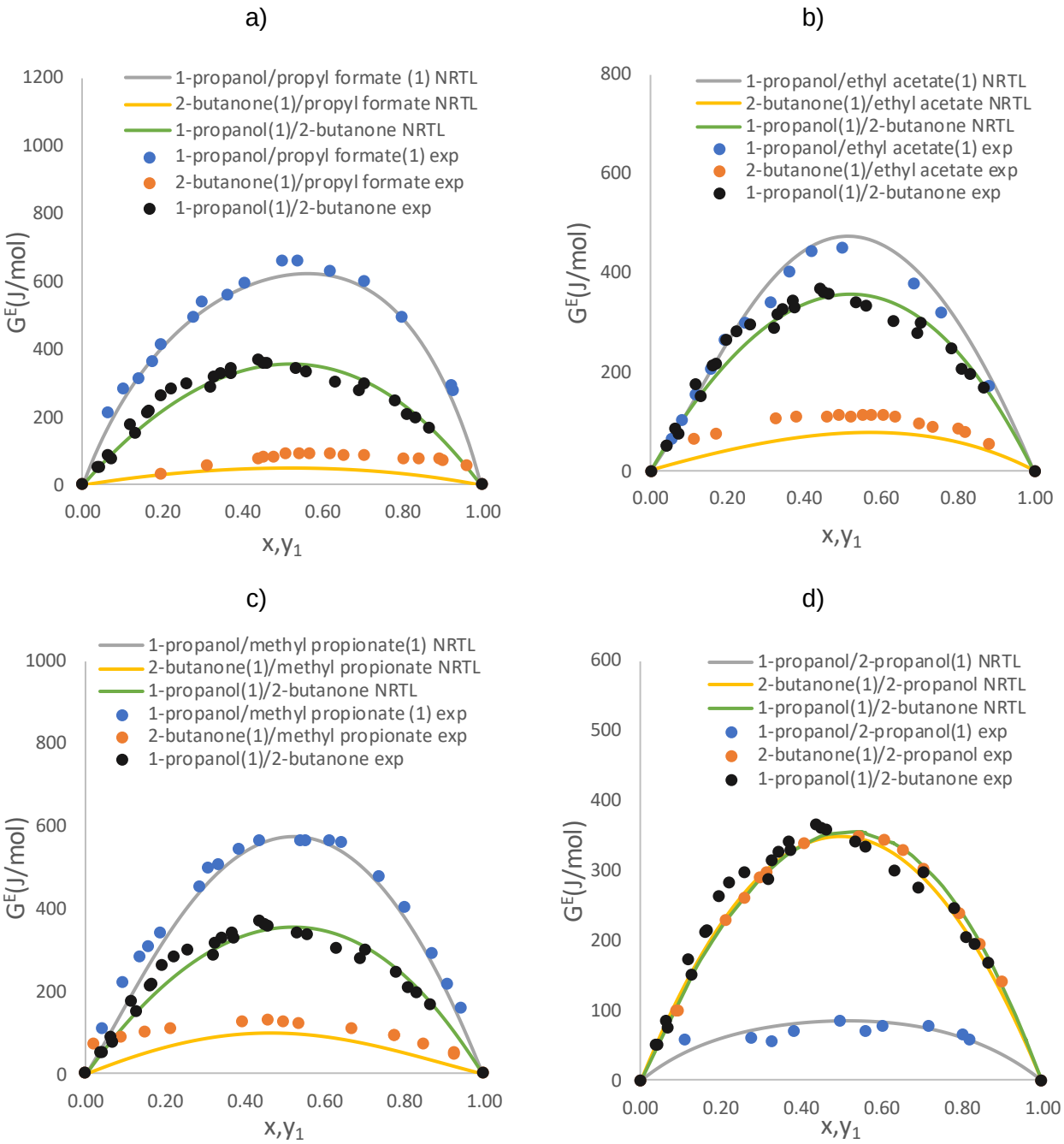

Figure 6.2: Excess Gibbs free energy of NRTL vs the excess free Gibbs energy of the experimental data in the four ternary systems. a) 1-propanol/2-butanone/propyl formate. b) 1-propanol/2-butanone/ethyl acetate. c) 1-propanol/2-butanone/methyl propionate. d) 1-propanol/2-butanone/2-propanol

The BIPs of Table 6.1 have been utilized to correlate the phase equilibria of the studied ternary systems. Table 6.2 lists the deviation of calculated temperature and vapor compositions regarding the ternary experimental VLE data.

Table 6.2: NRTL predictions for the four studied ternary systems, as well as the absolute average deviation of the model from temperature and vapour compositions

Ternary system	AAD (T)	AAD(y1)	AAD(y2)	AAD(y3)
1-propanol/2-butanone/propyl formate	0.588	0.024	0.014	0.021
1-propanol/2-butanone /ethyl acetate	0.419	0.011	0.007	0.009
1-propanol/2-butanone /methyl propionate	1.092	0.022	0.015	0.009
1-propanol/2-butanone /2-propanol	1.071	0.022	0.020	0.014
Average	0.793	0.02	0.014	0.013

Table 6.2 also shows good correlation of the ternary systems using the NRTL model. However, AAD values are slightly higher compared to those found in the binary systems. This is especially true in the methyl propionate and the 2-propanol system, when looking at the deviation in temperature.

This deviation would require ternary interaction parameters to lower this value and find a more accurate representation. This leads to the belief that there is a slight deviation from binary to ternary modelling. If a similar deviation is noticed with the ternary predictive models it can therefore be assumed that there is more work needed in the development of these models, bringing into question the assumption that accurate binary modelling will lead to accurate multicomponent modelling.

The results however, especially the propyl formate and ethyl acetate systems are still accurate. It is important to note that the results of the ternary prediction of the SAFT type EoS will be slightly less accurate than the binary predictions of these thermodynamic models, as seen with the NRTL model. As the complexities of the interactions increase with the addition of more components. This is especially true when there is not one dominant component in the interactions such as at high concentrations of 1-propanol.

Using the ternary systems containing propyl formate (Figure 6.3), as well as temperatures ranging from 354.15-356.60 K. This range allowing for an array of different compositions, while not completely overwhelming the graph to the point that predictions of the tie lines cannot be seen. A visual example of the NRTL correlations is shown, in which a good outcome of the model is noticed.

Similar results with the NRTL model and ternary systems can be seen in Appendix G.

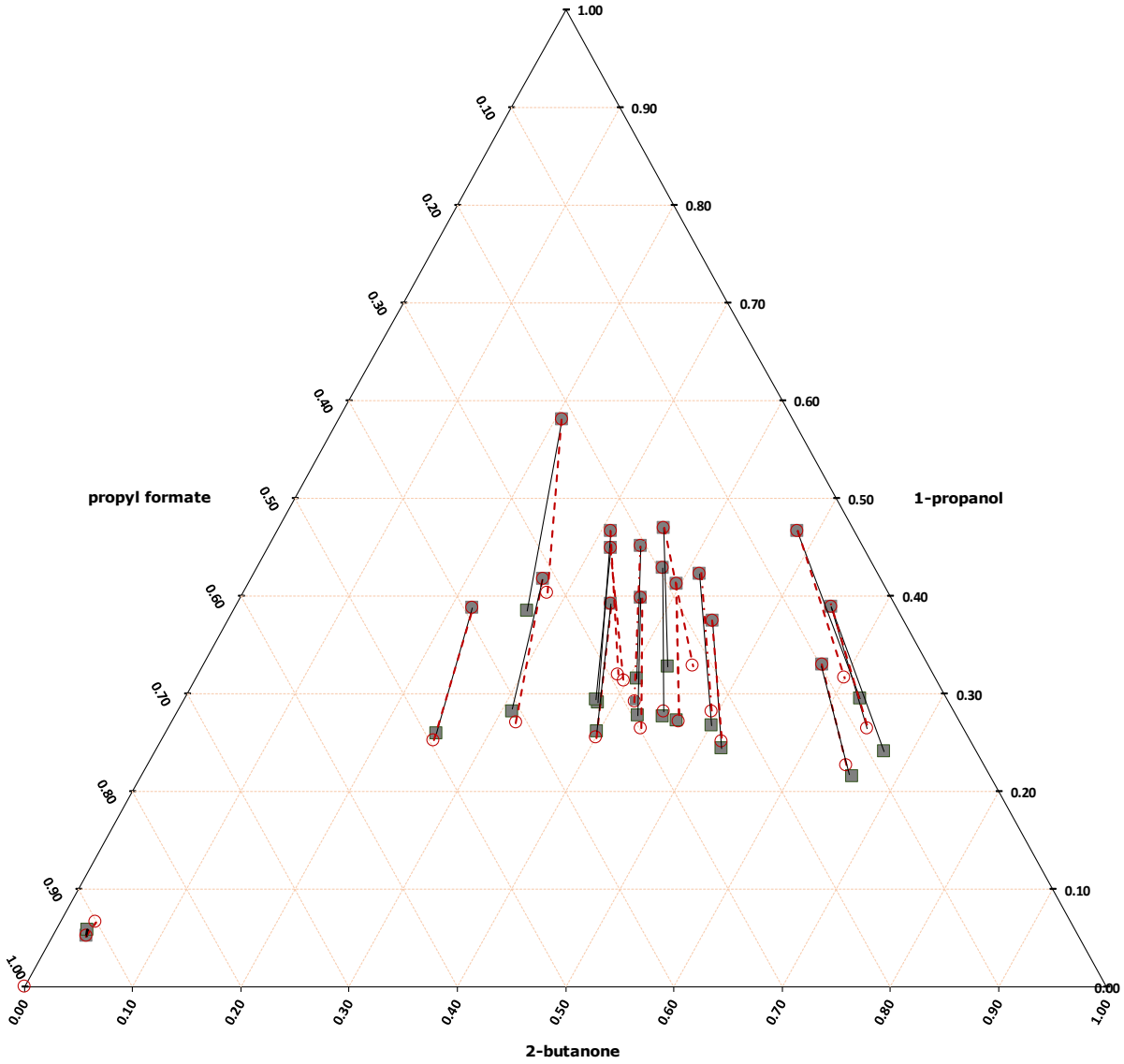

Figure 6.3: NRTL correlative outcomes of the ternary systems 1-propanol/2-butanone/propyl formate for T=354.13-358.55 K. solid lines with grey squares represent experimental tie-lines, and dashed lines with red circles represent the calculated tie-lines using the NRTL model

6.2. Pure component parameters

The TR*Solutions* software created by De Villiers, 2011 [35] in the Separations Technology group at Stellenbosch University was used in the VLE prediction results.

Before the VLE predictions can be made the choice of association scheme for the self-associating components, 1-propanol, and 2-propanol, is needed. These association schemes correspond to the three types of association sites: positive acceptor sites, negative donor sites, and bipolar sites [32].

Table 6.3: Association schemes for alcohols in the perturbation theory models, taken and re-drawn from Kontogeorgis et al. [9]

Formula	Scheme	Sites
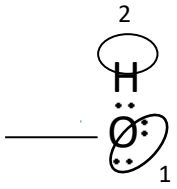	2B	1 electron donor 1 electron accepter
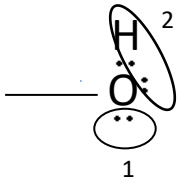	2C	1 bipolar 1 electron donor
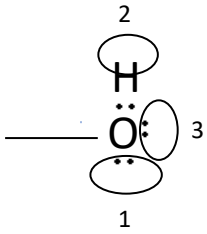	3B	2 electron donors 1 electron accepter

Although different schemes have different levels of accuracy depending on the types of interactions occurring, for example the 2C scheme results in better accuracy for alcohol/water interactions and worse for alcohol/alkane, it was decided to keep the scheme constant in this work. This would allow for direct comparison of the three models ability of modelling the ternary system in which alcohol/alcohol, alcohol/ester, and alcohol/ketone interactions are all involved. When looking at cross association between alcohol/ketone and alcohol/ester, the 2B scheme for the alcohol shows accurate predictions [32]. This led to both alcohols modelled with the 2B scheme having one positive and one negative site. Due to the ketones and esters not self-associating but cross associating these systems are modelled with one negative site, allowing the alcohol to cross-associate with these components.

The pure component parameters are available for SAFT-VR-Mie-GV and sPC-SAFT-GV for all the components used in previous research done by the Stellenbosch University's Separations Technology group [32], [33], [112]. Pure component parameters are also available for CPA-GV [32], [98], for all components except 2-propanol (Appendix F). Assessing the accuracy of the pure component parameters is not within the scope of this work. However, with no parameters existing, pure parameter regression was required.

An objective function using pure component properties including saturated vapour pressure (P^{sat}), liquid density (ρ^{liq}), and the heat of vaporisation (ΔH^{vap}) and binary data where the second component is an alkane (2-propanol/n-hexane[114]) [115] is used to regress the CPA-GV pure component parameters of 2-propanol (Equation 6.5).

$$OF = \sum_{i=1}^{NP} [\alpha \left(\frac{P_i^{sat,reg} - P_i^{sat,exp}}{P_i^{sat,exp}} \right)^2 + \beta \left(\frac{\rho_i^{sat,reg} - \rho_i^{sat,exp}}{\rho_i^{sat,exp}} \right)^2 + \gamma \left(\frac{\Delta H_i^{vap,reg} - \Delta H_i^{vap,exp}}{\Delta H_i^{vap,exp}} \right)^2 + \eta \, (X_i^{VLE,error})^2] \quad 6.8$$

Where α, β, ϒ, and ɳ are regression weights, values of 10, 8, 4, and 1 respectively were used as these are the common regression weights used for similar components in previous studies[32], [100], [112].These parameters can be seen in Appendix H.

Table 6.4: Regression results for 2-propanol for the pure component parameters of CPA-GV

Component	a0/R_b (K)	ε^{AB}/k (K)	κ^{AB}	B	c1	μ (D)	n_p
2-propanol	2061	2437	0.0060	0.0650	0.9300	1.560	0.9400

Property	Components	Np	Temperature (K)	%AAD		Ref
P^{sat}	2-propanol	30	254.15-457.47	0.128		[110]
ρ^{sat}	2-propanol	30	254.15-457.47	0.857		[110]
H^{vap}	2-propanol	30	254.15-457.47	0.954		[110]
VLE	2-propanol + n-Hexane	18	323.15	x 0.993	y 1.380	[114]

Due to 2-butanone and the three C_4 esters cross-associating and hydrogen bonding with the two alcohols, even though they do not self-associate themselves, pure component cross-association parameters are needed for these components.

The cross-association parameters for the sPC-SAFT-GV EoS were taken from de Villiers, 2011 [35], in which the 'universal cross-association approach' [35] was used. In this approach the association volume (κ^{AB}) is set to the same value as the association volume of the 1-alcohol that is a similar molecular weight, 1-pentanol for the C_4 esters and 1-butanol for 2-butanone. The second association parameter the association energy ($\frac{\varepsilon^{AB}}{K}$) is fitted to existing binary data, these parameters were available for the C_4 esters, however, were not available for 2-butanone. Using the same method described in de Villiers, 2011[35] cross-association parameters for the 2-butanone system was regressed using binary systems seen in Table 6.5.

Table 6.5: Mixtures used in the regression of the association energy

	ethanol	1-propanol	2-propanol	1-butanol	2-butanol
2-butanone	[59]	[59]	[59]	[116]	[117]

Physically significant bounds were chosen for the regression of the association energy, those being $\frac{\varepsilon^{AB}}{K}$ = 1400-3000 [118].

The cross-association parameters for 2-butanone have been taken and used from Cripwell et al. 2019 [118]. In this article, an approach for accounting for solvation in mixtures containing ketones and ethers is suggested in the SAFT-VR-Mie-GV EoS model. Using a discretised regression approach, functional group specific cross-association parameters were found that can be used for any component in that homologous group [116]. Unpublished cross-association parameters for esters done by the same group using the same method was used in this work. The cross-association parameters used in this work can be seen below.

This leaves three different models, with three different approaches to cross-association. In which the CPA-GV EoS model will not be able to account for the cross-association. CPA is an industry-standard for associating systems and is considered as a benchmark for the more advanced SAFT models. The sPC-SAFT-GV EoS model uses a simplified method, using assumptions and fitted data to calculate a universal cross-association parameter[35], and the SAFT-VR-Mie-GV model expands on the 'universal cross-association approach', by using parameters that are universal for a homologous group, such as the esters and ketones. sPC-SAFT is functionally similar to the widely used PC-SAFT, while SAFT-VR Mie is the most advanced variant considered. This gives us a tiered approach to consider modelling performance.

Table 6.6: CPA + GV pure component parameters CPA + GV pure component parameters

component	1-propanol [35]	2-propanol*	2-butanone [35]	propyl formate [35]	ethyl acetate [35]
a0	2164	2061	2520	2455	2404
association energy	2587	2437	0	0	0
association volume	0.0070	0.0060	0	0	0
b	0.0640	0.0650	0.0740	0.080	0.080
c1	0.8590	0.9300	0.7740	0.830	0.880
dipole moment	0.1680	1.5600	2.760	1.910	1.780
polar segment	0.6130	0.9400	0.5680	1.290	1.490

Table 6.7: sPC-SAFT + GV pure component parameters

component	1-propanol [35]	2-propanol [112]	2-butanone [35]	propyl formate [35]	ethyl acetate [35]	methyl propionate
association energy	2342	2224	1667	1639	1639	1639
association volume	0.0358	0.0301	0.0159	0.0139	0.0139	0.0139
dipole moment	1.6800	1.700	2.7600	1.9100	1.7800	1.700
dispersion energy	225.4	204.5	227.3	222.1	210.6	219.2
polar segment	1.627	2.323	1.757	3.516	4.194	3.900
segment diameter	3.309	3.197	3.416	3.366	3.297	3.299
segment number	2.818	3.138	2.972	3.240	3.497	3.434

Table 6.8: SAFT-VR-Mie + GV pure component parameters

component	1-propanol [120]	2-propanol [120]	2-butanone [33]	propyl formate [33]	ethyl acetate [33]	methyl propionate [33]
association distance	0.400	0.400	0.400	0.400	0.400	0.400
association energy	2746	2691	2550	1850	1850	1850
association range	0.354	0.359	0.334	0.418	0.418	0.418
attractive exponent	6.000	6.000	6.000	6.000	6.000	6.000
dipole moment	0	0	2.760	1.910	1.780	1.700
dispersion energy	227.7	208.0	257.9	253.3	276.9	273.5
polar segments	0	0	1.430	2.930	3.370	3.700
repulsive exponent	10.18	10.53	11.96	12.03	13.96	13.44
segment diameter	3.561	3.441	3.614	3.590	3.640	3.630
segment number	2.336	2.579	2.603	2.810	2.740	2.730

These pure component parameters for each component were used to predict the experimental data of the nine binary systems and the four ternary systems.

6.3. Modelling of binary systems containing 1-propanol/ester or ketone

The CPA-GV EoS model is unable to take into account the cross association between a component that self-associates, and one that cross-associates but does not self-associate. As a result, large deviations from the experimental data are noticed, resulting in an inaccurate prediction (Figure 6.4). This inability to be able to model cross-association leads to a minimum azeotrope that is at a much lower temperature and mole fraction of methyl propionate than what was found experimentally.

The 1-propanol systems were well predicted in every case by the sPC-SAFT-GV model, accurate azeotropes and good agreement with the phase envelopes are shown (Appendix I). In terms of the 1-propanol/2-butanone system (Figure 6.4), it can be seen that the vapour and liquid prediction agree with the experimental data.

Very similar results are noticed using the SAFT-VR-Mie-GV model, with accurate azeotropes and a similar phase envelope to that of all the binary experimental data (Appendix I). In the 1-propanol/2-butanone system it can be seen that the SAFT-VR-Mie-GV model is more accurate in terms of temperature, this in turn shows the slight superiority of the cross-association parameters used.

The better accuracy in terms of temperature is noticed for all the 1-propanol/(ketone or ester) systems, except for the ethyl acetate system, in which less cross-association is expected due to the steric hindrance that this component exhibits.

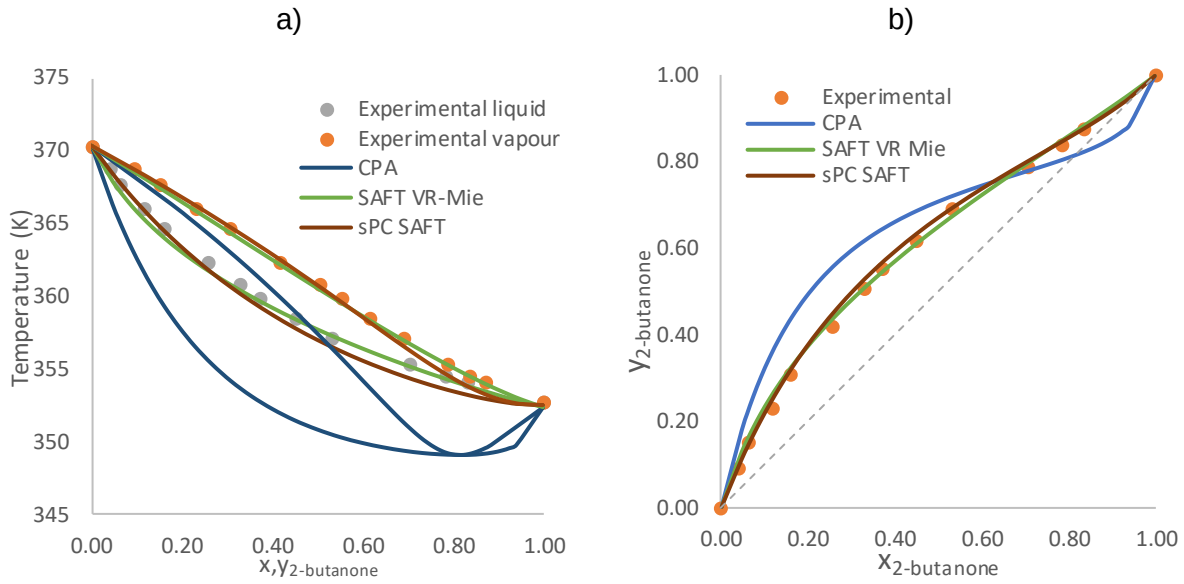

Figure 6.4: Modelling of the 1-propanol/2-butanone system with: CPA + GV; SAFT-VR-Mie + GV; and sPC-SAFT + GV. a) Txy representation of experimental data compared to the three models. b) xy representation of experimental data compared to the three models

Similar trends in all the 1-propanol/(ester-ketone) systems are noticed, in which the sPC-SAFT and the SAFT-VR-Mie models show a good prediction for the cross-association experienced(Appendix I).

6.4. Modelling of binary systems containing 2-butanone/ester

As with the NRTL correlation, prediction of the binary systems containing 2-butanone is difficult. With extremely close boiling points and little separation, visually inaccurate predictions occur. This little separation leads to the slight scatter seen in Figure 6.5 b, in which the y-x values are all below the uncertainty in concentration.

This manifests with all three of the models underestimating the deviation from the ideal state. With each model showing comparable outcomes for each system in the 2-butanone/ester systems. No model stands out with either accurate or inaccurate predictions, as all three models have similar downfalls (Figure 6.5).

With no cross-association occurring within the 2-butanone/ester systems it was expected for all three models to produce similar outcomes. Visually the models produced vastly different outcomes, however, because of the small separation and close boiling points, the differences are magnified for these systems in a very small temperature range. The similarities are shown with all three models having similar AAD values for the three systems.

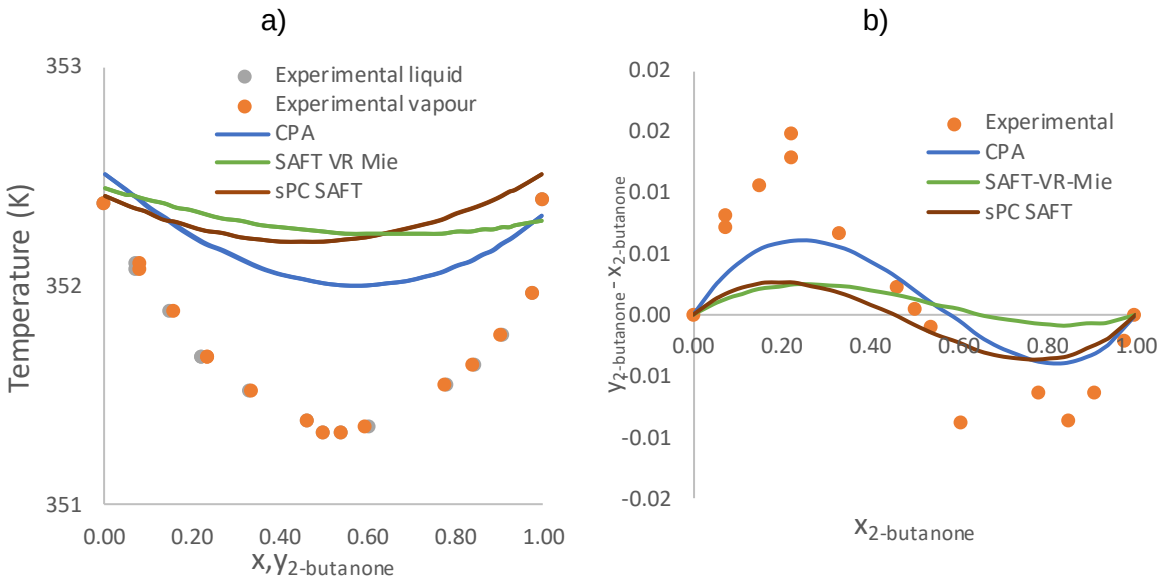

Figure 6.5: Modelling of the 2-butanone/methyl propionate system with: CPA + GV; SAFT-VR-Mie + GV; and sPC-SAFT + GV. a) Txy representation of experimental data compared to the three models. b) (y-x) vs x representation of experimental data compared to the three models

6.5. Modelling of binary systems containing 2-propanol

The modelling of the binary systems containing 2-propanol show slightly different results compared to the systems containing ketones or esters. With association parameters for both 2-propanol and 1-propanol the CPA-GV model more accurately predicts the cross-association between the two components (Figure 6.6 a). This is also noticed for the SAFT-VR-Mie-GV and sPC-SAFT-GV EoS models were near identical predictions are noticed.

Figure 6.6 c) shows that similar trends in the SAFT-VR-Mie-GV and the sPC-SAFT-GV models is noticed in the 2-butanone/2-propanol system, however, it can be seen that the SAFT-VR-Mie-GV EoS model is more accurate at predicting the azeotrope (Figure 6.6 d). The CPA-GV EoS model however still cannot account for the cross-association of the ketone and alcohol, and overpredicts the deviation from the ideal state. It can therefore be concluded that the 'universal cross-association approach' that relies on the primary alcohols, will show less accurate results compared to the more complex approach.

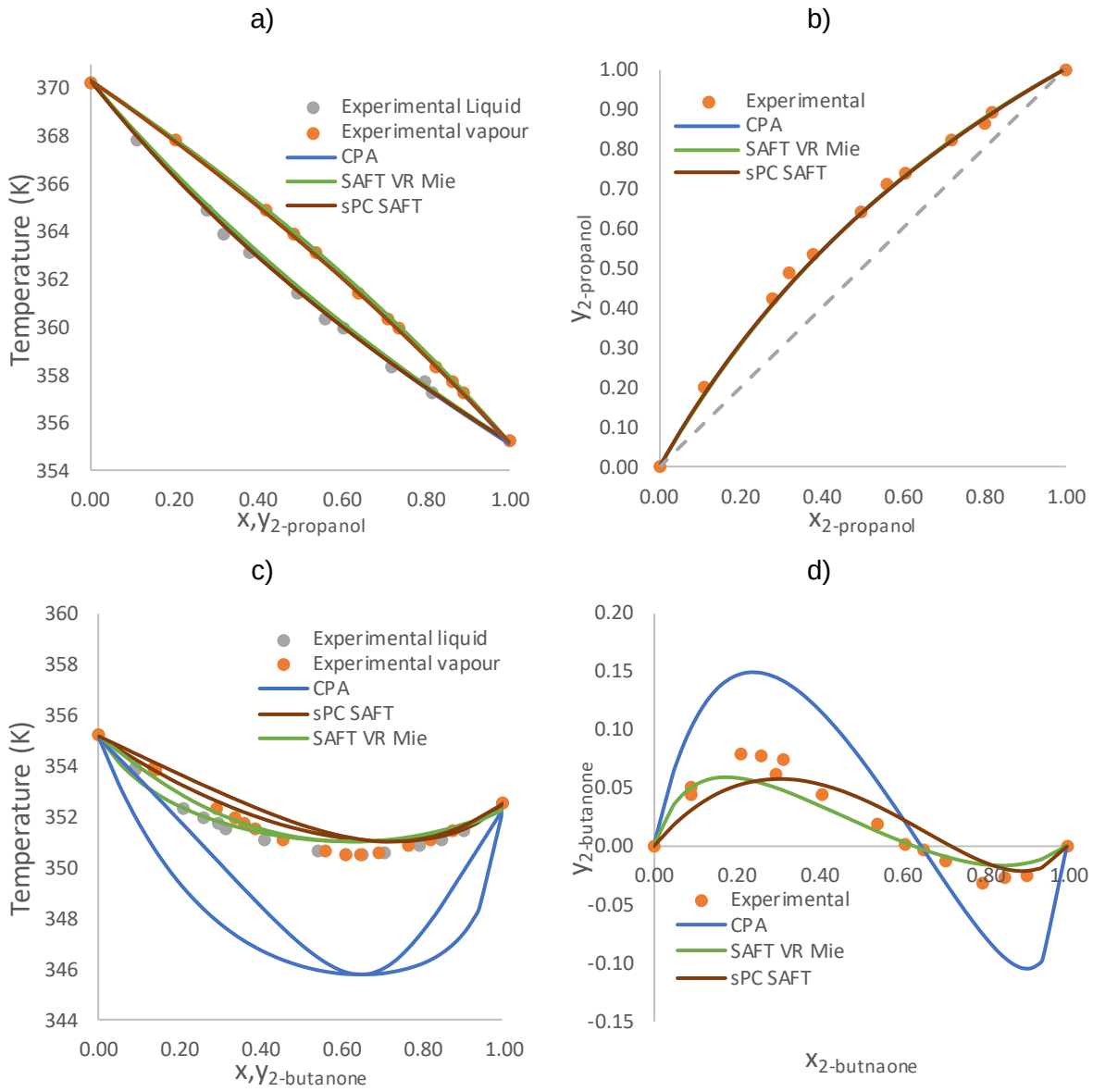

Figure 6.6:Modelling of the 1-propanol/2-propanol and 2-butanone/ 2-propanol systems witha) Txy representation of the 1-propanol/2-propanol. b) (y-x) vs x representation of the 1-propanol/2-propanol. c) Txy representation of the 2-butanone/2-propanol. d) (y-x) vs x representation of the 2-butanone/2-propanol.

6.6. Binary models in the ternary systems

Looking at the binary predictions for the systems that make up the ternary systems tested, it is possible to try see where the downfalls and the possible accurate modelling of the ternary systems will occur.

The three ternary systems containing the three C_4 esters show very similar trends when looking at the model predictions. At very low concentrations of 1-propanol the accuracy of the models is similar for all three models, overpredictions of the deviation from the ideal state for all models can be expected in this region (Figure 6.7 a, b, c).

The CPA-GV model will be expected to show large deviations from the experimental data and from the ideal state, especially at low concentrations of 1-propanol. It is expected that the CPA-GV EoS model will not be able to accurately model the ternary systems.

The sPC-SAFT-GV EoS model is expected to predict the ternary systems containing the C_4 esters well, like the other two models' small deviations at low concentrations of 1-propanol is expected. Due to the inability of the model to predict the binary azeotrope in the 2-butanone/propyl formate and 2-butanone/methyl propionate systems the prediction of the distillation boundary is not expected to be accurate.

The SAFT-VR-Mie-GV EoS model is expected to show more accurate predictions of the Ternary systems. It is also expected that the model will not be able to predict the distillation boundary that exists in these models (Figure 6.7 a, b, c), however, small deviations will be expected at low concentrations of 1-propanol.

A more accurate distillation boundary is expected in the ternary system containing methyl propionate, as the sPC-SAFT-GV and SAFT-VR-Mie-GV EoS model predicted the azeotropic point in the 2-butanone/methyl propionate system with a greater amount of accuracy, compared to the other 2-butanone/ester systems.

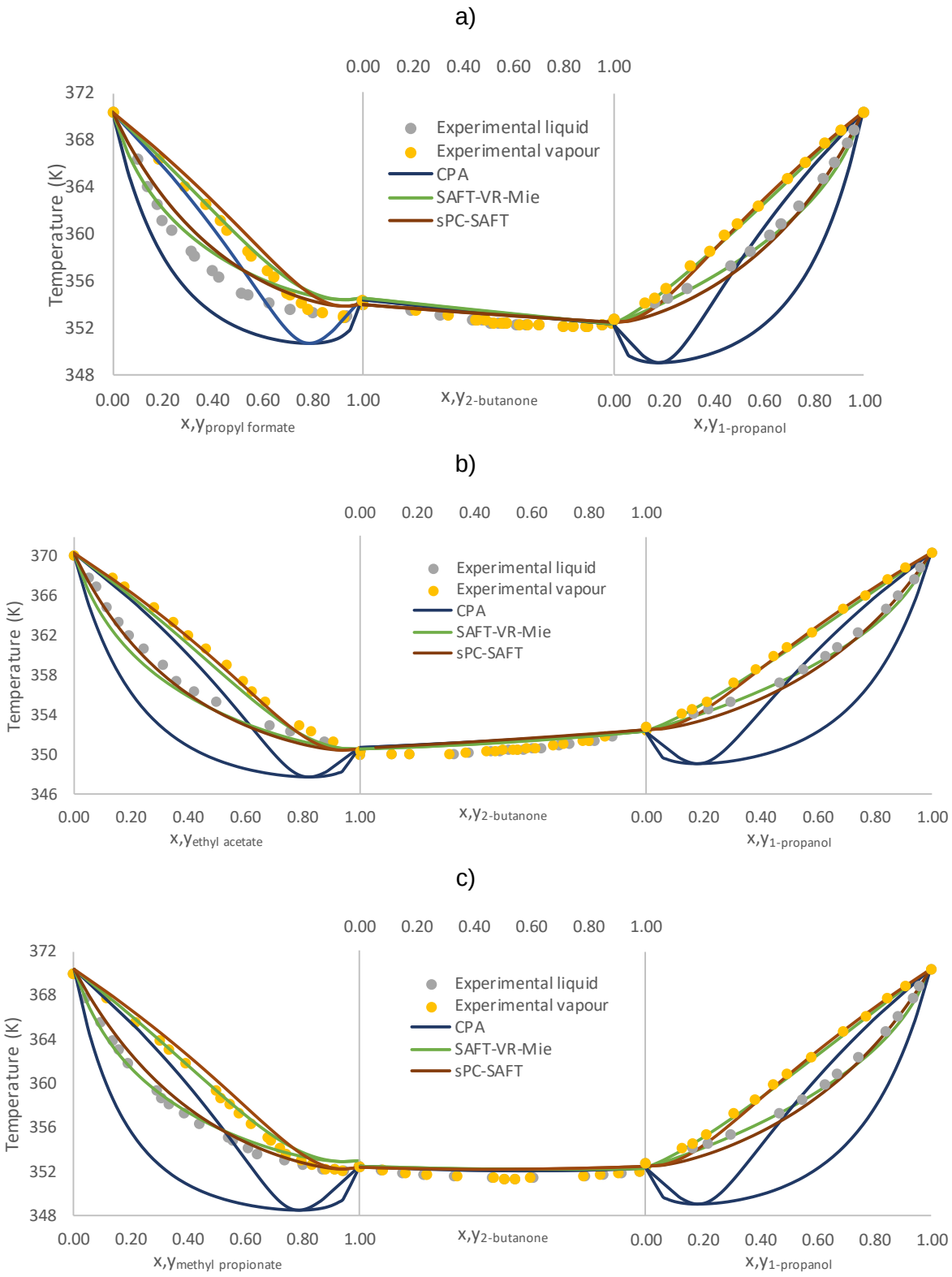

Figure 6.7: Model predictions of the binary systems contained in the ternary systems with C_4 esters. a) propyl formate. b) ethyl acetate. c) methyl propionate

The CPA-GV model is expected to more accurately predict the ternary system containing 2-propanol compared to the predictions in the C_4 ester ternary systems at high concentrations of both 1-propanol, and 2-propanol. However, due to the large deviation from the experimental

data in the 1-propanol/2-butanone and the 2-butanone/2-propanol systems less accurate predictions are expected at higher concentrations of 2-butanone (Figure 6.8).

The SAFT-VR-Mie-GV model is also expected to be more accurate compared to the C_4 ester systems as the deviation from the ideal state in the 1-propanol/2-propanol system is lower than that of the C_4 esters, the model is able to predict the cross association in this system more accurately. Similar outcomes are expected in the sPC-SAFT-GV model to that of the SAFT-VR-Mie-GV model.

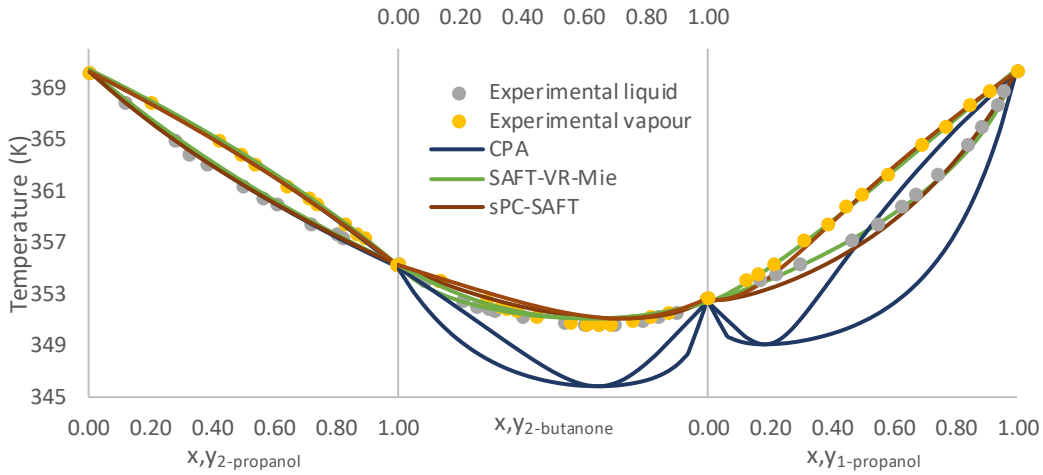

Figure 6.8: Model predictions of the binary systems contained in the ternary systems with 2-propanol.

Using the AAD values calculated for the nine binary systems it can be seen that the predictions are not as accurate as the correlations of the NRTL system (Table 6.9). However, because the perturbation theory models predict rather than correlate, it can be expected for slightly less accurate models. The CPA model which does not account for the cross-association between the ketone/esters and alcohols is expected to produce poor results for the ternary systems.

The sPC-SAFT-GV model predicts the systems contained in the four ternary models with accurate results, showing low AAD values. It is therefore expected for this model to accurately predict the ternary VLE data to a similar degree.

Similar outcomes were noticed with the SAFT-VR-Mie-GV EoS model. However, with the more complex cross-association parameter approach, it is expected for this model to have slightly better predictions than the sPC-SAFT model, as was shown in the binary systems.

Table 6.9: CPA-GV , SAFT-VR-Mie-GV, and sPC-SAFT-GV predictions for the nine binary systems, as well as the absolute average deviation of the model from temperature and vapour composition

1-propanol/2-butanone/propyl formate						
Mixture	CPA-GV		SAFT-VR-Mie-GV		sPC-SAFT-GV	
	AAD(T)	AAD(y1)	AAD(T)	AAD(y1)	AAD(T)	AAD(y1)
1-propanol/2-butanone	5.236	0.072	0.348	0.009	0.876	0.015
1-propanol/propyl formate	2.818	0.044	1.183	0.027	1.274	0.020
2-butanone/propyl formate	0.644	0.004	0.665	0.005	0.639	0.002
Average	2.899	0.040	**0.732**	**0.013**	0.930	0.012

1-propanol/2-butanone/ethyl acetate						
Mixture	CPA-GV		SAFT-VR-Mie-GV		sPC-SAFT-GV	
	AAD(T)	AAD(y1)	AAD(T)	AAD(y1)	AAD(T)	AAD(y1)
1-propanol/2-butanone	5.236	0.072	0.348	0.009	0.876	0.015
1-propanol/ethyl acetate	4.273	0.066	0.957	0.016	0.551	0.010
2-butanone/ethyl acetate	0.608	0.012	0.493	0.011	0.641	0.011
Average	3.372	0.050	**0.599**	**0.012**	0.689	0.012

1-propanol/2-butanone/methyl propionate						
Mixture	CPA-GV		SAFT-VR-Mie-GV		sPC-SAFT-GV	
	AAD(T)	AAD(y1)	AAD(T)	AAD(y1)	AAD(T)	AAD(y1)
1-propanol/2-butanone	5.236	0.072	0.348	0.009	0.876	0.015
1-propanol/methyl propionate	4.543	0.067	0.488	0.007	0.509	0.011
2-butanone/methyl propionate	0.451	0.003	0.860	0.006	0.561	0.004
Average	3.410	0.048	**0.565**	**0.007**	0.648	0.010

1-propanol/2-butanone/2-propanol						
Mixture	CPA-GV		SAFT-VR-Mie-GV		sPC-SAFT-GV	
	AAD(T)	AAD(y1)	AAD(T)	AAD(y1)	AAD(T)	AAD(y1)
1-propanol/2-butanone	5.236	0.072	0.348	0.009	0.876	0.015
1-propanol/2-propanol	0.128	0.011	0.269	0.012	0.094	0.010
2-butanone/2-propanol	3.479	0.047	1.066	0.017	0.446	0.012
Average	2.948	0.044	0.561	0.013	**0.472**	**0.012**

A graphical representation of the AAD values can be seen in Figure 6.9. The CPA-GV EoS model has poor results with deviations from the 45^0 line of the y vs y graph (Figure 6.9 a). This deviation is also shown in Figure 6.9 d), in which the deviations shown in blue are far larger than that of the other two models.

More accurate predictions can be seen with regards to the SAFT-VR-Mie-GV and the sPC-SAFT-GV models in which the deviations follow the 45^0 line (Figure 6.9 a), it can also be seen in Figure 6.9 d) that the two models, shown with the green and brown data points that the

deviations are far smaller than that of the CPA model. This shows that the predictions for these models are more accurate.

This same trend can be seen for the other binary systems in the other three ternary systems (Appendix G).

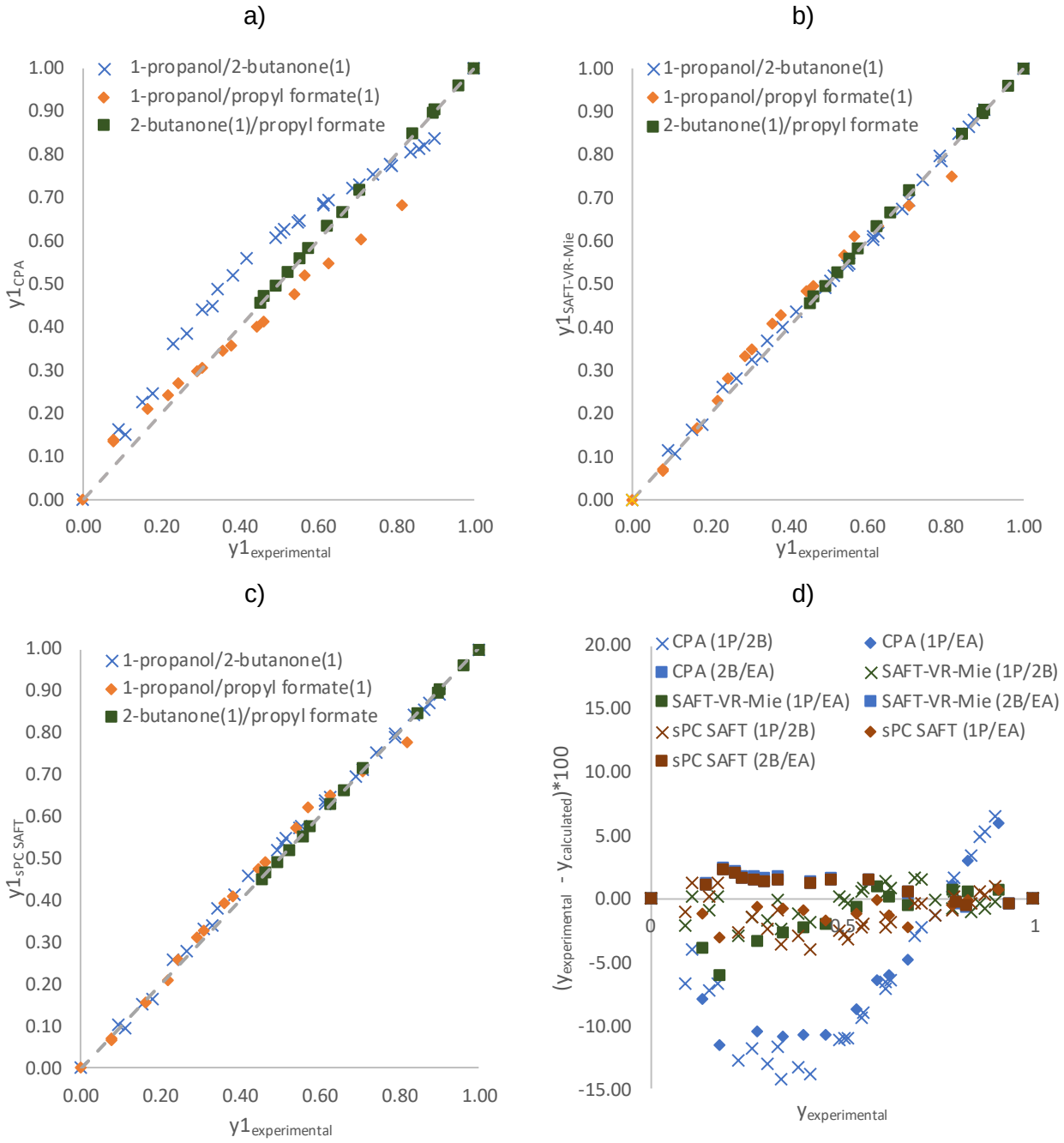

Figure 6.9: Graphical representation of the deviation of the experimental data from the predictive model of the binary systems in the propyl formate ternary system. a) $Y_{experimental}$ vs Y_{CPA}. b) $Y_{experimental}$ vs $Y_{SAFT\text{-}VR\text{-}Mie}$. c) $Y_{experimental}$ vs $Y_{sPC\ SAT}$. d) AADy(x10^2) values vs $y_{experimental}$

6.7. Modelling of the ternary systems

Using the same pure component parameters that were used for the binary systems (Table 6.6-8), the experimental data is compared to the predictions of CPA-GV, sPC-SAFT-GV, and SAFT-VR-Mie-GV. The accuracy of these ternary predictions can then be compared to the predictions of the binary systems.

As shown in Section 6.6 it is expected that the predictions of the ternary systems for CPA-GV would be inaccurate, whereas the predictions with the SAFT-VR-Mie-GV and sPC-SAFT-GV EoS models would be accurate. This is reiterated by Table 6.10.

The CPA-GV modelling of the ternary systems was poor, as this model does not take into account the cross-association that takes place between 2-butanone/C_4 esters and the alcohols. This results in AAD values in temperature and composition averaging 3.77 K and 0.038, 0.49, 0.035 mole fraction showing that the model is not accurate when predicting these systems.

While the CPA-GV model is shown to be inaccurate for ternary systems, the two SAFT type models sPC-SAFT-GV and SAFT-VR-Mie-GV, both of which take into account the cross-association of components that don't self-associate, are shown to predict more accurately. These systems have outcomes that are comparable to the NRTL ternary predictions with AAD values that average 0.720 K, and 0.019, 0.013, and 0.012 for sPC-SAFT-GV and 0.820 K, and 0.020, 0.014, and 0.016 mole fraction for the SAFT-VR-Mie-GV model.

These AAD values show that the sPC-SAFT-GV EoS model is the most accurate for the four ternary models tested, however the SAFT-VR-Mie-GV EoS models' predictions are comparable to that of the sPC-SAFT-GV model. It is also interesting to note that although the SAFT-VR-Mie-GV EoS model shows slightly less accurate predictions as a whole, it was better at predicting the vapour mole fractions compared to the sPC-SAFT-GV EoS model. However, both these models show accurate predictions.

Table 6.10: AAD values for the four ternary systems and the three predictive models

CPA-GV				
Ternary system	AAD (T)	AAD (y1)	AAD (y2)	AAD (y3)
1-propanol/2-butanone/propyl formate	4.27	0.037	0.034	0.026
1-propanol/2-butanone/ethyl acetate	4.19	0.042	0.026	0.021
1-propanol/2-butanone/methyl propionate	4.46	0.060	0.038	0.023
1-propanol/2-butanone/2-propanol	3.39	0.024	0.066	0.047
Average	4.08	0.041	0.041	0.029

sPC-SAFT-GV				
Ternary system	AAD (T)	AAD (y1)	AAD (y2)	AAD (y3)
1-propanol/2-butanone/propyl formate	0.75	0.020	0.013	0.022
1-propanol/2-butanone/ethyl acetate	0.40	0.013	0.009	0.012
1-propanol/2-butanone/methyl propionate	0.82	0.020	0.015	0.011
1-propanol/2-butanone/2-propanol	0.89	0.022	0.018	0.017
Average	0.72	0.020	0.014	0.016

SAFT-VR-Mie-GV				
Ternary system	AAD (T)	AAD (y1)	AAD (y2)	AAD (y3)
1-propanol/2-butanone/propyl formate	0.98	0.021	0.007	0.019
1-propanol/2-butanone/ethyl acetate	0.53	0.014	0.010	0.009
1-propanol/2-butanone/methyl propionate	0.99	0.022	0.015	0.009
1-propanol/2-butanone/2-propanol	0.79	0.022	0.020	0.011
Average	0.82	0.019	0.013	0.012

Looking at the deviations of the models from the vapour, and temperature predictions, allows for a systematic evaluation of the regions in which large deviations from the experimental data occur.

In the propyl formate ternary system it can be seen that the largest deviations occur at low concentrations of 1-propanol for the CPA-GV EoS model (Figure 6.10 a), with more accurate predictions at other compositions. Temperatures are also seen to deviate at lower temperatures of the system, however as the temperature increases, and the system becomes more ideal the CPA-GV EoS model shows better results.

The predictions of both the SAFT-VR-Mie-GV and the sPC-SAFT-GV EoS models show more accurate results, without the evidence of systematic deviations. It can be seen that the two models predict lower concentrations of propyl formate than were experimentally found, this deviation is however small, but can be attributed to the models slightly overpredicting the cross-association that occurs. Temperatures that are more accurate are also seen in the two models. Similar outcomes are noticed in the other two systems containing C_4 esters, this can be seen in Appendix J. It can also be seen that the reason that the SAFT-VR-Mie-GV EoS

model has a slightly higher AAD (T) value may be due to the amount of data collected at similar temperatures. This may artificially increase the AAD (T) value for this model.

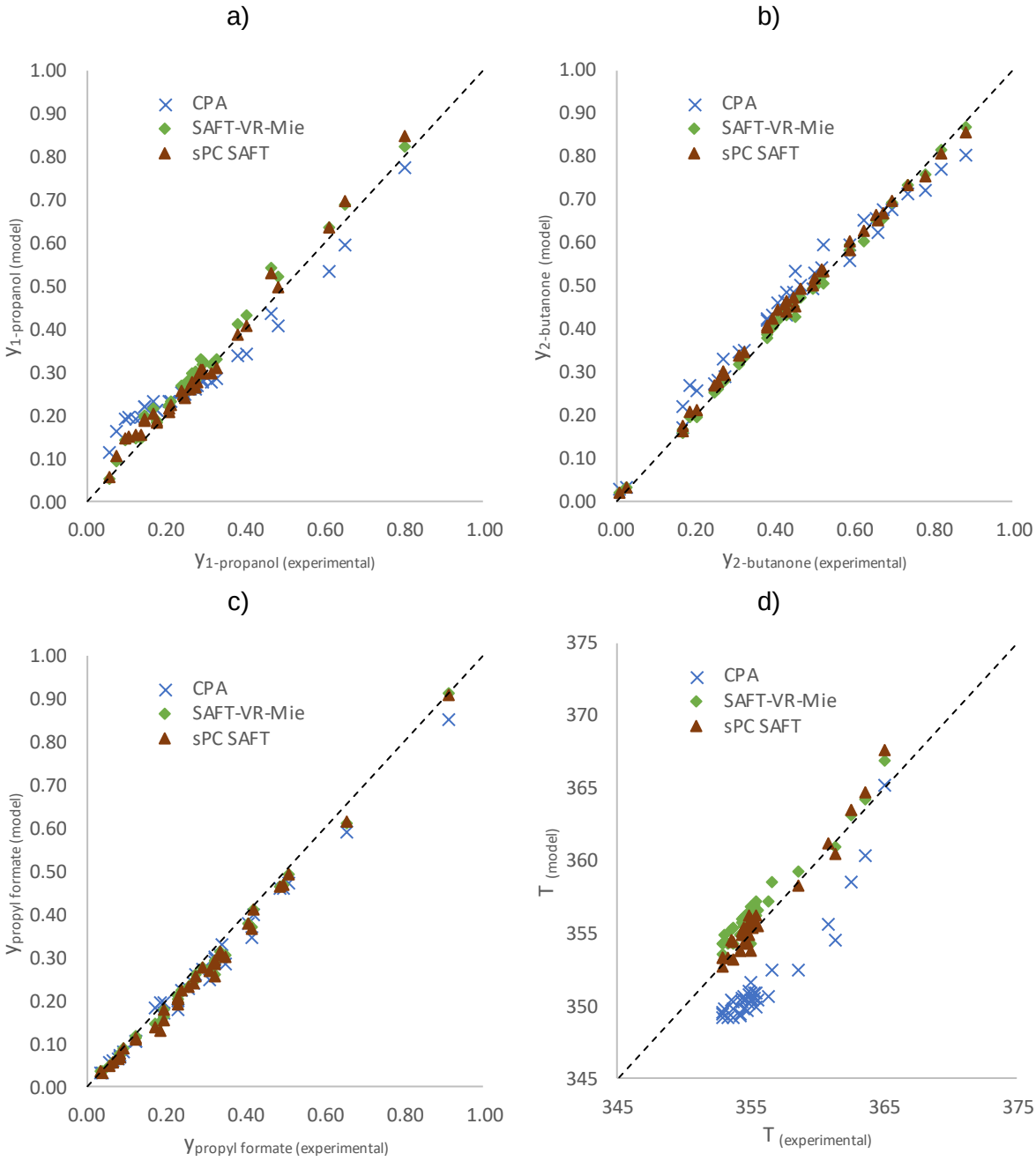

Figure 6.10: Graphical representation of the deviation of the experimental data from the predictive model in the propyl formate ternary system. a) $Y_{exp,1\text{-}propanol}$ vs $Y_{model,1\text{-}propanol}$. b) $Y_{exp,2\text{-}btunaone}$ vs $Y_{model,2\text{-}butanone}$. c) $Y_{exp,propyl\ formate}$ vs $Y_{model,propyl\ formate}$ d) $T_{exp,}$ vs T_{model}

Slightly different outcomes are noticed in the ternary system containing 2-propanol in the CPA-GV EoS model. As expected more accurate predictions of 1-propanol and 2-propanol are noticed. However, the predictions of 2-butanone show higher concentrations predicted compared to the experimental value, this is due to the 2-butanone component being the only non-self-associating, but cross-associating component in the system.

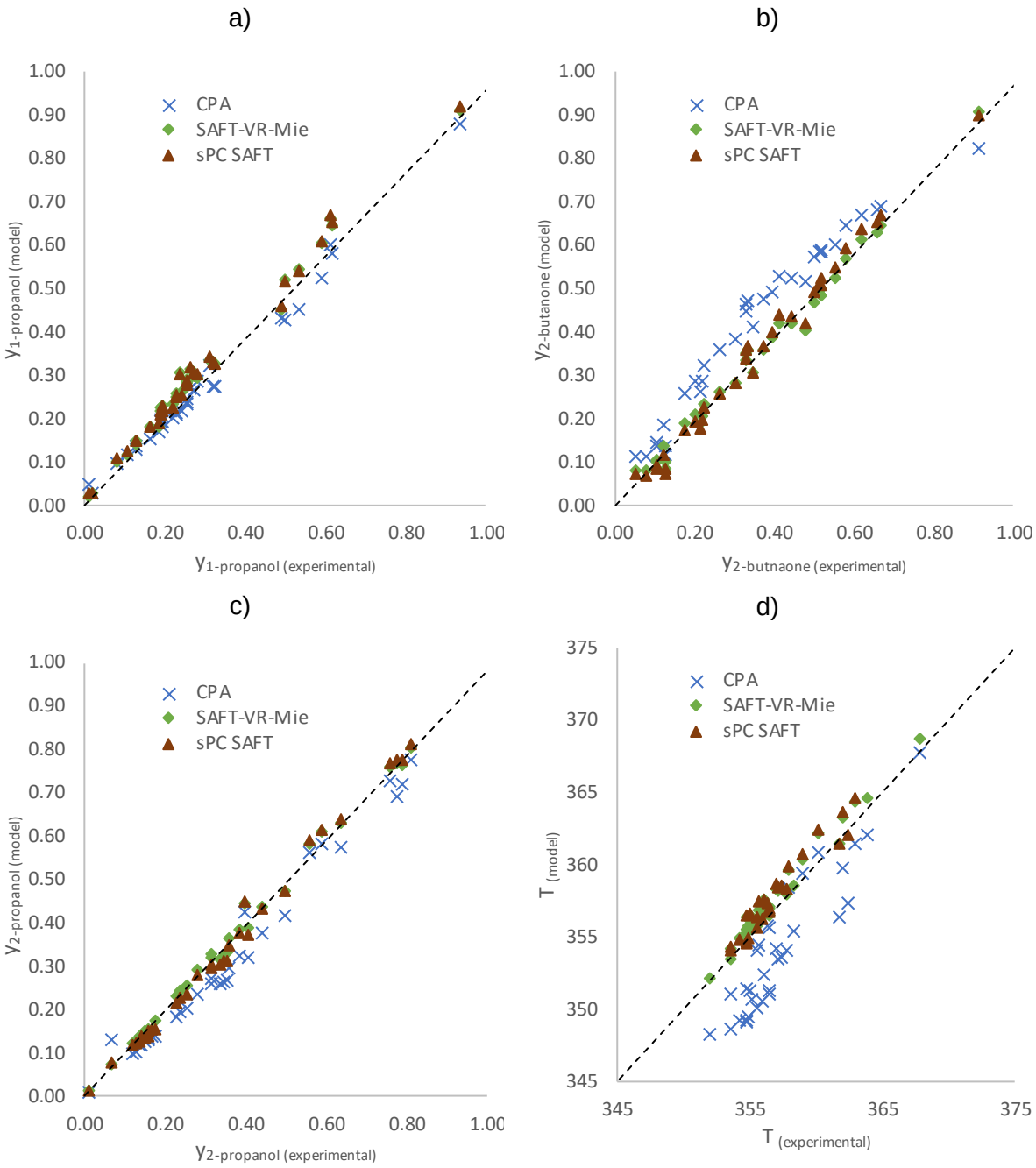

Figure 6.11: Graphical representation of the deviation of the experimental data from the predictive model in the 2-propanol ternary system. a) $Y_{exp,1\text{-}propanol}$ vs $Y_{model,1\text{-}propanol}$. b) $Y_{exp,2\text{-}btunaone}$ vs $Y_{model,2\text{-}butanone}$. c) $Y_{exp,2\text{-}propanol}$ vs $Y_{model,2\text{-}propanol}$ d) $T_{exp,}$ vs T_{model}

A graphical representation of the ternary prediction of the three models can be seen in Figures 6.12-6.14. for the ethyl acetate system. As with the NRTL graphical representation a range of temperatures with experimental data between 353.28-356.28 K was chosen, allowing for a good compositional range, while still being able to see the tie-line predications.

The CPA-GV EoS model shows the largest deviation from the experimental values, with completely different tie line sizes, as well as different tie-line slopes, this leads to a less accurate representation of the system. In the SAFT-VR-Mie-GV and sPC-SAFT-GV EoS

models good representations of the VLE can be seen (Figure 6.13 and Figure 6.14). Both models show similar vapour compositions and therefore tie-line slopes compared to the experimental data. This allows us to see that the predictions of the SAFT-VR-Mie-GV and sPC-SAFT-GV EoS models are visually accurate. Similar trends can be seen with the models and the other ternary systems in Appendix J.

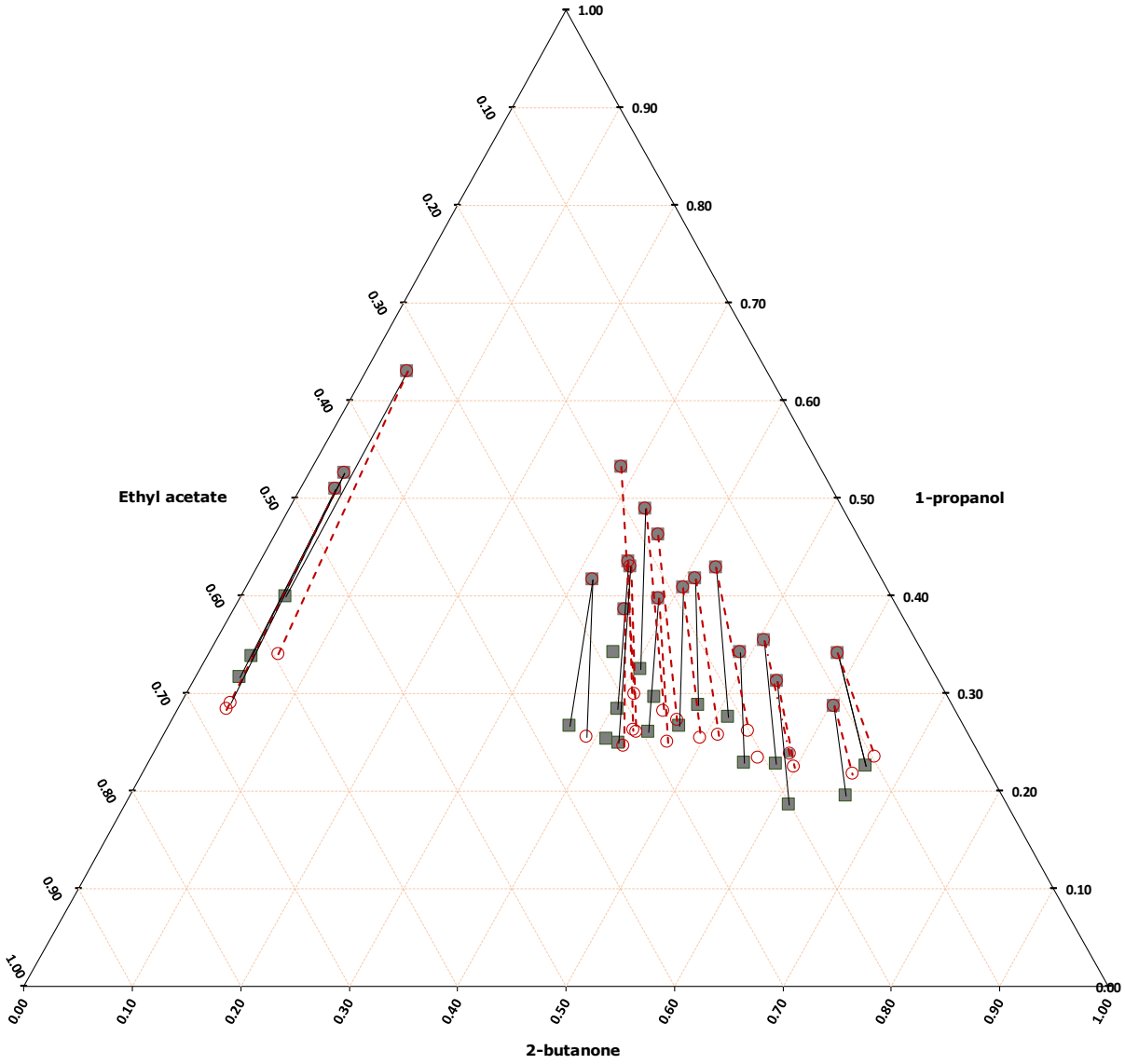

Figure 6.12: Predictions of the CPA-GV model of the ternary systems 1-propanol/2-butanone/ethyl acetate for T=353.28-356.28 K. Solid lines with grey squares represent experimental tie-lines, and dashed lines with red circles represent the calculated tie line

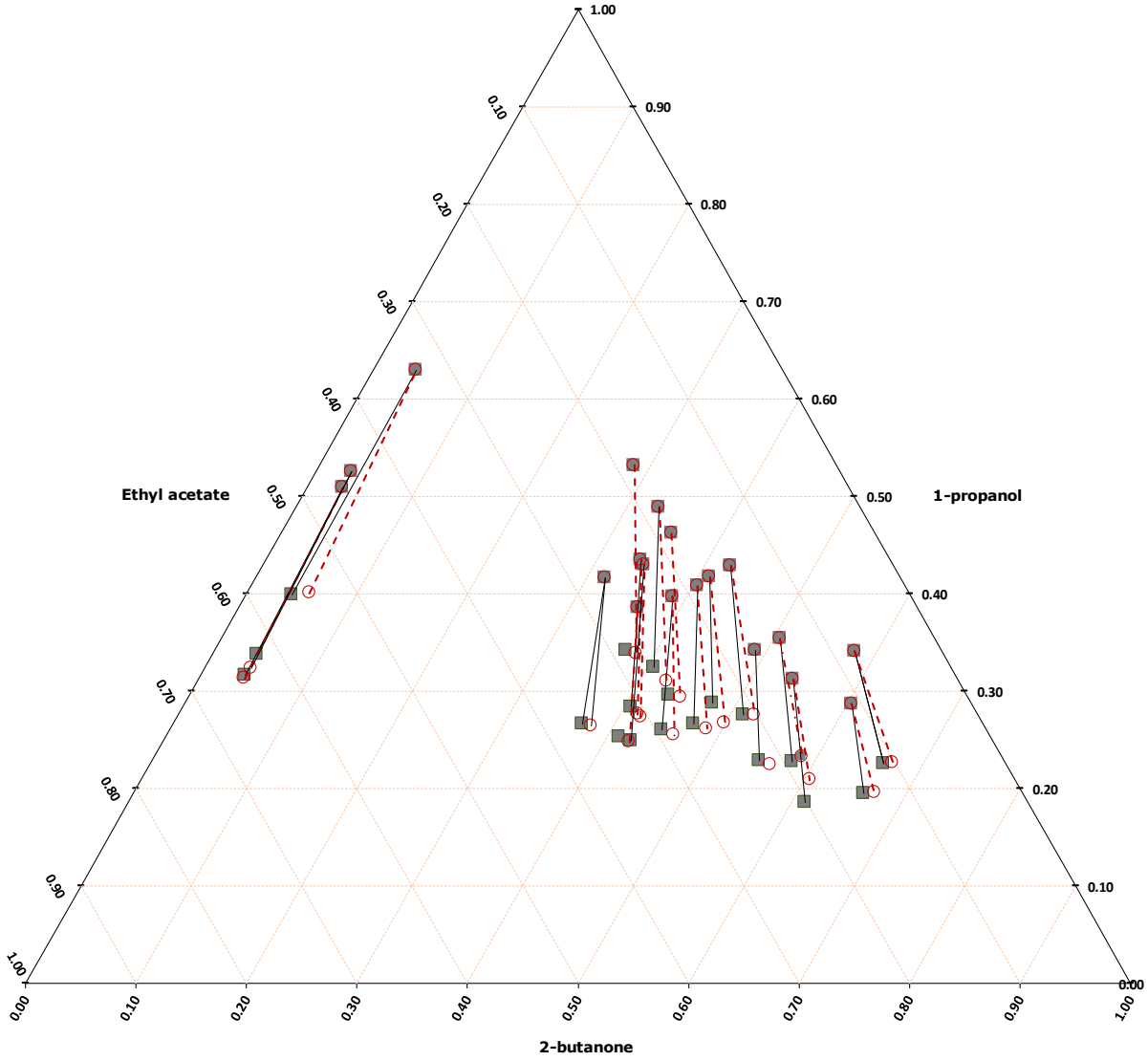

Figure 6.13: Predictions of the sPC-SAFT-GV model of the ternary systems 1-propanol/2-butanone/ethyl acetate for T=353.28-356.28 K. Solid lines with grey squares represent experimental tie-lines, and dashed lines with red circles represent the calculated tie line

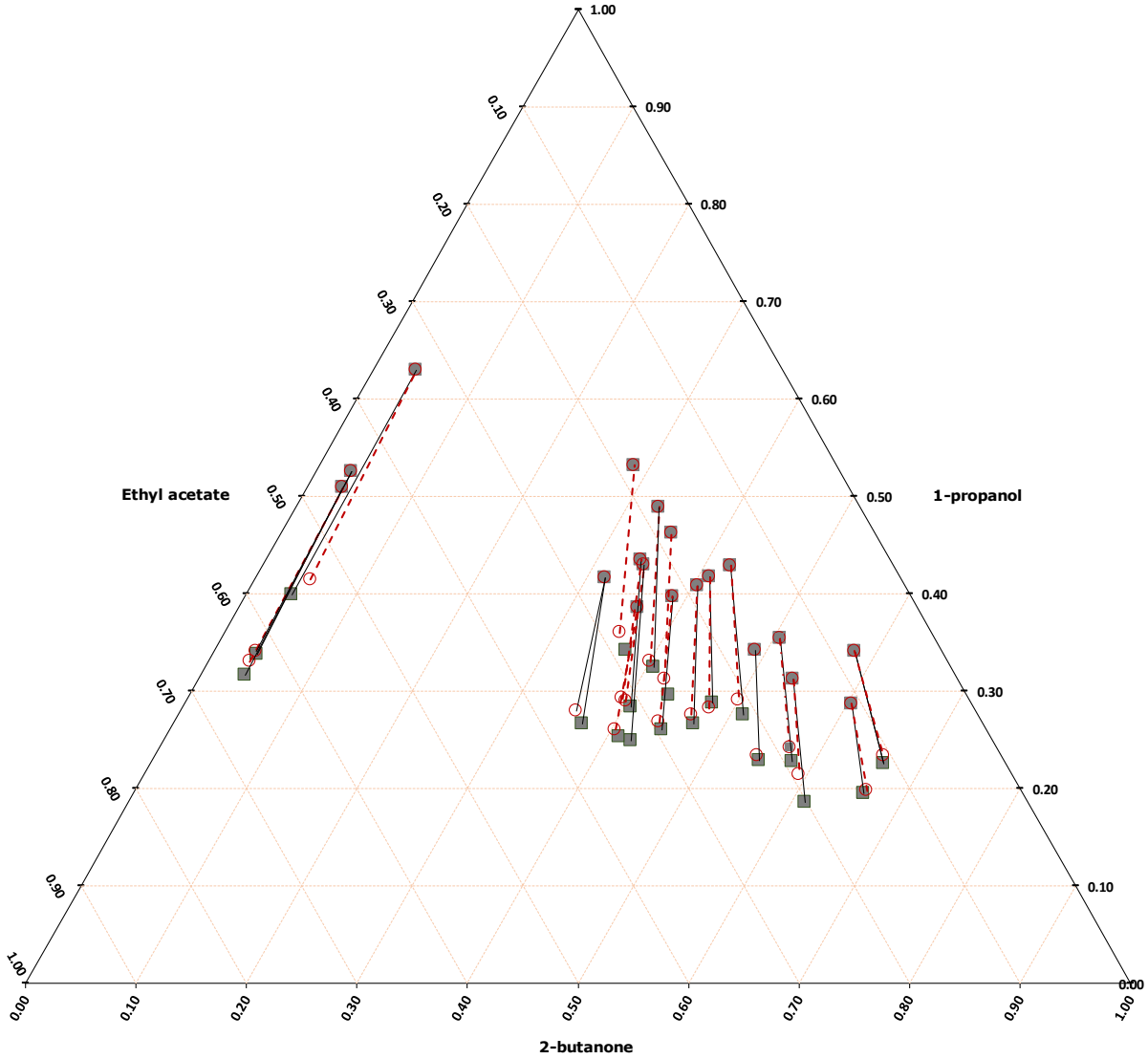

Figure 6.14: Predictions of the SAFT-VR-Mie-GV model of the ternary systems 1-propanol/2-butanone/ethyl acetate for T=353.28-356.28 K. Solid lines with grey squares represent experimental tie-lines, and dashed lines with red circles represent the calculated tie line

Although it is important to know how the tie lines in the xyz graph deviate from the experimental data, this does not tell the whole story. There is also a need to see where and by how much the temperature deviates. Using a colour scale in which blue is the lowest deviation and red is the highest deviation from the experimental temperature, it is useful to see which model will show the greatest deviations. This will allow for the systematic evaluation on where the model is not able to accurately predict the outcomes.

The CPA model as shown above does not have pure component cross-association parameters for the C_4 esters and 2-butanone. This model has therefore shown to be inaccurate when modelling the four complex ternary systems. This is again shown when looking at the deviations in temperature. It is however interesting to see that each system follows similar

deviations to those in the binary systems. This can easily be seen in the 2-propanol system, where accurate modelling is noticed at low concentrations of 2-butanone, however as the concentration increases the more inaccurate the model becomes (Figure 6.15 d). This can also be seen in the propyl formate system (Figure 6.15 a), Because of the larger deviation from ideal state in the 1-propanol/propyl formate interactions compared to the 1-propanol/2-butanone interactions it can be seen that the propyl formate system is more accurate at lower concentrations of 2-butanone.

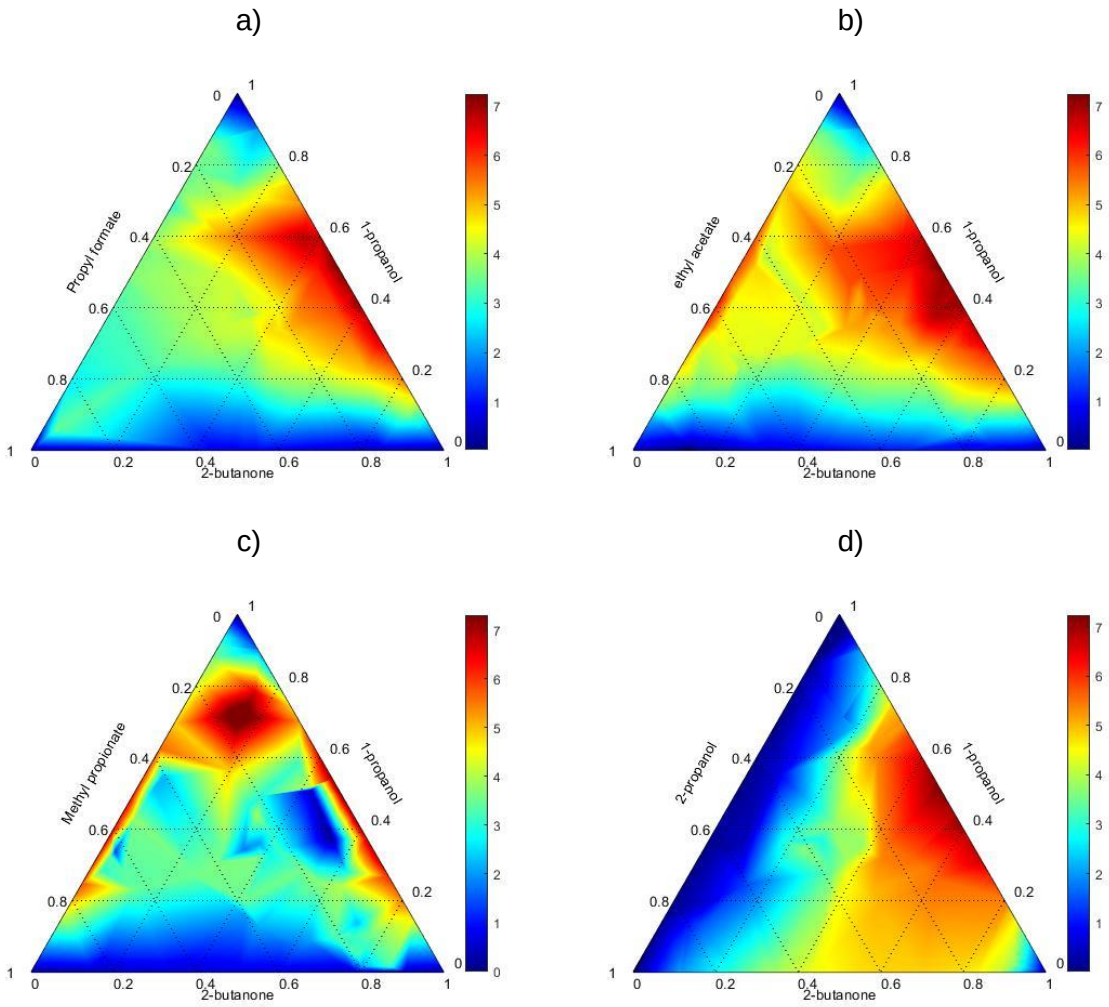

Figure 6.15: Colour map of temperature deviations of the CPA-GV model predictions from the experimental temperatures, for: a) Propyl formate system; b) ethyl acetate system; c) methyl propionate system; d) 2-propanol system

Looking at the four ternary systems temperature deviations using the sPC-SAFT-GV model it is important to note that the scale has been modified, to between 0-2 K instead of the 0-7 K as seen above. This is due to the more accurate predictions in this model.

From this it can be seen that the most ideal system ethyl acetate, also shows the lowest deviations from the experimental data, with only small deviations in the high 2-butanone concentrations (Figure 6.16 b). Deviations are expected at these concentrations with a binary azeotrope in the 2-butnaone/ethyl acetate system. This causes a more non-ideal region in the low concentration ethyl acetate high concentration 2-butanone region.

Similar to the ethyl acetate system, the deviations in the binary systems are similar to the concentrations where deviations occur in the ternary systems. For example, the deviation in the propyl formate system in a similar concentration to where the largest deviations occur in the 1-propanol/propyl formate occur (Figure 6.16 a). And at medium concentrations of 2-butanone/2-propanol, in the 2-propanol system (Figure 6.16 d).

These concentrations may not have the largest deviations from the ideal state, as these regions the model predicts well such as the azeotropes in the binary systems, but the deviations are in concentrations where strong intermolecular forces are noticed.

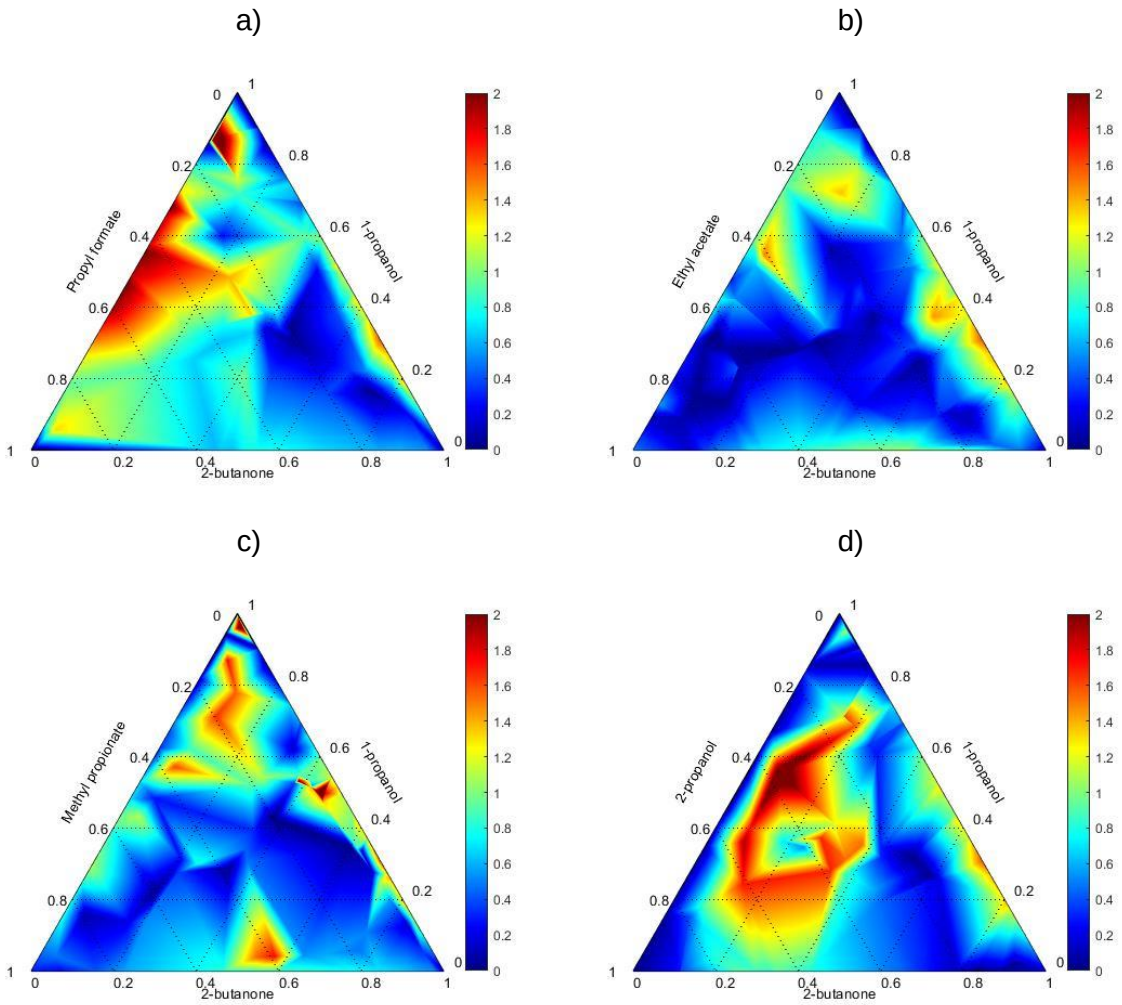

Figure 6.16: Colour map of temperature deviations of the sPC-SAFT-GV models predictions from the experimental temperatures, for: a) Propyl formate system; b) ethyl acetate system; c) methyl propionate system; d) 2-propanol system

The colourmap of the deviations in the SAFT-VR-Mie-GV model are also on a scale of 0-2 K showing very similar results to that in the sPC-SAFT-GV model.

The trends in the SAFT-VR-Mie-GV model show similarities to those of the sPC-SAFT-GV model and therefore no drastically different outcomes are noticed. It is however important to note that the type of cross-association pure component parameter method can be evaluated between these two models, when looking at the degree of deviations.

Similar to the sPC-SAFT-GV model the most ideal system is the most accurately modelled, the ethyl acetate system shows mostly accurate predictions of the temperatures. This system shows fewer poor predictions, however with more areas showing light blue, it can be seen that mostly average deviations are noticed.

This trend is repeated for the other three systems with the SAFT-VR-Mie-GV model, with fewer dark red areas, but more average light blue areas. With very similar AAD values between the

sPC-SAFT-GV and SAFT-VR-Mie-GV models, it can be seen that larger deviations are seen in the sPC-SAFT-GV systems, with more consistent results in the SAFT-VR-Mie-GV systems.

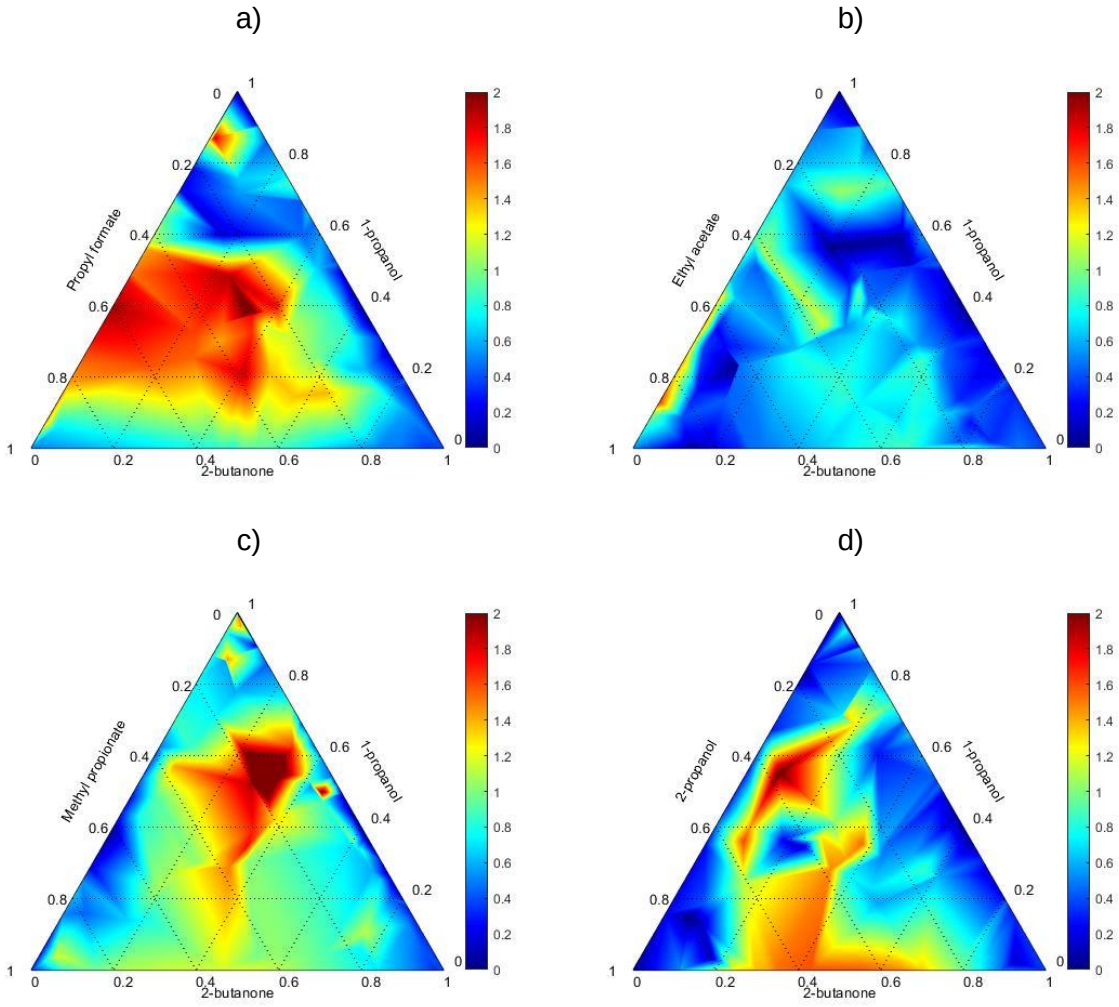

Figure 6.17: Colourmap of temperature deviations the SAFT-VR-Mie-GV models predictions from the experimental temperatures, for: a) Propyl formate system; b) ethyl acetate system; c) methyl propionate system; d) 2-propanol system

By looking at the vapour-liquid surfaces that are created at a specific temperature, it is possible to see the outcomes of the models in both temperature and in composition. It is however difficult to directly compare the two. This is seen even when looking at binary systems that are accurately modelled.

This can be seen looking at the binary systems that make up the ternary system containing propyl formate. By cutting the graph at 360 K (Figure 6.18), the vapour liquid surfaces of each model and the experimental data can be placed on one graph (Figure 6.19).

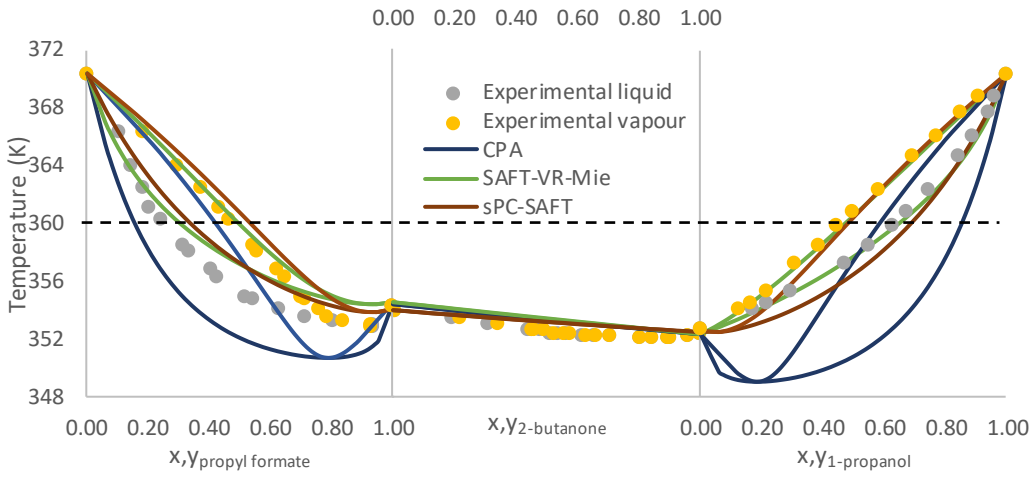

Figure 6.18: Cutting the binary systems in the propyl formate system at 360 K.

The resulting surfaces, which are present only on the axes as no ternary data is being taken into account, shows even a system that is accurately modelled will still show discrepancies. It can be seen that the experimental data of 1-propanol/propyl formate shows higher concentrations of 1-propanol compared to the 1-propanol/2-butanone system. This shows larger cross-association with the ketone. However, this is less pronounced with the modelled data of sPC-SAFT-GV showing almost identical concentrations. The SAFT-VR-Mie-GV model shows a more accurate prediction with a higher concentration of 1-propanol, however even with a more accurate model the surfaces are not identical. It is, therefore, more important to look at the trend, rather than the exact surface.

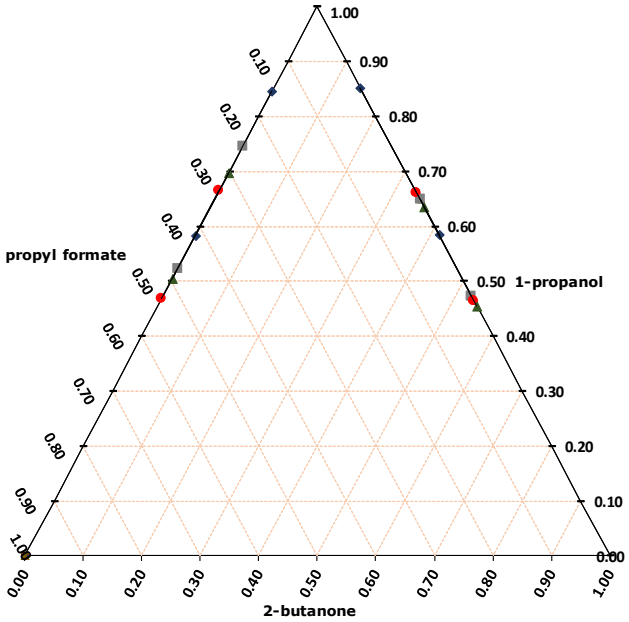

Figure 6.19: Liquid-vapour surfaces from the binary systems in the propyl formate ternary system at 360 K. Where the blue diamonds show CPA-GV, the red circles show sPC-SAFT-GV, the green triangles show SAFT-VR-Mie-GV, and the grey squares show the experimental values.

The system that was least accurately modelled, the propyl formate ternary system was used to assess the model's ability to predict the trends of the vapour-liquid surfaces. As is expected the CPA-GV model is not able to predict the trends with no differences noticed in the solvation effects of either 2-butanone or propyl formate, as well as lower temperatures noticed at higher concentrations of 1-propanol.

The sPC-SAFT-GV model also fails to accurately predict the trends of the vapour-liquid surfaces. This is seen again with little differences between the amount of solvation between 2-butanone and propyl formate.

SAFT-VR-Mie-GV with a more complex way of calculating the cross-association parameters, shows the most accurate trends in the vapour-liquid surfaces. This can be seen with sloping curves from lower concentration of 1-propanol, at high concentrations of 2-butanone, to higher concentrations of 1-propanol, at lower concentrations of 2-butanone.It should however be noticed that improvements to the model can still be made as deviations still occur, this can be seen with a saddle, and 'inversion' point shown at higher temperatures, than those noticed in the experimental data.

It can therefore be concluded that although slightly better AAD values are noticed for the sPC-SAFT-GV model, slightly more accurate results are predicted using the SAFT-VR-Mie-GV model. However, both models can be considered accurate.

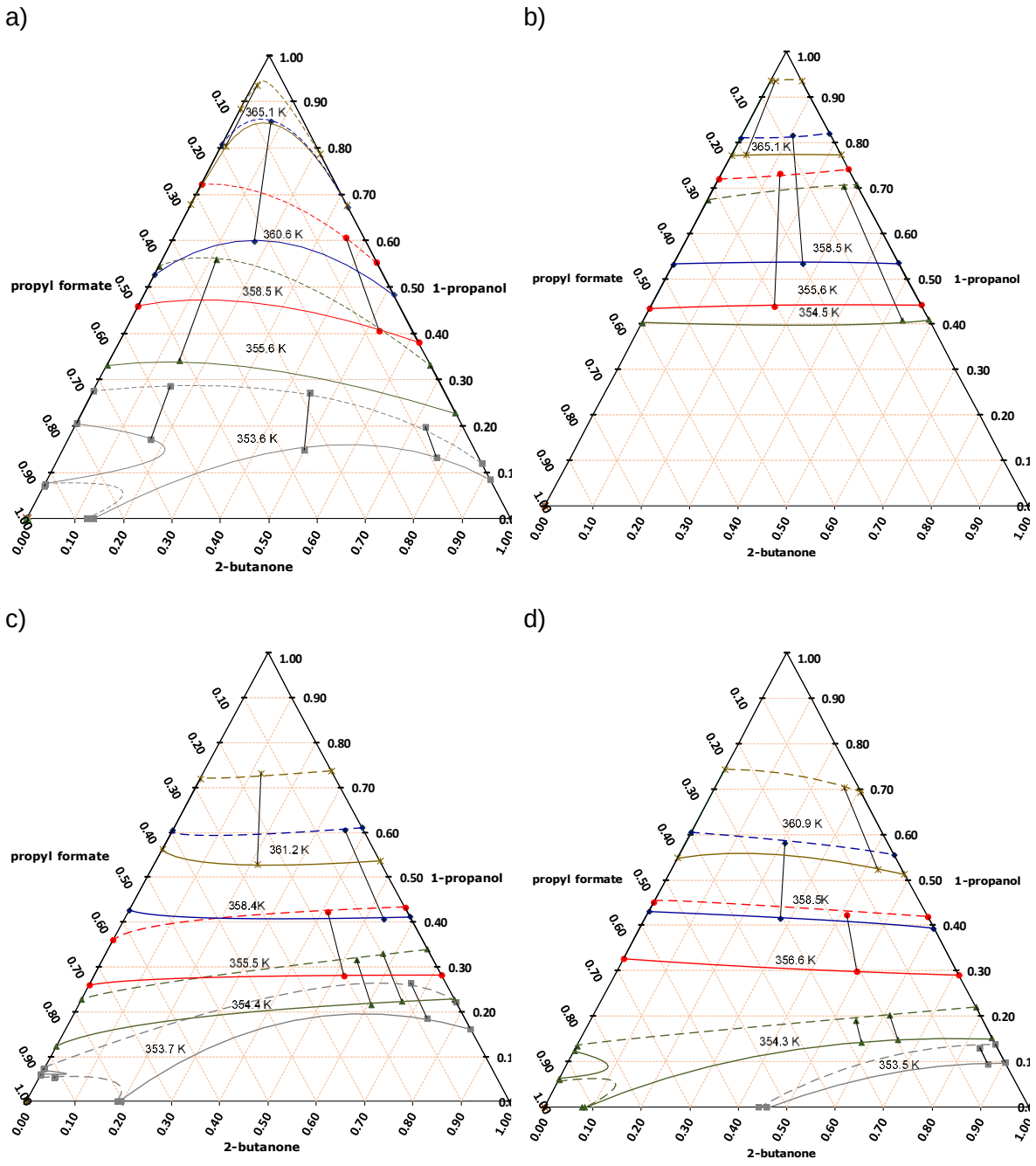

Figure 6.20: Vapour-liquid surfaces in the propyl formate system of: a) Experimental data; b) CPA-GV predictions; c) sPC-SAFT-GV predictions; d) SAFT-VR-Mie-GV predictions

In order to satisfy objective 3b the predictions of the binary systems need to be compared to the predictions of the ternary systems. The results of these predictions have been reprinted in Figure 6.8, for ease of reference.

Table 6.9 shows that the AAD results of the binary systems in the ternary systems show slightly more accurate predictions. However, this difference is small, and as noticed with the NRTL model, the ternary predictions can be assumed to be accurate. As it is expected for the

ternary predictions to be slightly less accurate compared to the binary systems, with more components creating more complex interactions.

It can therefore be assumed that for the SAFT-VR-Mie-GV and the sPC-SAFT-GV models, can accurately predict complex, polar, associating, and cross-associating multicomponent systems. There is however still room for improvement in these models.

Table 6.11: The Ternary AAD values for temperature and vapour fractions, compared to the average of the binary AADs for the binary systems involved in the ternary systems

1-propanol/2-butanone/propyl formate											
CPA-GV				SAFT-VR-Mie-GV				sPC-SAFT-GV			
AAD (T)	AAD (y1)	AAD (y2)	AAD (y3)	AAD (T)	AAD (y1)	AAD (y2)	AAD (y3)	AAD (T)	AAD (y1)	AAD (y2)	AAD (y3)
Average binary											
2.89	0.040			0.73	0.013			0.93	0.012		
Ternary outcomes											
4.27	0.037	0.034	0.026	0.98	0.021	0.007	0.019	**0.75**	**0.020**	**0.018**	**0.017**

1-propanol/2-butanone/ethyl acetate											
CPA-GV				SAFT-VR-Mie-GV				sPC-SAFT-GV			
AAD (T)	AAD (y1)	AAD (y2)	AAD (y3)	AAD (T)	AAD (y1)	AAD (y2)	AAD (y3)	AAD (T)	AAD (y1)	AAD (y2)	AAD (y3)
Average binary											
3.37	0.050			0.60	0.012			0.69	0.012		
Ternary outcomes											
4.19	0.042	0.026	0.021	0.53	0.014	0.010	0.009	**0.40**	**0.013**	**0.009**	**0.012**

1-propanol/2-butanone/methyl propionate											
CPA-GV				SAFT-VR-Mie-GV				sPC-SAFT-GV			
AAD (T)	AAD (y1)	AAD (y2)	AAD (y3)	AAD (T)	AAD (y1)	AAD (y2)	AAD (y3)	AAD (T)	AAD (y1)	AAD (y2)	AAD (y3)
Average binary											
3.41	0.048			0.56	0.007			0.65	0.010		
Ternary outcomes											
4.46	0.060	0.038	0.023	0.99	0.022	0.015	0.009	**0.82**	**0.020**	**0.015**	**0.011**

1-propanol/2-butanone/2-propanol											
CPA-GV				SAFT-VR-Mie-GV				sPC-SAFT-GV			
AAD (T)	AAD (y1)	AAD (y2)	AAD (y3)	AAD (T)	AAD (y1)	AAD (y2)	AAD (y3)	AAD (T)	AAD (y1)	AAD (y2)	AAD (y3)
Average binary											
2.94	0.044			0.56	0.013			0.47	0.012		
Ternary outcomes											
3.39	0.024	0.066	0.047	**0.79**	**0.022**	**0.020**	**0.011**	0.89	0.022	0.018	0.017

7. Conclusions and Recommendations

7.1. Conclusions

The primary aim of this study was to measure and model four ternary VLE systems of polar, self-associating, and cross associating components, and to evaluate the nine binary VLE systems that make up the four ternary systems. These systems were modelled by using predictive models: sPC-SAFT, SAFT-VR-Mie, and the CPA equations of state, with each model utilising the Gross and Vrabec polar term. The models were compared on their ability to predict the experimental data. The conclusions to the objectives laid out in Section 1.3 are now summarised below.

7.1.1. Objective 1: Generate binary VLE data

The nine binary systems evaluated in this study were based on the components of the four ternary systems. VLE data were found for the nine systems using a modified Gillespie still isobaric (P=1.013 bar). There were uncertainties in temperature of ± 0.62 K, in pressure of ± 0.046 bar and composition ± 0.016 mole fraction. The one binary system, which was common amongst all four ternary systems (1-propanol/2-butanone and literature data), was used to verify the experimental accuracy of the modified Gillespie still.

All nine binary systems passed the McDermott-Ellis consistency test and the L/W area test. This proved that the binary data generated were thermodynamically consistent.

In the binary systems containing 1-propanol at high concentration of 1-propanol, the VLE followed very similar trends, while differences occurred at low concentrations of 1-propanol. Minimum boiling azeotropes were apparent in the 1-propanol/propyl formate and the 1-propanol/methyl propionate system.

In the binary systems containing 2-butanone, the systems similar boiling points and intermolecular forces lead to all the systems containing minimum boiling azeotropes, with each azeotrope occurring close to the lower boiling component. With these trends and azeotropes, it was possible to predict the outcomes of the ternary systems.

7.1.2. Objective 2: Generate Ternary VLE data

To meet objective 2, VLE data were generated for the four ternary systems using the same modified Gillespie still with the same experimental uncertainties as the one used for the binary VLE.

All four ternary systems passed the McDermott-Ellis consistency test and the L/W area test. This again proved that the ternary data generated were thermodynamically consistent.

Definite distillation boundaries were found in the 1-propanol/2-butanone/propyl formate system and the 1-propanol/2-butanone/methyl propionate systems with tie lies at high concentrations of the C_4 ester being inverted.

Cutting the isomorphous graphs at certain temperatures allowed for the evaluation of the liquid-vapour surface for each system. The greatest differences between the systems occurred at high concentrations of the C_4 esters and 2-propanol, as the interactions of these components took precedence.

The deviations from an ideal state where noticed for each system in areas where the binary systems had large deviations. The 2-butanone/methyl propionate system has an azeotrope at medium concentrations (0.515 mole fraction of 2-butanone), and large deviations where noticed at medium concentrations of 2-butanone and methyl propionate in the ternary system. This is similar for the propyl formate ternary system, in which the binary azeotrope of 2-butanone/propyl formate has an azeotrope at high concentrations of propyl formate (0.10 mole fraction of 2-butanone). This leads to larger deviations at high concentrations of propyl formate. More ideal outcomes are noticed for the ethyl acetate system.

As the temperature increased and the concentration of 2-propanol increased, all four systems showed very small differences between each other with all four systems acting in a more ideal way.

7.1.3. Objective 3a: Modelling binary experimental data using CPA-GV sPC-SAFT-GV and SAFT-VR-Mie-GV

Objective 3 can be split into two separate objectives, viz: a) model the nine binary systems with the three perturbation EoS models and then compare their accuracies; and b) model the four ternary systems with the same three perturbation EoS models and then compare their accuracies with the accuracies obtained for the binary systems.

To evaluate and compare the accuracies of the selected EoS models (predicting, rather than correlating the phase equilibria), the classic NRTL activity coefficient model was used as benchmark. Using AAD values, the NRTL's average deviation from experimental values was found to be 0.24 K and 0.005 mole fraction.

Using the pure component parameters regressed within this work (2-propanol, CPA-GV) and those found in literature, the predictions of the nine binary systems were modelled. The CPA-GV EoS model struggled with the alcohol/(ketone ester) systems, showing large AAD values and not being able to predict the phase envelope, as this model does not take into account components that cross-associate but do not self-associate. Better, more comparable

outcomes with the experimental data and NRTL correlations, were found when considering mixtures that do not cross-associate and ones with two self-associating components.

The sPC-SAFT-GV EoS model showed more accurate predictions of the alcohol/(ketone ester), compared to the CPA-GV model systems predicting all nine systems with a high level of accuracy, showing agreement with the phase envelopes. SAFT-VR-Mie-GV predicted the binary systems with comparable results compared to sPC-SAFT-GV. This is reiterated when looking at the AAD's of the binary systems. Those being 0.589 K, and 0.011 mole fraction for sPC-SAFT-GV, and 0.614 K, and 0.011 mole fraction for SAFT-VR-Mie.

7.1.4. Objective 3b: Model experimental ternary data using sPC-SAFT-GV SAFT-VR-Mie-GV and CPA-GV

Both the SAFT-VR-Mie-GV and sPC-SAFT-GV EoS models produced comparable and acceptably accurate predictions for the ternary systems, with only slight differences in outcomes between the two models. These SAFT type EoS models could predict the VLE of the ternary systems to a very similar accuracy than the NRTL model, with the majority of the systems showing more accurate AAD values. The AAD values for SAFT-VR-Mie-GV were 0.820 K, and 0.019, 0.013, and 0.012 mole fraction, while sPC-SAFT produced AAD values of 0.72 K and 0.020, 0.014, and 0.016 mole fraction.

When comparing the modelled results of the ternary systems and the binary systems, there are slight differences, with the predictions of the binary systems showing slightly more accurate predictions. However, these differences are small. With AAD values approximately 0.2 K and 0.05 mole fraction higher, in the ternary systems. Although these predictions are slightly less accurate than the binary systems, with better predictions than those shown in the NRTL correlation it can be assumed that SAFT-VR-Mie-GV and sPC-SAFT-GV can both be used for accurate predictions of complex systems used in this study.

7.2. Recommendations

The following recommendations for future work, based on the outcomes in this thesis, are as follows:

1) Modifications to the still can be made, by using a more complex analogue-to-digital converter (ADC), to convert the electrical resistance to a temperature measurement rather than the analogue Arduino used. This will decrease the electrical resistance fluctuations, lowering the high uncertainty in temperature.
2) Regress cross-association parameters for both the sPC-SAFT-GV EoS model and the CPA-GV model using the same AAD contour method set out by Cripwell et al. 2019.

This will allow for more accurate predictions for both models, as well as group- specific pure component parameters that can be used for all ketones or esters.

3) Explore different association schemes to evaluate the effectiveness of the models using these schemes. This will allow for a systematic test between these schemes for ternary systems.
4) Evaluate the group contribution SAFT-γ-Mie model, which has recently been applied to ketones and esters, and added to the TRsolution software in work done in the Stellenbosch university Separation Technology research group [119].

References

[1] J. D. Seader and E. J. Henley, *Separation process principles*, 2nd ed. Hoboken: John Wiley & sons, 2006.

[2] G. Schlowsky, A. Erickson, and T. Schafer, “Generating your own VLE data,” *Chem. Eng.*, vol. 102, no. 3, pp. 139–142, 1995.

[3] D. Hill and C. Fred, “Understand Thermodynamics to Improve Process Simulations,” *Chem. Eng. Process*, vol. 107, no. 12, pp. 20–25, 2011.

[4] M. D. Koretsky, *Engineering and chemical thermodynamics*, 2nd ed. Hoboken: John Wiley & sons, 2013.

[5] S. I. Sandler, *Chemical, Biochemical, and engineering thermodynamics*, Fourth ed. Hoboken: John Wiley & sons, 2006.

[6] J. M. Prausnitz, R. N. Lichtenthaler, and E. Gomes de Azevedo, *Molecular thermodynamics of fluid phase equilibria*, Second ed. New Jersey, 1986.

[7] J. Servos, *Physical chemistry from Ostwald to pauling: the making of science in america*, Second ed. Chichester, west sussex: Princeton University Press, 1990.

[8] J. W. Tester and M. Modell, *Thermodynamics and Its Applications*, Second edi. Upper saddle River, New Jersey, 1997.

[9] G. Kontogeorgis and G. Folas, *Thermodynamic Models for Industrial Applications From Classical and Advanced Mixing Rules to Association Theories*, First ed. Chichester, west sussex: John Wiley and Sons, 2010.

[10] R. Dohrn and O. Pfohl, “Thermophysical properties — Industrial directions,” *Fluid Phase Equilib.*, vol. 197, no. 1, pp. 15–29, 2002.

[11] M. . Holmes and M. V. A. N. Winkle, “Prediction of Ternary Vapor-Liquid Equilibria from Binary Data Wilson equation used to predict vapor compositions,” *Ind. Eng. Chem.*, vol. 62, no. 1, pp. 21–31, 1970.

[12] D. P. Tassios, *Applied Chemical Enginnering Thermodynamics*, First Ed. Berlin: Spring-verlag Berlin Heidelberg GmbH, 1993.

[13] D. C. Silva, R. Guirardello, and A. C. D. Freitas, “Modeling Vapor Liquid Equilibrium of Binary and Ternary Systems of CO 2 + Hydrocarbons at High-Pressure Conditions,” *Ital. Assoc. Chem. Eng.*, vol. 57, pp. 1477–1482, 2017.

[14] R. V Orye and J. M. Prausimitz, “Multicomponent equilibria with the wilson equation,”

Ind. Eng. Chem., vol. 57, no. 5, pp. 18–26, 1965.

[15] K. Zheng, H. Wu, C. Geng, G. Wang, Y. Yang, and Y. Li, “A Comparative Study of the Perturbed-Chain Statistical Associating Fluid Theory Equation of State and Activity Coe ffi cient Models in Phase Equilibria Calculations for Mixtures Containing Associating and Polar Components,” *Ind. Eng. Chem. Reasearch*, vol. 57, no. 8, pp. 3014–3030, 2018.

[16] R. A. Heidemann and J. M. Prausnitz, “A van der Waals-type equation of state for fluids with associating molecules,” *Appl. Phys. Sci.*, vol. 73, no. 6, pp. 1773–1776, 1976.

[17] C. Panayiotou and I. . Sanchez, “Hydrogen bonding in fluids: an equation-of-state approach,” *J.Phys.Chem*, vol. 95, no. 1, pp. 10090–10097, 1991.

[18] W. G. Chapman, K. E. Gubbins, G. Jackson, and M. Radosz, “SAFT: Equation-of-state solution model for associating fluids,” *Fluid Phase Equilib.*, vol. 52, no. 1, pp. 31–38, 1989.

[19] W. Chapman, K. Gubbins, G. Jackson, and M. Radosz, “New reference equation of state for associating fluids,” *Ind. Eng. Chem. Res.*, vol. 29, pp. 1709–1721, 1990.

[20] G. M. Kontogeorgis, E. C. Voutsas, I. V Yakoumis, and D. P. Tassios, “An Equation of State for Associating Fluids,” *Ind. Eng. Chem. Res.*, vol. 35, no. 1, pp. 4310–4318, 1996.

[21] M. . Wertheim, “Fluids with Highly Directional Attractive Forces. I. Statistical Thermodynamics,” *J. Stat. Phys.*, vol. 35, no. 1–2, pp. 19–34, 1984.

[22] M. . Wertheim, “Fluids with highly directional attractive forces. II. Thermodynamic perturbation theory and integral equations,” *J. Stat. Phys.*, vol. 35, no. 1–2, pp. 35–47, 1984.

[23] M. . Wertheim, “Fluids with highly directional attractive forces. III. Multiple attraction sites,” *J. Stat. Phys.*, vol. 42, pp. 459–476, 1986.

[24] M. . Wertheim, “Fluids with highly directional attractive forces. IV. Equilibrium polymerization,” *J. Stat. Phys.*, vol. 42, no. 3, pp. 477–493, 1986.

[25] T. Lafitte, D. Bessières, M. M. Piñeiro, and J. L. Daridon, “Simultaneous estimation of phase behaviour and second-derivative properties using the statistical asso- ciating fluid theory with variable range approach,” *J.Chem.Phys*, vol. 124, p. 24509, 2006.

[26] J. Gross and J. Vrabec, “An equation-of-state contribution for polar components: Dipolar molecules,” *AIChE J.*, vol. 52, no. 3, pp. 1194–1204, 2006.

[27] I. Nagata, “Prediction of Ternary phase equilibria from binary data,” *Thermochim. Acta*, vol. 56, pp. 43–57, 1982.

[28] G. K. Folas, G. M. Kontogeorgis, M. L. Michelsen, and E. H. Stenby, “Vapor – liquid , liquid – liquid and vapor – liquid – liquid equilibrium of binary and multicomponent systems with MEG Modeling with the CPA EoS and an EoS / G E model,” vol. 249, no. 1, pp. 67–74, 2006.

[29] L. Yarborough, “Vapor-Liquid Equilibrium Data for Multicomponent Mixtures Containing Hydrocarbon and Nonhydrocarbon Components,” vol. 17, no. 2, pp. 129–133, 1972.

[30] T. . Anderson and J. M. Prausnitz, “Application of the UNIQUAC Equation to Calculation of multicomponent phase equilibria. 2. Liquid-Liquid Equilibria,” *Ind. Eng. Chem. Process Des.*, vol. 17, no. 4, pp. 561–567, 1978.

[31] C. . Guffey and A. . Wehe, “Calculation of multicomponent liquid-liquid equilibrium with Renon’s and Black’s activity equations,” *AIChE J.*, vol. 18, no. 5, pp. 913–922, 1972.

[32] A. J. de Villiers, C. E. Schwarz, and A. J. Burger, “Improving vapour-liquid-equilibria predictions for mixtures with non-associating polar components using sPC-SAFT extended with two dipolar terms,” *Fluid Phase Equilib.*, vol. 305, no. 2, pp. 174–184, 2011.

[33] J. T. Cripwell, C. E. Schwarz, and A. J. Burger, “SAFT-VR-Mie with an incorporated polar term for accurate holistic prediction of the thermodynamic properties of polar components,” *Fluid Phase Equilib.*, vol. 455, pp. 24–42, 2018.

[34] K. Mejbri, A. Taieb, and A. Bellagi, “Phase equilibria calculation of binary and ternary mixtures of associating fluids applying PC-SAFT equation of state,” *J. Supercrit. Fluids*, vol. 104, pp. 132–144, 2015.

[35] A. J. De Villiers, “Evaluation and improvement of the sPC-SAFT equation of state for complex mixtures,” no. December, 2011.

[36] J. M. Smith, H. van Ness, M. Abbott, and M. Swihart, *Introdction to chemical engineering themodynamics*, 7th editio. New York: McGraw-Hill, 2005.

[37] J. S. Rowlinson and F. L. Swinton, *Liquids and liquid mixtures*, Third ed. London: butterworth & Co., 1982.

[38] V. B. John, *Understanding phase diagrams*, 2nd editio. london: The Macmillan press LTD, 1974.

[39] E. Hala, I. Wichterle, J. Polak, and T. Boublik, *Vapour-liquid equilibrium data at normal*

pressures, First ed. Oxford: Pergamon Press, 1968.

[40] R. Rios, A. Sosa, L. Fernández, and J. Ortega, “Azeotropy: A limiting factor in separtion operations in chemical enginerring - Analysis, experimental techniques, modeling and simulation on solutions of ester-alkanes,” in *Laboratiry unit operations and experimental methods*, First edit., O. M. Basha and B. I. Morsi, Eds. IntechOpen, 2018, pp. 140–173.

[41] D. R. F. West, *Ternary Equilibrium Diagrams*, Second Ed. London: Chapman and Hall, 1982.

[42] F. C. Campbell, *Phase Diagrams, understanding the basics*, First Ed. Meterials Park: ASM international, 2012.

[43] S. Malanowski, “Experimental methods for vapour-liquid equilibria. Part 2. Dew-and bubble point method,” *Fluid Phase Equilib.*, vol. 9, no. 3, pp. 311–317, 1982.

[44] J. Raal and A. Muhlbauer, *Phase equilibria: measurement and computation*, First ed. washington Dc: Taylor and Francis, 1998.

[45] E. Hâla, J. Pick, V. Fried, and O. Vilim, *Vapour-liquid equilibrium*, Second eng. Oxford, UK: Pergamon Press, 1967.

[46] B. G. Scatchard, M. Grant, and F. G. Satkiewicz, “Vapor-Liquid Equilibrium. X. An Apparatus for Static Equilibrium Measurements,” vol. 86, no. 2, pp. 125–127, 1964.

[47] D. F. Othmer and H. B. Coats, “Measurement of surface temperature,” *Ind. Eng. Chem.*, vol. 20, no. 2, pp. 124–128, 1928.

[48] F. G. Cottrell, “On the determination of boiling points of solutions,” vol. 1618, no. 1918, pp. 721–729, 1919.

[49] D. T. C. Gillespie, “Vapor-Liquid Equilibrium Still for Miscible Liquids,” *Ind. Eng. Chem.*, vol. 18, no. 9, pp. 575–577, 1946.

[50] R. M. Rieder and A. R. Thompson, “Vapor-Liquid Equilibria Measured by a Gillespie Still,” *Ind. Eng. Chem.*, vol. 41, no. 12, pp. 2905–2908, 1949.

[51] I. Brown and A. H. Ewald, “Liquid-Vapour Equilibria. II. The System Benzene-n-Heptane,” *Austrian J. Sci. Res.*, vol. 4, no. 1, pp. 198–212, 1951.

[52] R. Gowda, “Phase equilibrium of limonene, p-cymene, indane, butylbenzene and 1,2,3-trimethylbenzene at sub- atmospheric conditions,” 2018.

[53] S. N. Vinogradov and R. H. Linnell, *Hydrogen bonding*. London: Van Nostrand Reinhold Company, 1971.

[54] N. von Solms, M. L. Michelsen, and G. M. Kontogeorgis, “Applying Association Theories to Polar Fluids,” *Ind. Eng. Chem. Res.*, vol. 43, no. 1, pp. 1803–1806, 2004.

[55] B. E. Poling, J. . Prausnitz, and J. . O’Connel, *The properties of gases and liquids*, 5th ed. New York: McGraw Hill, 2001.

[56] J. M. Prausnitz, R. N. Lichtenthaler, and E. Gomes de Azevedo, *Molecular thermodynamics of fluid-phase equilibria*, Third Ed., vol. 2, no. 1. New Jersey: Prentice-Hall. Inc., 1999.

[57] M. Kleiner and G. Sadowski, “Modeling of polar systems using PCP-SAFT: An approach to account for induced-association interactions,” *J. Phys. Chem. C*, vol. 111, no. 43, pp. 15544–15553, 2007.

[58] R. Garriga, F. Sánchez, P. Pérez, and M. Gracia, “Excess Gibbs free energies at seven temperatures and excess enthalpies and volumes at 298.15 K of butanone with 1-propanol or 2-propanol,” *Fluid Phase Equilib.*, vol. 124, no. 1–2, pp. 123–134, 1996.

[59] N. F. Martínez, E. Lladosa, M. C. Burguet, and J. B. Montón, “Isobaric vapour-liquid equilibria for binary systems of 2-butanone with ethanol, 1-propanol, and 2-propanol at 20 and 101.3 kPa,” *Fluid Phase Equilib.*, vol. 270, pp. 62–68, 2008.

[60] H. Yamamoto and J. Shibata, “Vapor−Liquid Equilibrium of Propan-2-ol + Propan-1-ol + Sodium Iodide at 298.15 K,” *J. Chem. Eng. Data*, vol. 44, no. 5, pp. 1071–1075, 1999.

[61] N. Gultekin, “Vapor-Liquid Equilibria for Binary and Ternary Systems Composed of Acetone, 2-Propanol, and 1-Propanol,” *J. Chem. Eng. Data*, vol. 34, no. 10, pp. 168–171, 1989.

[62] L. H. Ballard and M. Van Winkle, “Vapor-Liquid Equilibria at 760 Mm. Pressure. 2-Propanol-Methanol, 2-Propanol-Ethyl Alcohol, 2-Propanol-Propanol, and 2-Propanol-2-Butyl Alcohol Systems.,” *Ind. Eng. Chem.*, vol. 44, no. 10, pp. 2450–2453, 1952.

[63] C. Gabaldón, P. Marzal, J. B. Montón, and M. A. Rodrigo, “Isobaric vapor−liquid equilibria for binary and ternary systems composed of water, 1-propanol, and 2-propanol at 100 kPa,” *J. Chem. Eng. Data*, vol. 41, no. 6, pp. 1379–1382, 1996.

[64] P. Murti and M. Van Winkle, “Vapor-Liquid Equilibria for Binary Systems of Methanol, Ethyl Alcohol, 1-Propanol, and 2-Propanol with Ethyl Acetate and 1-Propanol-Water.,” *Ind. Eng. Chem. Chem. Eng. Data Ser.*, vol. 3, no. 1, pp. 72–81, 1958.

[65] J. Fernandez, C. Berro, and M. . Paz Andrare, “Excess thermodynamics functions of 1-propanol + methyl propanoate and 1-propanol + methyl butanoate systems,” vol. 20,

pp. 145–153, 1985.

[66] P. Susial, J. Ortega, C. de Alfonso, and C. Alonso, “Vapor—Liquid Equilibrium Measurements for Methyl Propanoate—Ethanol and Methyl Propanoate-Propan-1-ol at 101.32 KPa,” *J. Chem. Eng. Data*, vol. 34, no. 2, pp. 247–250, 1989.

[67] M. D. M. Olaya, V. Gomis, J. Moltó, and F. Ruiz, “Isobaric vapor-liquid equilibria for the binary system 2-propanol + methyl ethyl ketone and for the ternary system 1-butanol + 2-propanol + methyl ethyl ketone at 101.3 kPa,” *J. Chem. Eng. Data*, vol. 47, no. 1, pp. 65–67, 2002.

[68] Nagata I, “Isobaric vapour-liquid equilibrium data for binary systems,” *Can. J. Chem. Eng.*, vol. 41, no. 1, pp. 21–23, 1963.

[69] X. H. Yan, Q. Wang, G. H. Chen, and S. J. Han, “Azeotropes at elevated pressures for systems involving cyclohexane, 2-propanol, ethyl acetate, and butanone,” *J. Chem. Eng. Data*, vol. 46, no. 5, pp. 1235–1238, 2001.

[70] J. Falcón, J. Ortega, and E. González, “Densities and vapor-liquid equilibria in binary mixtures formed by propyl methanoate + ethanol, +propan-1-ol, and +butan-1-ol at 160.0 kPa,” *J. Chem. Eng. Data*, vol. 41, no. 4, pp. 859–864, 1996.

[71] P. Nikitas, “Applications of the Gibbs – Duhem Equation,” *J. Chem. Educ.*, vol. 78, no. 8, pp. 1070–1075, 2001.

[72] J. Wisniak, J. Ortega, and L. Fernández, “A fresh look at the thermodynamic consistency of vapour-liquid equilibria data,” *J. Chem. Thermodyn.*, vol. 105, pp. 385–395, 2017.

[73] J. C. . Li and B. C.-Y. LU, “A note on thermodynamic consistency of ternary vapour-liquid equilibrium data,” *Can. J. Chem. Eng.*, vol. 37, no. 3, pp. 117–120, 1959.

[74] C. McDermott and S. R. M. Ellis, “A multicomponent consistency test,” *Chem. Eng. Sci.*, vol. 20, no. 4, pp. 293–296, 1965.

[75] J. Wisniak, A. Apelblat, and H. Segura, “An Assessment of Thermodynamic Consistency Tests for Vapor-Liquid Equilibrium Data,” *phys. Chem. Liq*, vol. 35, no. 1, pp. 1–56, 1997.

[76] J. : A. T. Wisniak, “Correlation of the boiling points of Mixtures,” *Chem. Eng. Sci.*, vol. 31, no. 4, pp. 631–635, 1976.

[77] J. Wisniak, “A new test for the thermodynamic consistency of vapor-liquid equilibrium,” *Ind. Eng. Chem. Res.*, vol. 32, no. 7, pp. 1531–1533, 1993.

[78] J. van der Waal, “On the continuity of the gaseous and liquid states [Doctoral disertation],” Leiden University. Leiden, 1873.

[79] O. Redlich and J. N. . Kwong, “On the thermodynamics of solutions. An Equation of State. Fugacities of gaseous solutions,” *Chem. Rev.*, vol. 44, no. 1, pp. 233–244, 1948.

[80] G. Soave, “Equilibrium constants from a modified Redlich-Kwong equation of state,” *Chem. Eng. Sci.*, vol. 27, no. 6, pp. 1197–1203, 1972.

[81] D. Peng and D. B. Robinson, “A New Two-Constant Equation of State,” *Ind. Eng. Chem. fundimentals*, vol. 15, no. 1, pp. 59–64, 1976.

[82] G. M. Wilson, “A New Expression for the Excess Free Energy of Mixing,” *J. Am. Chem. Soc.*, vol. 86, no. 2, pp. 127–130, 1964.

[83] H. Renon and J. M. Prausnitz, “local compositions in thermodynamic excess functions for liquid mixtures,” *AIChE J.*, vol. 14, no. 1, pp. 135–144, 1968.

[84] G. Maurer and J. M. Prausnitz, “On the derivation equation and extension of the uniquac equation,” *Fluid Phase Equilib.*, vol. 2, pp. 91–99, 1978.

[85] A. Fredenslund, R. L. Jones, and J. M. Prausnitz, “Group contribution estimation of activity coefficients in nonideal liquid mixtures,” *AIChE J.*, vol. 21, p. 1086, 1975.

[86] J. Gross and G. Sadowski, “Application of the Perturbed-Chain SAFT Equation of State to Associating Systems Application of the Perturbed-Chain SAFT Equation of State to,” *Ind. Eng. Chem. Res.*, vol. 41, pp. 5510–5515, 2002.

[87] E. A. Müller and K. E. Gubbins, “Molecular-based equations of state for associating fluids: A review of SAFT and related approaches,” *Ind. Eng. Chem. Res.*, vol. 40, no. 10, pp. 2193–2211, 2001.

[88] S. Huang and M. Radosz, “Equation of State for small, large, polydisperse, and associating molecules,” *Ind. Eng. Chem. Res.*, vol. 29, pp. 2284–2294, 1990.

[89] J. Gross and G. Sadowski, “Perturbed-chain SAFT: An equation of state based on a perturbation theory for chain molecules,” *Ind. Eng. Chem. Res.*, vol. 40, no. 4, pp. 1244–1260, 2001.

[90] N. von Solms, M. L. Michelsen, and G. M. Kontogeorgis, “Equation of State for Highly Asymmetric and Associating Mixtures,” pp. 1098–1105, 2003.

[91] A. Gil-Villegas, A. Galind, P. Whitehead, S. Mills, G. Jackson, and A. Burgess, “Statistical associating fluid theory for chain molecules with attractive potentials of

variable range," *J. Chem. Phys.*, vol. 106, no. 10, pp. 4168–4186, 1997.

[92] A. Galindo, L. A. Davies, A. G. George, A. Gil-villegas, and G. Jackson, "The thermodynamics of mixtures and the corresponding mixing rules in the SAFT-VR approach for potentials of variable range The thermodynamics of mixtures and the corresponding mixing rules in the SAFT-VR approach for potentials of variable range," vol. 8976, 2010.

[93] T. Lafitte, M. M. Piñeiro, J. L. Daridon, and D. Bessières, "A comprehensive description of chemical association effects on second derivative properties of alcohols through a SAFT-VR approach," *J. Phys. Chem. B*, vol. 111, no. 13, pp. 3447–3461, 2007.

[94] G. M. Kontogeorgis, M. L. Michelsen, G. K. Folas, S. Derawi, N. Von Solms, and E. H. Stenby, "Ten Years with the CPA (Cubic-Plus-Association) Equation of State . Part 1 . Pure Compounds and Self-Associating Systems," *Ind. Eng. Chem. Res.*, vol. 45, no. 1, pp. 4855–4868, 2006.

[95] I. V Yakoumis, G. M. Kontogeorgis, E. C. Voutsas, and D. P. Tassios, "Vapor-liquid equilibria for alcohol/hydrocarbon systems using CPA Equation of State," *Fluid Phase Equilib.*, vol. 130, no. 1, pp. 31–47, 1997.

[96] E. C. Voutsas, G. M. Kontogeorgis, I. V Yakoumis, and D. P. Tassios, "Correlation of liquid-liquid equilibria for alcohol/hydrocarbon mixtures using the CPA eqaution of state," *Fluid Phase Equilib.*, vol. 130, no. 1, pp. 61–75, 1997.

[97] I. V Yakoumis, G. M. Kontogeorgis, E. C. Voutsas, E. Hendricks, and D. P. Tassios, "Prediction of phase equilibria in binary aqueous systems containing alkanes, cycloalkanes, and alkenes with Cubic-Plus-Association equation of state," *Ind. Eng. Chem. Res.*, vol. 37, pp. 4175–4182, 1998.

[98] A. J. De Villiers, C. E. Schwarz, and A. J. Burger, "Fluid Phase Equilibria Extension of the CPA equation of state with dipolar theories to improve vapour – liquid-equilibria predictions," *Fluid Phase Equilib.*, vol. 312, pp. 66–78, 2011.

[99] S. S. Chen and A. Kreglewski, "Applications of the augmented van der Waals theory of fluids.: 1. Pure fluids," *Berichte der Bunsen-Gesellschaft für Phys. Chemie*, vol. 81, no. 10, pp. 1048–1052, 1977.

[100] J. T. Cripwell, "Improvement of the Thermodynamic Description of Polar Molecules and Their Mixtures in the SAFT Framework by," *P.h.D Thesis*, no. March, 2017.

[101] J. Gross and G. Sadowski, "Application of perturbation theory to a hard-chain reference

fluid: An equation of state for square-well chains," *Fluid Phase Equilib.*, vol. 168, no. 2, pp. 183–199, 2000.

[102] A. Grenner, G. M. Kontogeorgis, N. Von Solms, and M. L. Michelsen, "Modeling phase equilibria of alkanols with the simplified PC-SAFT equation of state and generalized pure compound parameters," vol. 258, pp. 83–94, 2007.

[103] N. Von Solms, I. A. Kouskoumvekaki, M. L. Michelsen, and G. M. Kontogeorgis, "Capabilities, limitations and challenges of a simplified PC-SAFT equation of state," *Fluid Phase Equilib.*, vol. 241, no. 1–2, pp. 344–353, 2006.

[104] A. Grenner, J. Schmelzer, N. Von Solms, and G. M. Kontogeorgis, "Comparison of Two Association Models (Elliott - Suresh - Donohue and Simplified PC-SAFT) for Complex Phase Equilibria of Hydrocarbon - Water and Amine-Containing Mixtures," *Ind. Eng. Chem. Res.*, vol. 45, no. 1, pp. 8170–8179, 2006.

[105] A. Grenner, I. Tsivintzelis, I. G. Economou, C. Panayiotou, and G. M. Kontogeorgis, "Evaluation of the Nonrandom Hydrogen Bonding (NRHB) Theory and the Simplified Perturbed-Chain−Statistical Associating Fluid Theory (sPC-SAFT). 1. Vapor−Liquid Equilibria," *Ind. Eng. Chem. Res.*, vol. 47, no. 1, pp. 5636–5650, 2008.

[106] P. K. Jog and W. G. Chapman, "Application of Wertheim's thermodynamic perturbation theory to dipolar hard sphere chains," *Mol. Phys.*, vol. 97, no. 3, pp. 307–319, 1999.

[107] P. K. Jog, S. G. Sauer, J. Blaesing, and W. G. Chapman, "Application of dipolar chain theory to the phase behavior of polar fluids and mixtures," *Ind. Eng. Chem. Res.*, vol. 40, no. 21, pp. 4641–4648, 2001.

[108] J. T. Cripwell, "assessment of the capabilities of two polar sPC-SAFT terms through application to measured ketone-alkane phase equilibrium data (MEng)," 2014.

[109] J. 100:2008, "Evaluation of measurement data — Guide to the expression of uncertainty in measurement," 2008.

[110] DIPPR, "No Title," *801 database, Design Institute for Physical Properties. Sponsored by AIChE*. [Online]. Available: http://www.aiche.org/dippr.

[111] J. Gmehling and R. Bolts, "Azeotropic Data for Binary and Ternary Systems at Moderate," *J. Chem. Eng. Data*, vol. 41, pp. 202–209, 1996.

[112] S. A. M. Smith, "Measurement and modelling of the vapour-liquid equilibria of binary mixtures of water and alkanols," no. March, 2017.

[113] K. F. Al-Jiboury, "Modified NRTL Equation in Predicting Liquid – Liquid Equilibria," *Al-*

Nahrain Univ. Coll. Eng. J., vol. 17, no. 2, pp. 211–220, 2014.

[114] M. R. W. Marciel and A. Z. Francesconi, “Excess Gibbs free energies of (n-hexane + propan-1-ol) at 338.15 and 348.15 K and of (n-hexane + propan-2-ol) at 323.15, 338.15, and 348.1,” *J. Chem. Thermodyn.*, vol. 20, p. 539, 1988.

[115] A. Dominik, W. G. Chapman, M. Kleiner, and G. Sadowski, “Modeling of Polar Systems with the Perturbed-Chain SAFT Equation of State . Investigation of the Performance of Two Polar Terms,” *Ind. Eng. Chem. Res.*, vol. 44, no. 17, pp. 6928–6938, 2005.

[116] M. Do Seo, Y. Jo Kim, J. Sung Lim, and J. Won Kang, “Measurement and correlation of the isobaric vapor-liquid equilibrium for mixtures of alcohol + ketone systems at atmospheric pressure.,” *Korean J. Chem. Eng.*, vol. 29, no. 1, pp. 103–110, 2012.

[117] H. Tanaka, T. Muramatsu, and M. Kato, “Isobaric Vapor-Liquid Equilibria for Three Binary Systems of 2-Butanone with 3-Methyl-1-butanol, 1-Butanol, or 2-Butanol.,” *J. Chem. Eng. Data*, vol. 37, no. 1, pp. 164–166, 1992.

[118] J. T. Cripwell, F. J. Kruger, and A. J. Burger, “Accounting for cross association in non-self-associating species using a physically consistent SAFT-VR Mie approach,” *Fluid Phase Equilib.*, vol. 483, pp. 1–13, 2019.

[119] R. M. Hurter, “Comparing the group-contribution SAFT- γ Mie equation of state with SAFT-VR Mie by,” no. December, 2019.

[120] J. T. Cripwell, S. A. M. Smith, C. E. Schwarz, and A. J. Burger, “SAFT-VR Mie : Application to Phase Equilibria of Alcohols in Mixtures with n - Alkanes and Water,” *Ind. Eng. Chem. Res.*, vol. 57, no. 1, pp. 9693–9706, 2018.

Appendix A. Calibration Certification

WIKA Instruments (Pty) Ltd
South Africa

Certificate Number 14-00000978

Page 3 of 3 pages of calibration certificate dated 12/02/2020

Results

Immersion depth (mm)	Reference Temperature °C	DUT Indicated Reading Ω	DUT Indicated Reading mV	DUT Indicated Reading mA	DUT Indicated Temperature °C	DUT Deviation Temperature °C	Uncertainty of Measurement ±°C
150	19.994	-	-	-	20.028	0.034	0.61
150	79.992	-	-	-	80.040	0.048	0.62
150	139.991	-	-	-	140.030	0.039	0.61
150	199.989	-	-	-	199.890	-0.099	0.61

The reported expanded uncertainty of measurement is stated as the standard uncertainty of measurement multiplied by the coverage factor k=2, which for a normal distribution corresponds to a coverage probability of 95,45%, the uncertainty of measurement has been estimated in accordance with the principles defined in the GUM,'Guide to Uncertainty of Measurement, ISO, Geneva, 1993'.

Remarks

1. Standard used to convert resistance to temperature: IEC 60751:2008
2. Standard used to convert millivolts to temperature: IEC 60584-1:2013
3. The deviation must be subtracted algebraically from the DUT reading to obtain the correct temperature reading.

Label

The calibration object is labelled, which shows the number of this calibration certificate, serial/tag number and the date of calibration.

----------END OF CERTIFICATE----------

WIKA Instruments (Pty) Ltd
Unit 50-51 Gold Street , Northgate Business Park,
Maitland, 7405, Cape Town, South Africa
P.O. Box 475, Milnerton, 7435
Tel.: (021) 511 9228
Fax: (021) 511 5866
email: capetown@wika.co.za

ilac-MRA sanas Calibration Laboratory 246/S1 346/S1

WIKA Part of your business

Appendix B. Still PFD.

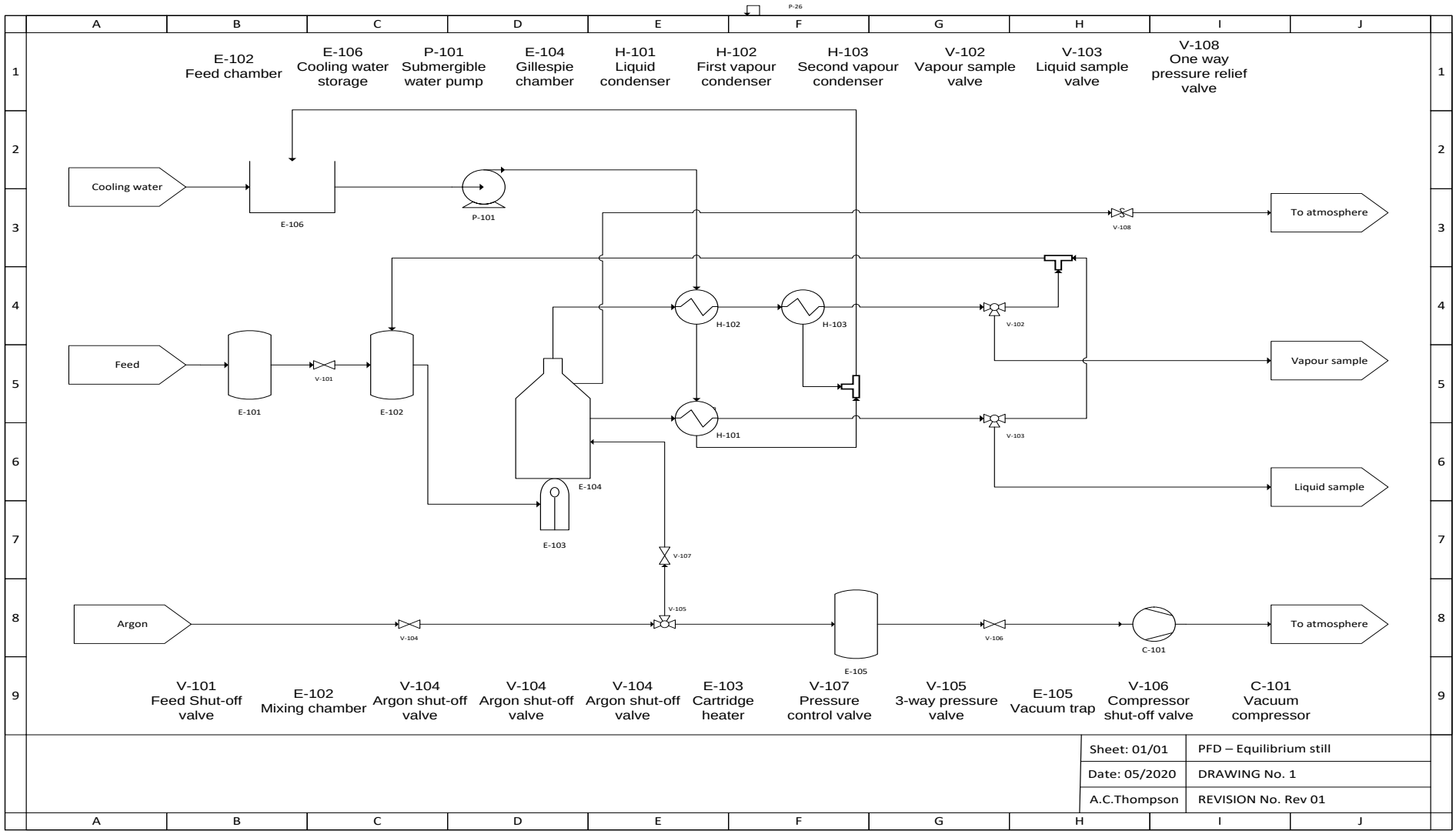

Appendix C. Detailed operating procedure

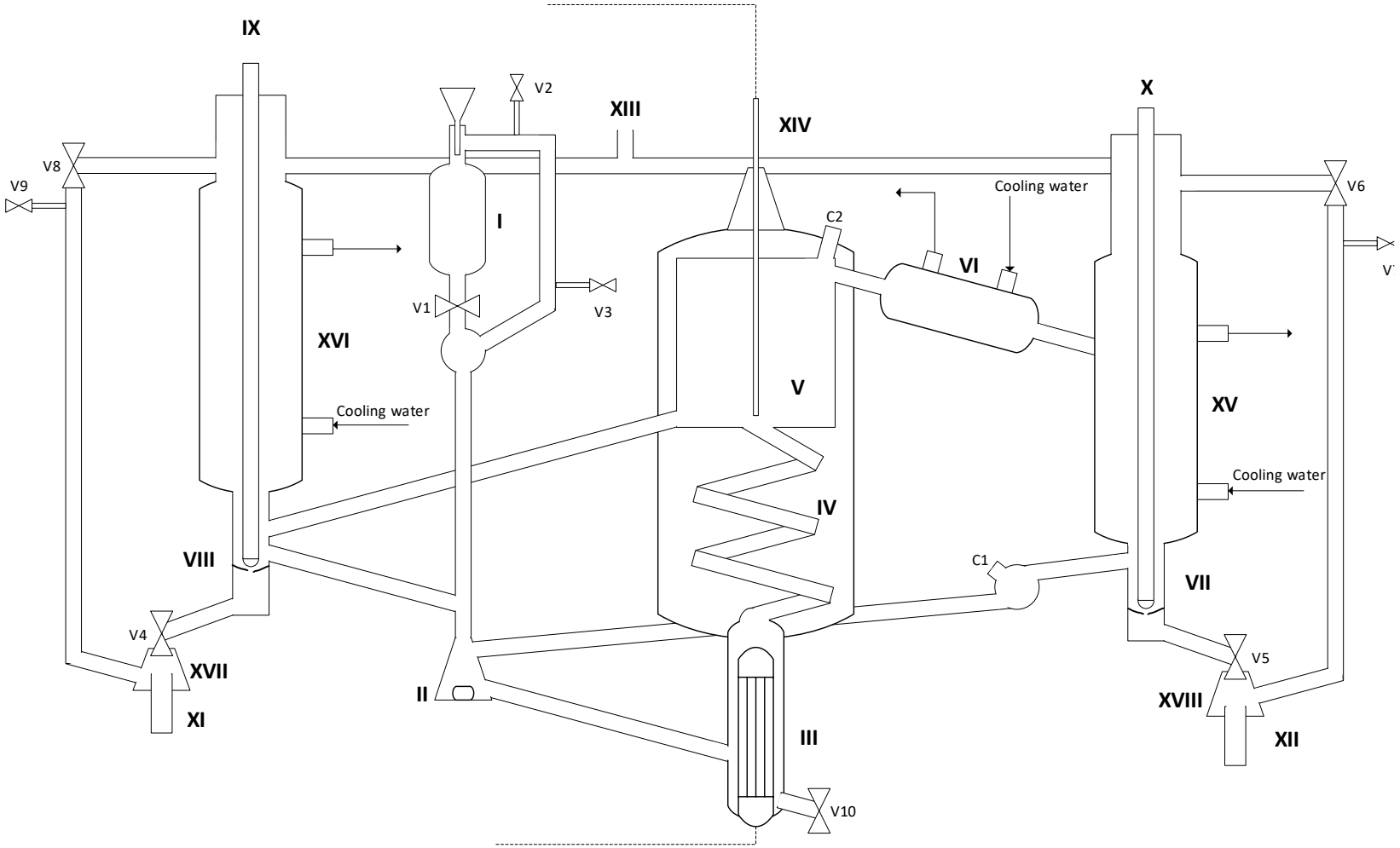

Figure C.1: Set-up of the glass Gillespie still used for phase equilibrium experimentation. Redrawn and adapted with permission from Gowda (2018)

Table C.1: annotations of the Gillespie type still

Notation	Description	Notation	Description
I	Feed chamber	XVI	Liquid condenser (Allihn style)
II	Mixing chamber and magnetic stirrer	XVII	Liquid collection point
III	Heating chamber and cartridge heater	XVIII	Vapour collection point
IV	Cottrell tube	V1	Feed chamber stop valve
V	Gillespie chamber	V2	Feed chamber aeration valve
VI	1st Vapour condenser (Liebig style)	V3	Feed piping aeration valve
VII	Vapour sample well	V4	Liquid sample valve
VIII	Liquid sample well	V5	Vapour sample valve
IX	Liquid glass rod with magnetic ends	V6	Vapour sample pressure valve
X	Vapour glass rod with magnetic ends	V7	Vapour sample aeration valve
XI	Liquid sample tube	V8	Liquid sample pressure valve
XII	Vapour sample tube	V9	Liquid sample aeration valve
XIII	Over and Under pressure control entry point	V10	Still drain valve
XIV	PT100 temperature probe	C1	Aeration cap 1 (possible vapour sample point)
XV	2nd Vapour condenser (Dimroth style)	C2	Aeration cap 2 (possible vapour sample point)

A detailed step-by-step guide on the operation of the Gillespie-type equilibrium still is presented in this chapter. With the still diagram (Figure A.0.1) and the annotations of the still (Table 0.1) presented and reprinted for reference.

C.1. Still preparation

Before operation of the still, the following should be ensured

i. Both the argon shut-off valve(V-104) and the vacuum pump shut-off valve (V-106) must be closed (Appendix B). The pressure regulator valve must also be closed.
ii. Ensure that the still is dry. If not wash the still with wash acetone, drain and open all aeration valves, and add compressed air. This process is discussed below.

iii. Turn on the cooling water pump. Ensure that water is flowing through the condensers and back into the bucket. Ice bricks must be added to the bucket to ensure the returning warmer water does not raise the temperature of the cooling water too high (these ice bricks are to be replaced every two hours).
iv. Ensure all valves on the equilibrium still are closed (V1-V10), Place caps on the aeration caps (C1 and C2). This will ensure that the still is airtight allowing the pressure in the still to remain constant.
v. The stills pressure indicator can be turned on, this is done on the red safety plug on the left-hand side of the still.
vi. By checking the ambient pressure of the still, it can be decided if over or under-pressure is required.

Under-Pressure

vii. If under-pressure is required check the pumps oil level. The oil level should be in the middle of the view glass. If the level is low top up with more lubrication oil.
viii. Turn the 3-way valve (V-104) so that it is open to the vacuum pump, open the vacuum pump shut-off valve, and crack open the pressure regulator valve. Ensure the argon shut-off valve is still closed.
ix. Turn on the Vacuum pump, the green switch on top of the pump, while looking at the pressure indication, adjust the pressure regulator valve, allowing for the system to settle at the required pressure.

Over-Pressure

vii. If over-pressure is required, open the valve on the argon canister to ensure argon is present.
viii. Open the argon-shut off valve and turn the three-way valve to open for over-pressure.
ix. Slowly open the pressure regulator valve allowing the pressure to settle, further adjustments can be made until the required pressure is met. Place the one-way pressure relief valve on the operating side of the still.

Liquid mixture can now be added to the still.

x. While keeping the feed chamber valve closed (V1), add approximately 110 ml of the mixture to the feed chamber (I).
xi. Open the valve (V1) and allow the mixture to fall into the mixing chamber and the heating chamber (II and III)
xii. Ensure that the mixture completely submerges the cartridge heater (III), and that the Chamber up to the base of the Cottrell tube (IV) is covered. If the volume of the liquid

isn't enough, add mixture until the chamber is filled. If the too much volume is added (The mixture is filling the vapour return pipe) open valve V10 and drain into a flask until the correct level is accomplished.

xiii. The still can now be turned on, by turning on the red plug on the right-hand side of the still.

C.2. Experimental runs

xiv. Now that the still is on, the pressure is constant, a mixture is in the heating chamber, the magnetic stirrer in the mixing chamber needs to be turned on. A setting of approximately 3 is needed to ensure constant mixing.

xv. The correct heater power is needed. Too low and the liquid boiling will not be carrying liquid and vapour through the Cottrell tube, too high and only vapour return will occur. At approximately 80-100^{o}C the dial should be turned approximately 40%.

xvi. After approximately 15 min the mixture should start boiling

xvii. Another 15 minutes and liquid and vapour return should be noticed. An ideal boiling rate will have a drop from the vapour return (VII) once every second, with comparable liquid return. If this is not the case adjust the cartridge heaters power.

xviii. If the boiling point of the mixture is greater than 100^{o}C set a heating jacket temperature 15^{o}C lower than the boiling point. This is accomplished by holding down the up or down arrows on the delta DTK temperature controller until the desired temperature is reached and pressing set.

xix. After approximately 20 minutes of continuous boiling, place magnets on points X and XI allowing the draining of the liquid building-up in the sample wells (VII and VIII), this is known as flushing

xx. Opening valves V4 and V5 allows the flushed liquids to into the liquid and vapour sample tubes these valves are then re-closed. This liquid is then discarded into a waste container.

xxi. Continuously check the pressure of the system, with the pressure in the gas canister slowly decreasing, the pressure in the still may start decreasing as well. adjust the pressure relief valve to ensure constant pressure throughout the run.

xxii. After another 20 minutes another flush of the build-up in the sample wells is done, as described above.

xxiii. After 60 minutes equilibrium should have been reached, this is indicated by small fluctuations in the temperature (indicated above the still) these fluctuations should be no larger than ±0.03K. This temperature is then noted down as the equilibrium temperature.

xxiv. A flush of the liquid in the sample wells (which is not at equilibrium), is done just before sampling, the Sample tubes containing this liquid are then replaced with clean and dry sample tubes, and a sample is taken with the same procedure used as that for flushing.

xxv. The sample is transferred to clean and dry green topped sample vials and placed in the fridge ready for analysis.

xxvi. The sample tubes used to sample the equilibrium mixture, are now washed with methanol, and allowed to dry before the next sample is needed.

xxvii. It is important to test the temperature of the cooling water, if an increase in temperature is noticed, the ice bricks are to be placed back in the freezer and new ice bricks placed in the cooling water.

The next component can now be added. The process for binary and ternary systems is slightly different

In a binary system.

xxviii. Assuming the initial mixture was pure component A, then pure component B is added to the Feed Chamber (I). This is approximately 10 ml, or the volume needed to get to the same level as that at the beginning of the first run. If too much mixture is now in the still it can be drained through valve V10 until the correct volume is reached.

xxix. Once this mixture has reached equilibrium and sampled, another 10 ml of pure component B is added to the still.

xxx. This is continued until the mixture is approximately 0.5 mole fraction of B.

xxxi. This still is washed and drained (below), dried and 110 ml pure component B is added to the still.

xxxii. Now pure component A is added 10 ml at a time until 0.5 mole fraction of a is reached

In a ternary system

xxviii. Once a binary system has been completely populated, both from pure A adding B and from pure B adding A. The still is drained but not washed. Approximately 110 ml of pure C is added to the still

xxix. This pure C will then have entrained amounts of A and B. This mixture is allowed to come to equilibrium and the sampled.

xxx. Approximately 10 ml of pure A is added to the mixture, this is allowed to come to equilibrium and sampled.

xxxi. Next approximately 10 ml of pure B is added to the still and allowed to come to equilibrium. Adding pure A and B until the mixture has a concentration of equal A, B, and C (0.33, 0.33, 0.33). The still is then drained, this same procedure is done starting with pure A and with pure B

xxxii. Once data is collected coming from the pure components and moving towards the centre of the Gibbs triangle, the spaces in which no data exists is investigated.

The still can now be drained and washed.

C.3. Washing and draining

xxxiii. Generally, after a day's run the still will not be ready to be drained and washed, in these cases the liquid in the still can be left over night.

xxxiv. When testing on a particular system is finished, the still can be turned off. This can be done by switching off at the wall. If running over or under-pressure the argon gas canister can be closed as well as the shut-off valve, or the vacuum pump can be turned off and the shut-off valve closed

xxxv. It is important to allow the still to cool down before any of the contents is drained, waiting approximately 45 min for this to occur.

xxxvi. Draining the still can be obtained by opening valve V10 and allowing the still to drain.

xxxvii. Some entrained liquid will still be in the still, it is therefore important to wash the still with a solvent that dissolves all the liquids used in the experiment. For the systems in this work wash acetone is used. Approximately 110 ml of wash acetone is added to the feed chamber (1), valve V1 is opened and the wash acetone fills the mixing and heating chambers, the still can be turned on again, however the heater power must be decreased to approximately 30%.

xxxviii. The still can be allowed to run for approximately an hour, flushing the sample ports often.

xxxix. After an hour, the still can be turned off at the wall, again it needs to be allowed to cool down.

xl. Once cool the still can be drained through valve V10.

xli. Leaving the magnetic stirrer on, cap C1 can be removed, and compressed air added to the opening. This allows as for as much draining as possible to occur.

xlii. After approximately five minutes Cap C1 can be replaced and Cap C2 removed. With the compressed air added to the evaporation chamber, pushing any liquid out of this area. In order to try drain different areas, different valves are opened and closed

The sample wells are dried by closing V10 opening Valves (V4,5,7, and 9) placing the compressed air either on open cap C1 or C2. While placing the magnet above the two magnetic rods

The feed chamber and mixing chamber are dried by closing all valves that are open and opening valves (V1-3) and placing the compressed air on the open caps

The over and under-pressure pipelines are drained by closing all valves and opening valves (V5-9)

xliii. Once the still has been adequately dried with the compressed air, all valves are opened, and the cartridge heater is unscrewed and removed. The compressed air is then placed where the cartridge heater was and allowed to flow through the still. After approximately 45 minutes the compressed air can be turned off

xliv. The valves are left open and the still can be left over night in order to completely dry.

Appendix D. GC error analysis

D.1. 1-propanol/2-propanol/2-butanone

Table D.1.: GC error analysis of 1-propanol + 2-propanol + 2-butanone

	1-prop mass	2-prop mass	MEK mass	IS mass	1-prop mole frac	2-prop mole frac	MEK mole frac	GC 1-propmass	GC 2-propmass	GC 2-MEK mass	GC 1-prop mole frac	GC 2-prop mole frac	GC 2-MEK mole frac	GC error mole frac	GC error lower mass	GC error higher mass	Ave Error
1a	7.64	16.32	24.16	22.08	0.173	0.370	0.457	7.95	16.54	24.85	0.176	0.366	0.458	0.007	0.007	0.007	
1b	7.64	16.32	24.16	22.08	0.173	0.370	0.457	7.98	16.48	24.81	0.177	0.365	0.458	0.009	0.009	0.008	
1c	7.64	16.32	24.16	22.08	0.173	0.370	0.457	7.94	16.57	24.79	0.176	0.367	0.457	0.006	0.006	0.006	0.007
2a	15.34	22.02	5.46	23.15	0.366	0.525	0.109	15.61	22.16	5.51	0.368	0.523	0.108	0.005	0.005	0.005	
2b	15.34	22.02	5.46	23.15	0.366	0.525	0.109	15.69	22.11	5.52	0.370	0.521	0.108	0.008	0.008	0.008	
2c	15.34	22.02	5.46	23.15	0.366	0.525	0.109	15.67	22.15	5.51	0.369	0.522	0.108	0.007	0.007	0.006	0.006
3a	21.1	6.1	12.42	22.89	0.562	0.162	0.276	22.05	6.24	12.62	0.568	0.161	0.271	0.008	0.008	0.008	
3b	21.1	6.1	12.42	22.89	0.562	0.162	0.276	22.05	6.25	12.62	0.568	0.161	0.271	0.008	0.007	0.008	
3c	21.1	6.1	12.42	22.89	0.562	0.162	0.276	22.08	6.25	12.65	0.568	0.161	0.271	0.008	0.007	0.008	0.008

D.2. 1-propanol/ethyl acetate/2-butanone

Table D.2: GC error analysis of 1-propanol + ethyl acetate+ 2-butanone

	1-prop mass	Eth ace mass	MEK mass	IS mass	1-prop mole frac	Ethyl ace mole frac	MEK mole frac	GC 1-prop mass	GC Eth ace mass	GC MEK mass	GC 1-prop mole frac	GC eth ace mole frac	GC MEK mole frac	GC error mole frac	GC error lower mass	GC error higher mass	Ave Error
1a	7.33	16.01	23.55	23.44	0.194	0.288	0.518	7.97	16.74	24.85	0.199	0.285	0.516	0.009	0.009	0.009	
1b	7.33	16.01	23.55	23.44	0.194	0.288	0.518	7.95	16.71	24.81	0.199	0.285	0.517	0.009	0.009	0.009	
1c	7.33	16.01	23.55	23.44	0.194	0.288	0.518	7.99	16.78	24.79	0.199	0.285	0.515	0.009	0.009	0.008	0.009
2a	17.28	21.42	7.22	23.21	0.456	0.385	0.159	17.65	22.14	7.51	0.452	0.387	0.160	0.005	0.005	0.005	
2b	17.28	21.42	7.22	23.21	0.456	0.385	0.159	17.64	22.18	7.53	0.452	0.387	0.161	0.006	0.006	0.006	
2c	17.28	21.42	7.22	23.21	0.456	0.385	0.159	17.68	22.15	7.57	0.452	0.386	0.161	0.005	0.005	0.005	0.005
3a	21.54	5.91	12.42	23.84	0.600	0.112	0.288	21.86	6.12	12.62	0.598	0.114	0.288	0.004	0.004	0.003	
3b	21.54	5.91	12.42	23.84	0.600	0.112	0.288	21.84	6.18	12.62	0.597	0.115	0.288	0.006	0.006	0.005	
3c	21.54	5.91	12.42	23.84	0.600	0.112	0.288	21.91	6.25	12.65	0.597	0.116	0.287	0.007	0.007	0.007	0.005

D.3. 1-propanol/methyl propionate/2-butanone

Table D.3.: GC error analysis of 1-propanol + methyl propionate + 2-butanone

sample	1-prop (mass)	Met prop (mass)	MEK (mass)	IS (mass)	1-propanol (mole frac)	Met prop (mole frac)	MEK (mole frac)	GC 1-propanol (mass)	GC Met prop (mass)	MEK (mass)	GC 1-propanol (mole frac)	GC Met prop (mole frac)	GC MEK (mole frac)	GC error mole frac	GC error lower mass	GC error higher mass	Ave Error
1a	6.91	15.92	21.25	22.15	0.195	0.306	0.499	7.44	16.21	22.15	0.201	0.299	0.499	0.013	0.014	0.013	
1b	6.91	15.92	21.25	22.15	0.195	0.306	0.499	7.48	16.28	22.18	0.202	0.300	0.499	0.014	0.014	0.013	
1c	6.91	15.92	21.25	22.15	0.195	0.306	0.499	7.45	16.24	22.19	0.201	0.299	0.500	0.013	0.013	0.013	0.013
2a	17.81	20.45	6.14	22.5	0.483	0.378	0.139	17.99	21	6.85	0.473	0.377	0.150	0.011	0.012	0.011	
2b	17.81	20.45	6.14	22.5	0.483	0.378	0.139	18.01	20.95	6.81	0.474	0.376	0.149	0.011	0.011	0.011	
2c	17.81	20.45	6.14	22.5	0.483	0.378	0.139	18	20.98	6.85	0.473	0.376	0.150	0.011	0.012	0.011	0.011
3a	20.65	7.12	13.15	23.18	0.566	0.133	0.301	21.01	7.32	14.15	0.556	0.132	0.312	0.011	0.011	0.011	
3b	20.65	7.12	13.15	23.18	0.566	0.133	0.301	21.03	7.31	14.12	0.557	0.132	0.311	0.011	0.011	0.011	
3c	20.65	7.12	13.15	23.18	0.566	0.133	0.301	21.05	7.31	14.15	0.556	0.132	0.312	0.011	0.011	0.011	0.011

D.4. 1-propanol/propyl formate/2-butanone

Table D.4: GC error analysis of 1-propanol + propyl formate + 2-butanone

	1-propanol (mass)	Prop-form (mass)	2-butanone (mass)	standard (mass)	1-propanol (mole frac)	Prop form (mole frac)	2-butanone (mole frac)	GC 1-propanol (mass)	GC Prop form (mass)	GC 2-butanone (mass)	GC 1-propanol (mole frac)	GC 2-prop form (mole frac)	GC 2-butanone (mole frac)	GC error mole frac	GC error -0.01mg	GC error +0.01 mg	Ave Error
1a	7.25	17.42	20.56	25.42	0.200	0.328	0.472	7.54	18.56	21.23	0.199	0.334	0.467	0.007	0.007	0.008	0.007
1b	7.25	17.42	20.56	25.42	0.200	0.328	0.472	7.52	18.42	21.19	0.199	0.333	0.468	0.006	0.006	0.006	
1c	7.25	17.42	20.56	25.42	0.200	0.328	0.472	7.56	18.55	21.19	0.200	0.334	0.466	0.007	0.007	0.007	
2a	16.49	22.02	5.42	21.23	0.458	0.417	0.125	16.95	23	6.15	0.449	0.415	0.136	0.010	0.010	0.010	0.011
2b	16.49	22.02	5.42	21.23	0.458	0.417	0.125	17	23.05	6.18	0.449	0.415	0.136	0.011	0.011	0.010	
2c	16.49	22.02	5.42	21.23	0.458	0.417	0.125	16.98	23.05	6.19	0.449	0.415	0.136	0.011	0.011	0.011	
3a	21.6	6.12	12.4	24,6	0,598	0,116	0,286	22,01	6,36	13.42	0.586	0.116	0.298	0,.012	0.012	0.012	0.012
3b	21.6	6.12	12.4	24.6	0.598	0.116	0.286	21.98	6.35	13.41	0.586	0.116	0.298	0.012	0.012	0.012	
3c	21.6	6.12	12.4	24.6	0.598	0.116	0.286	22.01	6.36	13.42	0.586	0.116	0.298	0.012	0.012	0.012	

Appendix E. GC Calibration

Table D.4: GC calibration curve gradients and R^2 values

Compound	K	R^2
1-propanol/2-butanone		
1-propanol	0.9834	0.9999
2-butanone	0.6984	0.9999
1-propanol/2-propanol		
1-propanol	0.9254	1.0000
2-propanol	0.7456	0.9999
1-propanol/methyl propionate		
1-propanol	1.035	0.9998
Methyl propionate	0.7012	0.9999
1-propanol/ethyl acetate		
1-propanol	1.0021	0.9997
Ethyl acetate	0.7564	1.0000
2-butanone/2-propanol		
2-butanone	0.8546	0.9999
2-propanol	0.7789	1.0000
2-butanone/propyl formate		
2-butanone	0.7664	0.9999
Propyl formate	0.6213	1.0000
2-butanonte/ethyl acetate		
2-butanone	0.7544	0.9998
Ethyl acetate	0.7001	0.9999
2-butanone/1-propanol/2-propanol		
2-butanone	0.7666	0.9999
1-propanol	1.0133	0.9998
2-propanol	0.6946	0.9999
2-butanone/1-propanol/ethyl acetate		
2-butanone	0.6899	0.9996
1-propanol	0.9956	0.9999
Ethyl acetate	0.7006	1.0000
2-butanone/1-propanol/methyl propionate		
2-butanone	0.7566	1.0000
1-propanol	1.1112	0.9999
Methyl propionate	0.6695	0.9998
2-butanone/1-propanol/propyl formate		
2-butanone	0.8001	0.9997
1-propanol	1.0332	0.9996
Propyl formate	0.6953	0.9996

Appendix F. Experimental results

F.1. Binary results

Table F.1.: 1-propanol/2-butanone (1) at 1.013 bar with consistency test results

Sample	Temperature (K)	Pressure (bar)	X1	X2	Y1	Y2	γ1	γ2	D	Dmax	L	W	L/W	D
1	370.31	1.01	0.000	1.000	0.000	1.000	0.000	1.002						
2	368.80	1.01	0.041	0.959	0.092	0.908	1.376	1.004			0.967	1.000	0.967	1.694
3	368.46	1.01	0.038	0.962	0.109	0.891	1.765	1.004	0.010	0.270	1.348	1.391	0.969	1.559
4	367.67	1.01	0.062	0.938	0.152	0.848	1.548	1.001	0.012	0.258	1.793	1.860	0.964	1.817
5	367.36	1.01	0.069	0.931	0.178	0.822	1.636	1.001	-0.024	0.260	1.999	2.067	0.967	1.670
6	366.01	1.01	0.117	0.883	0.230	0.770	1.307	1.029	0.008	0.269	2.653	2.754	0.963	1.867
7	365.70	1.01	0.129	0.871	0.264	0.736	1.367	1.029	-0.018	0.270	2.774	2.873	0.966	1.754
8	364.61	1.01	0.161	0.839	0.307	0.693	1.314	1.030	0.004	0.270	3.385	3.519	0.962	1.932
9	364.17	1.01	0.167	0.833	0.331	0.669	1.383	1.030	0.021	0.270	3.730	3.873	0.963	1.879
10	363.70	1.01	0.195	0.805	0.343	0.657	1.250	1.069	0.008	0.274	3.782	3.926	0.963	1.880
11	362.89	1.01	0.221	0.779	0.386	0.614	1.265	1.069	0.004	0.276	4.177	4.341	0.962	1.928
12	362.30	1.01	0.258	0.742	0.420	0.580	1.201	1.069	0.014	0.283	4.199	4.371	0.961	2.013
13	360.76	1.01	0.328	0.672	0.506	0.494	1.192	1.069	-0.006	0.287	4.603	4.798	0.959	2.069
14	360.49	1.01	0.343	0.657	0.517	0.483	1.174	1.118	0.021	0.291	4.633	4.823	0.961	2.003
15	359.81	1.01	0.373	0.627	0.555	0.445	1.185	1.072	-0.001	0.293	4.825	5.033	0.959	2.107
16	359.78	1.01	0.370	0.630	0.550	0.450	1.184	1.113	0.006	0.292	4.903	5.108	0.960	2.044
17	358.45	1.01	0.451	0.549	0.616	0.384	1.133	1.118	0.011	0.300	4.864	5.077	0.958	2.144
18	358.38	1.01	0.439	0.561	0.615	0.385	1.165	1.308	0.006	0.299	5.140	5.360	0.959	2.099
19	358.25	1.01	0.462	0.538	0.628	0.372	1.135	1.409	-0.010	0.302	4.883	5.090	0.959	2.080
20	357.16	1.01	0.533	0.467	0.691	0.309	1.120	1.113	-0.017	0.307	4.722	4.931	0.958	2.171
21	356.86	1.01	0.560	0.440	0.709	0.291	1.104	1.444	-0.018	0.309	4.541	4.734	0.959	2.087
22	356.22	1.01	0.632	0.368	0.752	0.248	1.058	0.000	-0.012	0.314	3.853	4.012	0.960	2.021
23	355.29	1.01	0.705	0.295	0.788	0.212	1.023	1.308	0.028	0.325	3.378	3.521	0.959	2.077
24	354.51	1.01	0.783	0.217	0.837	0.163	1.003	1.409	0.022	0.315	2.628	2.732	0.962	1.946

25	354.05	1.01	0.834	0.166	0.875	0.125	0.998	1.444	0.006	0.312	2.051	2.125	0.965	1.762
26	352.67	1.01	1.000	0.000	1.000	0.000	0.994	0.000						
													D	1.61273

Table F.2: 1-propanol/propyl formate (1) at 1.013 bar with consistency test results

Sample	Temperature (K)	pressure (bar)	X1	X2	Y1	Y2	γ1	γ2	D	Dmax	L	W	L/W	D
1	354.03	1.01	0.000	1.000	0.000	1.000								
2	352.69	1.01	0.071	0.929	0.076	0.924	2.153	1.043			2.736	2.880	0.950	2.556
3	352.64	1.01	0.076	0.924	0.076	0.924	2.029	1.050	0.003	0.29	2.883	3.028	0.952	2.459
4	352.93	1.01	0.203	0.797	0.164	0.836	1.624	1.091	0.004	0.34	4.989	5.172	0.965	1.806
5	353.32	1.01	0.296	0.704	0.217	0.783	1.451	1.142	0.013	0.32	6.296	6.499	0.969	1.590
6	353.80	1.01	0.381	0.619	0.244	0.756	1.241	1.235	-0.002	0.32	7.313	7.526	0.972	1.435
7	354.45	1.01	0.464	0.536	0.290	0.710	1.179	1.311	0.026	0.32	8.082	8.293	0.975	1.287
8	354.68	1.01	0.500	0.500	0.307	0.693	1.147	1.363	0.013	0.32	8.466	8.675	0.976	1.220
9	355.98	1.01	0.594	0.406	0.358	0.642	1.066	1.492	0.002	0.32	8.718	8.891	0.981	0.982
10	356.53	1.01	0.640	0.360	0.381	0.619	1.030	1.592	0.007	0.31	8.903	9.056	0.983	0.852
11	357.75	1.01	0.704	0.296	0.446	0.554	1.041	1.670	0.046	0.31	8.706	8.807	0.988	0.578
12	358.27	1.01	0.726	0.274	0.462	0.538	1.023	1.727	-0.006	0.30	8.536	8.613	0.991	0.451
13	360.06	1.01	0.803	0.197	0.541	0.459	1.007	1.940	0.031	0.30	7.934	7.920	1.002	0.087
14	360.82	1.01	0.828	0.172	0.569	0.431	0.996	2.034	0.000	0.28	7.545	7.491	1.007	0.359
15	366.03	1.01	0.940	0.060	0.818	0.182	1.026	2.099	0.060	0.30	3.994	3.660	1.091	4.359
16	363.74	1.01	0.899	0.101	0.710	0.290	1.019	2.135	-0.011	0.26	5.686	5.475	1.039	1.891
17	362.17	1.01	0.861	0.139	0.628	0.372	1.001	2.087	-0.035	0.27	6.694	6.569	1.019	0.944
18	370.31	1.01	1.000	0.000	1.000	0.000								
													D	1.130

Table F.3. 1-propanol/ethyl acetate(1) at 1.013 bar with consistency test results

Sample	Temperature (K)	X1	X2	Y1	Y2	γ1	γ2	D	Dmax	L	W	L/W	D
1	350.06	1.000	0.000	1.000	0.000	1.009							
2	351.38	0.879	0.121	0.907	0.093	0.996	1.663			1.827	1.929	0.947	2.701
3	352.33	0.758	0.242	0.830	0.170	1.027	1.444	0.00	0.52	3.623	3.823	0.948	2.689
4	353.01	0.685	0.315	0.790	0.210	1.057	1.336	0.00	0.50	4.513	4.761	0.948	2.667
5	355.41	0.500	0.500	0.671	0.329	1.139	1.191	-0.01	0.51	5.914	6.228	0.950	2.581
6	356.47	0.419	0.581	0.625	0.375	1.224	1.118	0.00	0.49	6.434	6.767	0.951	2.527
7	357.46	0.359	0.641	0.590	0.410	1.307	1.063	-0.01	0.48	6.582	6.917	0.952	2.481
8	359.08	0.311	0.689	0.536	0.464	1.303	1.048	-0.02	0.46	5.854	6.145	0.953	2.429
9	360.81	0.244	0.756	0.460	0.540	1.351	1.036	0.00	0.45	5.342	5.600	0.954	2.352
10	362.09	0.191	0.809	0.399	0.601	1.439	1.023	0.01	0.44	5.005	5.239	0.955	2.284
11	363.48	0.155	0.845	0.346	0.654	1.474	1.009	-0.02	0.43	4.244	4.437	0.957	2.221
12	364.97	0.117	0.883	0.280	0.720	1.512	1.003	0.00	0.42	3.420	3.570	0.958	2.143
13	367.03	0.079	0.921	0.179	0.821	1.347	1.012	-0.01	0.42	2.006	2.089	0.960	2.019
14	367.92	0.052	0.948	0.135	0.865	1.503	1.001	-0.01	0.41	1.570	1.632	0.962	1.912
15	370.22	0.000	1.000	0.000	1.000		1.005						
												D	2.23

Table F.4. 1-propanol(1)/methyl propionate at 1.013 bar with consistency test results

Sample	Temperature (K)	X1	X2	Y1	Y2	γ1	γ2	D	Dmax	L	W	L/W	D
1	370.06	0.000	1.000	0.000	1.000		1.011						
2	367.85	0.042	0.958	0.117	0.883	1.737	1.014			1.908	1.964	0.971	1.446
3	365.54	0.092	0.908	0.219	0.781	1.589	1.034	0.03	0.42	3.487	3.601	0.968	1.616
4	363.90	0.138	0.862	0.300	0.700	1.524	1.041	0.00	0.42	4.449	4.602	0.967	1.691
5	363.14	0.158	0.842	0.336	0.664	1.526	1.042	0.00	0.42	4.910	5.084	0.966	1.741
6	361.89	0.189	0.811	0.395	0.605	1.558	1.036	0.00	0.43	5.692	5.905	0.964	1.835
7	359.36	0.289	0.711	0.501	0.499	1.397	1.079	0.01	0.45	6.667	6.933	0.962	1.959
8	358.77	0.308	0.692	0.514	0.486	1.370	1.107	0.02	0.45	6.954	7.239	0.961	2.007
9	358.14	0.336	0.664	0.547	0.453	1.363	1.103	-0.01	0.46	7.132	7.430	0.960	2.047
10	357.34	0.386	0.614	0.578	0.422	1.286	1.149	0.01	0.47	7.111	7.413	0.959	2.083
11	356.38	0.438	0.562	0.619	0.381	1.251	1.179	0.01	0.47	7.197	7.514	0.958	2.153
12	355.14	0.540	0.460	0.680	0.320	1.160	1.274	0.01	0.48	6.661	6.964	0.956	2.230
13	354.88	0.556	0.444	0.692	0.308	1.156	1.284	0.00	0.48	6.630	6.936	0.956	2.257
14	354.13	0.613	0.387	0.724	0.276	1.124	1.363	0.02	0.48	6.342	6.645	0.954	2.339
15	353.64	0.645	0.355	0.745	0.255	1.117	1.401	0.01	0.48	6.236	6.544	0.953	2.408
16	353.02	0.740	0.260	0.795	0.205	1.060	1.579	0.00	0.49	5.034	5.291	0.951	2.492
17	352.64	0.802	0.198	0.832	0.168	1.036	1.727	0.01	0.48	4.177	4.399	0.950	2.578
18	352.31	0.874	0.126	0.884	0.116	1.021	1.901	0.01	0.48	3.023	3.192	0.947	2.718
19	352.26	0.912	0.088	0.915	0.085	1.015	1.999	0.00	0.46	2.267	2.398	0.946	2.799
20	352.16	0.945	0.055	0.943	0.057	1.012	2.154	0.01	0.46	1.655	1.756	0.942	2.969
21	352.58	1.000	0.000	1.000	0.000	1.001							
												D	2.017

Table F.5.: 1-propanol(1)/2-propanol at 1.013 bar with consistency test results

Sample	Temperature (K)	X1	X2	Y1	Y2	γ1	γ2	D	Dmax	L	W	L/W	D
1	370.25	0.000	1.000	0.000	1.000		1.004						
2	367.85	0.112	0.888	0.202	0.798	1.117	0.988			0.794	0.838	0.947	2.700
3	364.90	0.277	0.723	0.422	0.578	1.049	0.987	-0.03	0.30	1.265	1.306	0.968	1.625
4	363.90	0.320	0.680	0.488	0.512	1.092	0.965	-0.01	0.29	1.627	1.679	0.969	1.565
5	363.14	0.381	0.619	0.537	0.463	1.039	0.988	0.00	0.29	1.479	1.516	0.976	1.217
6	361.42	0.496	0.504	0.641	0.359	1.016	1.009	0.00	0.30	1.475	1.494	0.987	0.638
7	360.36	0.560	0.440	0.712	0.288	1.042	0.966	-0.01	0.31	1.593	1.607	0.991	0.454
8	359.94	0.605	0.395	0.738	0.262	1.016	0.996	0.00	0.31	1.341	1.337	1.003	0.165
9	358.35	0.719	0.281	0.825	0.175	1.016	0.997	0.00	0.33	1.234	1.205	1.024	1.165
10	357.69	0.801	0.199	0.865	0.135	0.981	1.117	0.00	0.33	0.670	0.600	1.116	5.489
11	357.28	0.818	0.182	0.892	0.108	1.007	0.994	0.00	0.33	0.827	0.762	1.086	4.102
12	355.28	1.000	0.000	1.000	0.000	1.000							
												D	1.248

Table F.6. 2-butanone(1)/propyl formate at 1.013 bar with consistency test results

Sample	Temperature (K)	X1	X2	Y1	Y2	γ1	γ2	D	Dmax	L	W	L/W	D
1	352.41	1.000	0.000	1.000	0.000	1.003	0						
2	352.06	0.960	0.040	0.961	0.039	1.014	1.058			0.505	0.511	0.987	0.644
3	352.06	0.901	0.099	0.902	0.098	1.015	1.057	0.001	0.320	0.609	0.614	0.991	0.432
4	352.06	0.893	0.107	0.896	0.104	1.016	1.047	0.000	0.290	0.622	0.627	0.992	0.411
5	352.15	0.842	0.158	0.844	0.156	1.013	1.053	-0.003	0.300	0.63	0.631	0.999	0.039
6	352.18	0.803	0.197	0.805	0.195	1.012	1.059	-0.001	0.290	0.667	0.665	1.002	0.104
7	352.26	0.705	0.295	0.709	0.291	1.012	1.05	-0.003	0.300	0.754	0.748	1.008	0.376
8	352.28	0.653	0.347	0.662	0.338	1.02	1.035	0.001	0.290	0.822	0.816	1.008	0.414
9	352.31	0.618	0.382	0.626	0.374	1.019	1.039	0.001	0.290	0.851	0.843	1.009	0.472
10	352.35	0.566	0.434	0.576	0.424	1.022	1.036	0.001	0.290	0.899	0.889	1.011	0.527
11	352.4	0.541	0.459	0.556	0.444	1.031	1.023	-0.001	0.290	0.889	0.879	1.012	0.612
12	352.46	0.509	0.491	0.524	0.476	1.029	1.025	0.000	0.290	0.881	0.869	1.014	0.704
13	352.61	0.479	0.521	0.494	0.506	1.026	1.022	-0.006	0.290	0.781	0.766	1.02	1.01
14	352.64	0.454	0.546	0.463	0.537	1.014	1.033	0.001	0.290	0.792	0.776	1.021	1.018
15	352.69	0.440	0.560	0.455	0.545	1.026	1.021	-0.002	0.290	0.765	0.748	1.022	1.111
16	353.03	0.310	0.690	0.345	0.655	1.094	0.984	0.001	0.300	0.632	0.613	1.031	1.532
17	353.51	0.195	0.805	0.216	0.784	1.072	0.994	0.005	0.290	0.335	0.317	1.056	2.713
18	354.42	0.000	1.000	0.000	1.000	0	0.991						
												D	0.665

Table F.7. 2-butanone/ethyl acetate(1) at 1.013 bar with consistency test results

Sample	Temperature (K)	X1	X2	Y1	Y2	γ1	γ2	D	Dmax	L	W	L/W	D
1	350.01	1.000	0.000	1.000	0.000	1.009							
3	349.94	0.830	0.170	0.830	0.170	1.013	1.083	0.005	0.458	0.761	0.768	0.990	0.485
4	349.98	0.674	0.326	0.688	0.312	1.032	1.039	0.008	0.458	1.051	1.098	0.957	2.186
5	350.09	0.622	0.378	0.633	0.367	1.026	1.049	-0.001	0.480	1.051	1.098	0.957	2.192
6	350.25	0.541	0.459	0.558	0.442	1.035	1.034	-0.002	0.453	1.066	1.114	0.957	2.197
7	350.30	0.510	0.490	0.528	0.472	1.037	1.033	0.001	0.454	1.082	1.130	0.957	2.199
8	350.38	0.481	0.519	0.503	0.497	1.043	1.026	-0.001	0.450	1.063	1.111	0.957	2.191
9	350.43	0.447	0.553	0.467	0.533	1.041	1.030	0.003	0.450	1.087	1.135	0.957	2.192
10	350.46	0.428	0.572	0.448	0.552	1.043	1.029	0.001	0.449	1.099	1.148	0.957	2.192
11	350.55	0.396	0.604	0.421	0.579	1.057	1.019	-0.001	0.448	1.078	1.126	0.957	2.177
12	350.64	0.366	0.634	0.390	0.610	1.054	1.021	0.000	0.449	1.052	1.098	0.958	2.159
13	350.94	0.302	0.698	0.327	0.673	1.060	1.014	-0.006	0.447	0.890	0.928	0.960	2.059
14	351.09	0.268	0.732	0.290	0.710	1.055	1.015	-0.002	0.448	0.815	0.848	0.961	1.989
15	351.30	0.198	0.802	0.221	0.779	1.081	1.009	0.003	0.445	0.757	0.786	0.963	1.879
16	351.42	0.180	0.820	0.200	0.800	1.072	1.009	-0.002	0.449	0.678	0.702	0.965	1.774
17	351.77	0.120	0.880	0.144	0.856	1.144	0.995	-0.005	0.441	0.460	0.472	0.975	1.257
18	352.41	0.000	1.000	0.000	1.000		1.003						
												D	1.388

Table F.8. 2-butanone(1)/methyl propionate at 1.013 bar with consistency test results

Sample	Temperature (K)	X1	X2	Y1	Y2	γ1	γ2	D	Dmax	L	W	L/W	D
1	352.38	0.000	1.000	0.000	1.000		1.007	0.000					
2	352.07	0.073	0.927	0.081	0.919	1.112	1.009	0.000		0.517	0.540	0.958	2.157
3	352.10	0.072	0.928	0.080	0.920	1.128	1.007	-0.002	0.28	0.487	0.509	0.958	2.163
4	351.88	0.150	0.850	0.160	0.840	1.092	1.011	-0.001	0.30	0.699	0.730	0.958	2.146
5	351.67	0.222	0.778	0.235	0.765	1.086	1.014	0.003	0.29	0.902	0.942	0.958	2.166
6	351.67	0.221	0.779	0.236	0.764	1.095	1.011	0.000	0.29	0.902	0.942	0.958	2.166
7	351.52	0.331	0.669	0.338	0.662	1.052	1.026	-0.002	0.30	1.040	1.087	0.957	2.212
8	351.38	0.464	0.536	0.466	0.534	1.041	1.036	0.004	0.30	1.166	1.220	0.955	2.278
9	351.33	0.502	0.498	0.502	0.498	1.039	1.041	0.003	0.29	1.211	1.268	0.955	2.300
10	351.33	0.541	0.459	0.540	0.460	1.036	1.045	0.000	0.29	1.207	1.264	0.955	2.318
11	351.35	0.605	0.395	0.596	0.404	1.022	1.065	0.001	0.29	1.180	1.237	0.954	2.345
12	351.96	0.979	0.021	0.977	0.023	1.015	1.124	0.011	0.88	0.527	0.552	0.956	2.247
13	351.77	0.912	0.088	0.905	0.095	1.016	1.101	0.000	0.37	0.725	0.760	0.954	2.360
14	351.64	0.849	0.151	0.840	0.160	1.017	1.090	-0.001	0.30	0.863	0.905	0.953	2.389
15	351.54	0.785	0.215	0.778	0.222	1.022	1.066	0.000	0.29	0.970	1.017	0.953	2.390
16	352.40	1.000	0.000	1.000	0.000	1.003							
												D	2.590

Table F.9. 2-butanone(1)/2-propanol at 1.013 bar with consistency test results

Sample	Temperature (K)	X1	X2	Y1	Y2	γ1	γ2	D	Dmax	L	W	L/W	D
1	355.23	0.000	1.000	0.000	1.000		1.002						
2	353.85	0.095	0.905	0.135	0.919	1.365	1.075			1.171	1.264	0.926	3.818
3	353.91	0.097	0.936	0.13	0.947	1.281	1.068	-0.02	0.30	1.113	1.203	0.925	3.888
4	352.31	0.21	0.825	0.289	0.923	1.384	1.262	0.32	0.33	2.466	2.619	0.942	3.004
5	351.97	0.258	0.798	0.335	0.817	1.32	1.169	-0.15	0.30	2.709	2.872	0.943	2.917
6	351.74	0.296	0.704	0.358	0.743	1.237	1.217	0.02	0.31	2.815	2.979	0.945	2.841
7	351.53	0.315	0.685	0.389	0.611	1.273	1.038	-0.20	0.32	2.98	3.152	0.945	2.81
8	351.09	0.409	0.591	0.453	0.547	1.16	1.095	0.00	0.33	3.187	3.363	0.948	2.695
9	350.65	0.542	0.458	0.561	0.439	1.098	1.156	0.00	0.33	3.277	3.447	0.95	2.54
10	350.51	0.609	0.391	0.61	0.39	1.067	1.21	0.01	0.33	3.232	3.395	0.952	2.454
11	350.5	0.653	0.347	0.649	0.351	1.059	1.227	0.00	0.32	3.118	3.27	0.953	2.385
12	350.57	0.704	0.296	0.691	0.309	1.044	1.263	0.00	0.32	2.9	3.036	0.955	2.285
13	350.82	0.795	0.205	0.764	0.236	1.014	1.379	0.00	0.33	2.378	2.476	0.96	2.018
14	351.1	0.847	0.153	0.82	0.18	1.012	1.393	0.00	0.32	1.936	2.005	0.966	1.735
15	351.46	0.902	0.098	0.877	0.123	1.005	1.464	0.00	0.32	1.401	1.434	0.977	1.176
16	352.54	1.000	0.000	1.000	0.000	0.998							
												D	2.26

F.2. Ternary results

Table F.10. 1-propanol(1)/2-butanone(2)/propyl formate(3) at 1.013 bar with consistency test results

Sample	Temperature (K)	X1	X2	X3	Y1	Y2	Y3	γ1	γ2	γ3	D	Dmax	L	W	L/W	D
1	365.10	0.937	0.008	0.055	0.804	0.009	0.187	0.907	1.569	2.619			4.738	4.970	0.953	2.391
2	363.55	0.857	0.077	0.066	0.598	0.171	0.231	1.013	1.334	1.930	0.39	0.45	5.139	5.396	0.952	2.440
3	362.55	0.817	0.104	0.079	0.612	0.190	0.198	0.978	1.284	1.742	0.48	0.53	4.561	4.758	0.959	2.107
4	361.34	0.704	0.267	0.028	0.486	0.453	0.062	0.924	1.320	1.787	0.13	0.52	5.549	5.862	0.947	2.738
5	360.84	0.731	0.121	0.148	0.466	0.207	0.327	1.064	1.219	1.589	0.35	0.61	5.745	6.024	0.954	2.367
6	358.55	0.606	0.356	0.038	0.406	0.525	0.069	1.040	1.289	1.673	0.20	0.52	7.679	8.101	0.948	2.679
7	356.73	0.608	0.236	0.156	0.369	0.348	0.283	1.143	1.165	1.482	0.40	0.47	7.397	7.821	0.946	2.783
8	356.60	0.581	0.206	0.214	0.385	0.272	0.342	1.120	1.250	1.647	0.33	0.47	7.991	8.429	0.948	2.669
9	356.52	0.614	0.232	0.154	0.398	0.329	0.273	1.099	1.151	1.422	0.10	0.57	5.512	5.810	0.949	2.632
10	356.39	0.467	0.481	0.052	0.295	0.625	0.080	1.145	1.108	1.340	0.14	0.52	5.729	6.070	0.944	2.886
11	355.48	0.423	0.412	0.165	0.268	0.501	0.231	1.124	1.120	1.358	0.13	0.53	5.138	5.436	0.945	2.818
12	355.36	0.389	0.551	0.060	0.241	0.674	0.085	1.082	1.169	1.471	0.17	0.52	6.730	7.120	0.945	2.817
13	355.34	0.470	0.356	0.174	0.280	0.455	0.265	1.275	1.087	1.302	0.35	0.49	6.475	6.858	0.944	2.872
14	355.28	0.451	0.344	0.205	0.316	0.408	0.276	1.175	1.104	1.338	0.16	0.48	6.072	6.435	0.944	2.901
15	355.28	0.429	0.375	0.197	0.277	0.451	0.273	1.281	1.063	1.233	0.26	0.48	5.687	6.038	0.942	2.987
16	355.13	0.398	0.371	0.231	0.278	0.428	0.294	1.218	1.087	1.323	0.18	0.49	5.993	6.353	0.943	2.916
17	355.06	0.413	0.396	0.192	0.273	0.466	0.261	1.204	1.110	1.349	0.25	0.47	6.690	7.088	0.944	2.889
18	355.05	0.449	0.317	0.235	0.294	0.381	0.326	1.204	1.083	1.292	0.21	0.50	5.478	5.814	0.942	2.973
19	354.87	0.375	0.448	0.177	0.244	0.522	0.234	1.154	1.158	1.414	0.26	0.48	7.183	7.603	0.945	2.846
20	354.87	0.467	0.308	0.225	0.291	0.384	0.325	1.252	1.066	1.280	0.34	0.49	6.414	6.809	0.942	2.982
21	354.84	0.418	0.270	0.312	0.282	0.310	0.409	1.220	1.073	1.276	0.19	0.59	4.736	5.030	0.941	3.019
22	354.69	0.330	0.572	0.098	0.216	0.657	0.127	1.255	1.080	1.284	0.20	0.51	6.212	6.592	0.942	2.970
23	354.54	0.392	0.346	0.261	0.262	0.398	0.340	1.266	1.072	1.233	0.30	0.48	6.310	6.705	0.941	3.037
24	354.48	0.388	0.220	0.392	0.260	0.251	0.489	1.270	1.062	1.220	0.22	0.58	4.785	5.091	0.940	3.100
25	354.42	0.315	0.526	0.159	0.212	0.593	0.195	1.263	1.068	1.229	0.23	0.51	6.174	6.562	0.941	3.050
26	354.30	0.370	0.229	0.401	0.246	0.258	0.496	1.366	1.047	1.184	0.33	0.50	5.804	6.172	0.940	3.074

27	354.28	0.351	0.293	0.356	0.252	0.324	0.423	1.286	1.051	1.203	0.12	0.66	3.927	4.190	0.937	3.247
28	354.20	0.264	0.664	0.072	0.178	0.735	0.087	1.285	1.052	1.191	0.06	0.49	4.063	4.335	0.937	3.248
29	354.15	0.266	0.628	0.106	0.179	0.695	0.126	1.380	1.039	1.164	0.21	0.57	5.467	5.820	0.939	3.128
30	353.74	0.298	0.256	0.446	0.212	0.276	0.512	1.273	1.050	1.185	0.12	1.01	3.304	3.547	0.931	3.550
31	353.73	0.211	0.755	0.034	0.138	0.822	0.039	1.058	1.077	1.287	0.07	0.74	4.907	5.231	0.938	3.193
32	353.63	0.273	0.449	0.278	0.148	0.500	0.352	1.164	1.075	1.197	0.41	0.53	5.501	5.856	0.939	3.125
33	353.61	0.287	0.153	0.560	0.171	0.170	0.659	2.933	0.900	0.898	0.27	0.95	1.896	2.078	0.912	4.581
34	353.58	0.132	0.781	0.087	0.198	0.725	0.077	1.184	1.080	1.146	-0.03	0.53	3.735	4.009	0.932	3.533
35	353.28	0.207	0.707	0.086	0.124	0.781	0.095	1.132	1.075	1.277	0.14	0.59	5.403	5.751	0.940	3.115
36	353.05	0.265	0.395	0.340	0.150	0.431	0.419	2.258	0.923	1.033	0.50	0.86	1.959	2.127	0.921	4.103
37	353.00	0.052	0.031	0.918	0.058	0.029	0.913	1.200	1.048	1.130	0.14	2.94	2.434	2.657	0.916	4.379
38	352.94	0.130	0.833	0.037	0.078	0.883	0.040	1.076	1.069	1.292	0.08	0.65	4.126	4.422	0.933	3.452
39	352.91	0.202	0.612	0.186	0.108	0.661	0.231	1.041	1.066	1.246	0.20	0.52	4.051	4.340	0.933	3.442
															D	2.20

Table F.11 1-propanol(1)/2-butanone(2)/ethyl acetate(3) at 1.013 bar with consistency test results

	T (K)	X1	X2	X3	Y1	Y2	Y3	γ1	γ2	γ3	D	Dmax	L	W	L/W	D
1	352.55	0.129	0.762	0.108	0.092	0.776	0.132	1.452	1.017	1.130						
2	354.79	0.341	0.580	0.079	0.226	0.664	0.110	1.230	1.065	1.209	0.04	0.76	2.648	2.646	1.000	0.021
5	358.05	0.460	0.476	0.064	0.289	0.608	0.103	1.019	1.072	1.271	-0.02	0.64	5.760	5.993	0.961	1.989
6	358.47	0.608	0.342	0.049	0.411	0.504	0.085	1.077	1.220	1.331	0.14	0.64	5.541	5.765	0.961	1.986
7	359.15	0.636	0.319	0.046	0.399	0.516	0.085	0.973	1.315	1.410	0.09	1.18	5.391	5.614	0.960	2.027
8	360.15	0.688	0.270	0.043	0.483	0.444	0.073	1.046	1.296	1.261	0.04	0.72	1.959	1.917	1.022	1.097
9	352.23	0.084	0.780	0.136	0.062	0.780	0.158	1.528	1.009	1.090	0.06	0.71	2.920	2.945	0.991	0.431
10	352.89	0.161	0.713	0.126	0.115	0.731	0.154	1.445	1.011	1.126	0.08	0.70	4.302	4.424	0.972	1.398
11	354.05	0.287	0.604	0.109	0.195	0.661	0.143	1.304	1.041	1.172	0.12	0.70	5.106	5.288	0.966	1.749
12	353.63	0.312	0.539	0.149	0.186	0.613	0.202	1.160	1.097	1.217	0.12	0.69	5.118	5.305	0.965	1.793

13	354.43	0.354	0.506	0.140	0.228	0.580	0.192	1.215	1.078	1.203	0.10	0.69	5.077	5.267	0.964	1.837
14	354.18	0.342	0.490	0.168	0.229	0.550	0.222	1.273	1.063	1.167	0.16	0.68	5.866	6.108	0.960	2.021
15	355.04	0.429	0.424	0.146	0.276	0.512	0.212	1.184	1.113	1.243	0.10	0.68	5.782	6.024	0.960	2.050
16	354.84	0.417	0.411	0.172	0.288	0.478	0.234	1.279	1.079	1.179	0.14	0.70	5.768	6.013	0.959	2.074
17	354.64	0.408	0.404	0.189	0.266	0.472	0.262	1.223	1.092	1.205	-0.34	0.71	6.082	6.348	0.958	2.138
18	355.36	0.463	0.364	0.173	0.347	0.525	0.127	1.362	1.316	0.627	0.17	0.69	6.082	6.357	0.957	2.212
19	354.74	0.435	0.340	0.224	0.284	0.406	0.310	1.213	1.111	1.199	0.38	1.05	5.989	6.267	0.956	2.268
20	354.38	0.416	0.317	0.267	0.266	0.371	0.363	1.208	1.103	1.192	0.07	0.73	2.366	2.508	0.944	2.906
21	350.51	0.100	0.075	0.825	0.077	0.075	0.848	1.716	1.060	1.023	0.12	0.74	3.666	3.882	0.944	2.869
22	351.12	0.184	0.068	0.747	0.120	0.082	0.798	1.410	1.256	1.041	0.03	0.72	3.197	3.368	0.949	2.602
23	350.97	0.148	0.157	0.695	0.122	0.156	0.723	1.799	1.042	1.018	0.15	0.71	5.121	5.402	0.948	2.668
24	351.93	0.280	0.136	0.584	0.186	0.148	0.665	1.397	1.110	1.081	0.21	0.73	4.549	4.799	0.948	2.678
25	352.41	0.275	0.136	0.589	0.184	0.140	0.675	1.377	1.031	1.073	0.08	0.70	5.556	5.834	0.952	2.437
26	352.41	0.309	0.250	0.441	0.227	0.266	0.508	1.508	1.066	1.076	0.25	0.70	5.660	5.943	0.952	2.438
27	352.89	0.337	0.246	0.417	0.218	0.267	0.516	1.302	1.068	1.139	0.17	0.69	6.779	7.112	0.953	2.397
28	353.43	0.413	0.274	0.313	0.273	0.314	0.413	1.301	1.115	1.191	0.20	1.00	5.864	6.149	0.954	2.369
29	353.52	0.373	0.277	0.350	0.239	0.313	0.449	1.254	1.092	1.156	0.02	0.60	6.232	6.521	0.956	2.269
30	361.76	0.846	0.112	0.042	0.720	0.193	0.087	1.188	1.292	1.447	0.00	0.61	5.018	5.244	0.957	2.195
31	362.86	0.838	0.125	0.037	0.757	0.183	0.061	1.206	1.060	1.109	0.09	0.65	4.874	5.101	0.956	2.275
32	363.68	0.884	0.076	0.040	0.818	0.116	0.066	1.197	1.074	1.091	0.00	0.64	6.571	6.886	0.954	2.342
33	360.44	0.790	0.114	0.096	0.649	0.175	0.176	1.209	1.198	1.332	0.22	0.66	6.317	6.623	0.954	2.370
34	358.68	0.673	0.158	0.169	0.456	0.236	0.307	1.072	1.232	1.393	0.20	0.66	6.329	6.619	0.956	2.241
35	357.39	0.592	0.261	0.147	0.392	0.358	0.251	1.103	1.176	1.358	0.21	0.67	6.369	6.668	0.955	2.294
36	356.70	0.559	0.253	0.188	0.364	0.337	0.299	1.118	1.167	1.295	0.18	0.67	6.145	6.420	0.957	2.192
37	355.73	0.489	0.329	0.182	0.325	0.406	0.269	1.188	1.114	1.241	0.18	0.68	6.895	7.218	0.955	2.289
38	355.73	0.532	0.285	0.182	0.342	0.373	0.286	1.147	1.179	1.316	0.13	0.69	6.332	6.615	0.957	2.183
39	355.06	0.462	0.354	0.184	0.296	0.434	0.270	1.179	1.129	1.258	0.26	0.69	6.093	6.368	0.957	2.207
40	354.64	0.430	0.345	0.224	0.249	0.424	0.326	1.084	1.148	1.265	0.17	0.69	5.855	6.109	0.958	2.128
41	354.30	0.397	0.387	0.216	0.260	0.446	0.294	1.240	1.089	1.198	0.22	1.76	5.837	6.098	0.957	2.187
42	354.03	0.386	0.361	0.252	0.253	0.411	0.336	1.255	1.083	1.182	0.03	0.90	1.136	1.044	1.089	4.241

43	351.51	0.019	0.797	0.184	0.018	0.776	0.205	2.057	1.005	1.071	0.06	0.69	2.605	2.611	0.998	0.123
44	352.06	0.111	0.724	0.165	0.090	0.722	0.189	1.694	1.010	1.080	0.08	0.70	2.759	2.782	0.992	0.421
45	351.79	0.109	0.690	0.201	0.083	0.687	0.229	1.608	1.018	1.090	0.09	0.69	2.637	2.666	0.989	0.543
46	351.51	0.097	0.639	0.263	0.077	0.626	0.296	1.694	1.010	1.084	0.08	0.69	2.565	2.597	0.987	0.635
47	351.44	0.095	0.606	0.299	0.076	0.594	0.330	1.716	1.014	1.063	0.08	0.72	2.610	2.654	0.984	0.831
48	351.22	0.091	0.569	0.339	0.072	0.556	0.373	1.700	1.016	1.067	0.13	0.71	3.432	3.540	0.970	1.546
49	351.57	0.150	0.491	0.359	0.107	0.485	0.408	1.519	1.018	1.090	0.16	0.71	4.113	4.271	0.963	1.884
50	351.75	0.193	0.435	0.372	0.129	0.438	0.433	1.409	1.031	1.113	0.10	1.52	4.722	4.918	0.960	2.040
51	352.18	0.243	0.408	0.349	0.158	0.421	0.421	1.354	1.040	1.137	0.05	0.70	1.057	0.942	1.122	5.729
52	351.77	0.019	0.868	0.112	0.014	0.855	0.131	1.529	1.007	1.116	0.06	0.70	1.111	1.005	1.105	4.999
53	351.64	0.018	0.845	0.137	0.014	0.827	0.160	1.560	1.005	1.119	0.07	0.80	1.093	0.997	1.097	4.624
54	351.54	0.018	0.804	0.178	0.013	0.783	0.204	1.592	1.004	1.098	0.09	0.75	1.758	1.707	1.030	1.490
55	351.76	0.058	0.771	0.171	0.040	0.759	0.201	1.471	1.006	1.125	0.32	1.52	2.721	2.735	0.995	0.260
56	352.23	0.123	0.718	0.159	0.085	0.722	0.192	1.437	1.015	1.138	0.47	0.66	4.890	5.134	0.953	2.433
57	362.91	0.845	0.043	0.112	0.578	0.127	0.295	0.911	2.161	1.768	0.65	0.68	8.158	8.593	0.949	2.600
58	356.91	0.692	0.040	0.267	0.401	0.049	0.550	0.985	1.069	1.663	0.50	0.69	7.623	8.038	0.948	2.648
59	356.28	0.630	0.039	0.331	0.399	0.042	0.559	1.106	0.954	1.395	0.50	0.68	7.613	8.041	0.947	2.730
60	354.25	0.525	0.033	0.442	0.316	0.041	0.643	1.144	1.161	1.282	0.28	0.70	7.447	7.867	0.947	2.741
61	354.10	0.509	0.033	0.459	0.338	0.041	0.621	1.272	1.175	1.199	0.40	0.71	6.421	6.791	0.945	2.802
62	353.36	0.421	0.033	0.546	0.254	0.036	0.710	1.190	1.059	1.179	0.29	0.72	6.282	6.647	0.945	2.818
63	352.89	0.391	0.032	0.577	0.253	0.031	0.716	1.302	0.964	1.142	0.31	0.77	5.925	6.272	0.945	2.846
64	352.44	0.353	0.028	0.619	0.215	0.031	0.754	1.250	1.104	1.138			5.755	6.082	0.946	2.763
65	352.65	0.349	0.077	0.574	0.221	0.084	0.694	1.290	1.092	1.122						

														D		2.186

Table F.12. 1-propanol(1)/2-butanone(2)/methyl propionate (3) at 1.013 bar with consistency test results

	T (K)	X1	X2	X3	Y1	Y2	Y3	γ1	γ2	γ3	D	Dmax	L	W	L/W	D
1	363.21	0.927	0.025	0.048	0.812	0.057	0.132	1.154	1.600	1.976	0.143					
2	363.76	0.927	0.023	0.050	0.803	0.053	0.145	1.116	1.636	2.042	0.109	0.560	5.524	5.762	0.959	2.103
3	361.63	0.876	0.077	0.047	0.741	0.145	0.115	1.187	1.409	1.831	0.171	0.648	6.894	7.201	0.957	2.177
4	365.76	0.991	0.006	0.003	0.989	0.008	0.003	1.189	0.850	0.807	0.173	2.009	4.456	4.639	0.961	2.003
5	365.63	0.980	0.016	0.005	0.948	0.038	0.013	1.159	1.614	1.975	0.148	0.742	4.423	4.603	0.961	2.000
6	360.73	0.854	0.088	0.058	0.659	0.180	0.161	1.122	1.585	2.154	0.115	1.115	7.475	7.813	0.957	2.216
7	356.18	0.532	0.319	0.149	0.322	0.441	0.238	1.061	1.228	1.422	0.059	0.794	6.804	7.132	0.954	2.351
8	355.94	0.516	0.324	0.160	0.343	0.411	0.246	1.178	1.136	1.381	0.164	0.682	6.765	7.091	0.954	2.356
9	352.39	0.061	0.918	0.021	0.042	0.933	0.025	1.425	1.019	1.199	0.354	1.517	1.452	1.527	0.950	2.538
10	353.18	0.166	0.815	0.019	0.090	0.886	0.024	1.075	1.063	1.265	0.073	0.809	2.896	3.044	0.951	2.496
11	353.95	0.237	0.738	0.025	0.162	0.807	0.031	1.315	1.044	1.191	0.274	0.748	3.569	3.748	0.952	2.444
12	354.54	0.308	0.669	0.023	0.192	0.777	0.031	1.173	1.087	1.280	0.159	0.711	4.368	4.585	0.953	2.422
13	354.92	0.339	0.633	0.028	0.215	0.746	0.039	1.173	1.092	1.280	0.159	0.696	4.587	4.813	0.953	2.400
14	355.70	0.416	0.560	0.025	0.256	0.707	0.037	1.103	1.141	1.356	0.098	0.699	5.235	5.489	0.954	2.369
15	355.78	0.420	0.549	0.031	0.265	0.689	0.046	1.127	1.130	1.338	0.119	0.685	5.234	5.488	0.954	2.362
16	356.13	0.464	0.507	0.029	0.264	0.688	0.048	0.998	1.211	1.491	-0.002	0.699	5.689	5.963	0.954	2.354
17	356.02	0.437	0.523	0.040	0.259	0.679	0.063	1.045	1.160	1.415	0.044	0.696	5.301	5.556	0.954	2.348
18	356.78	0.569	0.401	0.030	0.426	0.528	0.047	1.279	1.150	1.366	0.246	0.692	6.869	7.198	0.954	2.344
19	356.89	0.594	0.370	0.036	0.403	0.537	0.060	1.154	1.263	1.475	0.143	0.662	7.181	7.526	0.954	2.344
20	357.63	0.569	0.389	0.042	0.373	0.556	0.071	1.081	1.216	1.459	0.078	0.657	6.019	6.301	0.955	2.285
21	358.15	0.604	0.352	0.044	0.462	0.469	0.069	1.236	1.115	1.315	0.212	0.665	6.075	6.357	0.956	2.264
22	358.44	0.634	0.325	0.041	0.404	0.517	0.078	1.018	1.322	1.588	0.018	0.671	6.301	6.592	0.956	2.257
23	358.28	0.591	0.359	0.050	0.437	0.484	0.080	1.188	1.124	1.322	0.172	0.671	5.732	5.995	0.956	2.248
24	358.65	0.748	0.222	0.030	0.459	0.463	0.078	0.972	1.717	2.149	-0.028	0.708	7.926	8.296	0.955	2.284
25	358.94	0.699	0.262	0.039	0.544	0.386	0.069	1.218	1.207	1.446	0.197	0.674	6.861	7.177	0.956	2.252
26	358.13	0.651	0.294	0.055	0.442	0.455	0.103	1.098	1.298	1.572	0.093	0.648	6.885	7.207	0.955	2.285
27	358.13	0.625	0.312	0.063	0.439	0.453	0.109	1.135	1.217	1.445	0.126	0.647	6.456	6.756	0.955	2.276

28	357.89	0.616	0.310	0.073	0.437	0.441	0.123	1.157	1.199	1.412	0.146	0.644	6.544	6.851	0.955	2.288
29	352.86	0.178	0.049	0.773	0.140	0.053	0.807	1.584	1.073	1.035	0.460	1.440	3.505	3.627	0.967	1.702
30	352.52	0.156	0.160	0.684	0.120	0.175	0.705	1.577	1.091	1.034	0.456	0.779	3.397	3.518	0.966	1.746
31	352.42	0.154	0.208	0.638	0.133	0.209	0.658	1.775	1.008	1.037	0.574	0.704	3.458	3.585	0.964	1.809
32	352.94	0.261	0.183	0.556	0.189	0.199	0.612	1.452	1.074	1.089	0.373	0.725	5.057	5.279	0.958	2.141
33	353.55	0.337	0.204	0.458	0.215	0.233	0.551	1.251	1.104	1.166	0.224	0.719	5.903	6.177	0.956	2.266
34	354.03	0.375	0.194	0.431	0.250	0.223	0.527	1.279	1.095	1.168	0.246	0.702	6.129	6.417	0.955	2.289
35	353.97	0.364	0.236	0.400	0.238	0.271	0.491	1.261	1.094	1.173	0.232	0.699	5.973	6.254	0.955	2.297
36	354.28	0.368	0.347	0.286	0.243	0.395	0.363	1.254	1.076	1.201	0.227	0.711	5.745	6.020	0.954	2.338
37	353.60	0.357	0.311	0.333	0.222	0.360	0.418	1.216	1.118	1.217	0.196	0.704	6.218	6.517	0.954	2.344
38	354.16	0.424	0.317	0.259	0.262	0.384	0.355	1.178	1.148	1.301	0.164	0.709	6.902	7.239	0.953	2.384
39	354.60	0.448	0.320	0.232	0.337	0.364	0.299	1.410	1.061	1.211	0.344	0.702	6.899	7.235	0.953	2.382
40	355.13	0.545	0.267	0.188	0.399	0.330	0.270	1.343	1.137	1.325	0.295	0.682	8.073	8.470	0.953	2.398
41	354.59	0.559	0.282	0.159	0.302	0.422	0.276	1.012	1.402	1.627	0.012	0.711	8.868	9.310	0.952	2.433
42	355.57	0.634	0.247	0.119	0.392	0.385	0.223	1.113	1.414	1.697	0.107	0.681	9.143	9.595	0.953	2.409
43	355.05	0.663	0.228	0.109	0.376	0.397	0.227	1.042	1.604	1.930	0.041	0.669	10.146	10.653	0.952	2.439
44	356.13	0.667	0.220	0.113	0.405	0.371	0.224	1.066	1.501	1.776	0.064	0.658	9.128	9.575	0.953	2.390
45	356.48	0.667	0.220	0.113	0.405	0.371	0.224	1.051	1.484	1.756	0.049	0.646	8.778	9.205	0.954	2.374
46	356.70	0.660	0.225	0.115	0.422	0.359	0.219	1.099	1.393	1.669	0.094	0.652	8.440	8.848	0.954	2.362
47	356.60	0.608	0.231	0.161	0.433	0.315	0.252	1.226	1.199	1.378	0.204	0.674	7.679	8.049	0.954	2.350
48	366.36	0.919	0.073	0.009	0.763	0.206	0.031	0.967	1.853	2.331	-0.033	1.312	2.810	2.915	0.964	1.837
49	363.52	0.854	0.080	0.066	0.704	0.134	0.162	1.072	1.188	1.754	0.070	0.813	4.675	4.873	0.959	2.072
50	361.76	0.821	0.061	0.118	0.606	0.122	0.273	1.030	1.500	1.728	0.029	0.622	5.921	6.185	0.957	2.179
51	359.44	0.739	0.055	0.206	0.504	0.094	0.402	1.045	1.370	1.573	0.044	0.633	6.955	7.278	0.956	2.269
52	357.89	0.699	0.048	0.254	0.444	0.077	0.479	1.038	1.360	1.595	0.037	0.638	7.846	8.218	0.955	2.316
53	356.51	0.588	0.047	0.365	0.379	0.066	0.555	1.114	1.234	1.342	0.108	0.679	7.393	7.745	0.955	2.323
54	355.60	0.520	0.041	0.439	0.343	0.054	0.603	1.185	1.185	1.247	0.170	0.682	7.133	7.471	0.955	2.312
55	352.28	0.138	0.732	0.130	0.078	0.786	0.136	1.170	1.081	1.056	0.157	1.767	3.226	3.386	0.953	2.422
56	352.06	0.063	0.769	0.168	0.054	0.766	0.180	1.789	1.010	1.089	0.582	0.779	1.845	1.929	0.957	2.213
57	351.80	0.055	0.692	0.253	0.041	0.692	0.266	1.592	1.022	1.081	0.465	0.713	1.940	2.021	0.960	2.032

58	351.72	0.051	0.640	0.309	0.039	0.637	0.324	1.607	1.020	1.080	0.474	0.707	1.950	2.026	0.963	1.896
59	351.67	0.046	0.571	0.383	0.036	0.570	0.393	1.678	1.025	1.058	0.517	0.709	1.891	1.956	0.967	1.678
60	351.72	0.043	0.526	0.431	0.034	0.527	0.438	1.702	1.027	1.046	0.532	0.702	1.780	1.834	0.971	1.490
61	351.73	0.040	0.040	0.920	0.045	0.040	0.915	2.381	1.024	1.023	0.868	1.361	1.800	1.807	0.996	0.183
															D	2.202

Table F.13. 1-propanol(1)/2-butanone(2)/2-propanol (3) at 1.013 bar with consistency test results

	T(K)	P(bar)	X1	X2	X3	Y1	Y2	Y3	γ1	γ2	γ3	D	Dmax	L	W	L/W	D
1	353.63	1.01	0.246	0.445	0.309	0.129	0.553	0.318	1.024	1.199	1.098			4.92	4.88	1.01	0.32
2	355.89	1.01	0.403	0.371	0.226	0.231	0.514	0.255	1.017	1.243	1.102	0.18	0.76	5.40	5.32	1.02	0.75
3	356.49	1.01	0.446	0.342	0.211	0.256	0.504	0.239	0.994	1.298	1.079	0.36	0.72	5.55	5.46	1.02	0.84
4	356.44	1.01	0.440	0.359	0.201	0.254	0.518	0.228	1.002	1.273	1.083	0.37	0.71	5.49	5.39	1.02	0.87
5	355.60	1.01	0.400	0.450	0.150	0.241	0.583	0.176	1.083	1.173	1.161	0.38	0.73	5.56	5.48	1.01	0.72
6	354.85	1.01	0.358	0.506	0.136	0.219	0.623	0.157	1.137	1.143	1.176	0.28	0.71	5.53	5.46	1.01	0.59
7	354.71	1.01	0.344	0.526	0.130	0.190	0.660	0.150	1.029	1.168	1.186	0.20	0.72	5.40	5.33	1.01	0.62
8	354.70	1.01	0.330	0.548	0.122	0.191	0.669	0.140	1.079	1.139	1.173	0.33	0.73	5.14	5.07	1.02	0.75
9	356.49	1.01	0.198	0.043	0.758	0.106	0.080	0.814	0.925	1.632	1.022	0.53	1.46	1.91	1.78	1.07	3.52
10	355.60	1.01	0.176	0.079	0.745	0.083	0.124	0.792	0.852	1.431	1.049	0.48	0.76	2.39	2.29	1.04	2.11
11	356.39	1.01	0.237	0.054	0.709	0.130	0.107	0.763	0.951	1.753	1.030	0.13	0.76	2.60	2.48	1.05	2.23
13	358.27	1.01	0.457	0.135	0.407	0.274	0.226	0.499	0.965	1.395	1.089	0.21	0.80	4.11	3.96	1.04	1.84
14	357.78	1.01	0.439	0.176	0.385	0.254	0.303	0.443	0.948	1.459	1.043	0.07	0.70	4.28	4.14	1.03	1.61
15	356.02	1.01	0.480	0.190	0.331	0.264	0.349	0.388	0.970	1.644	1.139	0.36	0.71	6.68	6.65	1.00	0.21
17	357.39	1.01	0.499	0.226	0.275	0.321	0.332	0.347	1.073	1.260	1.160	0.37	0.71	5.60	5.50	1.02	0.92
18	357.15	1.01	0.497	0.233	0.270	0.328	0.334	0.338	1.110	1.239	1.163	0.22	0.68	5.81	5.72	1.02	0.79
19	356.06	1.01	0.469	0.278	0.253	0.240	0.480	0.280	0.903	1.545	1.069	0.05	0.73	6.41	6.36	1.01	0.38
20	355.07	1.01	0.398	0.306	0.296	0.228	0.415	0.357	1.052	1.251	1.216	0.55	0.75	6.21	6.18	1.00	0.20
21	354.82	1.01	0.369	0.277	0.354	0.195	0.399	0.406	0.980	1.340	1.166	0.22	0.73	6.01	5.99	1.00	0.14

22	355.13	1.01	0.351	0.314	0.335	0.194	0.445	0.361	1.013	1.303	1.083	0.30	0.73	5.35	5.30	1.01	0.45
23	354.20	1.01	0.295	0.409	0.296	0.163	0.521	0.316	1.053	1.207	1.114	0.32	0.74	5.23	5.20	1.01	0.34
24	351.96	1.01	0.029	0.910	0.061	0.013	0.917	0.070	0.933	1.025	1.307	0.18	1.74	1.59	1.44	1.10	4.84
25	366.91	1.01	0.967	0.027	0.006	0.938	0.052	0.011	1.105	1.224	1.229	0.33	5.30	3.51	3.09	1.14	6.37
28	362.89	1.01	0.813	0.082	0.105	0.616	0.217	0.167	1.011	1.920	1.186	0.71	1.39	5.14	4.87	1.06	2.72
29	361.97	1.01	0.804	0.092	0.104	0.619	0.222	0.159	1.066	1.800	1.178	0.23	0.61	5.93	5.70	1.04	1.97
30	362.02	1.01	0.776	0.128	0.097	0.594	0.264	0.142	1.059	1.540	1.125	0.16	0.62	5.44	5.19	1.05	2.31
31	362.44	1.01	0.727	0.180	0.093	0.537	0.333	0.130	1.002	1.361	1.063	0.06	0.64	4.26	3.97	1.07	3.53
32	361.78	1.01	0.706	0.202	0.092	0.503	0.376	0.121	0.994	1.396	1.016	0.18	0.64	4.57	4.30	1.06	3.00
33	353.51	1.01	0.050	0.146	0.804	0.018	0.202	0.780	0.706	1.339	1.041	-0.25	2.43	2.36	2.31	1.02	1.07
34	355.69	1.01	0.302	0.112	0.586	0.186	0.176	0.638	1.102	1.420	1.071	0.59	1.28	4.24	4.18	1.02	0.75
36	357.98	1.01	0.441	0.047	0.512	0.281	0.128	0.591	1.037	2.292	1.037	0.24	0.74	4.20	4.08	1.03	1.50
37	358.96	1.01	0.486	0.039	0.475	0.314	0.127	0.559	1.010	2.660	1.018	0.25	0.66	3.93	3.77	1.04	2.06
38	360.12	1.01	0.615	0.046	0.339	0.492	0.107	0.401	1.193	1.834	0.978	0.25	0.67	4.78	4.61	1.04	1.91
																D	1.58

Appendix G. NRTL model correlations

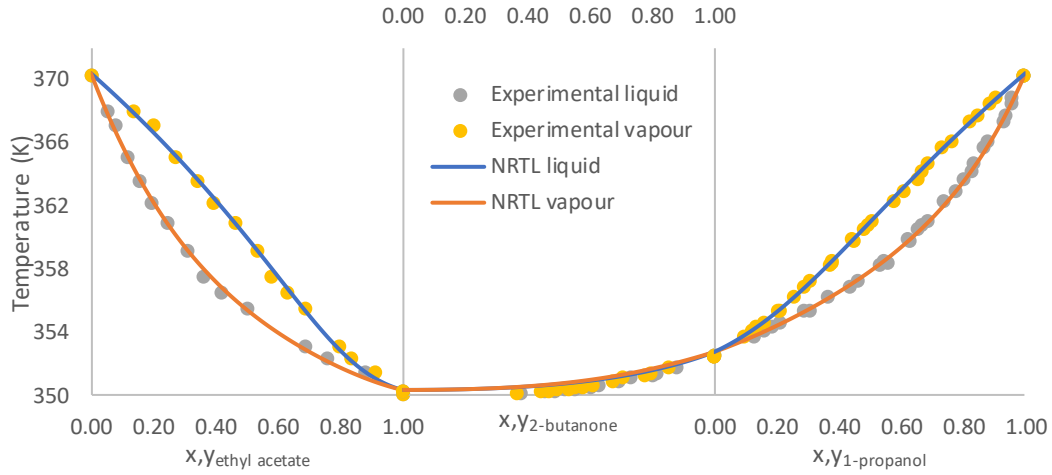

Figure G.1. NRTL correlative outcomes of the binary systems 1-propanol/2-butanone. 2-butanone/ethyl acetate. and 1-propanol/ethyl acetate used to create a ternary diagram of 1-propanol/2-butanone/ethyl acetate

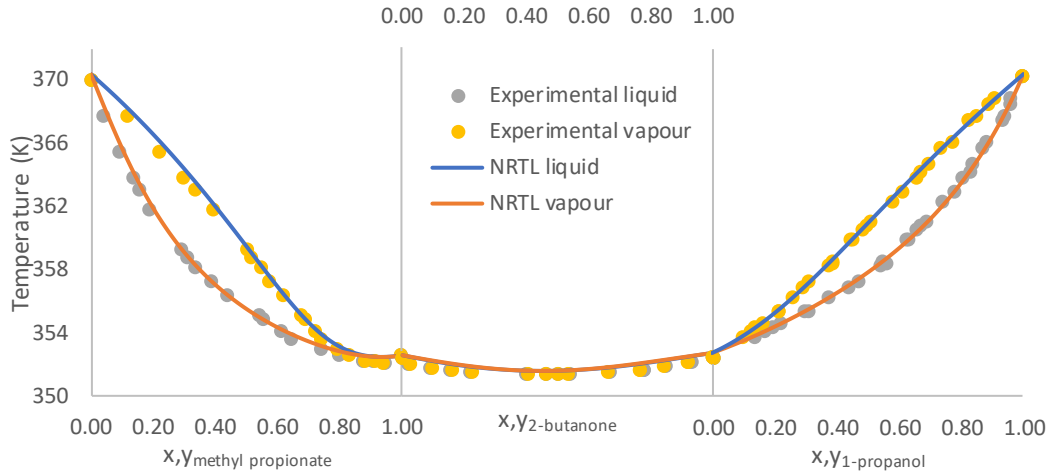

Figure G.2. NRTL correlative outcomes of the binary systems 1-propanol/2-butanone. 2-butanone/methyl propionate. and 1-propanol/methyl propionate used to create a ternary diagram of 1-propanol/2-butanone/methyl propionate

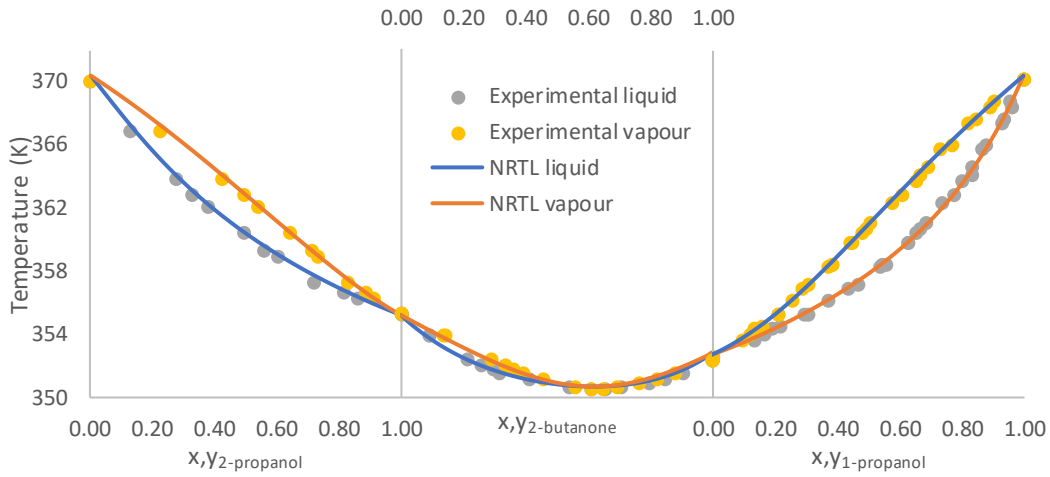

Figure G.3. NRTL correlative outcomes of the binary systems 1-propanol/2-butanone. 2-butanone/2-propanol. and 1-propanol/2-propanol used to create a ternary diagram of 1-propanol/2-butanone/2-propanol

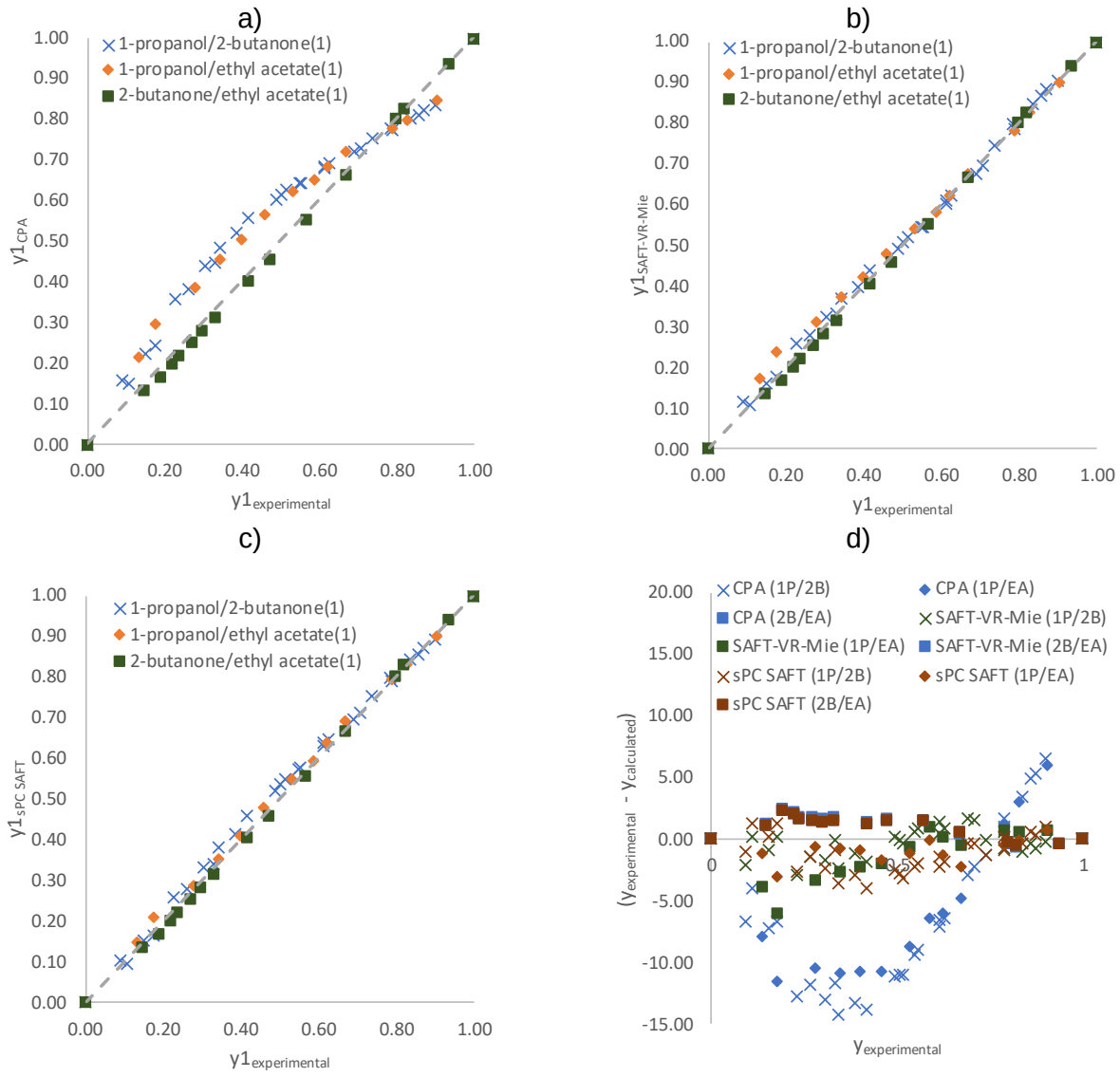

FigureG.4. Graphical representation of the deviation of the experimental data from the predictive model of the binary systems in the ethyl acetate ternary system. a) $Y_{experimental}$ vs Y_{CPA}. b) $Y_{experimental}$ vs $Y_{SAFT\text{-}VR\text{-}Mie}$. c) $Y_{experimental}$ vs $Y_{sPC\text{-}SAFT}$. d) AADy(x10^2) values vs $y_{experimental}$

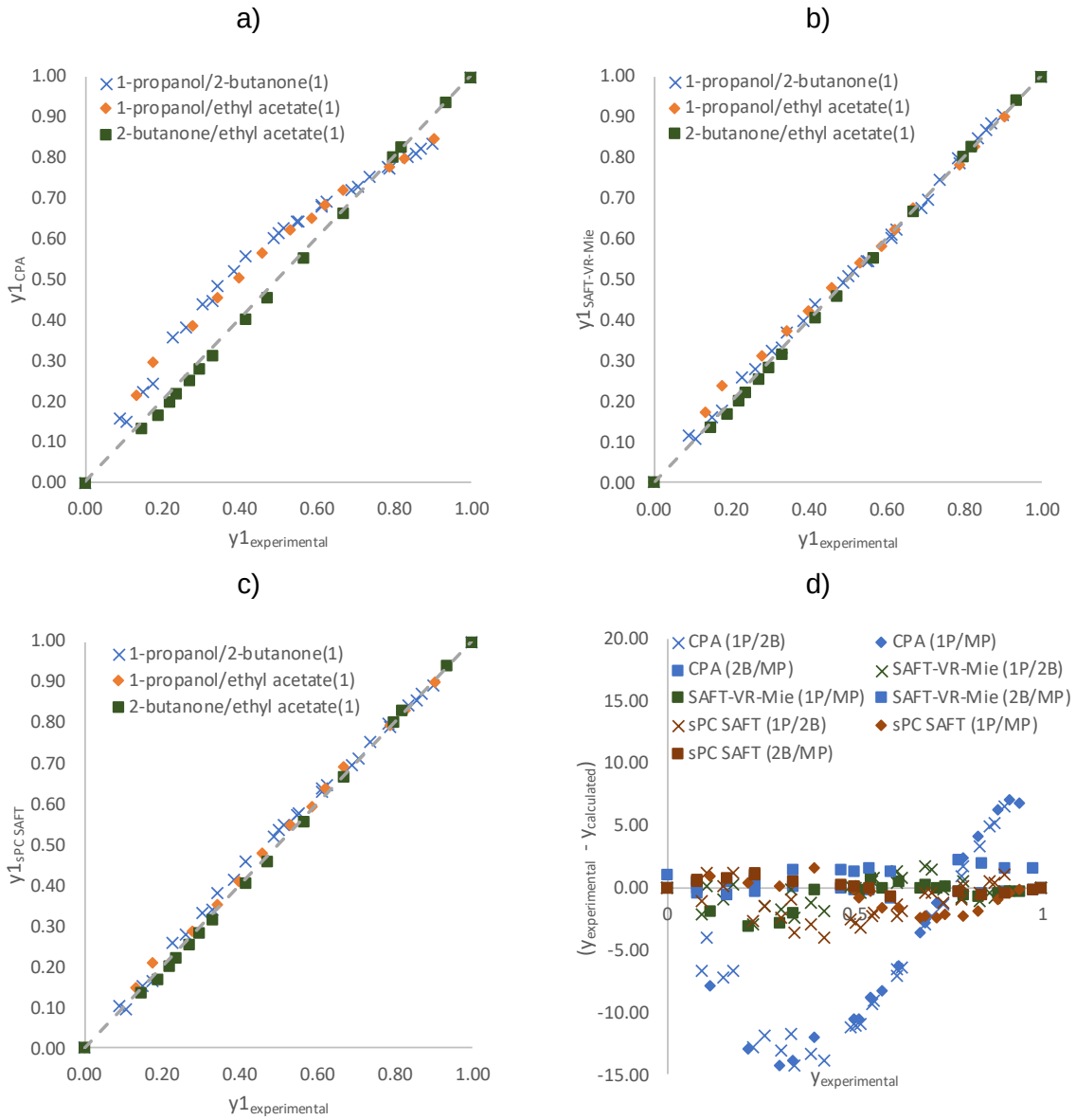

Figure G.5. Graphical representation of the deviation of the experimental data from the predictive model of the binary systems in the methyl propionate ternary system. a) $Y_{experimental}$ vs Y_{CPA}. b) $Y_{experimental}$ vs $Y_{SAFT\text{-}VR\text{-}Mie}$. c) $Y_{experimental}$ vs $Y_{sPC\text{-}SAFT}$. d) AADy(x10^2) values vs $y_{experimental}$

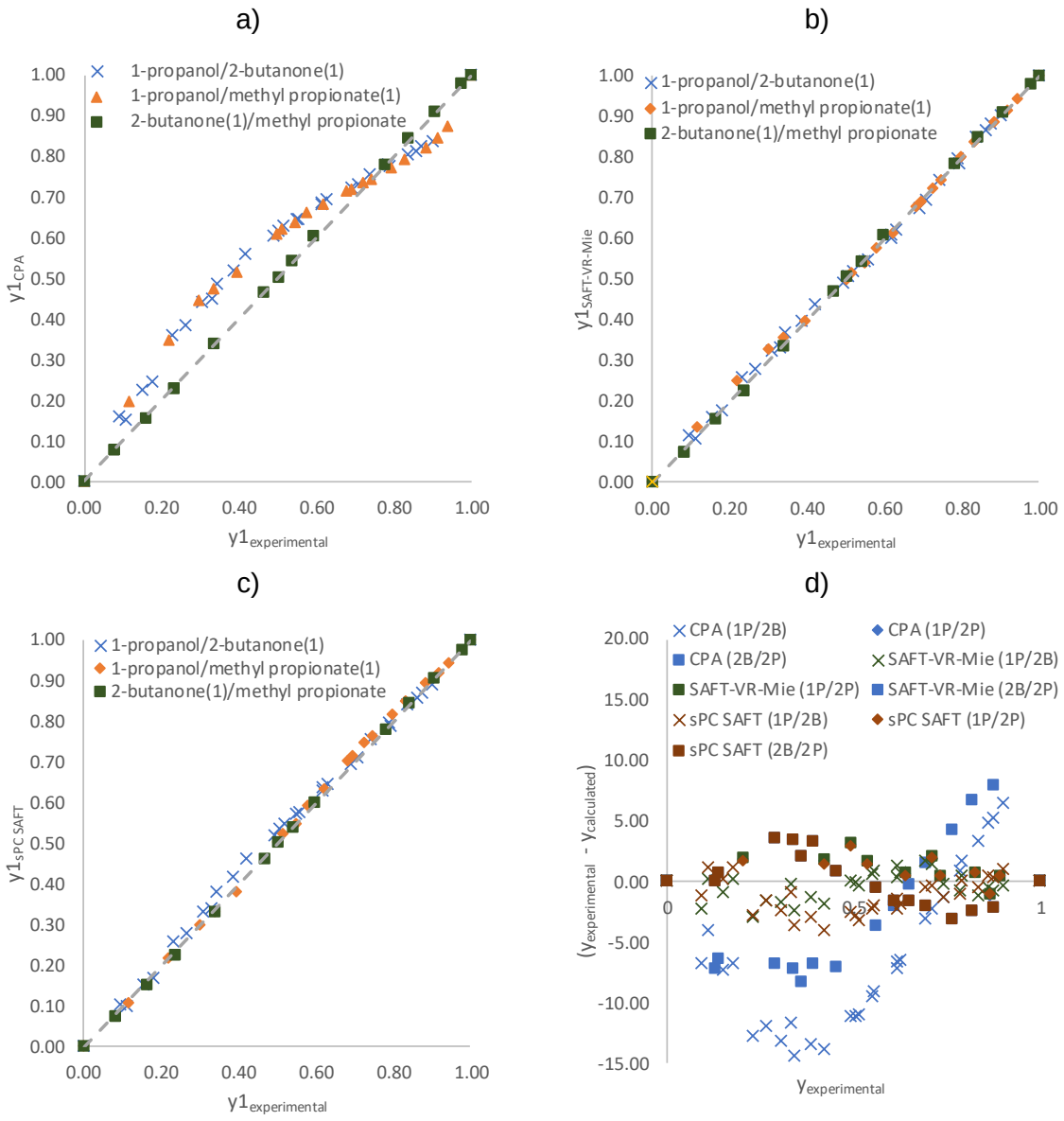

Figure G.6. Graphical representation of the deviation of the experimental data from the predictive model of the binary systems in the 2-propanol ternary system. a) $Y_{experimental}$ vs Y_{CPA}. b) $Y_{experimental}$ vs $Y_{SAFT\text{-}VR\text{-}Mie}$. c) $Y_{experimental}$ vs $Y_{sPC\text{-}SAFT}$. d) AADy(x10^2) values vs $y_{experimental}$

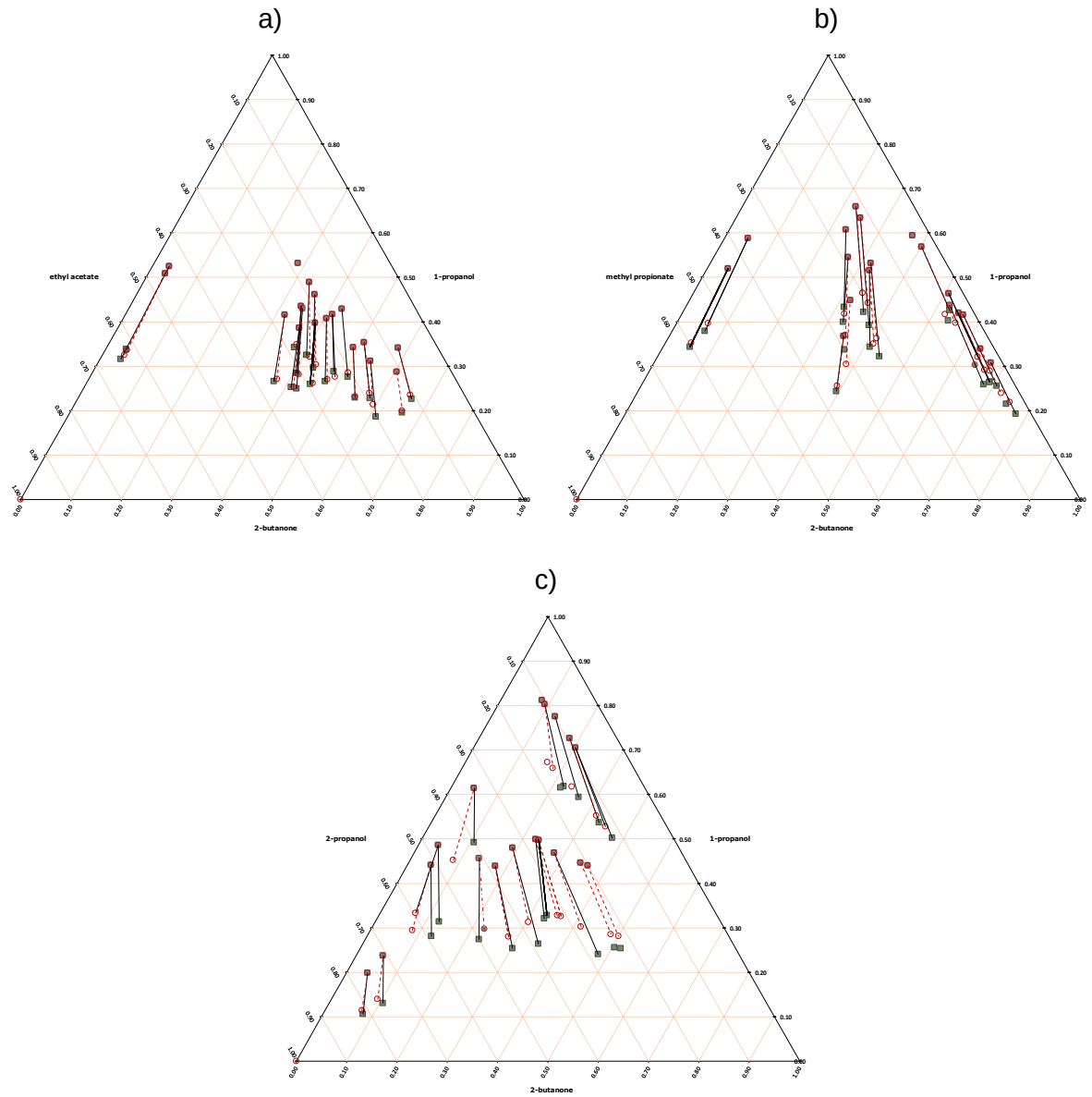

Figure G.7. NRTL correlative outcomes. solid lines with grey squares represent experimental tie-lines. and dashed lines with red circles represent the calculated tie-lines using the NRTL model. a) 1-propanol/2-butanone/ethyl acetate (353.63-356.28 K). b) 1-propanol/2-butanone/methyl propionate (354.28-356.89 K). c) 1-propanol/2-butanone/2-propanol (355.06-363.89 K)

Appendix H. Pure Component parameters

TableH.1. CPA + GV pure component parameters

component	1-propanol [35]	2-propanol*	2-butanone [35]	propyl formate [35]	ethyl acetate [35]	methyl propionate
a0	2164	2060.77	2520	2455	2404	2295
association energy	2587	2436.5	0	0	0	0
association volume	0.007	0.006	0	0	0	0
b	0.064	0.065	0.074	0.080	0.080	0.084
c1	0.859	0.930	0.774	0.830	0.880	0.850
dipole moment	0.168	1.560	2.760	1.910	1.780	1.700
polar segment	0.613	0.940	0.568	1.290	1.490	2.000

Table H.2 SAFT-VR-Mie + GV pure component parameters

component	1-propanol [120]	2-propanol [120]	2-butanone [33]	propyl formate [33]	ethyl acetate [33]	methyl propionate [33]
association distance	0.400	0.400	0.400	0.400	0.400	0.4
association energy	2746	2691	2550	1850	1850	1850
association range	0.354	0.359	0.334	0.418	0.418	0.418
attractive exponent	6.000	6.000	6.000	6.000	6.000	6
dipole moment	0	0	2.7600	1.9100	1.7800	1.700
dispersion energy	227.7	208.0	257.9	253.3	276.9	273.5
polar segments	0	0	1.430	2.930	3.370	3.700
repulsive exponent	10.18	10.56	11.96	12.03	13.96	13.44
segment diameter	3.561	3.441	3.614	3.590	3.640	3.630
segment number	2.336	2.579	2.603	2.810	2.740	2.730

Table H.3. sPC-SAFT + GV pure component parameters

component	1-propanol [35]	2-propanol* [112]	2-butanone [35]	propyl formate [35]	ethyl acetate [35]	methyl propionate
association energy	2342	2224	1667	1639	1639	1639
association volume	0.036	0.030	0.0159	0.0139	0.0139	0.0139
dipole moment	1.680	1.700	2.760	1.910	1.780	1.700
dispersion energy	225.4	204.5	227.3	222.1	210.6	219.2
polar segment	1.627	2.323	1.757	3.516	4.194	3.900
segment diameter	3.309	3.197	3.416	3.366	3.297	3.299
segment number	2.818	3.138	2.972	3.240	3.497	3.434

Appendix I. Perturbation model predictions for binary systems

The three perturbation type models used in the work can be seen below. in which CPA-GV. SAFT-VR-Mie-GV and sPC-SAFT-GV were used to predict the nine binary systems. As shown in Chapter 6 the SAFT-VR-Mie-GV model best predicted the binary systems,This appendix allows for the graphical representation of each system to be shown. with T-xy, xy, (y-x) vs x and excess Gibbs free energy plots.

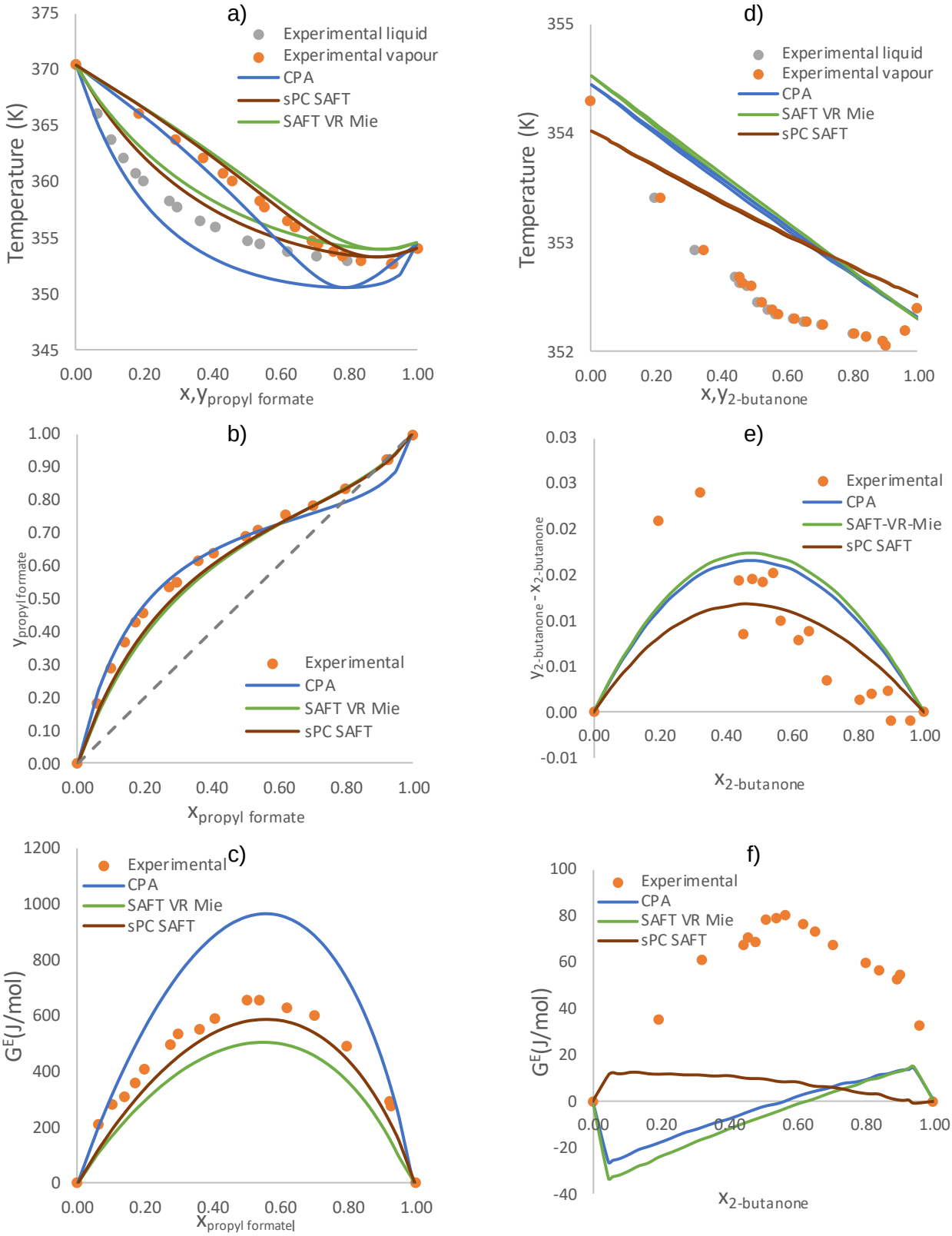

Figure I.1: Modelling without BIPs a) Experimental T-xy data compared to T-xy models of SAFT-VR Mie + GV and CPA + GV for 1-propanol/propyl formate. b) Experimental xy data compared to xy models of SAFT-VR-Mie + GV and CPA + GV for 1-propanol/propyl formate. c) Excess Gibbs free energy of experimental data compared to SAFT-VR-Mie + GV and CPA + GV for 1-propanol/propyl formate. d) Experimental T-xy data compared to T-xy models of SAFT-VR Mie + GV and CPA + GV for 2-butanone/propyl formate e) Experimental (y-x) vs x data compared to (y-x) vs x models of SAFT-VR-Mie + GV and CPA + GV for 2-butanone/propyl formate. f) Excess Gibbs free energy of experimental data compared to SAFT-VR-Mie + GV and CPA + GV for 2-butanone/propyl formate.

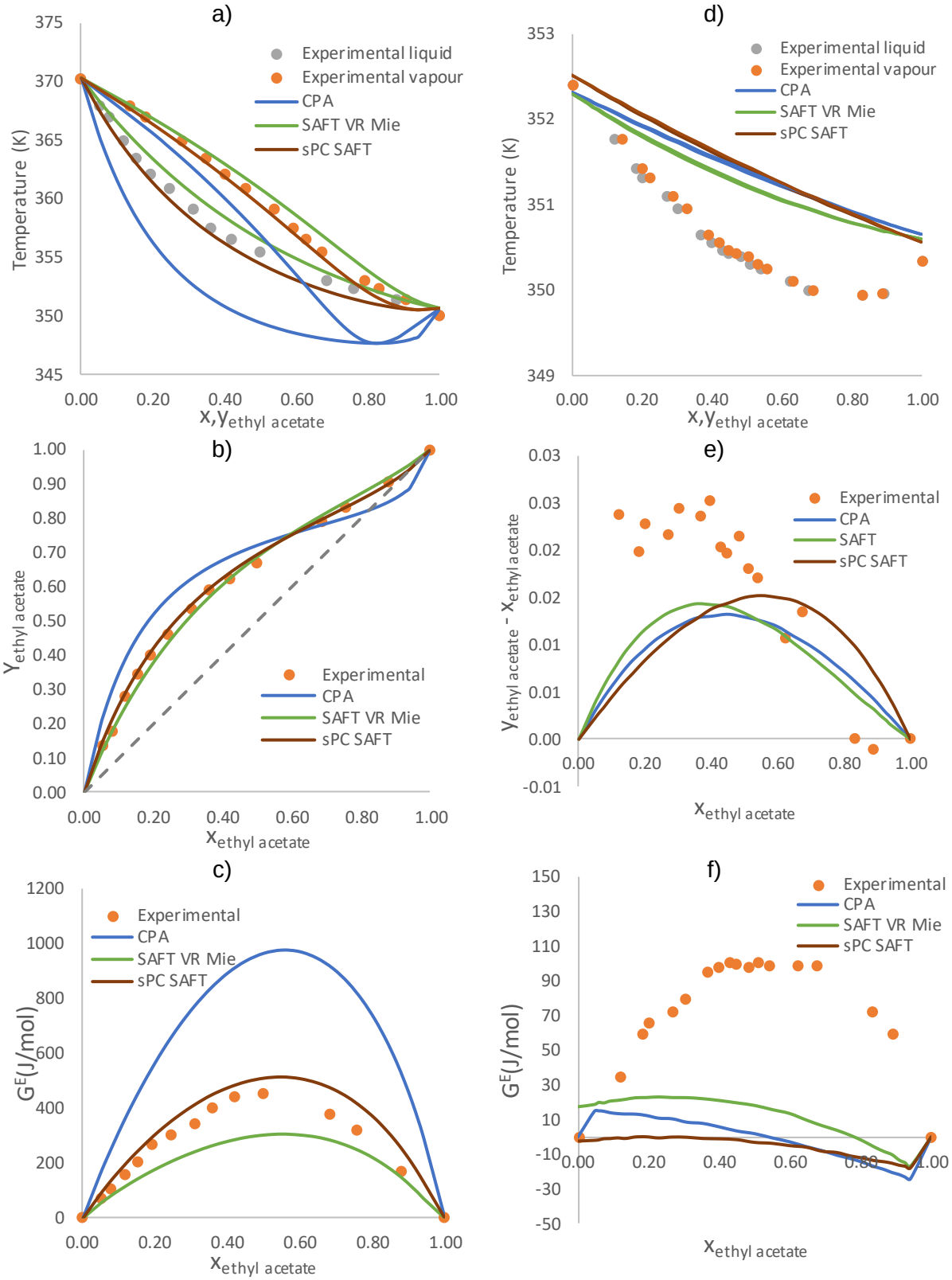

Figure I.2. Modelling without BIPs a) Experimental T-xy data compared to T-xy models of SAFT-VR Mie + GV and CPA + GV for 1-propanol/ethyl acetate. b) Experimental xy data compared to xy models of SAFT-VR-Mie + GV and CPA + GV for 1-propanol/ethyl acetate. c) Excess Gibbs free energy of experimental data compared to SAFT-VR-Mie + GV and CPA + GV for 1-propanol/ethyl acetate. d) Experimental T-xy data compared to T-xy models of SAFT-VR Mie + GV and CPA + GV for 2-butanone/ethyl acetate. e) Experimental (y-x) vs x data compared to (y-x) vs x models of SAFT-VR-Mie + GV and CPA + GV for 2-butanone/ethyl acetate. f) Excess Gibbs free energy of experimental data compared to SAFT-VR-Mie + GV and CPA + GV for 2-butanone/ethyl acetate.

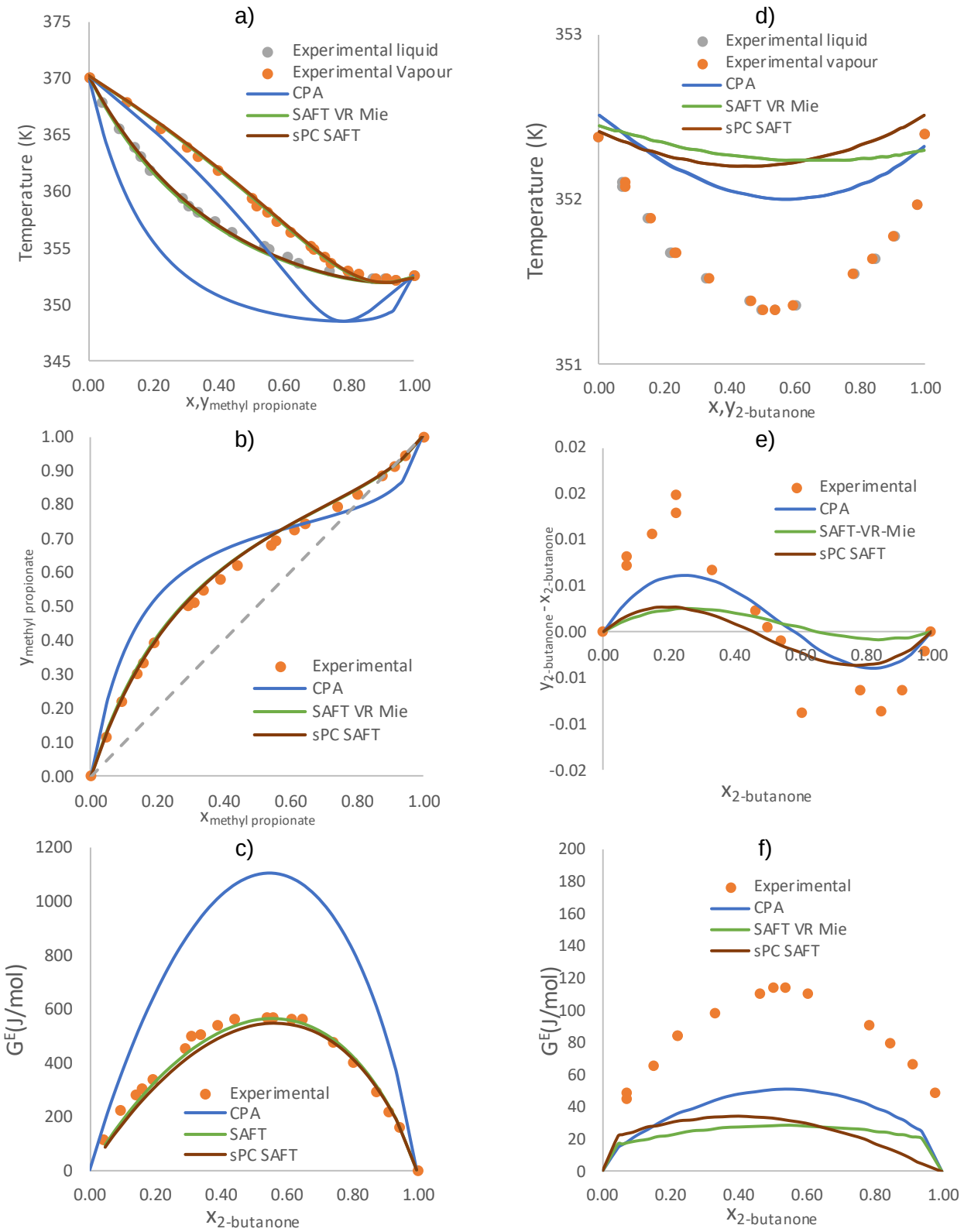

Figure I.3. Modelling without BIPs a) Experimental T-xy data compared to T-xy models of SAFT-VR Mie + GV and CPA + GV for 1-propanol/methyl propionate. b) Experimental xy data compared to xy models of SAFT-VR-Mie + GV and CPA + GV for 1-propanol/methyl propionate. c) Excess Gibbs free energy of experimental data compared to SAFT-VR-Mie + GV and CPA + GV for 1-propanol/methyl propionate. d) Experimental T-xy data compared to T-xy models of SAFT-VR Mie + GV and CPA + GV for 2-butanone/methyl propionate e) Experimental (y-x) vs x data compared to (y-x) vs x models of SAFT-VR-Mie + GV and CPA + GV for 2-butanone/methyl propionate. f) Excess Gibbs free energy of experimental data compared to SAFT-VR-Mie + GV and CPA + GV for 2-butanone/methyl propionate

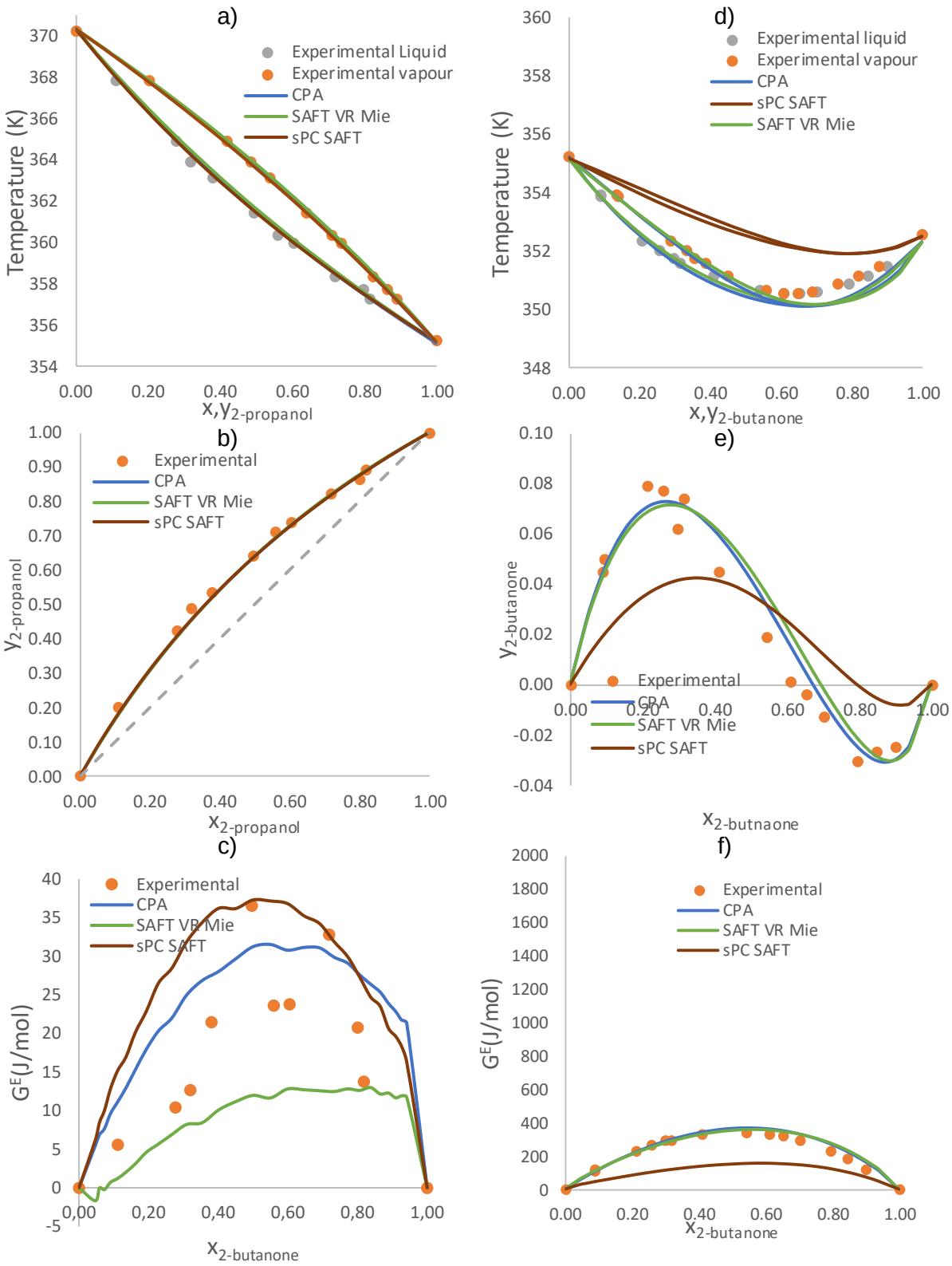

Figure I.4. Modelling without BIPs a) Experimental T-xy data compared to T-xy models of SAFT-VR Mie + GV and CPA + GV for 1-propanol/2-propanol. b) Experimental xy data compared to xy models of SAFT-VR-Mie + GV and CPA + GV for 1-propanol/2-propanol. c) Excess Gibbs free energy of experimental data compared to SAFT-VR-Mie + GV and CPA + GV for 1-propanol/2-propanol. d) Experimental T-xy data compared to T-xy models of SAFT-VR Mie + GV and CPA + GV for 2-butanone/2-propanol e) Experimental xy data compared to xy models of SAFT-VR-Mie + GV and CPA + GV for 2-butanone/2-propanol. f) Excess Gibbs free energy of experimental data compared to SAFT-VR-Mie + GV and CPA + GV for 2-butanone/2-propanol.

Appendix J. Perturbation model predictions for ternary systems

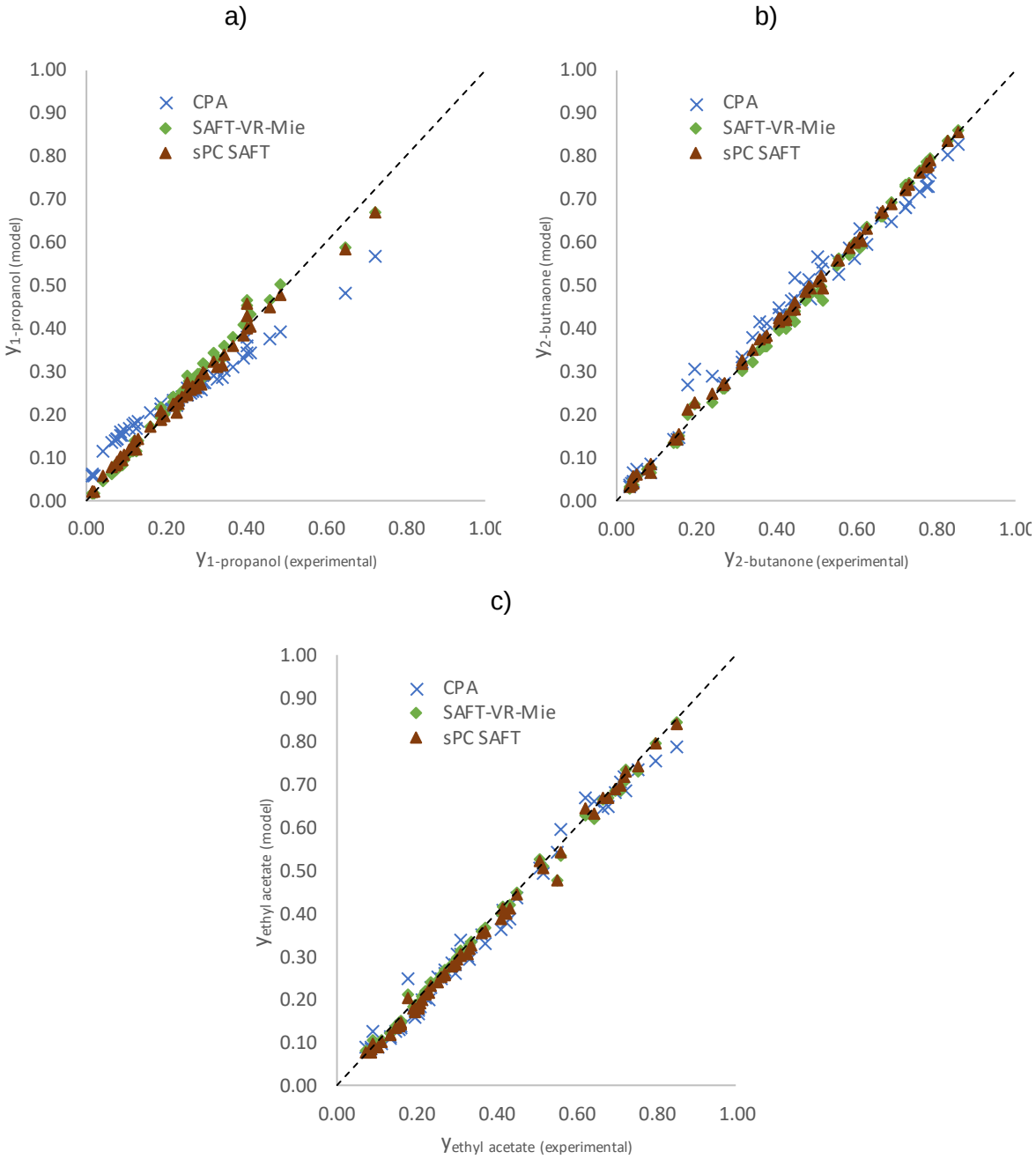

Figure J.1. Graphical representation of the deviation of the experimental data from the predictive model in the propyl formate ternary system. a) $Y_{exp.1\text{-}propanol}$ vs $Y_{model.1\text{-}propanol}$. b) $Y_{exp.2\text{-}btunaone}$ vs $Y_{model.2\text{-}butanone}$. c) $Y_{exp.ethyl\ acetate}$ vs $Y_{model.ethyl\ acetate}$ d) $T_{exp.}$ vs T_{model}

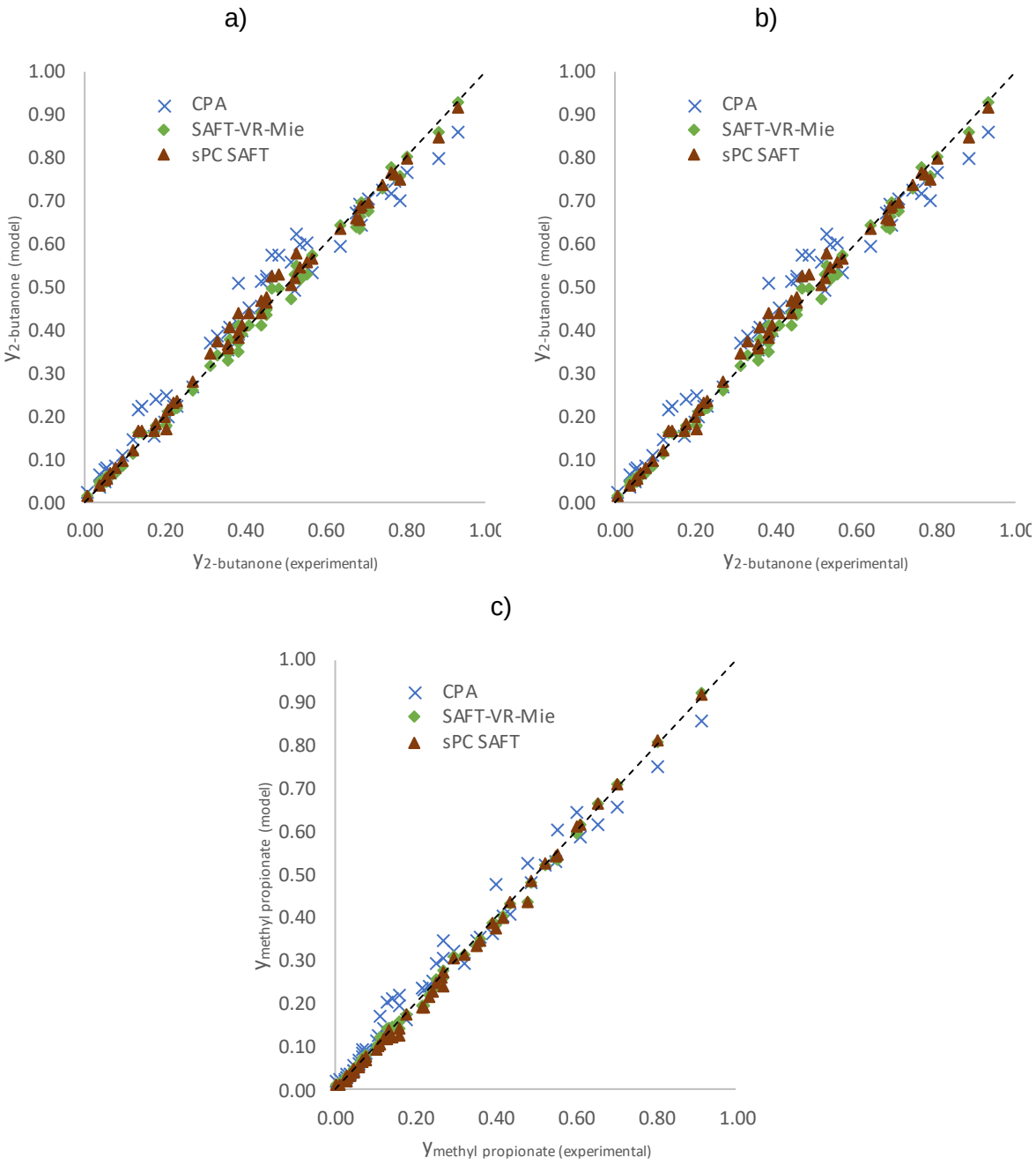

Figure J.2. Graphical representation of the deviation of the experimental data from the predictive model in the propyl formate ternary system. a) $Y_{exp.1\text{-}propanol}$ vs $Y_{model.1\text{-}propanol}$. b) $Y_{exp.2\text{-}btunaone}$ vs $Y_{model.2\text{-}butanone}$. c) $Y_{exp.methyl\ propionate}$ vs $Y_{model.metly\ propionate}$ d) $T_{exp.}$ vs T_{model}

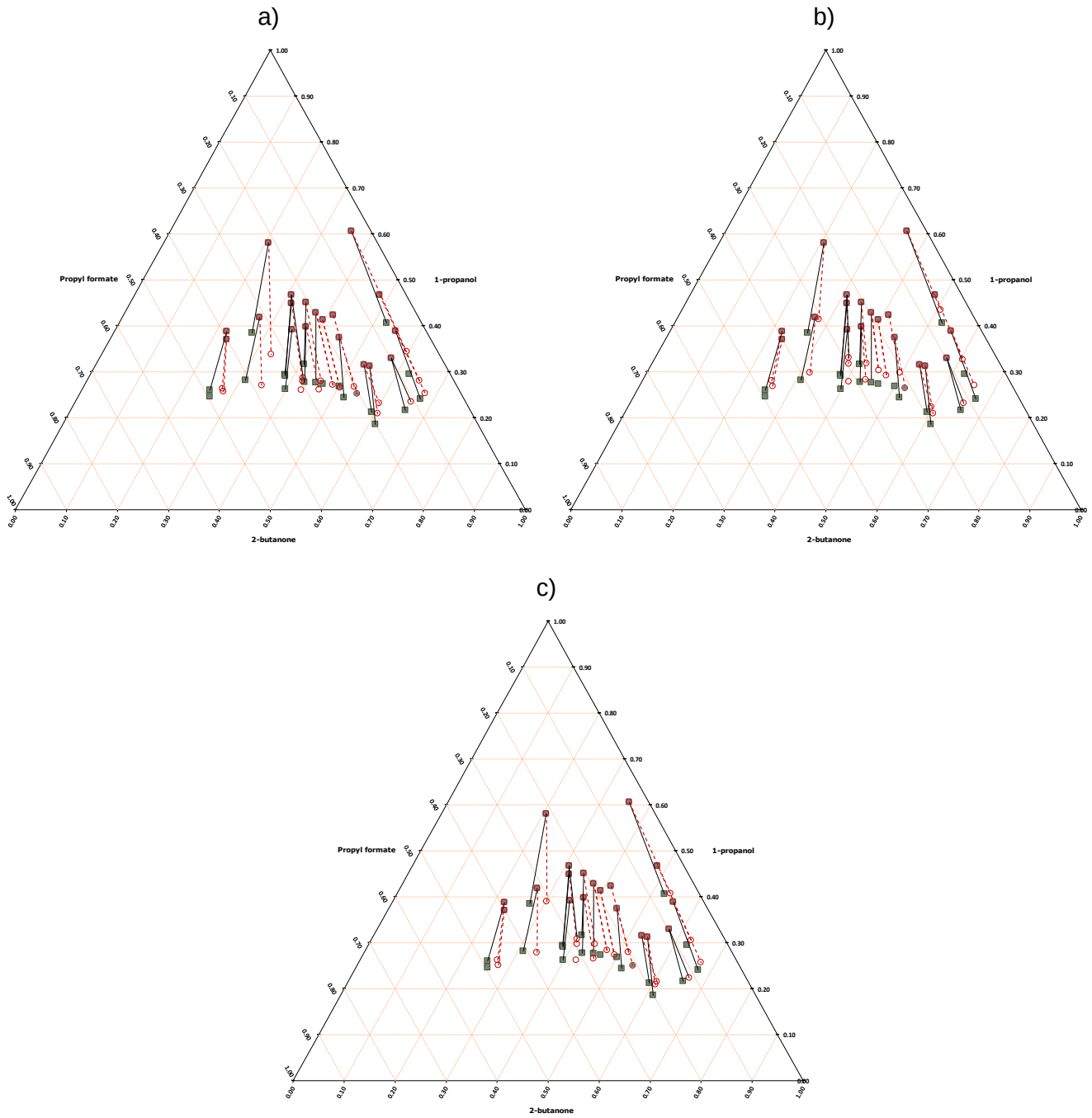

Figure J.3. Predictions of the three thermodynamic models of the ternary systems 1-propanol/2-butanone/propyl formate for T=354.52-358.55 K. Solid lines with grey squares represent experimental tie-lines. and dashed lines with red circles represent the calculated tie-lines using a predictive model. a) Prediction using CPA-GV. b) predictions using SAFT-VR-Mie-GV. c) prediction using sPC-SAFT-GV

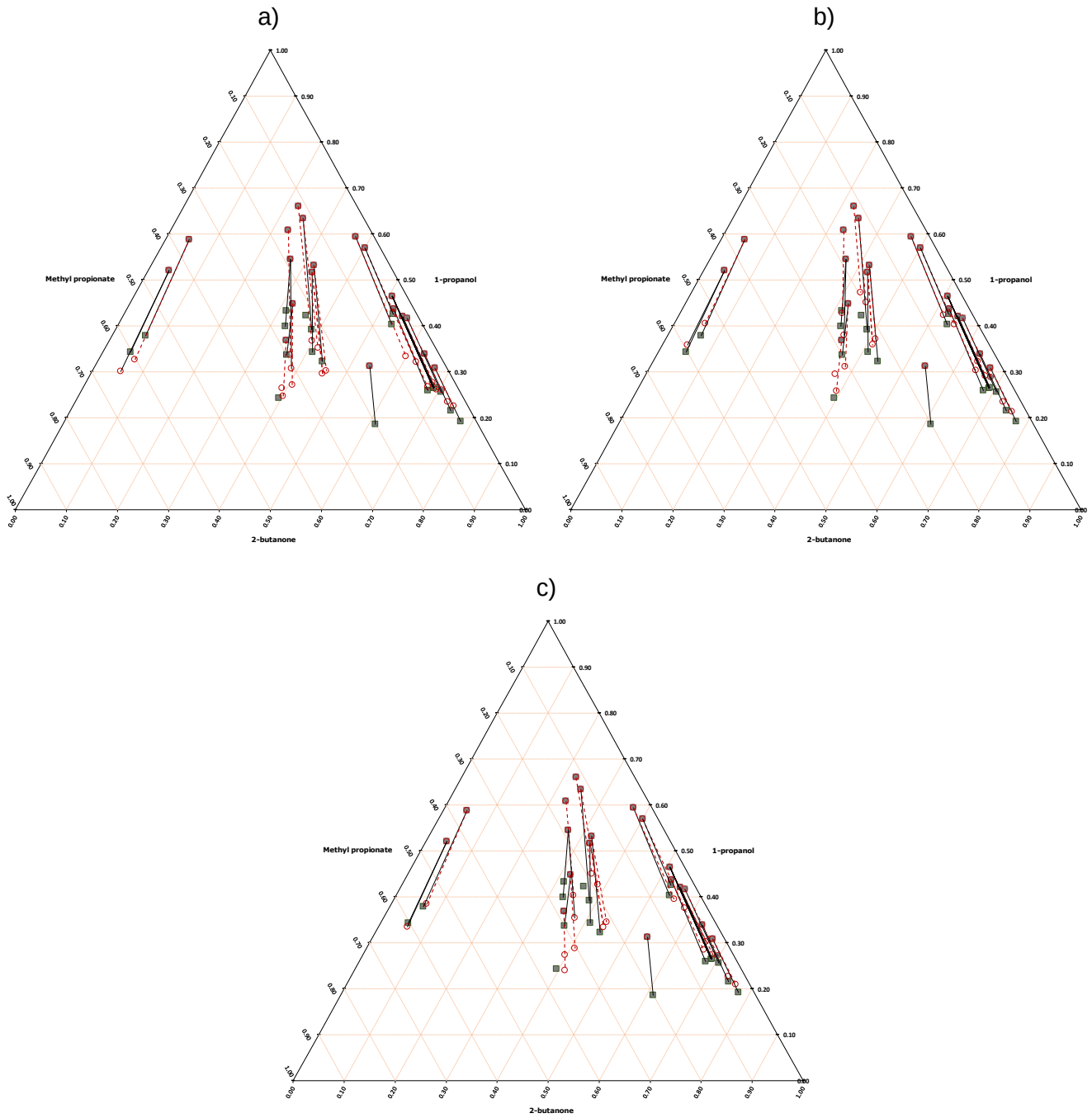

Figure J.4. Predictions of the three thermodynamic models of the ternary systems 1-propanol/2-butanone/propyl formate for T=354.28-356.02 K. Solid lines with grey squares represent experimental tie-lines. and dashed lines with red circles represent the calculated tie-lines using a predictive model. a) Prediction using CPA-GV. b) predictions using SAFT-VR-Mie-GV. c) prediction using sPC-SAFT-GV

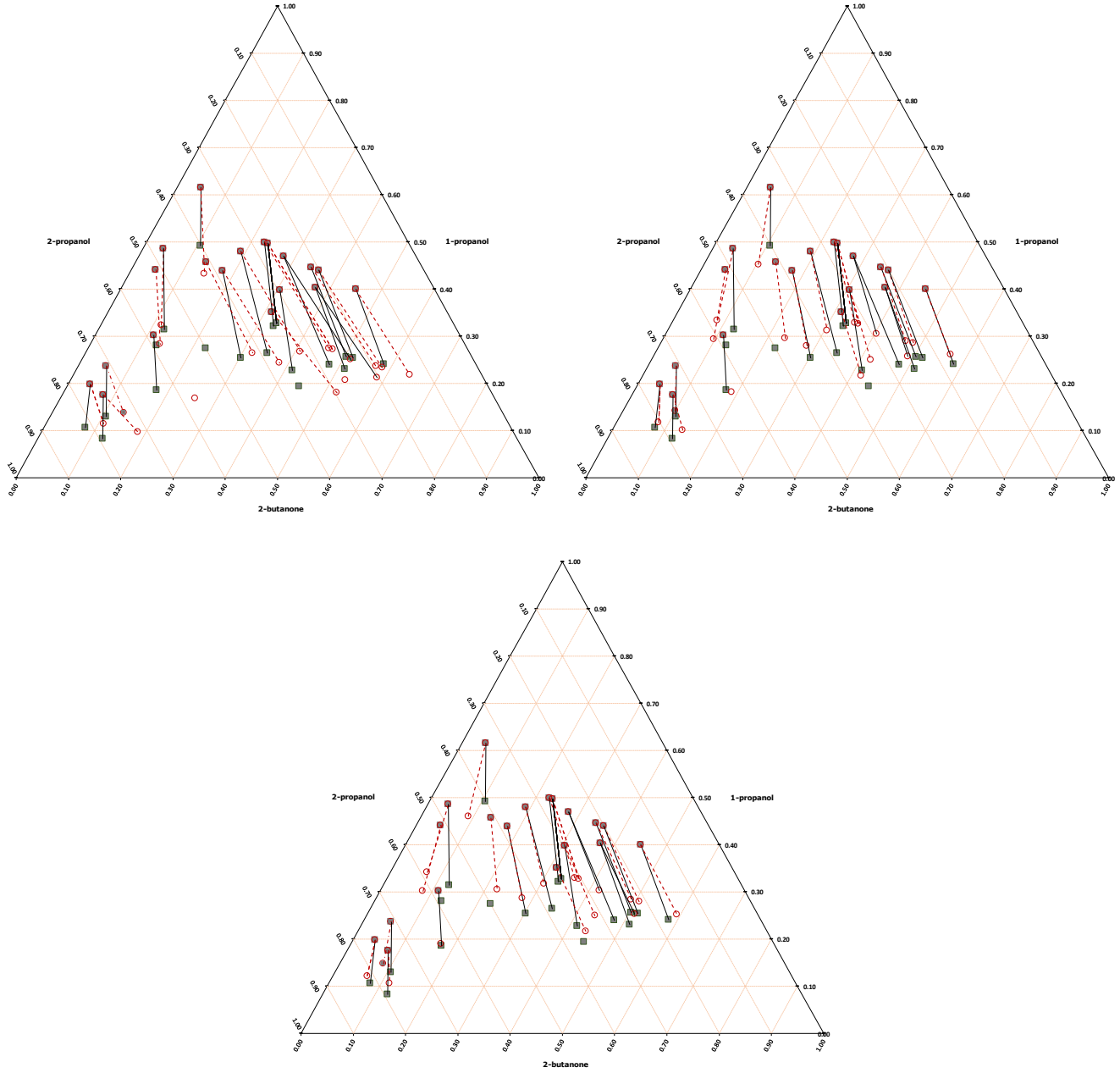

Figure J.5. Predictions of the three thermodynamic models of the ternary systems 1-propanol/2-butanone/propyl formate for T=355.07-360.12 K. Solid lines with grey squares represent experimental tie-lines and dashed lines with red circles represent the calculated tie-lines using a predictive model. a) Prediction using CPA-GV, b) predictions using SAFT-VR-Mie-GV, c) prediction using sPC-SAFT-GV